Thermal and Hydraulic Aspects of Falling Film Evaporation

A thesis presented for the degree of
Doctor of Philosophy
in
Chemical and Process Engineering
at the
University of Canterbury
Christchurch, New Zealand

by

A.R. Mackereth

1995

VOLUME 1: ACKNOWLEDGEMENTS - REFERENCES

This work is dedicated to Jesus Christ, with the sentiment expressed in the following passage from 1 Cor 13:9-10,12 (New American Standard Version):

> *For we know in part, and we prophesy in part; but when the perfect comes the partial will be done away...*
>
> *For now we see in a mirror dimly, but then face to face; now I know in part, but then I shall know fully just as I have been fully known.*

ACKNOWLEDGEMENTS

This work was carried out, in part, at the Chemical & Process Engineering Department, University of Canterbury and, in part, at the New Zealand Dairy Research Institute (NZDRI), Palmerston North.

The author would like to extend his deepest appreciation and thanks to the following people at the University of Canterbury: Dr P.J. Jordan for his encouragement, advice and guidance and Prof A.G. Williamson, Dr R.M. Allen and Dr R Kabel for their advice.

The author gratefully acknowledges the contributions of the following NZDRI staff: Dr G. Page and Dr R. Norris for their support during the project; Dr C B Bloore for proposing and setting up the PhD programme, and Dr K Pearce for his forbearance as deadlines passed and the end was still not in sight; the Milk Powder & Drying Section, in particular, Robbie Buwalda, the other process hall staff and the laboratory staff for their assistance during the experimental programme; the support of the process hall maintenance staff and, in particular, the boiler operator, Jeff Hardy in keeping both the plant running and services supplied; the Starters and Microbiology section staff for microbiological testing during the skim milk trials; Grant Winter who was the prime mover behind the design and installation of the Research Evaporator; Pat Janssen for writing the operating and data logging program and Ken Morison for his assistance with instrumentation and control; Ian Horley, Mark Dillon and Don McLean for their assistance in the design and fabrication of the non-condensable gas measurement apparatus. The assistance of the NZDRI Illustrations staff with the drawings and photos is appreciated.

The author acknowledges the generosity of the NZDRI in completely financing the PhD programme.

The author gratefully acknowledges the patience and prayerful support of his wife, Diana, during this seemingly never-ending programme. To Michael, Aaron and Joel who arrived during this programme to brighten up our lives, welcome.

SUMMARY

Some thermal and hydraulic aspects of falling film evaporation were investigated. Experiments were made on two single effect evaporators. The first with a tube, 15 m long and 48 mm in diameter and the second which had the choice of one of three tubes, all 10 m long, with diameters (23,40 & 48 mm). The apparatus was designed to enable the measurement of overall heat transfer coefficients. The effects of process variables, on the product-side and on the steam-side heat transfer coefficients, were determined by fixing conditions on the other side of the tube.

Experiments were conducted on water, sucrose solution and skim milk. Aspects evaluated were temperature driving force, boiling temperature, tube liquid loading, feed temperature, non-condensable gas concentration in steam, de-aeration rates, product concentration (sucrose solution, milk) and feed thermal history (milk). The results obtained have been compared with theory and empirical data from the literature. A numerical integration procedure for the boiling side Nusselt number was developed to account for the change in boiling-side fluid properties over the length of the tube. The effect of boiling film Reynolds number on the overall heat transfer coefficient proved complicated with a local maximum being found in the transition flow region.

A model description was developed to mimic the steam flow and condensation behaviour in the steam-side annulus of a single tube falling film evaporator. The numerical method initially chosen to solve the model proved inapplicable.

A range of methods for measuring the amount of non-condensable gases present in vacuum steam were considered. The in-line measurement of pressure and temperature and the comparison of the pressure of a collected sample before and after freezing out the component were evaluated.

CONTRIBUTIONS

A large body of experimental heat transfer data was obtained on well-instrumented, commercial sized evaporator tubes at commercial operating conditions. Data was obtained on water, sucrose solutions, and, skim milk concentrates. Variables investigated on water were tube liquid loading, temperature driving force, boiling temperature, feed temperature (degree of flash), tube diameter, and, steam-side factors. The steam-side factors studied were the non-condensable gas concentration, the location of de-aeration ports, and, de-aeration flow rate. Variables evaluated on sucrose solutions were feed concentration, tube liquid loading, boiling temperature, temperature driving force, degree of flash on entry, and, tube diameter. For skim milk, the effects of pre-heat treatment and feed concentration were investigated.

There are two major sets of boiling film Nusselt number correlations in the literature. This work demonstrated that the local modified Nusselt number correlations proposed by Chun & Seban (1971) were far superior to those proposed by Billet (1989).

The presence of a local maximum overall heat transfer coefficient in the transitional flow regime was confirmed on water. Struve (1969) had obtained data on Refrigerant R11 which also exhibits a local maximum. This shows that the transitional flow behaviour is more complex than previously thought. The reason for this maximum is not understood, but is possibly due to changes in wave formation.

Heat transfer data were obtained at high Prandtl numbers (up to 250) under conditions which ensured large changes in the local Reynolds and Prandtl numbers over the length of the tube. Numerical integration of Chun & Seban local Nusselt number correlations over the length of the tube, demonstrated that mean Reynolds and Prandtl numbers could be reasonably approximated by using arithmetic means of entry and exit values.

The dramatic effect of the presence of low concentrations of non-condensable gases in condensing steam on the overall heat transfer coefficient was confirmed.

The method of Wassner (1981) for calculating an overall heat transfer coefficient, given the boiling film Nusselt number, was extended to permit use of Zazuli's correction or the correlation of Chun and Kim(1990) in place of Nusselt's theory for $\bar{Nu}_c$.

GLOSSARY

AP	"absolute pressure".
BPE	"boiling point elevation" - the difference in the liquid boiling temperature of a solution and that of the pure solute. This leads to a step change in temperature at the liquid-vapour interface.
calandria	a cylindrical body containing a bundle of tubes.
CIP	"cleaning-in-place" *i.e.* cleaning of plant without manual dismantling of plant and scrubbing.
DSE	"direct steam expansion" - a method of supplying steam to evaporator
DSI	"direct steam injection" - a DSI unit is a device which heats a liquid stream by injection of steam.
dairy season	in New Zealand the dairy cows are not housed inside so the milk supply is seasonal in nature. The seasons vary depending on location and climatic conditions but commonly run from August to May. Calves are usually born in July-September so the cow's lactation period runs in parallel with the season.
degree of flash (DOF)	the difference between the feed temperature and the liquid boiling temperature at the top of the tube. For positive degrees of flash, vapour is flashed off on entry into the calandria.
DP	"differential pressure".
effect	a technical term for all the calandria-separators in an evaporator that operate with the same steam supply pressure and the same boiling temperature. The number. of effects in an evaporator indicates the number of times the heat in the steam is reused.
end of season	this refers to the period during February-May where climatic conditions and the late lactation period produces milk with a higher protein content.
flow plate	a manifold of pipes arranged so one or more U bends can be used to route the fluids to the desired location. They are cheaper than valve systems and can ensure complete isolation of CIP fluids from the milk stream.

fouling	the deposit of mineral and protein material on heat transfer surfaces.
GC	gas chromatograph.
HP	"high(er) pressure".
HS	"high steam" flow condition.
HTC	"heat transfer coefficient".
LF	"low" feed "flow" condition.
LP	"low(er) pressure".
liquid distributor	a device at the top of the calandria body which attempts to evenly distribute the feed stream over all the tubes.
liquid loading	mass flow per unit tube perimeter.
MVR	"mechanical vapour recompression" - the compression of the milk vapour by fan or compressor so that the vapour can be used for heating the same calandria or one operating at a higher boiling temperature. The term "recompression" is a misnomer as only the heat is recycled not the steam.
NCG	"non-condensable gases".
NCN	"non-casein nitrogen".
NPN	"non-protein nitrogen".
NZDRI	"New Zealand Dairy Research Institute".
pass(es)	the number of "passes" refers to the number of times the milk is pumped to the top of a calandria and passes down through separate sets of tubes.
PHE	"plate heat exchanger".
S	"standard" condition.
SPC	"standard plate count" - a microbiological test.
separator	a cyclone-type device which separates the boiled-off vapour from the concentrate at the bottom of the calandria.
steam (jet) ejector	a device which forces high pressure steam through a nozzle which converts the pressure energy to kinetic energy. The low pressure zone created can be used to draw in low pressure steam or air. After the low pressure zone, there is a recovery section where part of the kinetic energy is converted back to pressure energy.
TA	"titratable acidity".
TN	"total nitrogen".

TS	"total solids" - the concentration of solid material in the sample
TVR	"thermal vapour recompression" - the compression of some of the vapour from one effect using a steam ejector (see above) so that the vapour can be used to heat the same effect or another operating at a higher temperature (see MVR above).
temperature driving force	the temperature difference between the steam side of the calandria and the boiling vapour temperature.
temperature excess	the difference between the wall temperature and the boiling vapour temperature or the temperature drop across the boiling film.
UHT	"ultra high temperature" - refers to a process where liquid streams are subjected to very high temperatures for a short time to sterilize the product.
WPNI	"whey protein nitrogen index" - a measure of the amount of un-denatured whey proteins.

TABLE OF CONTENTS

VOLUME 1

SYMBOLS

ROMAN

A	surface area (m^2)
BPE	boiling point elevation (°C)
C	specific heat of fluid (J kg^{-1} K^{-1})
d	tube diameter (m)
E	evaporation rate (kg s^{-1})
g	acceleration due to gravity (m s^{-2})
k	fluid conductivity (W m^{-1} K^{-1})
L	length (m)
m	mass flow rate (kg s^{-1})
n	power term defined in Equation 10.15
N	number of tubes in effect (-)
p	absolute pressure (Pa)
q	heat flow (W)
R	specific gas constant (J kg^{-1} K^{-1})
s	tube wall thickness (m)
S	concentration (% w/w)
T	temperature (K)
u	mean stream velocity (m s^{-1})
U	overall heat transfer coefficient (W m^{-2} K^{-1})
x	mole fraction
w	mass fraction
z	vertical distance from top of tube (m)

GREEK

α	heat transfer coefficient (W m^{-2} K^{-1})
Γ	mass flow per unit tube perimeter [or liquid loading] (kg s^{-1} m^{-1})
δ	liquid film thickness (m)
Δp	pressure difference or pressure drop (Pa)
ΔT	temperature difference (K)
Δz	step size in z direction (m)
κ	mean height of pipe wall roughness (m)
λ	latent heat of vaporization (J kg^{-1})
Λ	coefficient of pipe friction (-)
μ	dynamic viscosity (kg m^{-1} s^{-1})
ν	kinematic viscosity (m^2 s^{-1})
ρ	density (kg m^{-3})
τ	shear stress (kg m^{-1} s^{-2})

HEBREW

ן	percentage of steam inlet flow vented through top vent
מ	mass evaporation rate (kg s^{-1})
נ	mass condensation rate (kg s^{-1})
ש	dimensionless steam consumption (defined on page 2.15)

SUBSCRIPTS

1	condition of water vapour
B	Billet (1989) equation
boil	boiling vapour condition
c	condensate stream condition
CS	Chun & Seban (1971) equation
e	evaporating film condition
i	condition at boiling liquid/vapour interface
ID	condition at wall inner surface
l	liquid phase condition
lam	laminar flow regime
m	mean
max	maximum value
MM	Micromotion meter output
o	condition of pure solvent
OD	condition at wall outer surface
p	at constant pressure
prod	condition of liquid product leaving tube
r	radial direction component
S	combined property of all solutes
sat	saturated steam condition
SS316	condition of 316 stainless steel
steam	bulk steam condition
tra	transitional flow regime
tur	turbulent flow regime
U	overall
v	vapour phase condition
vent	venting stream condition
w	wall condition
μ	capillary viscometer condition
ρ	condition in density meter
τ	condition at top of tube
$\perp$	condition at bottom of tube

SUPERSCRIPTS

-	mean value
*	based on ΔT_U rather than ΔT_e or ΔT_c (see Section 28.1)

DIMENSIONLESS GROUPS

Jacob numbers:

$$Ja = \frac{C_p \Delta T_e}{\lambda} \quad , \quad Ja^* = \frac{C_p \Delta T_U}{\lambda}$$

Modified Nusselt number:

$$Nu = \frac{\alpha}{k}\left(\frac{\nu^2}{g}\right)^{1/3}$$

Boiling point elevation numbers:

$$N_{BPE} = \frac{\Delta T_e - BPE}{\Delta T_e}$$

$$N^*_{BPE} = \frac{\Delta T_U - BPE}{\Delta T_U}$$

Tube aspect ratio:

$$N_{L/d} = \frac{L}{d_{ID}}$$

Vapour/liquid loading ratio:

$$N_{\Gamma_v/\Gamma_e} = \frac{\Gamma_v}{\Gamma_e}$$

Prandtl number:

$$Pr = \frac{C_p \mu}{k}$$

Film Reynolds number:

$$Re = \frac{4\Gamma}{\mu}$$

Wassner's material parameter:

$$x = \frac{k_e}{k_c}\left(\frac{\nu_c^2}{\nu_e^2}\right)^{1/3}$$

Wassner's pipe wall parameter:

$$y = \frac{s}{\left(\frac{\nu^2}{g}\right)^{1/3}} \frac{k_e}{k_w} \frac{A_{ID}}{A_m}$$

Wassner's condensation parameters

$$Z = \frac{C_{p_c} L \Delta T_c}{\lambda_c Pr_c \left(\frac{\nu_c^2}{g}\right)^{1/3}}$$

$$Z^* = \frac{C_{p_c} L \Delta T_U}{\lambda_c Pr_c \left(\frac{\nu_c^2}{g}\right)^{1/3}}$$

PART I: INTRODUCTION

1. EVAPORATION

Evaporation is the process of turning a liquid into a vapour. Where there is a mixture of components in the liquid, the composition of the vapour is dependent on the relative vapour pressures of the components. With liquid mixtures, this means that distillation or rectification is normally required to separate out a particular component. With a solution, however, the vapour pressures of the solid components are negligible, so the solvent can be separated off simply by the application of heat.

There are a variety of ways in which heat is applied. The Dead Sea is a natural example of an evaporation process. With no natural outlet, the only way water leaves the lake is by solar powered surface evaporation. Solar power is also used for the evaporation of water from clothes hanging on a line. In industry, the heat is usually supplied by condensation of steam. A general review can be found in Coulson & Richardson (1968).

Evaporation is used industrially for recovering a purified solvent and/or a concentrated solute. Drinking water is produced from sea water by flash evaporation (Al-Zubaidi, 1987). Black liquor, a by-product of paper manufacture containing high levels of sodium hydroxide, has been concentrated by falling film evaporation (Mackereth, 1987). The concentrated effluent is reduced further by combustion. This eliminates a high volume liquid effluent stream, and enables process water recirculation. Processes in which the solute is the desired product include the concentration of fruit juices, milk and whey. Drying processes such as roller drying, spray drying and tray drying are all technically evaporation processes, but the term evaporation usually refers to processes which increase the concentration of liquid streams.

A wide variety of evaporation techniques are used for concentration of liquid streams. These have been classified by Billet (1989) as follows:

Natural circulation
Forced circulation
Climbing film
Falling film
Thin film
Flash

Simplified schematics of each type are shown in Figure 1.1.

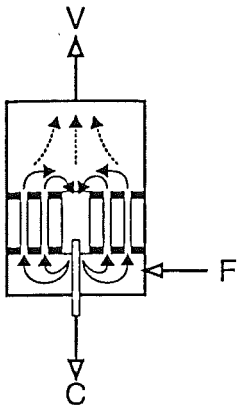

Natural circulation

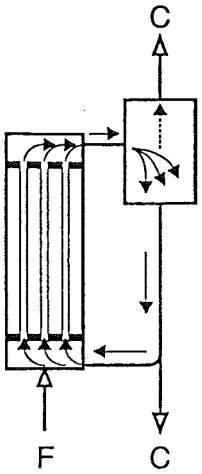

Natural or forced circulation

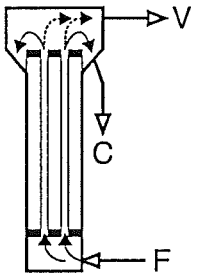

Climbing film

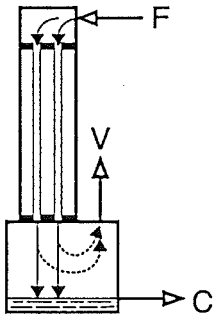

Falling film

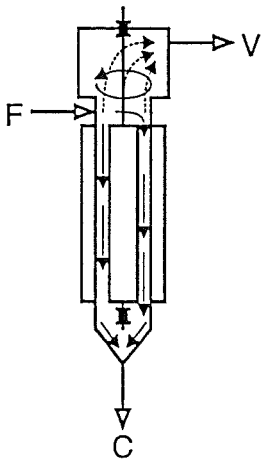

Thin film - wipers

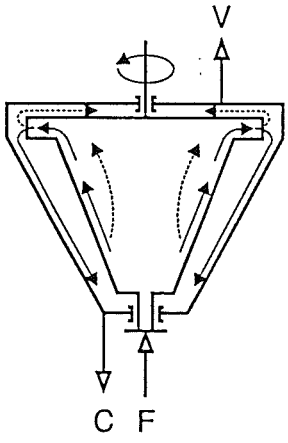

Thin film - centrifugal

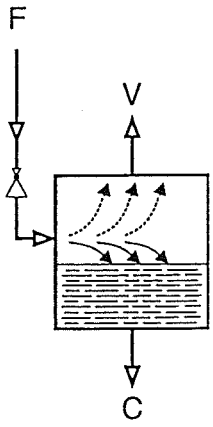

Flash

Figure 1.1: Types of Evaporators (Adapted from Billet (1989); F = Feed, C = Concentrate, V = Vapour; Graphics by Garnett Davy, NZDRI)

1.1 Natural Circulation

Bubbles of vapour are produced on short vertical or inclined tube walls. The bubbles flow upwards through the tubes, dragging with them a portion of the surrounding liquid. The vapour is separated above the tubes and the liquid is returned in a down pipe to the bottom of the tubes. The tube wall needs to be 10-20°C above the boiling point for natural circulation. The residence time is extremely long and the tubes are prone to excessive fouling, salting or scaling due to low liquid velocities and high wall temperatures (Billet, 1989).

1.2 Forced Circulation

Essentially the same as for *natural circulation* except that the liquid is pumped upwards through the tubes. The higher liquid velocities reduce the degree of fouling (Billet, 1989).

1.3 Climbing Film

The feed is pumped into the bottom of vertical tubes. The production of vapour bubbles carries the liquid up the tube. By the top of the tube there is an upwardly flowing film of liquid on the tube wall, with a high velocity vapour core. The vapour and concentrate leave the tubes at the top and are separated in a centrifugal separator. The liquid level is about one third of the way up the tubes and usually there is no re-circulation (Billet, 1989). Thus, the residence time is much less than for circulating evaporators, but longer than for falling film evaporators. The high wall temperatures required and the potential dry areas of tube wall mean that these evaporators are prone to excessive fouling.

1.4 Falling Film

In falling film evaporators, the feed is carefully distributed to the top of vertical tubes and flows down the inner walls. The vapour and concentrate leave the tubes at the bottom and are separated in a centrifugal separator. The tube length can vary from 3 to 18 m. The residence time is less than 1 min per pass. The thin film of product reduces the wall temperature required for effective heat transfer. Falling film evaporators will work successfully with wall temperatures of 2-3°C above the feed boiling temperature. The degree of fouling depends on the liquid coverage of the tube walls, the film's flow behaviour and on the temperature difference across the product film. Milk evaporators made to modern designs exhibit negligible fouling (Mackereth, 1990). The maximum

liquid viscosity for falling film evaporators is 0.1-1.0 kg m^{-1} s^{-1} (Billet, 1989) because of the very slow film flow rate, the difficulty in maintaining adequate tube coverage and the high temperature driving force required.

1.5 Thin Film

These are evaporators which have been designed to have low residence times, and can be operated at very low temperatures. There are two basic types. The first employs wipers to scrap the feed off the tube walls, thus maintaining a clean wall. These can operate on products with viscosities up to 10 kg m^{-1} s^{-1} (Billet, 1989). The cleaning action of the wipers enables the use of high wall temperatures which reduces the area required, and thus the residence time. The high wall temperatures can cause thermal damage to sensitive products.

The second type introduces the feed onto the centre of a spinning, upward-inclined heated disc. The centrifugal force causes the feed to travel up the inclined surface as a thin film. The thickness of the film is controlled by the rotational speed, and products with viscosities of 20 kg m^{-1} s^{-1} (Billet, 1989) can be evaporated successfully. The high speed ensures that the steam condensing on the underside of the disc forms droplets which are thrown away from the surface. The thin product film and the drop-wise condensation ensures that the heat transfer coefficient (HTC) is very high. This enables the use of very low wall temperatures and thus minimises thermal product damage.

1.6 Flash

Flash evaporation is simply the process of introducing a hot feed into a low pressure chamber. The absence of nucleation and potential dry surfaces in the heaters allows the use of these evaporators for solutions which are prone to salting or scaling (*e.g.* sea water). The concentration ratio for each stage is small, so multiple stages and recirculation are required. Therefore residence times will be longer than for falling film evaporation (Billet, 1989).

1.7 Effect of Product Characteristics on Evaporator Selection and Design

The characteristics of the product during concentration, determine the choice of evaporator design and the operating conditions. Important product factors to consider are:

Viscosity
Thermal conductivity
Boiling point elevation
Tendency to salting, scaling and/or fouling
Thermal instability

The properties of the solvent are also important, in particular:

Vapour pressure
Latent heat of vaporization
Temperature excess required for nucleation
Critical temperature excess

The properties of the product stream and water vapour are discussed with respect to milk in Chapter 2.

2 EVAPORATION OF MILK

A paper given to a New Zealand Dairy Industry Conference in July 1992 is attached as Appendix A. It discusses the transfer of heat from the condensing steam, through the calandria tube wall and through the milk film. It summarizes a lot of the information provided in this chapter and later chapters, and the reader may find it an appropriate introduction to the falling film evaporation of milk.

2.1 Properties of Milk

Composition

Milk is the natural secretion from a cow's udder. The composition of milk varies widely depending on breed, climatic conditions and period of lactation. Mean weight percentage values (Grey, 1988) for the main constituents of milk (assuming 50% Jersey and 50% Friesian are:

Water	86.6%	
Fat	4.2%	Total solids 13.4%
Protein	3.6%	
Lactose	4.9%	
Minerals	0.7%	

The fat is in the form of globules with a protective protein surface layer. The globules are dispersed in the skim milk aqueous phase. There are two main types of proteins (Gordon & Kalan, 1974):

Casein (76-86%) which is heat stable at temperatures below 100°C.

Whey proteins (14-24%) which are sensitive to heat. The main whey proteins are;

beta-lactoglobulin	7-12% (of skim milk proteins)
alpha-lactalbumin	2-5%
blood serum albumin	0.7-1.3%

Minerals present in milk include calcium, potassium, sodium and magnesium salts (Johnson, 1974). Some are bound in the protein structures, with the remainder being in solution.

Effect of heat on milk

Denaturation of whey proteins occurs at temperatures as low as 55°C (Parry, 1974). The denaturation of whey proteins changes the characteristics of the final product and

increases the viscosity of the milk.

Calcium phosphate is less soluble at high temperatures and its precipitation may cause the formation of the initial fouling layer in preheating equipment (Bird & Fryer, 1991). Once a mineral layer is formed, the aggregation of denatured beta-lactoglobulin appears to be the controlling step in the fouling process.

To prevent excessive fouling of evaporative heat transfer surfaces, and to minimise denaturation of whey proteins during concentration, the maximum recommended boiling temperature for milk at low concentrations is 70°C. At high concentrations the limit is reportedly 58-60°C (Fergusson, 1989).

Viscosity

The viscosity of milk during the evaporation process varies from $< 10^{-3}$ to 0.3 kg m^{-1} s-1. The viscosity is dependent on milk solids composition, concentration (see Figure 2.1) and temperature (Wood, 1982). The major contributions to the viscosity of milk come from the protein structures in the milk, and also the fat globules in the case of whole milk. Preheat treatment of the milk which changes protein structures can affect the concentrate viscosity (Bloore, 1981). Milk is reported to be pseudoplastic (Liu *et al*, 1991) and at above 40-42% w/w thixotropic (Snoeren *et al*, 1984). However, recent work has indicated (Trinh, 1993) that milk is essentially Newtonian under evaporation conditions except perhaps at concentrations above 40-42% w/w.

Thermal conductivity

Thermal conductivity data of water, skim milk and whole milk from the literature (Wood, 1982, p5:1-8) are shown in Figure 2.2. The concentration of the whole milk and skim milk was not given. The data indicates that unhomogenised whole milk has a significantly lower thermal conductivity than skim milk, but that homogenisation significantly increases the thermal conductivity of whole milk. The thermal conductivity of whole milk (see Figure 2.3) decreases with increasing concentration and increases with increasing temperature (Hall & Hedrick, 1966, p35).

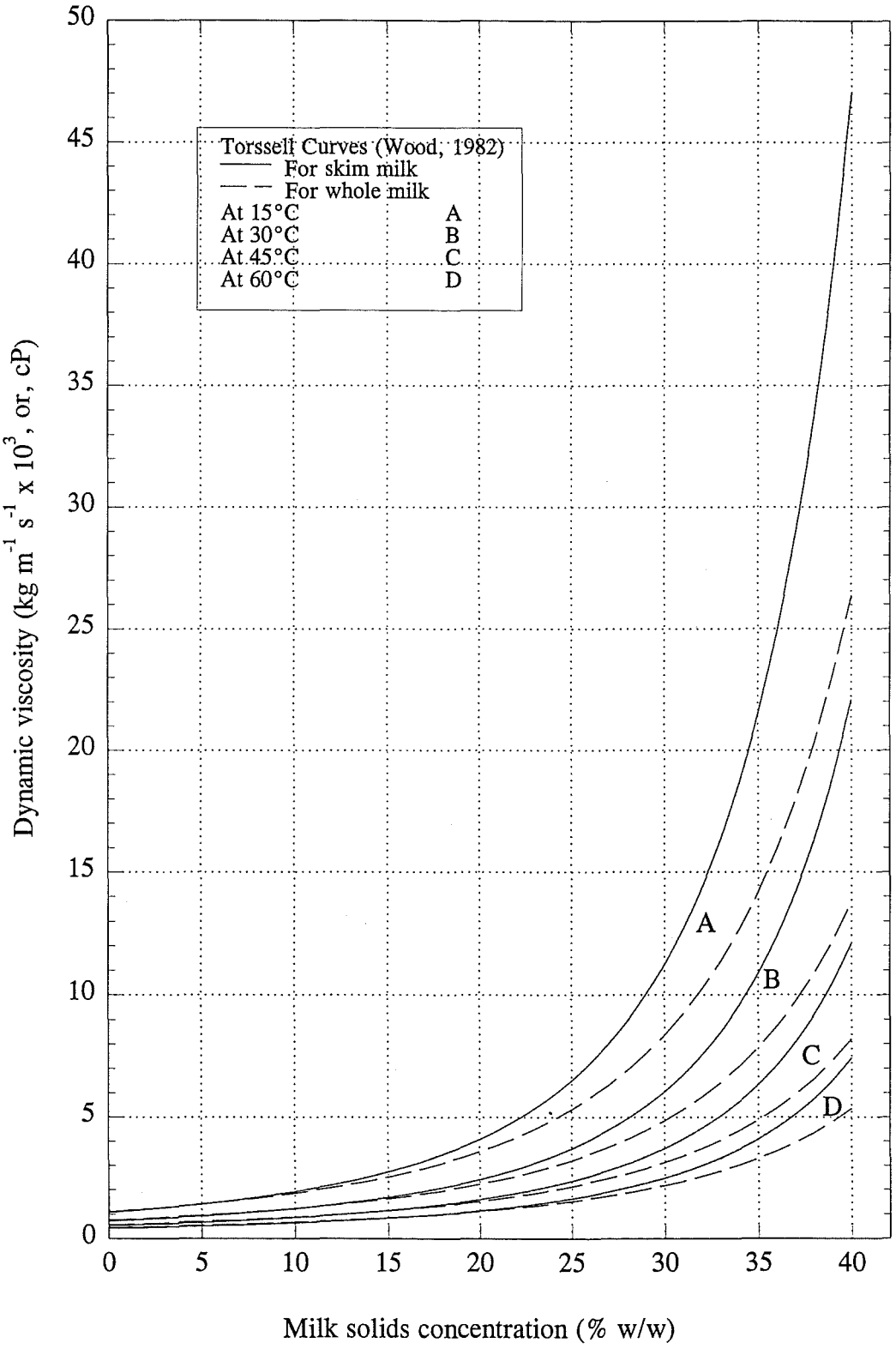

Figure 2.1: Viscosity of Skim Milk and Whole Milk Concentrates.

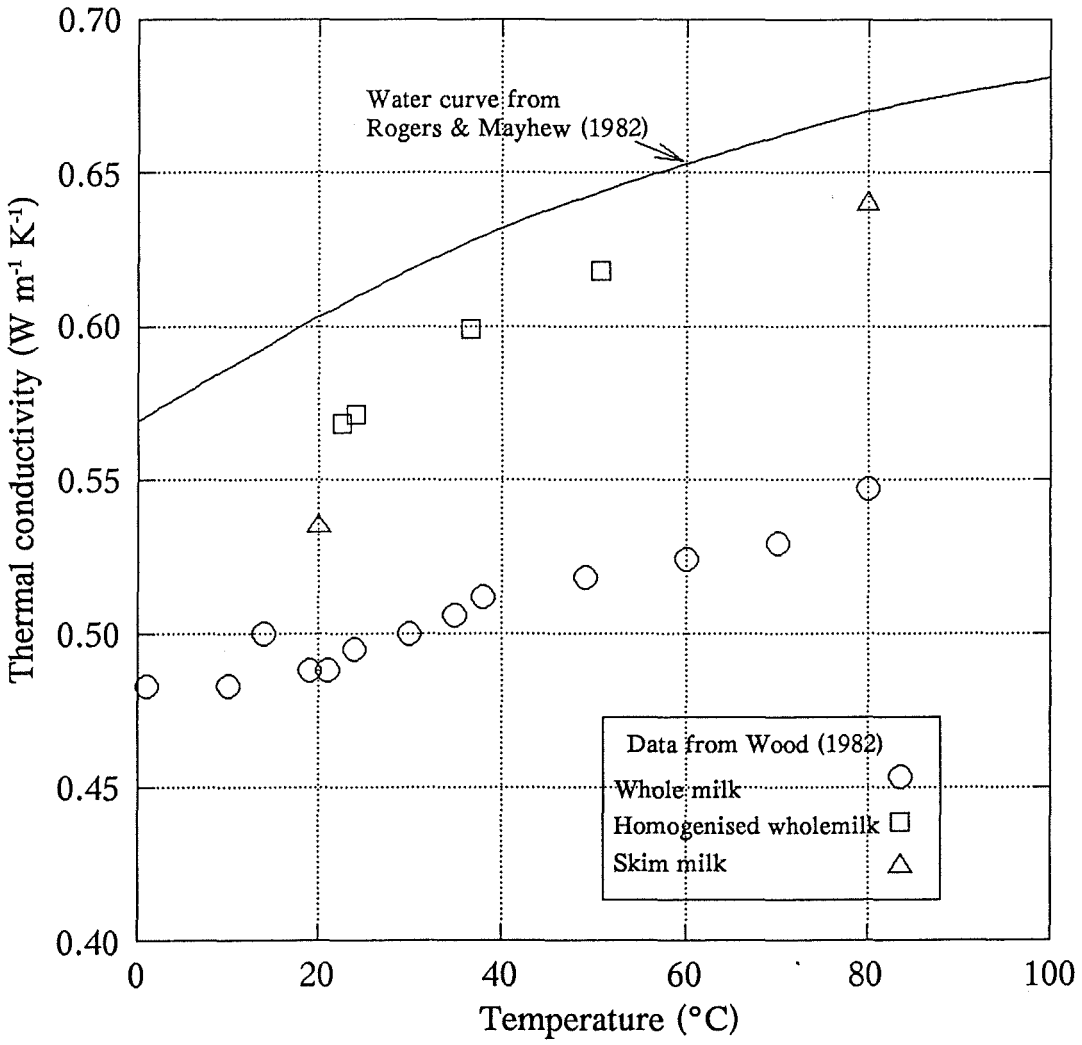

Figure 2.2: Thermal Conductivity Data for Skim Milk and Whole Milk.

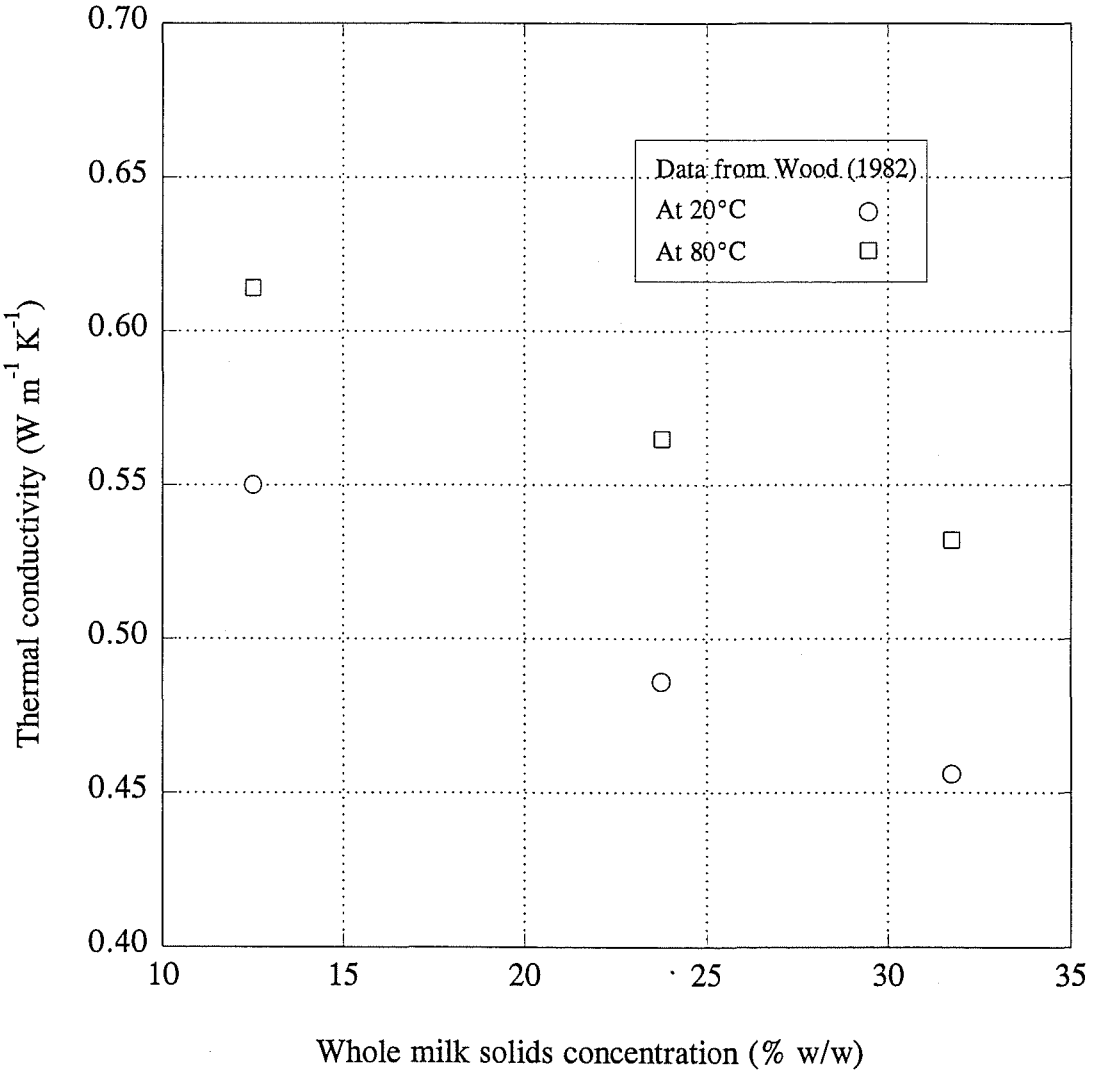

Figure 2.3: Thermal Conductivity Data for Whole Milk Concentrates.

Boiling point elevation (BPE)

Aqueous solutions boil at a higher temperature than water. Predicted BPE values for skim milk and whole milk were determined using the following equation (Castellan, 1972):

$$BPE = \left[\frac{1}{\left(\frac{1}{T_o}\right) + \frac{R \ln(1 - x_S)}{\lambda_e}} \right] - T_o \qquad (2.1)$$

Lactose and salts contribute almost all the moles of solute in milk, because the size and close association of both the protein and fat components severely limit their contribution. Lactose makes up ~52% w/w of skim milk solids and ~38% w/w of whole milk solids. The ratio of salts to lactose in skim milk is typically 0.142/0.160 mole/mole (Creamer, 1988). This information was used to determine BPE curves for skim milk and whole milk concentrates at 60°C (see Figure 2.4). The BPE effectively reduces the available temperature driving force, and in conjunction with increasing Pr_e, prevents the use of ΔT_U (T_{steam} - T_v) of less than 6-7°C for the final stages of milk concentration (~ 40 to 50% w/w). Experimental BPE data for skim milk is presented in Chapter 31.

2.2 Properties of Solvent (Water)

Vapour pressure

The vapour pressure of water ensures that to boil at temperatures less than 70°C, the evaporation has to be done under vacuum. The relationship between vapour pressure and saturation temperature is shown in Table 2.1.

A combination of factors ensures that the minimum practical temperature for milk evaporation is 40°C. Lower pressures are difficult to maintain and very low vapour densities lead to large vapour ducts. The high viscosity and the low thermal conductivity of milk concentrate at low temperatures hinders heat transfer. The cooling water required and cooling tower costs increase at low temperatures.

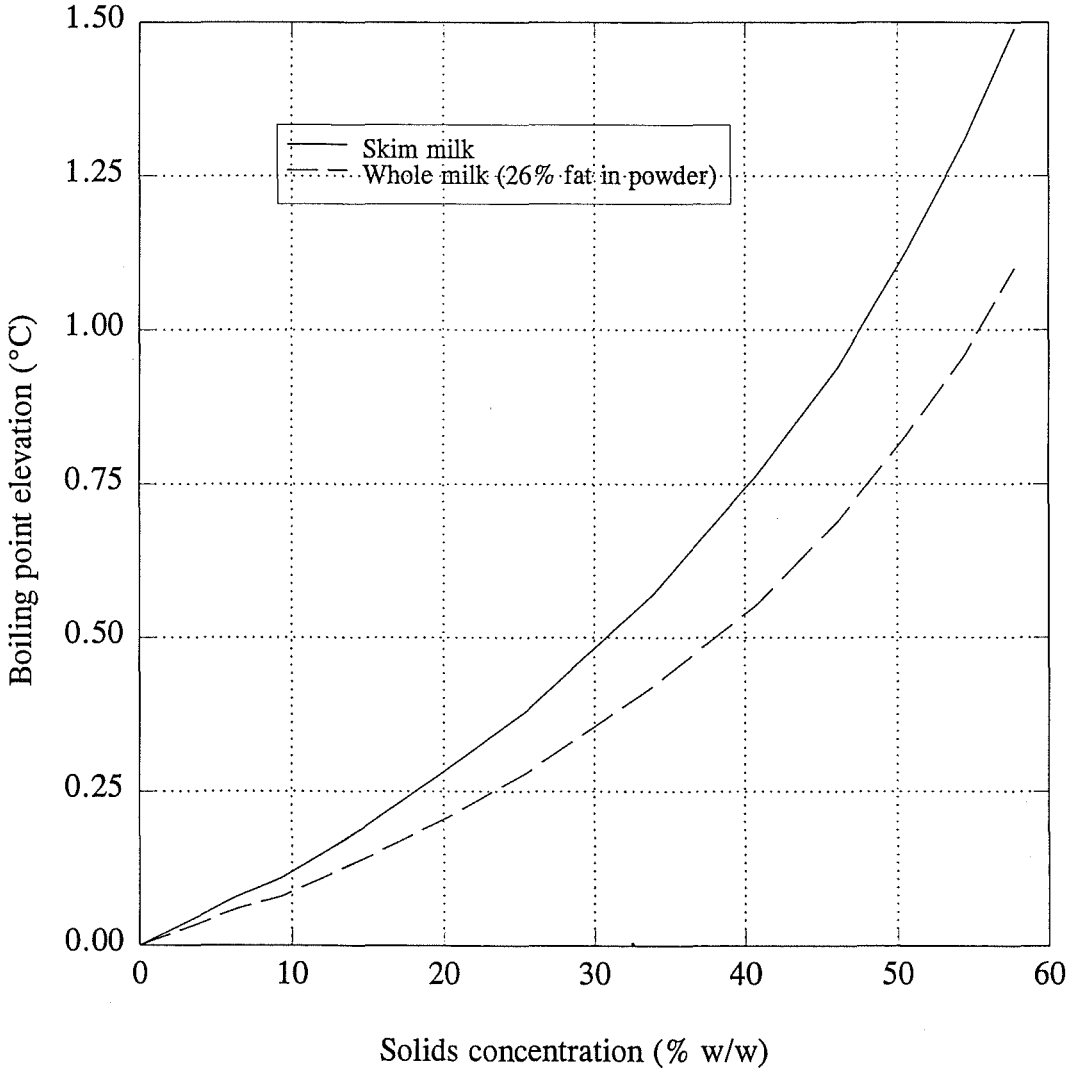

Figure 2.4: Predicted Boiling Point Elevation for Skim Milk and Whole Milk Concentrates at 60°C.

Table 2.1: Relationship between the vapour pressure and saturation temperature of water.[1]

Saturation Temperature (°C)	Vapour Pressure (kPa)
30	4.24
40	7.38
50	12.3
60	19.9
70	31.1
80	47.4
90	70.1
100	101.3

[1]Adapted from Rogers & Mayhew (1982).

Latent heat of Vaporization

Water has an extremely high latent heat of vaporization, so the evaporation process is energy intensive. Modern evaporator designs ensure that the heat contained in the boiled-off vapour is reused many times.

Temperature excess

The temperature excess, ΔT_e required for nucleate boiling of water is 5°C at atmospheric pressure under free convection (pool boiling) conditions. Under conditions of forced convection, the temperature excess required is higher. Nucleate boiling involves the formation of bubbles on the wall that grow and travel out to the film-vapour interface. Heat transfer coefficients for nucleate boiling, without fouling, are much higher than for free and forced convection boiling due to increased turbulence. Nucleate boiling creates additional free surface, which potentially could lead to the formulation of denatured proteins which could deposit on temporarily dried surfaces. The critical temperature excess of water is approximately 32°C and effectively limits the maximum available ΔT_U to 35-45°C when evaporating pure water. On milk, however, rapid fouling of the heating surfaces would be expected at these high temperatures, severely restricting run length. Boiling regimes are discussed further in Chapter 10.

2.3 Milk Powder Manufacture

The milk powder process involves a number of unit operations (Figure 2.5) The milk arriving at the factory is stored in refrigerated silos. The milk then goes through the following process steps:

Separation
Pasteurization
Standardization
(Storage)
Preheat Treatment
Evaporation
Concentrate Handling
Spray Drying
Cooling
Storage
Packing

Separation

The milk is separated in a centrifugal separator into skim (9% TS) and cream (45% TS) fractions. The skim milk contains less than 1.5% fat (dry basis) and the cream contains 88% fat (dry basis).

Pasteurization

The skim milk is usually pasteurized by regenerative heating to 72°C and holding for 15 s. A higher temperature (80°C) is used for cream.

Standardization

For whole milk powder production, a portion of the cream is metered back into the skim milk stream to achieve the desired fat content in the final product (26-30% w/w). Vitamins and minerals may also be added to suit customer specifications. Lactose may be added to *end of season* milk to reduce the protein level to that of mid-season milk.

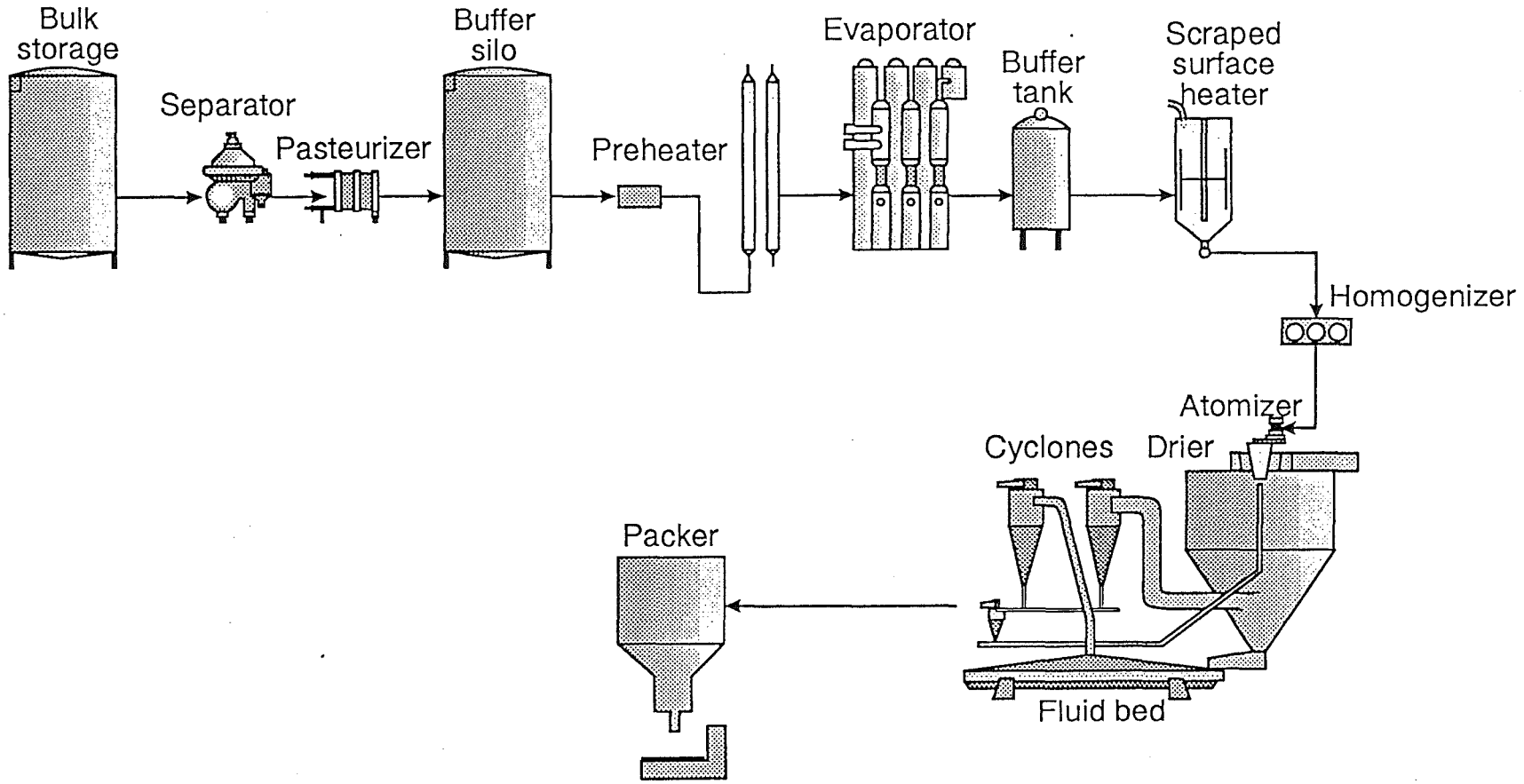

Figure 2.5: Milk Powder Process Schematic (Graphics by Chris Thomasen, NZDRI).

Preheat treatment

The milk is preheated, prior to evaporation, to a temperature of between 75°C and 125°C. The milk is held at the preheat temperature for a period of between 1 s and 3 min. Preheating is done for the following reasons.

a. To raise the milk temperature to above the first effect temperature. This ensures that the evaporative heat transfer area is not used for sensible heating. It also ensures that there is some flashing, when the milk enters the first effect, which assists in the distribution of liquid to the tubes.

b. To kill bacteria and de-activate enzymes. There are bacteria and enzymes which can survive pasteurization, but will not survive the higher temperatures of preheating. However, some bacteria can survive even very high heat treatments.

c. To denature a proportion of the whey proteins to meet an end-product specification. For example, skim milk powder, destined for recombined evaporated milk manufacture, requires a high heat treatment (120°C for 3 min) to ensure the end-product survives in-can sterilization without gelation. Powder destined for recombined cheese manufacture requires a minimal heat treatment (100°C for 1 s). This avoids extensive cross-linking between denatured whey proteins and κ casein. The extensive cross-linking can give the cheese a sticky texture.

d. For whole milk powder, the milk is heated to above 85-90°C to encourage the formation of free sulphydryl groups that act as antioxidants and delay oxidation of the fat (Knipschildt, 1986).

Evaporation

Skim milk is concentrated from 8.5-9.5% w/w to 45-50% w/w total solids in a falling film evaporator. Whole milk is concentrated from 12-13% w/w to 50% w/w. The evaporation is carried out at temperatures between 40-70°C. The flow is essentially co-current with the concentrate leaving the plant at between 40-58°C.

Concentrate handling

The concentrate is heated immediately prior to spray drying to 70-80°C, to reduce the concentrate viscosity and the drier heat load. Whole milk concentrate is homogenized to reduce the milk fat globule size.

Spray drying

The concentrate is atomized by a centrifugal disc or a pressure nozzle. The resultant droplets are dried in a co-current drier. Inlet air temperatures of 180-245°C are used and the outlet air temperatures are usually between 70-75°C for plants with secondary driers. Secondary drying is carried out on both static and vibrating fluid beds. Skim milk powder and whole milk powder have moisture contents of 3.5-4% w/w and 2.5-3% w/w respectively.

2.4 Falling Film Evaporation of Milk

Since the 1960's falling film evaporators have been used for the evaporation of milk in New Zealand. The advantages of falling film evaporation are the short residence time and, latterly, the ability to use a low temperature driving force.

The original plants installed were three effect evaporators with or without thermal vapour compression. Since their introduction, the increasing cost of energy, especially after 1973, has led to an increase in the number of effects and the extent of thermal vapour compression. Latterly, plants with mechanical vapour compression have been introduced.

The evaporation and spray drying of milk powder is an energy intensive process. It has been calculated (Jebson & Iyer, 1991) that in New Zealand 1% of the total energy consumed is used in the evaporation and drying of milk.

2.5 Milk Evaporator Designs

Single effect evaporator components

A single effect evaporator is shown schematically in Figure 2.6. The components shown are discussed below.

Preheating

The milk is preheated using a variety of different heater designs. In the DSE evaporators and older TVR evaporators, coils mounted either around the bundle of tubes in the

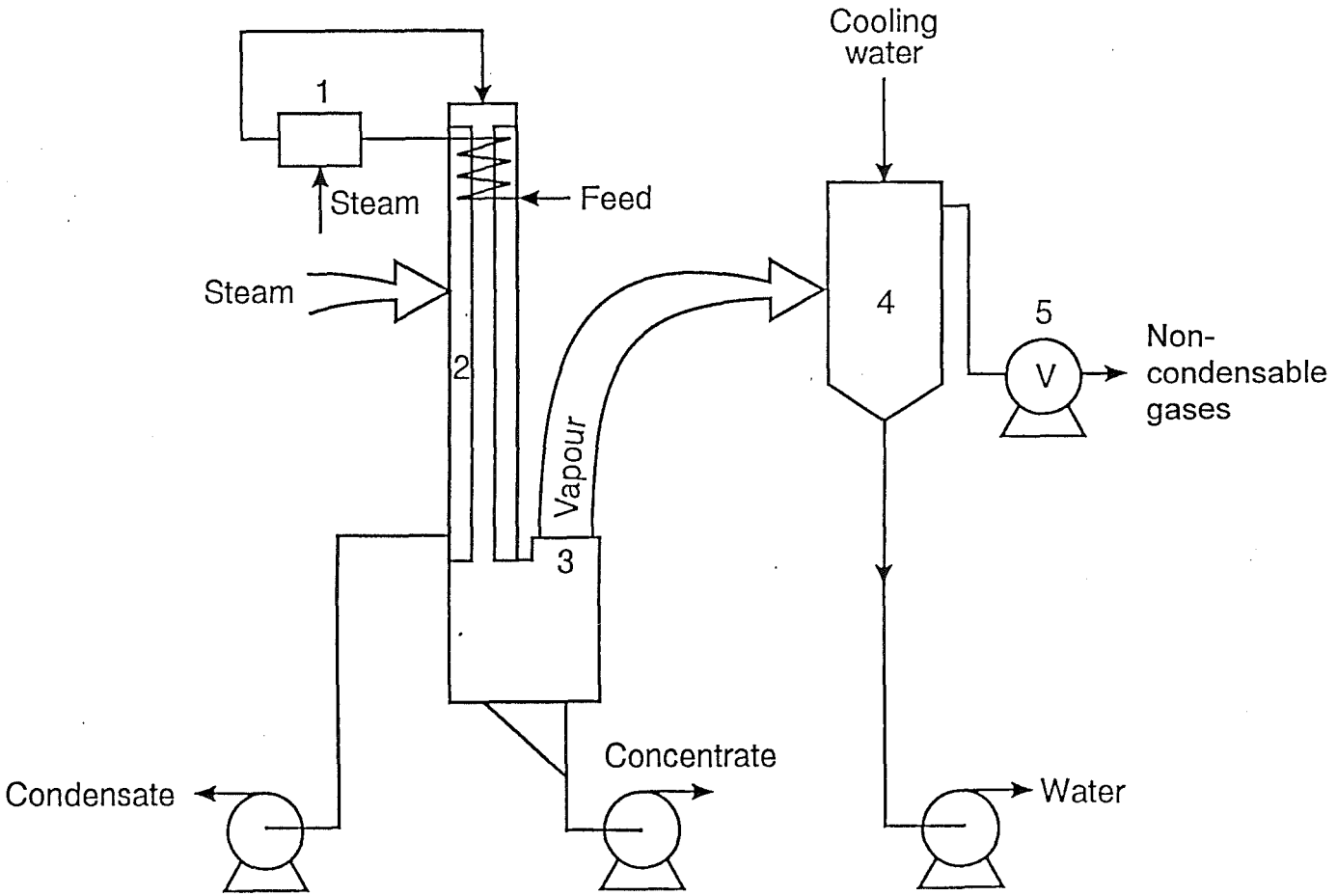

Key:

1 Preheat equipment
2 Calandria
3 Vapour-liquuid separator
4 Condenser
5 Vacuum pump

Figure 2.6: Single Effect DSE Evaporator (Graphics by Garnett Davy, NZDRI).

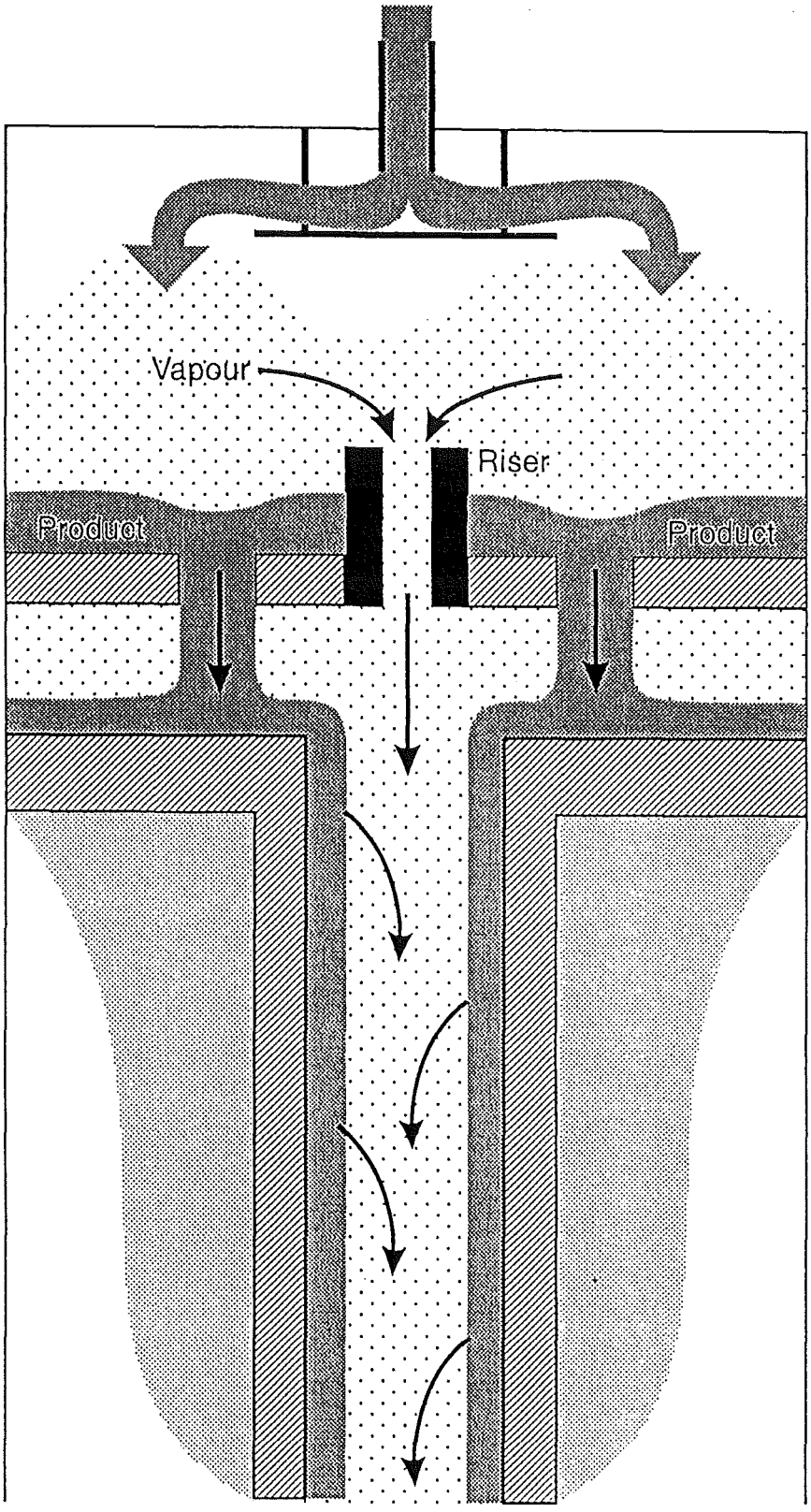

Figure 2:7: Liquid Distribution Detail (Graphics by Chris Thomasen, NZDRI).

calandria or in the separator duct outlet are used to preheat, in stages, the milk up to the first effect temperature. In modern TVR and MVR evaporators a plate heat exchanger (PHE) is normally used to do the same duty using condensate as the heating source. The final preheating step to 75-125°C can be done using indirect heating (with a coil or straight tube heater) or using direct heating (with direct steam injection or steam infusion). Multiple steam infusion vessels connected to flash vessels are used to reduce the steam required for preheating. The steam required for most preheating duties exceeds the amount of steam required for MVR evaporators and thus extra condensing capacity is required to remove this extra heat. One use for this low grade heat is for preheating the drier air.

Liquid distribution

The milk is distributed to the tubes (See Figure 2.7) through small holes drilled in the distribution plate. The tubes are usually positioned in a triangular pitch pattern with three holes per tube. Flash vapours assist in spreading the liquid out over the distribution plate. The small tubes rising up from the distributor plate are known as vapour risers. These allow the flashed vapour to bypass the liquid distribution holes, thus ensuring no deformation of the distributor plate is caused by pressure differential. If the plate is not flat, or if holes are blocked with solid material, or if the holes are too large (no liquid level on the plate) then certain tubes can become starved of feed. The small amount of feed entering the tube becomes highly concentrated and burns on. In severe cases, the tube can become completely blocked.

Heat transfer

The vertical tubes range in length from 3 to 18 m and from 32 to 50 mm in diameter. The number of tubes in a calandria can vary from 20 to 1500. The liquid film flowing down the inner surface of the tubes is heated by steam condensing on the shell-side of the vertical tube bundle. The condensate is extracted at the bottom and returned to the boiler. There is a small port at both the top and bottom of the calandria to remove non-condensable gases. The mass flow rate through each port is restricted by an orifice plate to 0.5-0.75% of the steam condensed in the calandria. The steam consumption of a single effect evaporator is slightly greater than 1 kg per kg of water evaporated. If a dimensionless steam consumption, $\dot{W}$ is defined as:

$$\dot{W} = \frac{\text{steam flow rate}}{\text{evaporation rate}}$$

then a one effect evaporator has a $\dot{W}$ of ≈ 1.

Vapour/concentrate separation

The concentrate and vapour leave the tubes at the bottom, and are separated firstly by gravity and then by centrifugal separation in a cyclone-type device (separator). These are designed to have a low pressure drop (typically the equivalent of 0.5°C temperature drop). Centrifugal pumps are used for product removal.

Vacuum/condensation

The vapour produced is condensed in either a mixing condenser or a surface condenser. The condensate is either removed by gravity through a barometric leg, or by pump. Mechanical vacuum pumps or steam ejectors are used to remove non-condensable gases. The boiling temperature in the effect is usually controlled by adjusting the condenser cooling water flow. A small air bleed into the suction-side of the vacuum pump has also been used for control.

Multiple effects

The vapour boiled off the milk has almost the same enthalpy as the condensing steam. By supplying this vapour to a second effect operating at a lower boiling temperature, the dimensionless steam consumption, $\dot{W}$ drops to approximately 0.5. Obviously, the vapour from the second and subsequent effects can be likewise reused. The highest practical boiling temperature for the evaporation of milk is 70°C (see Section 2.1) and the minimum practical temperature is 40°C (see Section 2.2). This fixes the maximum boiling temperature difference between the first effect and the last effect at 30°C. Now $\dot{W}$ is inversely proportional to the number of effects for a DSE evaporator. The available ΔT_U for each effect drops (see Table 2.2) as the number of effects increase. As ΔT_U is reduced, the area must go up, so the savings in steam consumption are offset by an increase in capital cost.

To prevent fouling the effect may need to be split into a number of product passes to increase tube liquid coverage. This has been done either by having split-body effects (That is, two or more calandrias all using the same steam source) or by dividing off groups of tubes in a calandria and providing them with separate liquid supplies and separate concentrate collection systems. These groups of tubes are known as passes. The product flows into the first pass in a calandria, and the resultant concentrated product from that pass is pumped to the second pass and so on.

Table 2.2 Dependence of steam consumption and available ΔT_U on the number of effects

No of Effects	$\mathbb{U}$	Available ΔT_U per effect (°C)
1	1.00	35-45*
2	0.50	30
3	0.33	15
4	0.25	10
5	0.20	7.5
6	0.17	6
7	0.14	5

*Limited by critical excess temperature (see Section 2.2).

Thermal vapour recompression (TVR)

A thermal vapour recompressor is a steam jet ejector designed to increase the pressure of vacuum steam by mixing it with high pressure steam (0.5-1.2 MPa absolute). The high pressure steam passes through a sonic nozzle, converting pressure energy to kinetic energy and creating a low pressure zone into which the vacuum steam is drawn. The mixed steam goes through an expansion section, converting the kinetic energy back to pressure energy. TVR units can run with a pressure rise equivalent to 20°C in saturation temperature rise. A rise in saturation temperature of ≤12°C is normal (Gray, 1981) to ensure a reasonable suction vapour to supplied steam ratio. The introduction of TVR units improved the economy of evaporators but required high pressure steam. A TVR unit (see Figure 2.8) operating around one effect saves approximately the same amount of steam as adding one effect. TVR units can operate around up to four effects. A TVR unit also enables the amount of evaporation in effects around which thermo-compression takes place to be approximately double that occurring in each of the remaining effects. This ensures that more evaporation takes place at high boiling temperatures (and therefore with better HTCs). In addition, less evaporation occurs in the last effects which simplifies the problems associated with liquid coverage.

Mechanical vapour recompression (MVR)

A simple schematic of an MVR evaporator is shown in Figure 2.9 The principle behind MVR (and TVR) evaporators is that when steam is compressed, its saturation temperature is increased. Fans and compressors are used to compress the steam, and

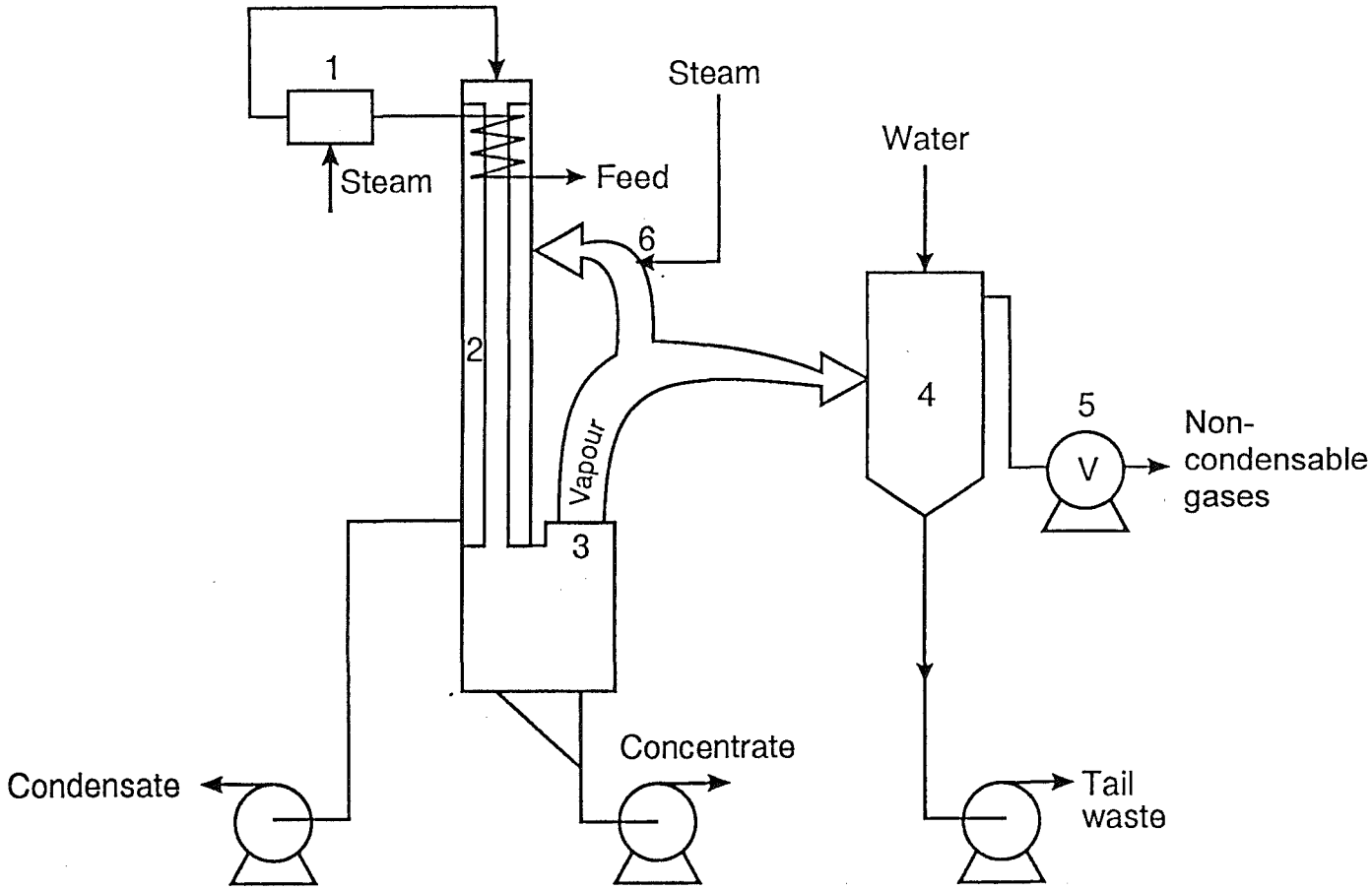

Key:

1 Preheat equipment
2 Calandria
3 Vapour-liquid separator
4 Condenser
5 Vacuum pump
6 TVR

Figure 2.8: Single Effect TVR Evaporator (Graphics by Garnett Davy, NZDRI).

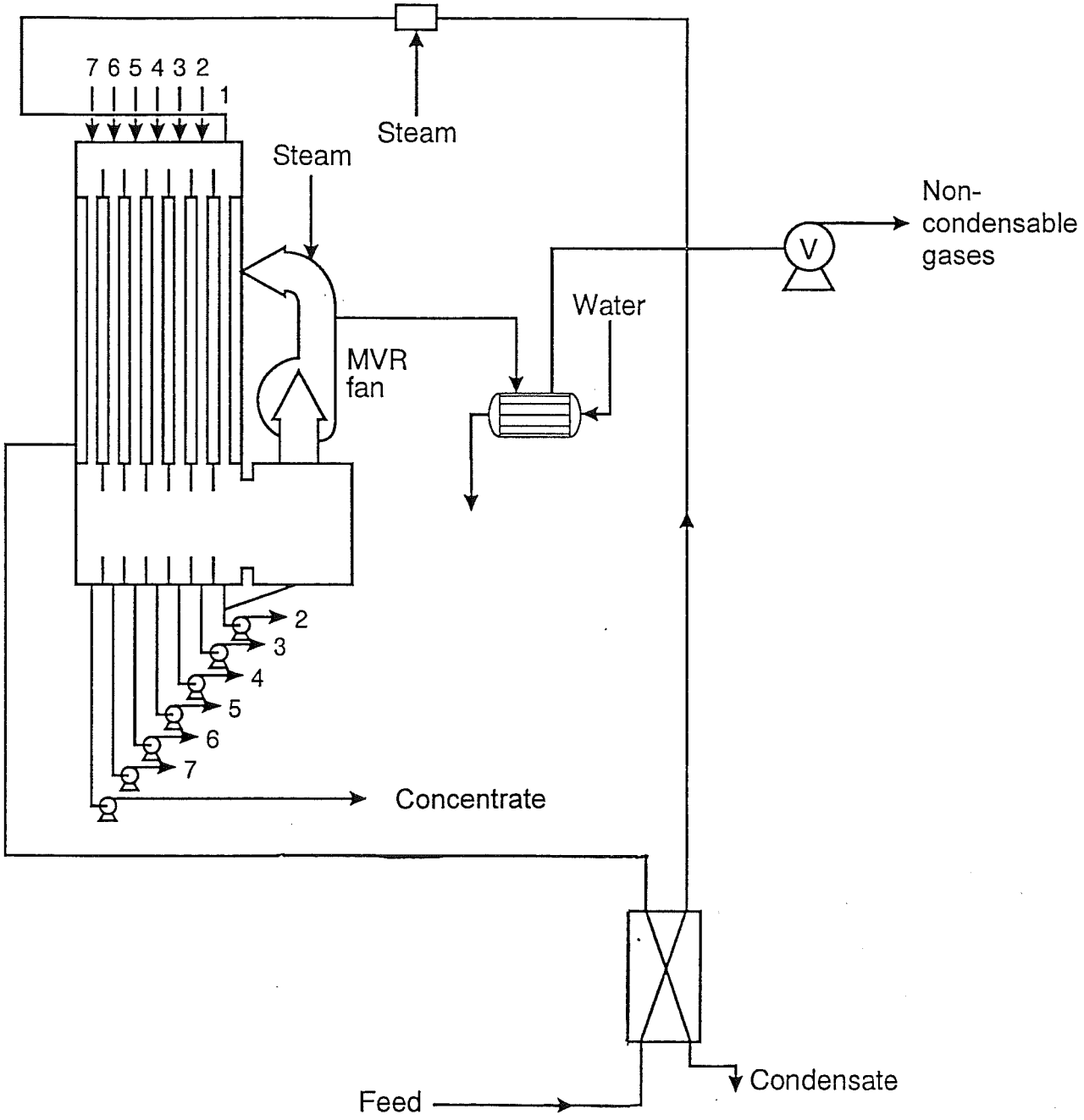

Figure 2.9: Single "Effect" MVR Evaporator (Graphics by Garnett Davy, NZDRI).

thus enable the heat in the steam to be recycled. A compressor can raise the saturation temperature of the vapour by 15-20°C and thus the heat can be recycled around three effects. Fans can raise the saturation temperature by 4-6°C and thus only operate around one effect. Fans are now the preferred option because of their simplicity in design and ease of operation and hence lower cost.

Since the late 1980's the new evaporators being installed are MVR evaporators not TVR evaporators. DSE evaporators are still installed on sites which have co-generation of electricity and steam. MVR evaporators have a number of advantages over TVR plants including;

- less energy usage and usually less energy cost,
- lower first effect boiling temperatures can be used (less product damage),
- higher final effect temperatures can be used (better heat transfer),
- no cooling water required, and,
- lower ΔT_U so less fouling.

There is an increased maintenance cost with MVR evaporators - namely a fan and motor. A major disadvantage is that because ~95% of the heat in the evaporator is being recirculated there is no convenient place to use heat flashed off the milk after preheating. This has led to a huge variety of preheat systems designed to minimise energy consumption largely at the expense of plant product mix flexibility. MVR evaporators are usually driven by variable speed electric motors and thus are sensitive to power flicks. This can lead to sudden forced shutdowns, and fouling.

Now MVR fan evaporators generally run with a 3-5°C temperature difference across the tubes. This is satisfactory for concentration up to 40-42% w/w. For the final concentration to 50% w/w a high ΔT_U is required to counteract the effects of boiling point elevation, lower thermal conductivity and high viscosity. This final concentration can be done in two ways (see Appendix A, Figures 14 and 15);

- by a TVR or DSE finisher, or,
- by using a second fan which removes vapour from a second effect and supplies it to the suction side of the main fan.

In the latter case, steam from the main fan is supplied to both calandria shell-sides. This gives a ΔT_U of 4°C in the first effect and a ΔT_U of 7°C in the second effect.

3 THIS WORK

The purpose of this work was to look at thermal and hydraulic aspects of falling film evaporation. In 1989, there was limited published information available on heat transfer coefficients for water, sucrose, skim milk and whole milk. The limited information available had been collected on short tube evaporators and often at unrealistic operating conditions. The availability of a research evaporator provided a well-instrumented plant to study heat transfer in commercially sized evaporator tubes under normal operating conditions.

The work provides a foundation for further work designed to provide an understanding of the evaporation process and tools for plant troubleshooting. There is a need to be able to modify existing plant to improve plant capacity and flexibility. Process understanding is required to enable both existing plants and new plants to successfully process commercially sensitive products without supplying details of the product to evaporator supply firms. The evaporation and spraying drying of milk are energy intensive processes. Extensive work by evaporator supply firms has minimised the energy consumption of evaporators. In some cases this has adversely affected product quality and reduced process flexibility. Evaporators need to be designed to meet product quality and process flexibility requirements while minimising energy consumption.

The plant was installed but not commissioned at the start of the PhD programme. Problems with level control and product transfer pumps prevented the use of multiple effects. The work was carried out using two of the evaporator calandrias in single effect mode. Most of the work was done on a 15 m long tube with an internal diameter of 48 mm. The other calandria had three 10 m long tubes with internal diameters of 23 mm, 40 mm and 48 mm.

The experimental programme included extensive work on water, of which a subset was repeated on sucrose solutions, and some limited work on skim milk. The objective was to investigate a wide range of variables on water, which had known properties and a constant composition over the length of the tube. Variables that were likely to be affected by changing composition over the length of the tube, were evaluated using a Newtonian single solute solution. Sucrose solutions were used because of their ready availability and because there were more physical property data available than for lactose (the milk sugar). Skim milk contains proteins, lactose, minerals and fat, varies in composition, foams and, under certain conditions, has pseudoplastic and thixotropic properties. Skim milk was used to check the applicability of models proposed from the water and sucrose work for the evaporation of milk.

The variables investigated using water were boiling temperature, temperature driving force, tube

liquid loading, degree of flash on entry (flash temperature difference), tube diameter and steam-side factors. The steam-side factors were the non-condensable gas concentration in steam, the location of de-aeration ports, and, de-aeration flow rates. Variables evaluated on sucrose solutions were feed concentration, tube liquid loading, boiling temperature, temperature driving force, degree of flash on entry, and, tube diameter. For skim milk, the effects of preheat treatment and feed concentration were investigated.

Previous models of local boiling side Nusselt number were integrated with respect to length to account for changes in liquid loading, film fluid properties and pressure drop in the vapour core. A dimensional analysis of the heat transfer process across the tube wall was also undertaken.

Several methods were considered for measuring the concentration of non-condensable gases (NCG) in evaporator liquid and vapour streams. Two methods were experimentally evaluated but were found wanting in several aspects. An analytical description of the distribution of NCG in the steam side of a single tube calandria was developed. Efforts to provide a working numerical model using the above description failed due to the use of an inappropriate technique.

PART II: APPARATUS & MATERIALS

4. THE NZDRI RESEARCH EVAPORATOR

In 1988, a research evaporator (herein after referred to as the Research Evaporator) was installed in the Process Hall of the New Zealand Dairy Research Institute (NZDRI) in Palmerston North. The Research Evaporator consists of five single effect evaporator units, each evaporator unit having its own steam supply and independent control of boiling pressure. A flow plate was installed to enable the plant to be run as a 1, 2, 3, 4, or 5 effect (or pass) evaporator. The Research Evaporator has a combined maximum evaporative capacity of 250-300 kg h^{-1}.

The evaporator design, fabrication and installation programme was run by Mr G Winter (NZDRI). The number, length and diameter of the tubes in each evaporator unit were determined in conjunction with the author, who was on secondment in the evaporator design office at APV Anhydro A/S in Copenhagen, Denmark at the time. The author took over the project during the final stages of installation and undertook the commissioning programme.

Table 4.1: Research Evaporator Tube Details

Calandria	Number of Tubes	Tube Diameter (mm)	Tube Length (m)
First	4	48	15
Second	2	48	15
Third	1	48	15
Fourth	1	40	15
Fifth	1 of 3	23 40 48	10

4.1 Calandria Design

The number and diameter of the tubes in each evaporator unit (see Table 4.1) were selected to enable the plant to mimic a five effect evaporator, with a reasonable tube liquid coverage in each effect. In this work, only the third and fifth calandrias were used as single effect evaporators. A simplified piping and instrument diagram showing just the Third and Fifth Evaporators is shown in Figure 4.1.

4.2 Feed Handling System

The 60 litre balance tank can be supplied with reticulated soft water, or gravity fed from

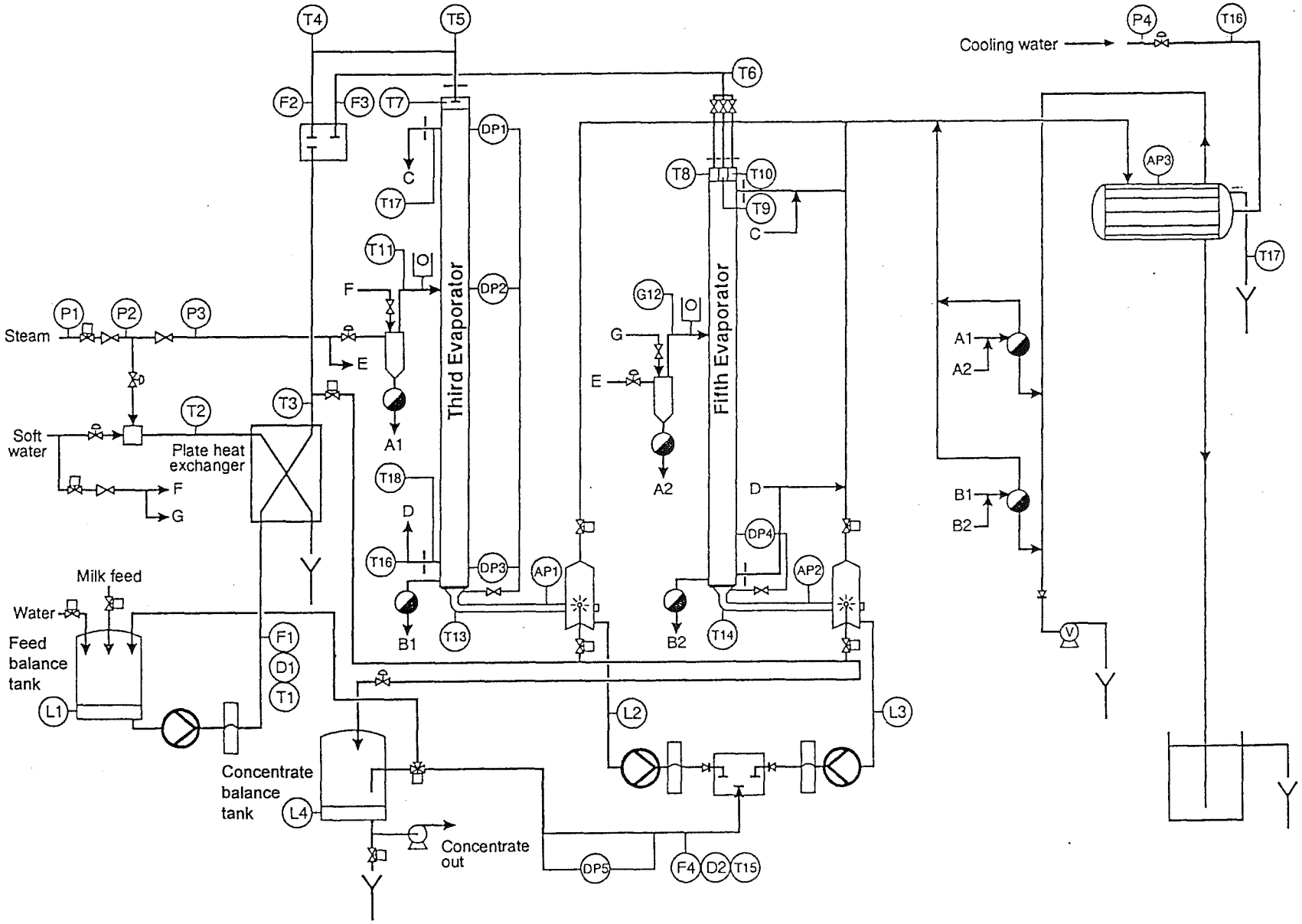

Figure 4.1: Piping and Instrument Diagram for Third and Fifth Evaporators (Graphics by Garnett Davy, NZDRI).

List of symbols for Figure 4.1

three 500 litre tanks (used for cleaning-in-place (CIP) chemicals). Milk can be pumped directly from a 20,000 litre refrigerated silo. For the skim milk trials however, the milk was gravity fed using a temporary flexible line from a 1000 litre tank.

4.3 Feed Preheat System

The preheat system consisted of a PHE (Type T4RV, Pasilac Therm A/S, Kolding, Denmark) designed to heat milk up to a maximum of 70°C. The heating water for the PHE was obtained initially by mixing cold and hot water streams. Oscillations in the temperature and supply pressure of the hot water forced the installation of a small DSI unit to heat cold water to the desired temperature. All experimental work reported here was done using the water DSI unit. The PHE was used to heat water to temperatures of up to 100°C and sucrose to temperatures in excess of 80°C. A 3 mm diameter orifice was installed in the last union before entering the calandria to ensure that no flash cooling occurred in the feed line.

4.4 Liquid Distribution

The feed entering the calandria hit a splash plate (see Figure 4.2) and flowed over onto a distributor plate which had one central vapour riser. Three small holes, equidistant on a pitch-diameter circle slightly larger than the tube, spread the liquid flow around the circumference of the tube. Vapour, flashed off on entry to the effect, travelled through the vapour riser down into the centre of the tube. The liquid stream flowed as a film down the tube, while giving off vapour by surface evaporation.

4.5 Vapour/Concentrate Separation

On leaving the calandria tube, the concentrated liquid and the vapours travelled through a short duct with a 90° bend to the vapour-liquid separator. A cyclone-type separator was used to separate the liquid from the vapour by centrifugal force. The vapours leaving the separator passed through a control valve to the surface condenser.

4.6 Product Transfer

In commercial evaporation plants, centrifugal pumps are used for product transfer. The pumps are usually run in scavenging mode, with either an orifice or a valve fitted down stream to minimise cavitation. Small single-stage centrifugal pumps do not have the head required and so positive displacement pumps had to be used on the Research Evaporator. The pumping of the feed to the evaporator and product transfer between the evaporator

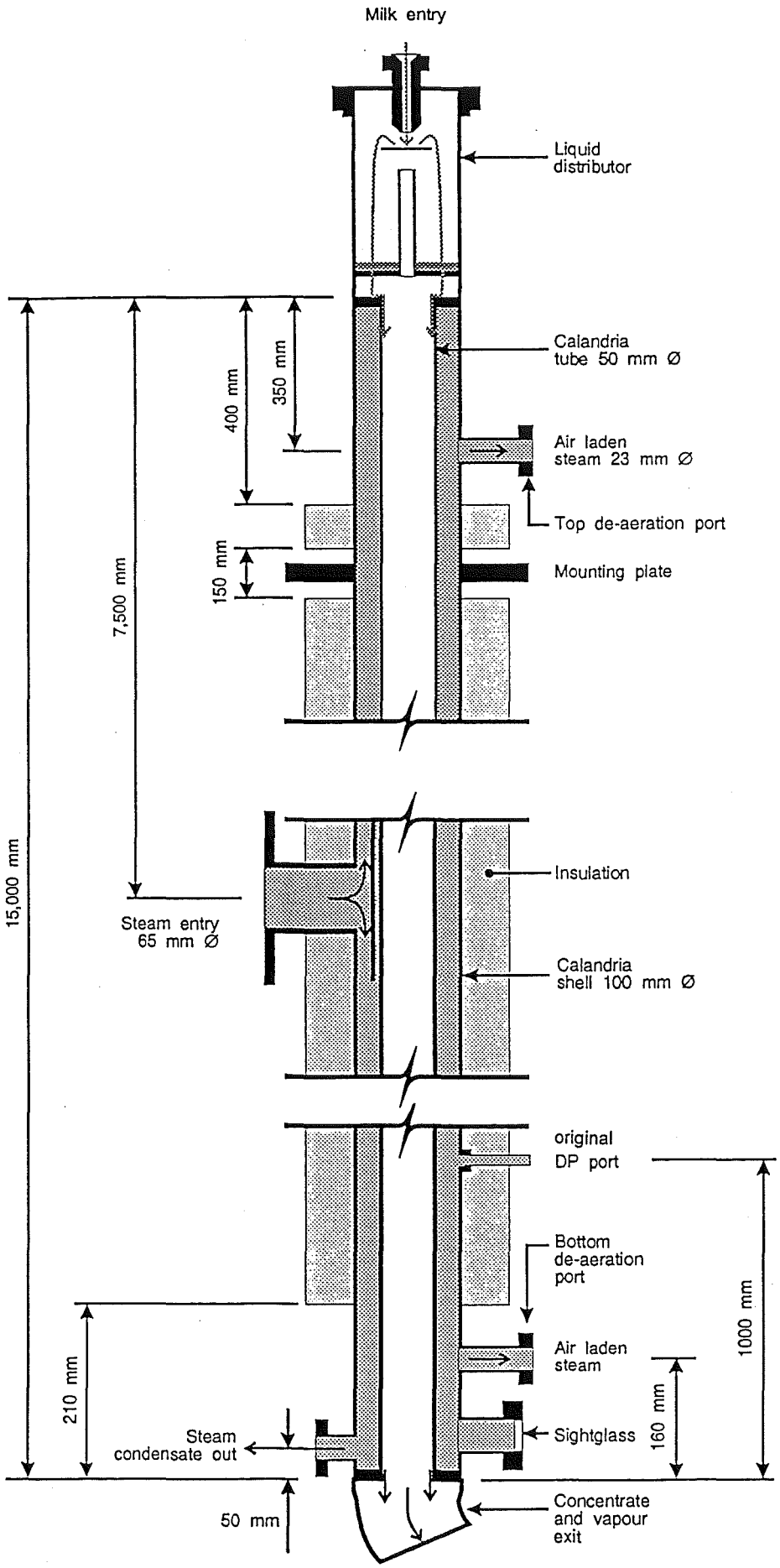

Figure 4.2: Third Evaporator Calandria Detail (Graphics by Garnett Davy, NZDRI).

units was done using rotary lobe pumps (Model SR/1/005/SS, SSP Pumps Ltd, Eastbourne, Sussex, England) with nitrile rubber rotors. Each pump was driven by a vee belt drive using an AC motor with a variable speed drive (PDL Mk II Model MD4-3.0, PDL Electronics Ltd, Napier, NZ). The product transfer pump arrangement is shown in Figure 4.3.

4.7 Calandria De-aeration and Condensate Removal

There was a de-aeration line at both the top and bottom of each calandria to remove non-condensable gases from the calandria shell. The flow through the de-aeration lines was controlled by an orifice plate.

The condensate from each calandria was extracted through a steam trap and flashed down to the condenser operating pressure. The remaining liquid was gravity fed to the vacuum pump.

4.8 Concentrate Handling

The concentrate leaving the evaporator was fed into a 60 litre concentrate balance tank. The skim milk concentrate was pumped from this tank and stored in a refrigerated vat, before collection by a local pig farmer. For CIP purposes, a line connected the ex-concentrate tank pump to the ex-silo pump so that the feed line from the milk silo could be cleaned-in-place. A drain valve was installed under the concentrate tank to dispose of rinse water and spent CIP solutions.

4.9 Condenser and Vacuum System

A surface condenser with a barometric leg was used to condense the boiled off vapour and extract the condensate. A liquid ring vacuum pump (Model LEM90, Sihi, Itzehoe, Germany) was used to extract air and other non-condensable gases from the plant.

4.10 Steam Supply

Steam was supplied at 2 bar (gauge) at the header. Soft water was sprayed into the steam through a full cone spray nozzle to remove the superheat. The location of the de-superheating nozzle for the third and fifth evaporators is shown in Figure 4.4. A small cyclone was employed to remove any excess water added during de-superheating. The excess water was flashed down to the condenser temperature and the remaining liquid was extracted by the vacuum pump. The steam entered the calandria (see

(a) For Third Evaporator

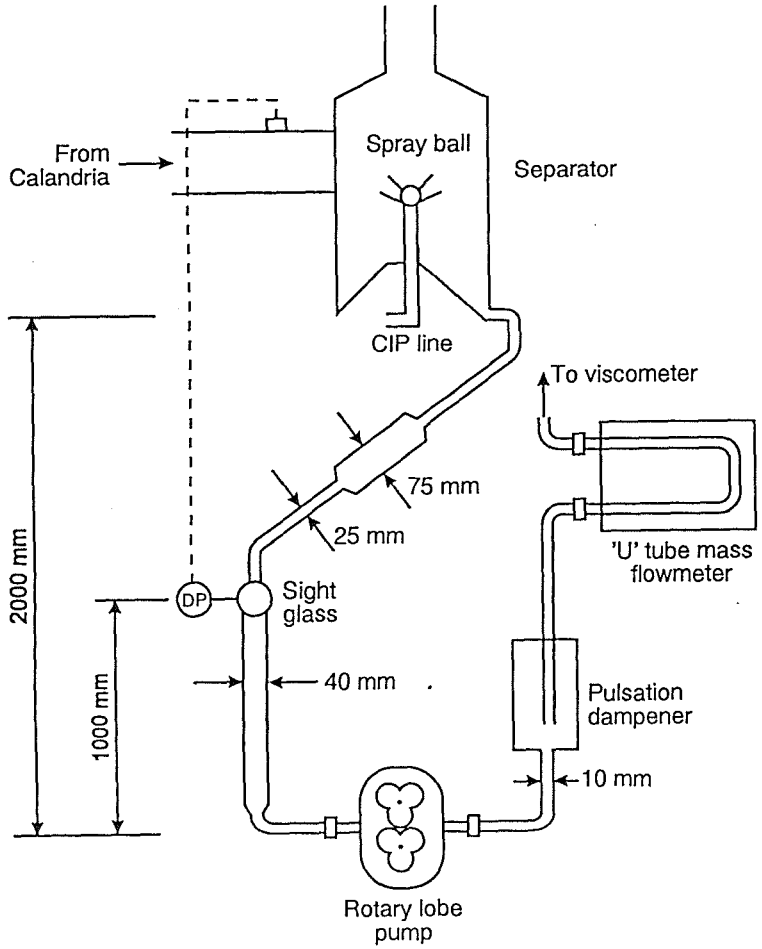

(b) For Fifth Evaporator

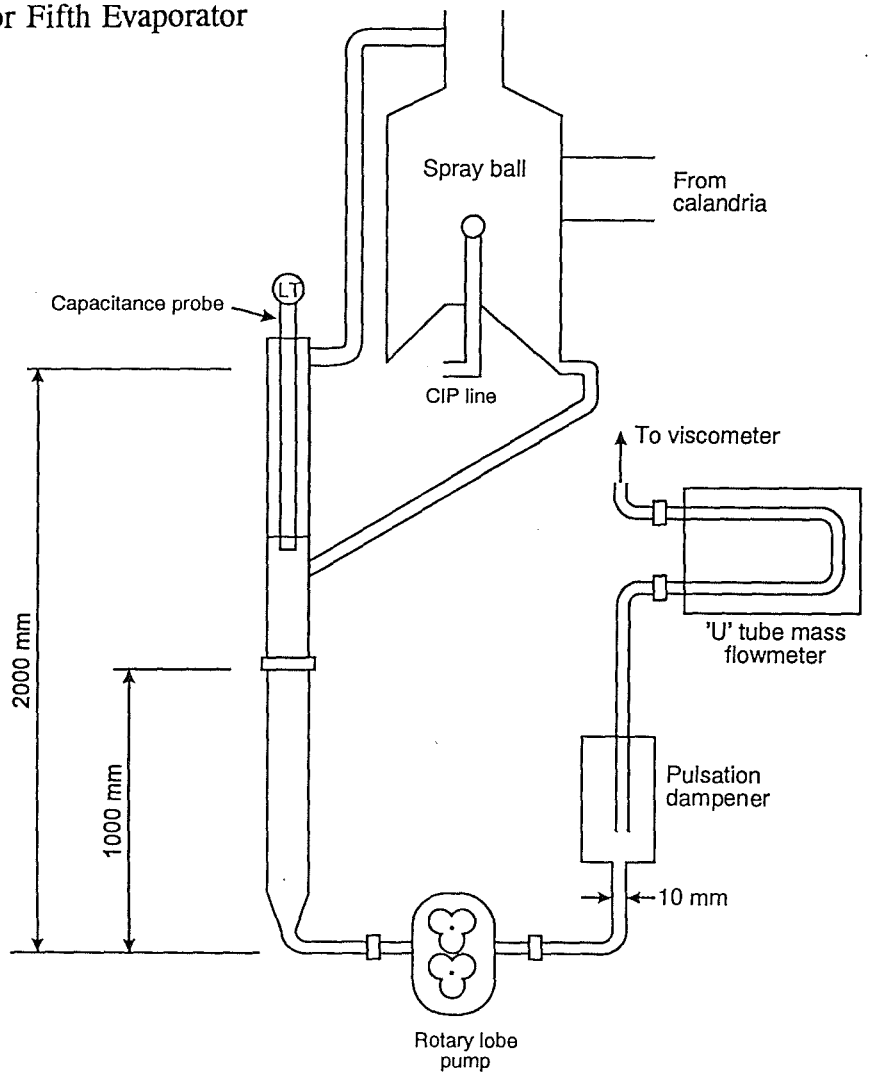

Figure 4.3: Product Transfer Pump Assembly and Suction Side Level Control (Graphics by Maria Wind, NZDRI).

(a) For Third Evaporator

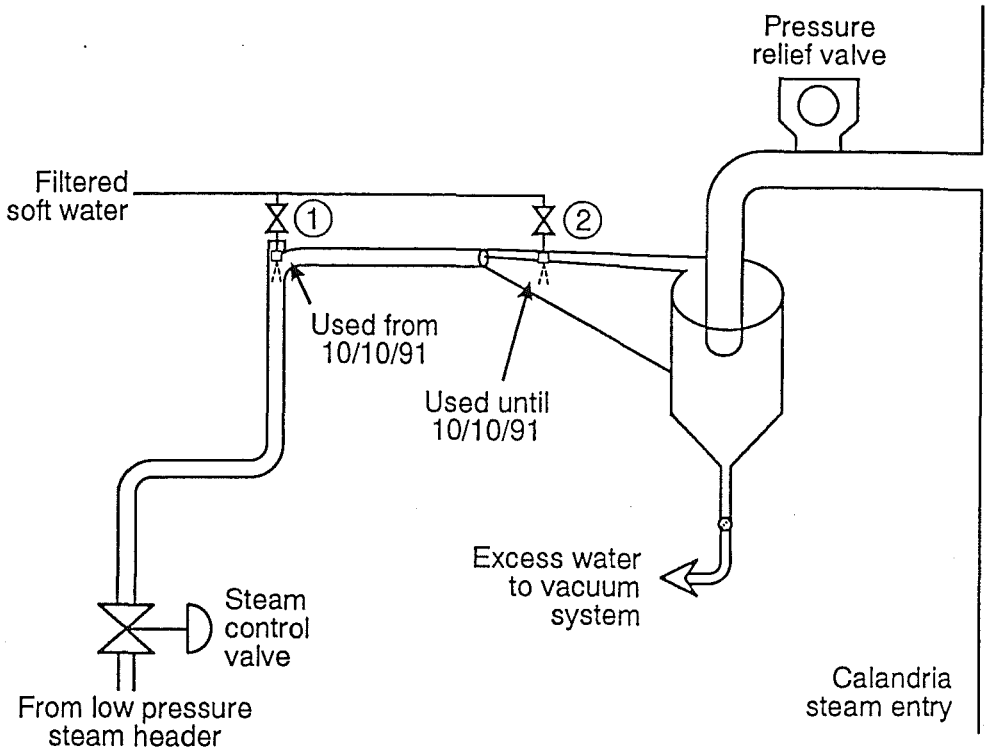

(b) For Fifth Evaporator

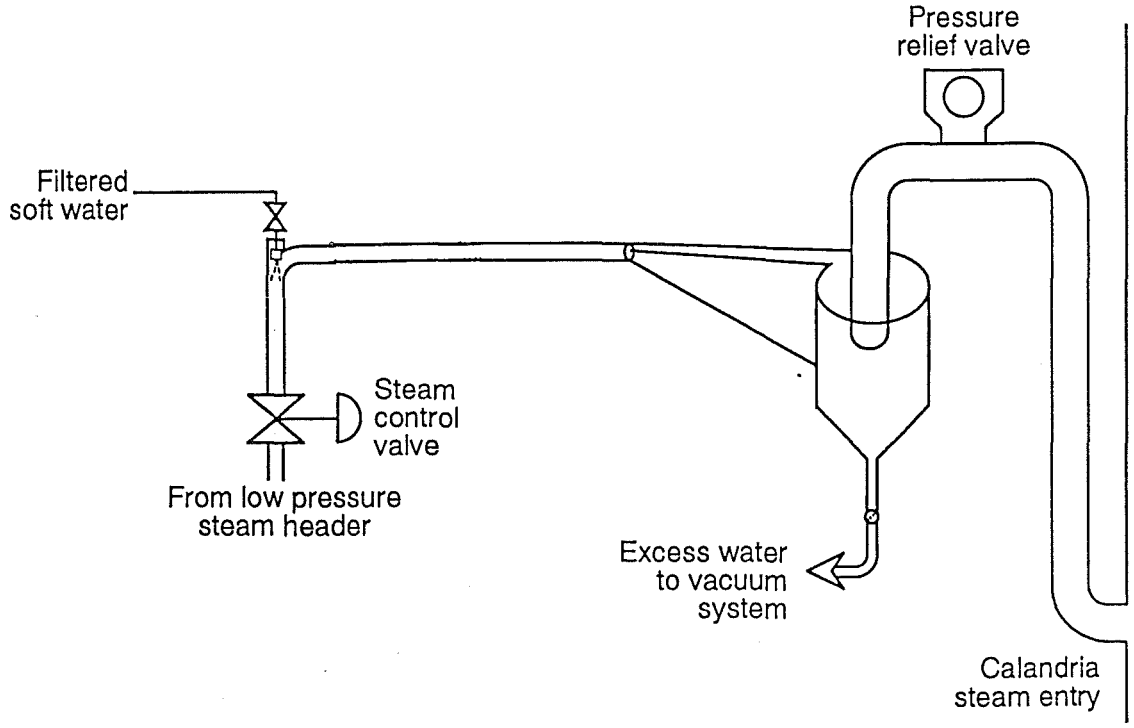

Figure 4.4: Detail of Steam Pre-conditioning for Third and Fifth Evaporators (Graphics by Maria Wind, NZDRI).

Figure 4.2) at the mid point. A deflector plate was installed at the entrance to prevent any solid or liquid material impinging onto the tube(s).

4.11 Evaporator CIP System

Spray balls were installed in each of the separators. While the CIP fluids are circulating through the plant, fluid was delivered in short pulses to the spray balls to clean the internal surfaces of the separators and connecting ducts.

4.12 Third Evaporator Experimental Set Up

The majority of the experimental work was done using the Third Evaporator as a single effect evaporator. Dimensions of the calandria are shown in Figure 4.2. The non-condensable gas experiments were done on the Third Evaporator because it had a single tube of commercial diameter. The single tube made the steam side flow patterns easier to model. The modifications made for the experiment are listed below.

Air bleed nozzle

A small line complete with ball valve (4 mm bore) and nozzle holder was connected onto the steam supply line just before the separator (see Figure 4.5). By fitting the appropriate nozzle (Unijet Solid Stream Tip Series, Spraying Systems Co, Wheaton, Illinois, USA) in the nozzle holder and opening the valve, a known flow rate of air was bled into the steam.

De-aeration line modifications

The de-aeration lines were modified to include a nozzle holder in place of the orifice plate and to enable samples of steam/non-condensable gas mixture to be extracted for measurement purposes (see Chapter 7).

Differential pressure measurement

Three transmitters were installed temporarily on the Third Evaporator to measure the differential pressure between three locations (steam entry, top and bottom de-aeration ports) on the steam side of the calandria and the calandria-separator connecting duct on the boiling side.

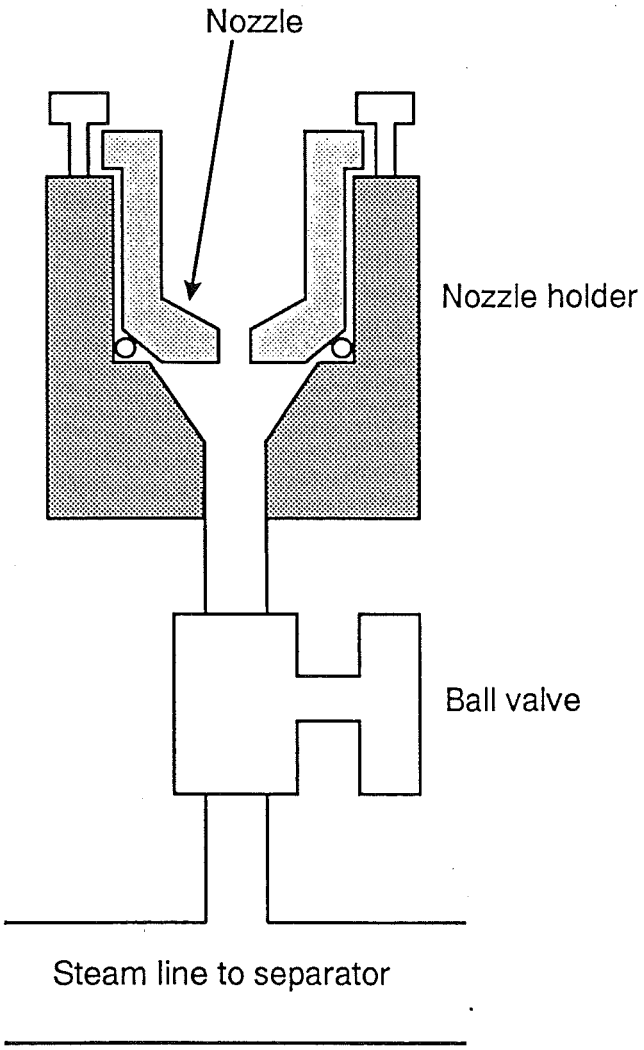

Figure 4.5: Air Bleed Nozzle Assembly Detail (Graphics by Maria Wind, NZDRI).

Temperature measurement

Probes were installed to measure the condensate temperature and the temperature of the top and bottom de-aeration entry sections (see Section 5.1).

4.13 Fifth Evaporator Experimental Set Up

The remainder of the experimental work was done using the Fifth Evaporator as a single effect evaporator. Dimensions of the calandria are shown in Figure 4.6. The modifications made for the experiments are listed below.

Absolute pressure measurement

The Third Evaporator AP sensor was attached to the old sanitary DP low pressure connection port on the Fifth Evaporator calandria-separator connecting duct to check the reliability of the Fifth Evaporator AP sensor.

De-superheat water addition

The nozzle size for the de-superheating water spray was increased during the water trials (see Section 13.9).

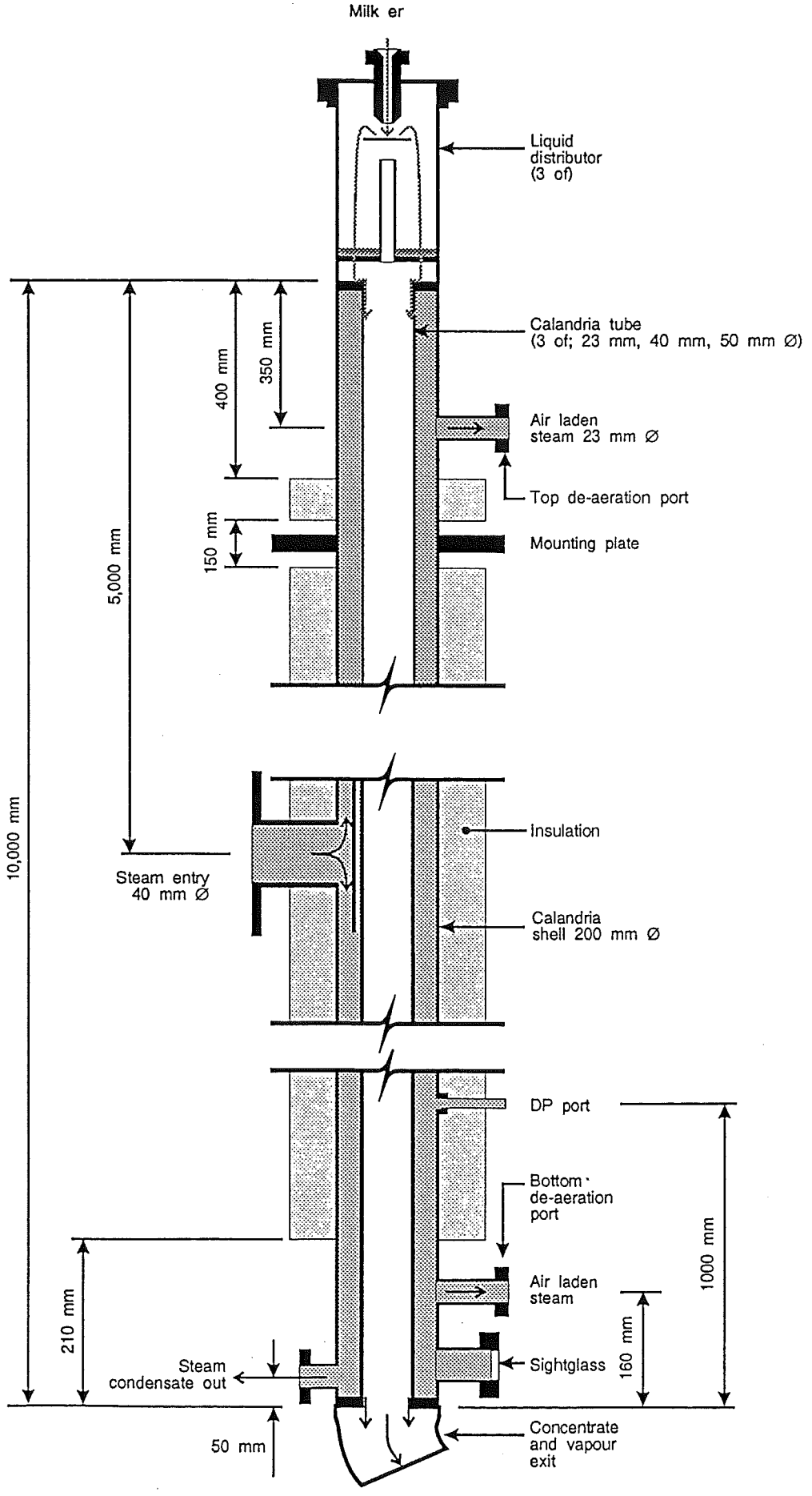

Figure 4.6: Fifth Evaporator Calandria Detail (Graphics by Garnett Davy, NZDRI).

5 INSTRUMENTATION

A piping and instrument diagram showing the set up of the Third and Fifth Evaporators is shown in Figure 4.1. The calibration procedures used, for all relevant instruments, are detailed in Appendix B.

5.1 Temperature

There were three types of platinum resistance bulb sensors used, two surface and one insert sensor. The first type of surface sensors used were Degussa platinum resistance elements (Type GR2101 Pt100, Degussa AG, Hanau, Germany) mounted in silicon epoxy as shown in Figure 5.1a. These proved difficult to calibrate and were prone to mechanical failure. For the trial work reported here they were used only for non-critical measurements. The second type of surface sensors employed for critical temperatures were Minco 3-wire, strip sensing thermal ribbons (Type 536PD10236A, Minco Products Inc, Minneapolis, Minnesota, USA) and mounted as shown in Figure 5.1b. A standard platinum resistance sensor (Therafilm 100 P30 100Ω, Matthey, Stoke-on-Trent, England) mounted in a socket was used to measure temperatures where a probe could be inserted into the line or vessel (see Figure 5.1c). Three types of temperature transmitters (Analog Devices TRD 2 wire 0-100°C, Norwood, Massachusetts, USA; Servotech R11 3-wire, 0-150°C, Auckland, New Zealand; INOR 3-wire, 0-150°C, Malmo, Sweden) were used to convert the resistance to a 4-20 mA signal. The type of sensor and transmitter used for each temperature measurement is listed in Table 5.1.

5.2 Pressure & Level

Pressure and level measurement was done using Rosemount (Rosemount Inc, Minneapolis, Minnesota, USA) instruments. The type, range and special features of each pressure sensor are shown in Table 5.2.

5.3 Flow

The feed flow rate was measured using a D25 (Micromotion Inc, Boulder, Colorado, USA) Coriolis force "U" tube mass flow meter (F1) and by a Micromotion D12 mass flow meter (F2 or F3). The concentrate flow rate was measured using a Micromotion D12 mass flow meter (F4).

(a) Degussa sensor mounting

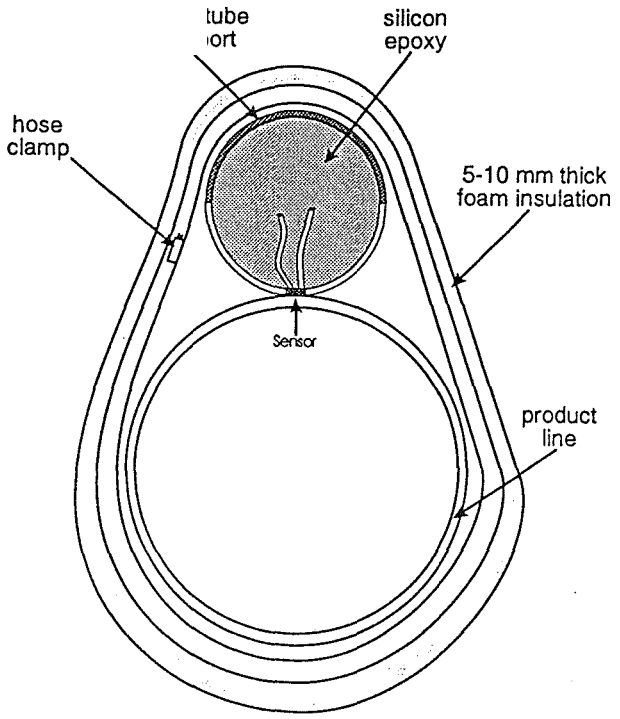

(b) Minco sensor mounting

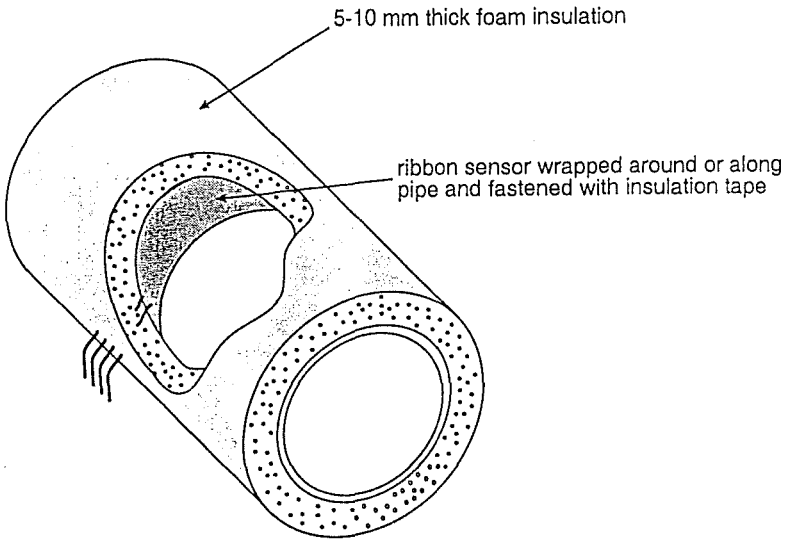

(c) Thermafilm sensor housing

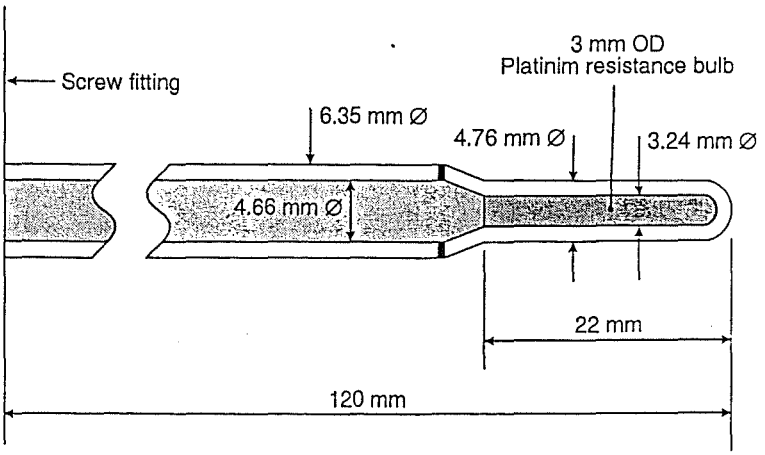

Figure 5.1: Temperature Probe Mounting (Graphics by Garnett Davy and Maria Wind, NZDRI).

Table 5.1 : Details of Temperature Probes & Transmitters

Point of Temperature Measurement[1]	Probe Type	Transmitter Type
Feed ex-balance tank[2] (T1)	Micromotion	Micromotion
PHE water supply (T2)	Thermafilm	Analog Devices
Feed ex-PHE (T3)	Degussa	Analog Devices
Feed at 3 m from top of Third Evaporator (T4), Fifth Evaporator feed at 0.3 m from top (T6)	Minco	INOR
Feed at 0.3 m from top of Third Evaporator (T5)	Minco	ServoTech
Vapour in liquid distributor (T7, T8, T9, T10)	Thermafilm	Analog Devices
Product until 26 August 1991 (T13, T14)	Degussa	Analog Devices
Product after 26 August 1991 (T13, T14)	Minco	Analog Devices
Concentrate[2] (T15)	Micromotion	Micromotion
Steam entry until 26 August 1991 (T11, T12)	Degussa	Analog Devices
Steam entry after 27 August 1991 (T11, T12)	Minco	Analog Devices
Condensate exit (T16)	Minco	Analog Devices
Top de-aeration line entry (T17)	Minco	Analog Devices
Bottom de-aeration line entry (T18)	Minco	Analog Devices
Ambient at top of third calandria	Thermafilm	Analog Devices
Ambient at middle of third calandria	Degussa	Analog Devices
Ambient at bottom of third calandria	Degussa	Analog Devices

[1]Instrument labels from Figure 4.1 are shown in brackets.

[2]Integral part of Micromotion mass flow meter. Probe actually measures temperature of U tube in the Micromotion flow meter.

Table 5.2: Pressure and Level Measurement Details

Pressure Measurement	Rosemount Model	Range	Special Features
Feed balance tank level (L1)	1151GP3E22B1	0-20 kPa	Level sanitary seal
Boiling-side (AP1, AP2)	1151AP5E22S1B1	0-110 kPa	Remote sanitary seal
Difference between steam and boiling side[2] (DP1, DP2, DP3, DP4)	1151DP4E22B1	0-20 kPa	
Pump suction-side level[1] (L2, L3)	1151DP4E22S1B1	0-15 kPa	Level sanitary seal (HP) and remote seal (LP)
Viscometer (DP5)	1151DP5E22S2	0-100 kPa	Remote sanitary seals
Concentrate tank level (L4)	1151GP4E22B1	6 kPa	Level sanitary seal
Cooling water supply (P4)	1151GP7E22B1	0-1600 kPa	
Steam mains pressure (P1)	1151GP7E22B1	0-1600 kPa	
Steam pressure ex regulator (P2) or Steam header pressure (P3)	1151GP7E22B1	0-1600 kPa	
Condenser shell-side (AP3)	1151AP5E22B1	0-187 kPa	

1 For Experiments Wa1-Wa4 on the Third Evaporator and all Fifth Evaporator Experiments, a capacitance probe (Vega 22.02, Instrumatics, Auckland, New Zealand) was used to measure the suction side level.

2 For Experiments Wa1-Wa4 a single 1151DP4E22S1 transmitter was used (instead of DP1-3) with a non-sanitary HP connection to the steam-side (1 m above bottom of tube) and a sanitary LP fitting attached to the vapour duct between the calandria and separator.

5.4 Density

The two meters (Model DMS-2-NA-1-C-S, Micromotion Inc., Boulder, Colorado, USA) were sensitive to temperature changes and, in the case of the concentrate density meter, flow rate. The output from the feed density has been corrected to account for the temperature effect (see Appendix B). The output from the concentrate density meter was not used due to its extremely non-linear nature.

5.5 Viscosity

The detailed design of the capillary viscometer is shown in Figure 5.2. The differential pressure sensor details can be found in Table 5.2.

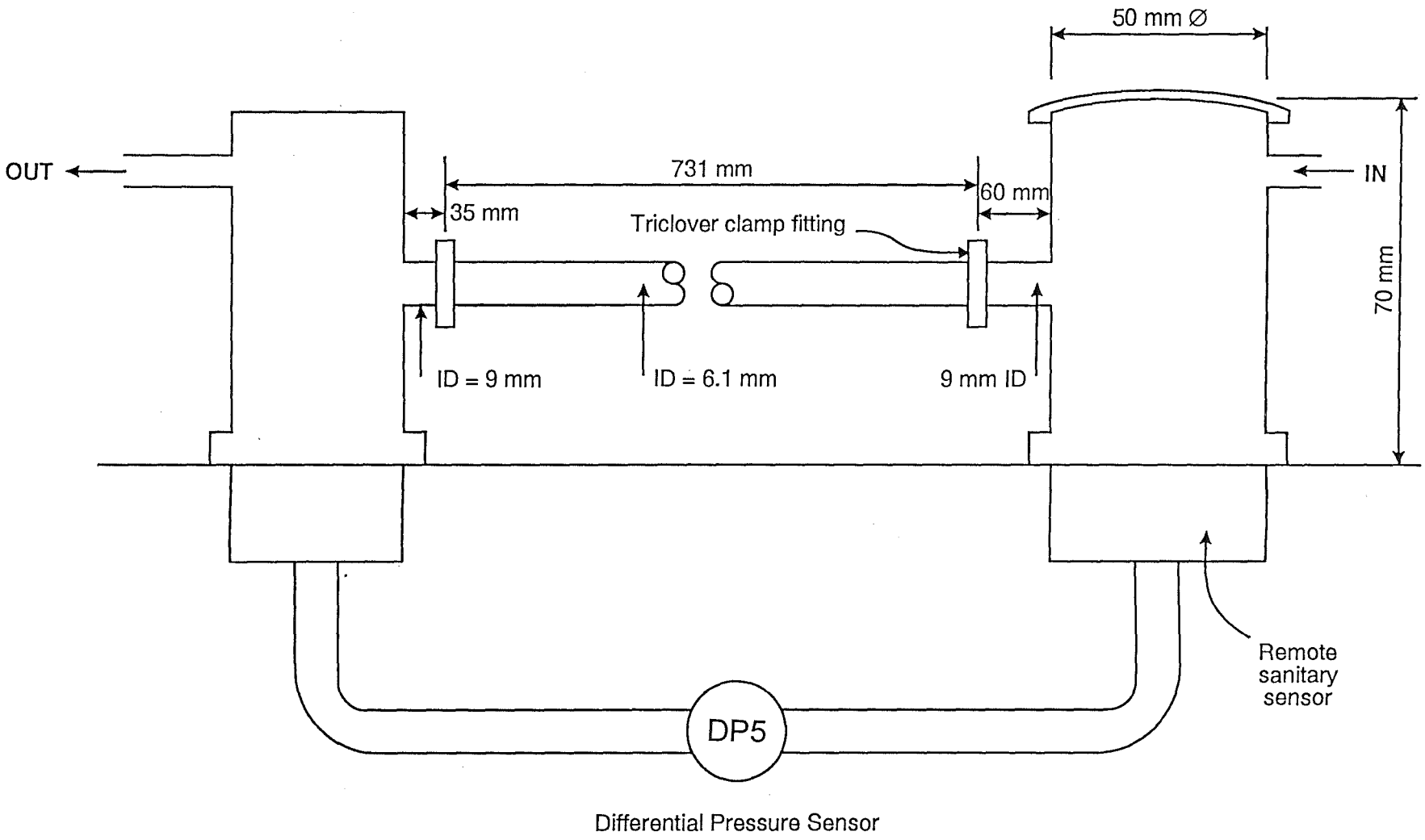

Figure 5.2: Viscometer Detail (Graphics by Maria Wind, NZDRI).

6 PROCESS CONTROL AND DATA LOGGING

6.1 Control System

The introduction to the Research Evaporator Control System Operation Manual (Janssen, 1989) states:

> "The evaporator control system consists of two interconnecting computers, one of which provides the operator interface and the other the measurement and control operations.
>
> The operator interface is an IBM PS2/80 with a 70 Mbyte hard disk and printer. It uses the DOS operating system and is programmed in Turbo Pascal. Its functions include all interaction with the operator, real-time data display, maintenance of configuration databases, and historical data storage and retrieval.
>
> The control computer is a Macsym 320 which consists of an HP CS Vectra personal computer linked to a Macsym 200 interface unit. This machine uses the CCPM operating system and is programmed in a multi-tasking version of the BASIC language called MacBasic. Its responsibility includes all input/output and control.
>
> The two computers are linked by a RS232 serial communications line operating at 19200 baud. This is used to down-load the control configuration from the operator interface to the control computer and to send real-time data back to the operator interface for display and storage.
>
> Once down-loading of the control configuration is complete, the control computer can operate independently of the operator interface. Similarly, the operator interface can be used for the development of control configurations without the control computer operating."

Examples of the operator interface displays are shown in Figure 6.1.

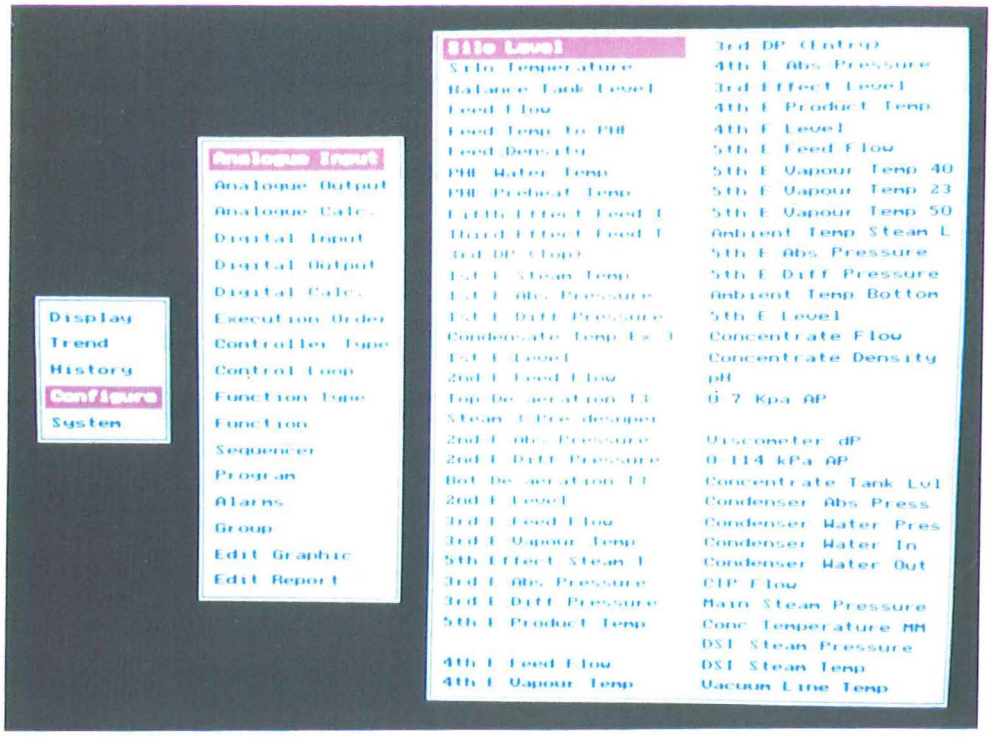

(a) Menu

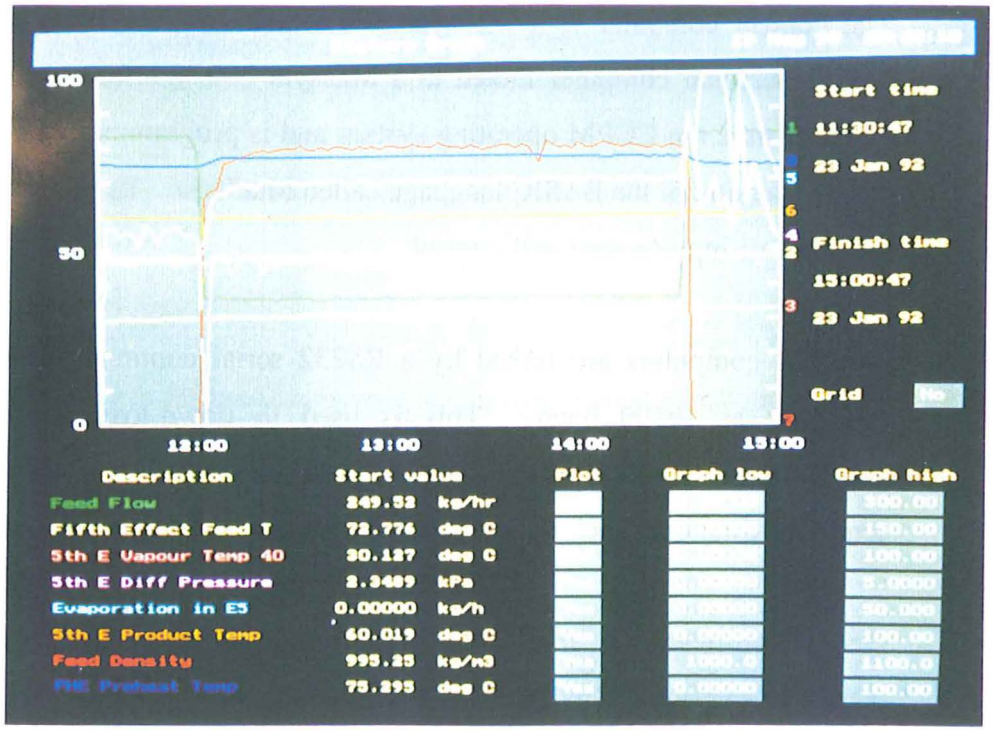

(b) Historical graph page

Figure 6.1: Examples of Operator Interface Displays (Photos by Paul Le Ceve, NZDRI).

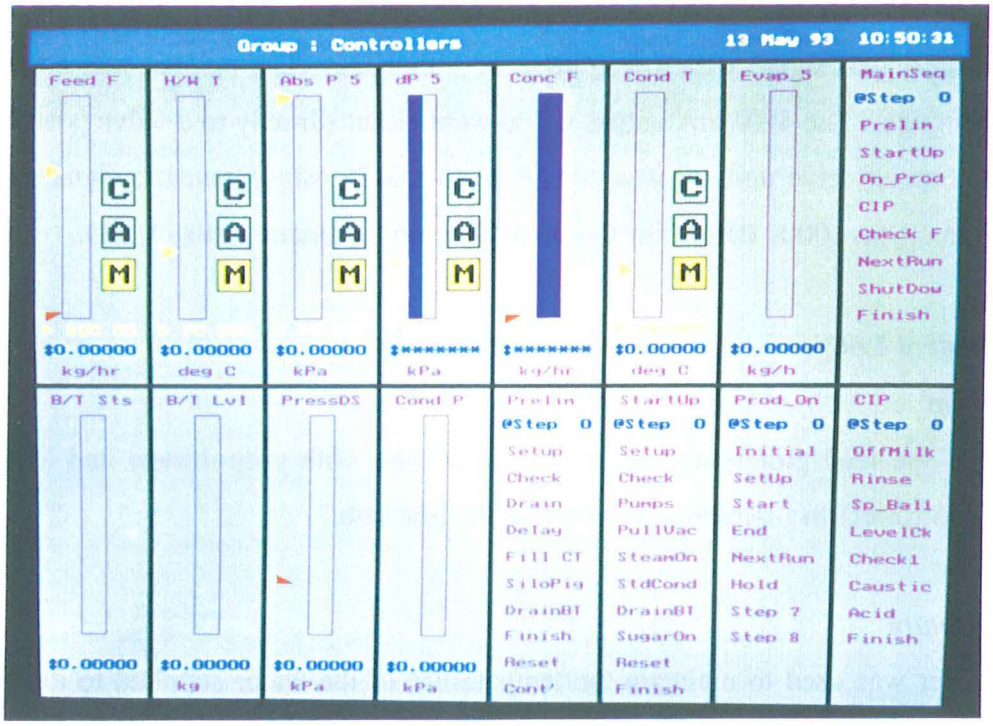

(c) Controller group page

(d) Sequencer configuration page

Figure 6.1 continued.

6.2 Analog Inputs and Outputs

All analog inputs coming in from the plant were 4-20 mA signals, and these were converted to a digital signal with a resolution of 1 in 1024. The reverse was done for the analog outputs. The 4-20 mA output signal went either directly to a valve positioner or a variable speed drive unit, or was converted to a 3-15 psig pneumatic signal by an I/P converter (Type 1000, Bellofram Corp, Burlington, Massachusetts, USA).

6.3 Process Control Loops

Feed flow rate

The speed of the feed pump was varied by a controller with proportional and integral action (PI controller) to maintain a constant feed flow rate.

Feed temperature

A PI controller was used to maintain the temperature of the water supplied to the PHE by adjusting a valve (Fisher ½" GS globe valve with a linear flow characteristic and a 513R actuator and a 3661 positioner, Fisher Controls International Inc., Marshalltown, Iowa, USA) in the steam line to the water DSI unit. The set point for this controller was adjusted to maintain the desired feed temperature as follows:

<u>For Third Evaporator</u>

The set point of the controller was determined from the sum of the following:

- the feed temperature set point
- 1.12 times the 100 second weighted average of the difference between the feed temperature ex-PHE[1] and the feed temperature at 3 m below the calandria top
- a 5 minute filtered average of the difference between the PHE hot water supply temperature and the feed temperature ex-PHE.

<u>For Fifth Evaporator</u>

The set point of the controller was determined from the sum of the following:

- the feed temperature set point
- the 100 second weighted average of the difference between the feed temperature ex-PHE and the feed temperature at the calandria top
- a 5 minute filtered average of the difference between the PHE hot water supply temperature and the feed temperature ex-PHE.

---

[1] The temperature ex-PHE was modified by dead-time and lead/lag functions to ensure that the temperatures being compared were of approximately the same fluid.

```
!Example of Procedure Code
!          Written by A R Mackereth, 11 May 1993
!
Equivalent  !This section defines words used in the code
            !to make the code easier to read.
! Balance tank level control stati
  "B/T none" = "0", "B/T off" = "1", "B/T water" = "2",
  "B/T Ex Vat 1" = "3"
! General definitions
  "set " = "", "switch " = "","  to" = ":=", " is" = "="
  "true" = "1", "false" = "0", " on" = "1", " off" = "0"
!************************************************************
Procedure Balance_Tank_Level
!  Actioned in Block No. 2 currently every 5 s.
     Case 'B/T Sts'
     Of B/T none
!
     Of B/T off
          CIP_Tank_Valves_Off  !Calls another procedure
          Switch 'Feed V' to off
          Switch 'Water V' to off
          Switch 'SiloPmp' to off
!
     Of B/T water
          CIP_Tank_Valves_Off
                 Switch 'SiloPmp' to off
                 Switch 'Feed V' to off
          If 'B/T Lvl' < 2.0 Then
                     Switch 'Water V' to on
                     Switch 'CIP B/T' to off !Opens valve
          Else
                     If 'B/T Lvl' > 5.0 Then
               Switch 'Water V' to off
               Switch 'CIP B/T' to on !Closes valve
                  Endif
          EndIf
!
     Of B/T Ex Vat 1 !This was used for the skim trial
          CIP_Tank_Valves_Off
          Switch 'Water V' to off
          Switch 'CIP B/T' to on !Closes valve
          If 'B/T Lvl' < 5.0 then
               Switch 'Feed V' to on
               If 'B/T Lvl' < 0.5 then
                Set 'B/T Sts' to B/T Water
                Ring_Operator  !Calls another procedure
                Endif
          Else
               If 'B/T Lvl' > 10.0 Then
               Switch 'Feed V' to off
               Endif
          Endif
!    Other cases were removed to keep this on one page
     EndCase
```

Figure 6.2: Example of Procedure Code.

Product transfer suction side level control

The signal from the level sensor was scaled to 0-100% and fed directly to the pump speed control. Thus the control action was proportional only with respect to level. However, because the level measurement is the integral of the concentrate flow rate, the control action was essentially integral only with respect to flow rate.

Boiling side absolute pressure

A PI controller was used to adjust a valve mounted in the separator vapour exhaust duct to maintain the required absolute pressure. The valve details are as follows:

Third Evaporator

Fisher 1½" GS globe valve with 667 actuator and 3661 positioner

Fifth Evaporator

Foxboro V250UE globe valve with P25 actuator (Foxboro Proprietary Ltd., Lilydale, Victoria, Australia)

Differential pressure

The steam flow to each calandria is regulated by a control valve with a linear flow characteristic (Fisher ½" GS globe valve with 513R actuator and 3661 positioner). The sonic flow through the valve ensured the steam mass flow rate was proportional to the valve position. When differential pressure control was required, a PI controller was used to adjust the steam valve.

Condenser cooling water exit temperature

A PI controller was used to maintain the temperature of the cooling water leaving the surface condenser at 25°C by adjusting a valve (Fisher 1" GS globe valve with GS513R actuator) mounted in the supply line.

6.4 Sequencers & Procedures

The plant was automatically run using a series of sequences. One main sequence called a range of sequences to undertake preliminary checks, start the plant up, set up and run at each experimental condition, CIP the plant and shutdown the plant. An example of part of a sequence can be see in Figure 6.1d. The sequences call procedures which were written in simple English-like code and are compiled by a single pass compiler. An example of the code is given in Figure 6.2.

6.5 Data Logging

All inputs, outputs, calculated variables, controller set-points were read every 10 s and every minute the average of the six readings during that minute was saved to disk. In addition, operator changes, alarms and event messages were also saved to disk.

7 NON-CONDENSABLE GAS MEASUREMENT APPARATUS

7.1 General Functional Specification

The apparatus was designed to do the following:

In-line measurement of non-condensable gas (NCG) concentration

(1) Measure the temperature of a saturated steam / NCG mixture flowing through a process line.

(2) Measure the pressure of a saturated steam / NCG mixture flowing through a process line.

Residual pressure measurement to determine NCG concentration (check on in-line measurement)

(3) Extract a known volume of steam (which may containing NCG) from a process line. Condensation during sampling must be prevented.

(4) Measure the pressure of the extracted sample during sampling and immediately after extraction.

(5) Condense the water vapour by reducing the temperature of the sample to below 0°C.

(6) Measure the residual pressure, which should be equal to the partial pressure of the NCG (plus known water vapour pressure).

GC analysis of extracted sample to determine composition

(7) Add helium to the extracted sample to bring the pressure up to above atmospheric pressure. Measure final pressure.

(8) Extract a small sample of the gas and put into a GC column to analyze for N_2, O_2 and CO_2.

7.2 Non-condensable Gas Apparatus Description

The NCG apparatus is shown in Figure 7.1, and a piping and instrument diagram in Figure 7.2. The location of the apparatus with respect to the plant de-aeration lines both at the top and bottom of the calandria is shown in Figure 7.3. The extra instrumentation installed on the Third Evaporator calandria for the NCG experiments is covered in Section 4.12.

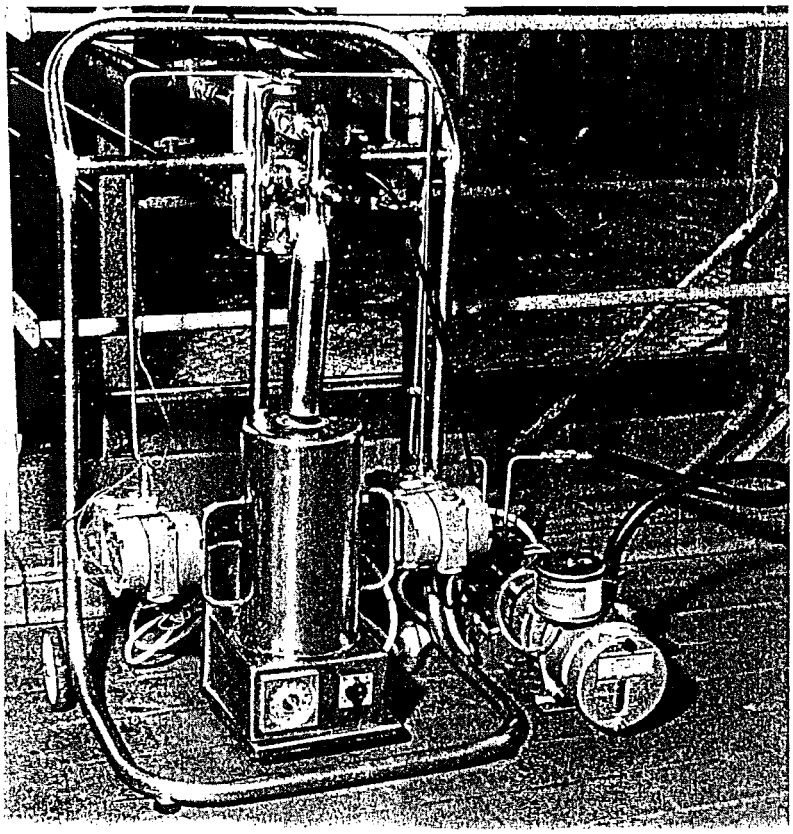

(a) Non-condensable gas apparatus

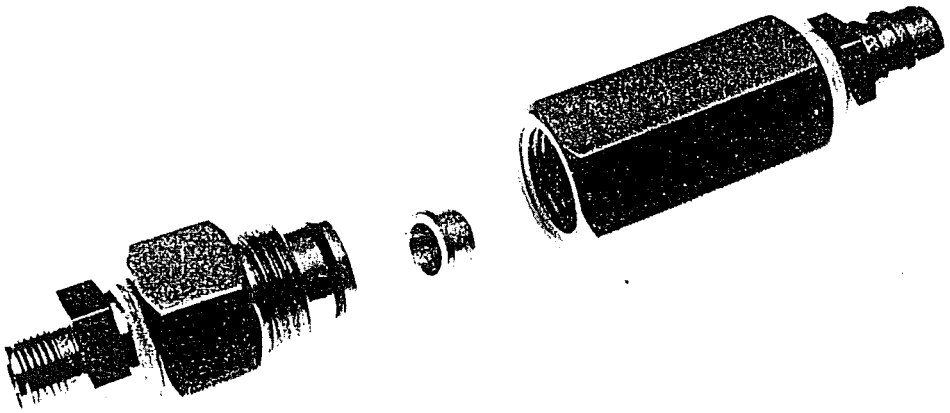

(b) De-aeration nozzle assembly

Figure 7.1: NCG Apparatus and De-aeration Nozzle Assembly (Photos by Paul Le Ceve, NZDRI).

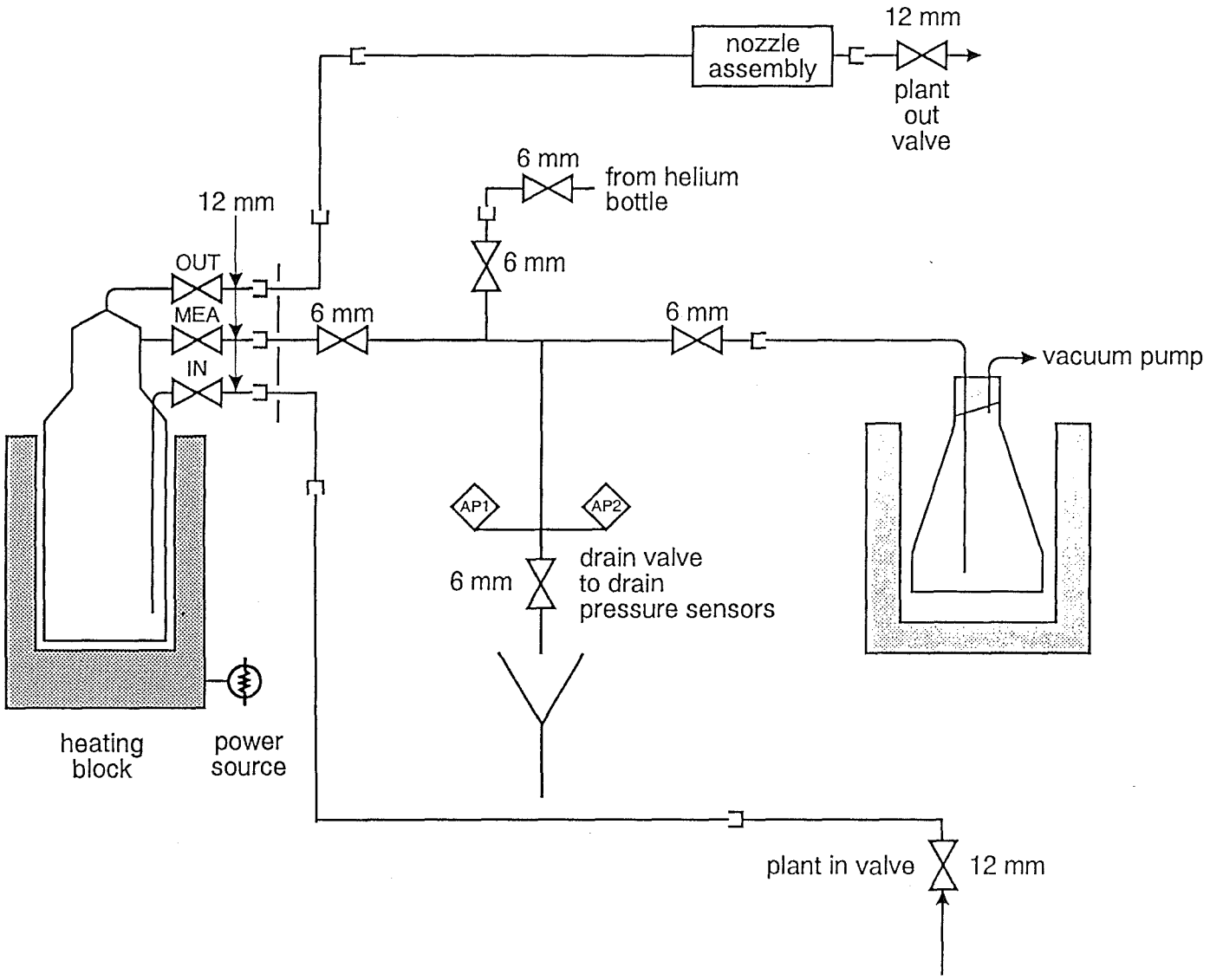

Figure 7.2: Non-condensable Gas Apparatus Piping and Instrument Diagram (Graphics by Maria Wind, NZDRI)

(a) At top of calandria

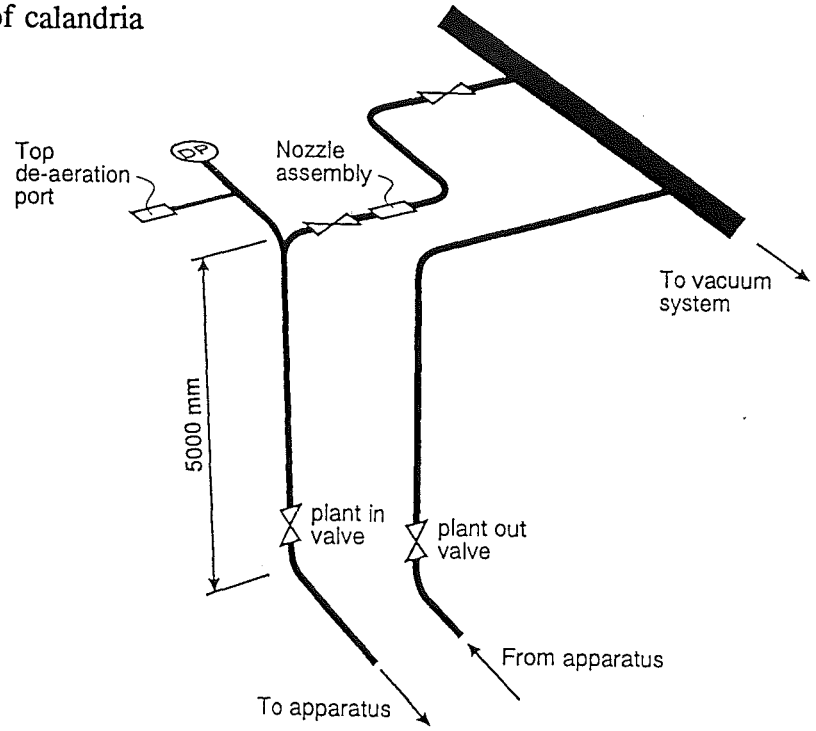

(b) At bottom of calandria

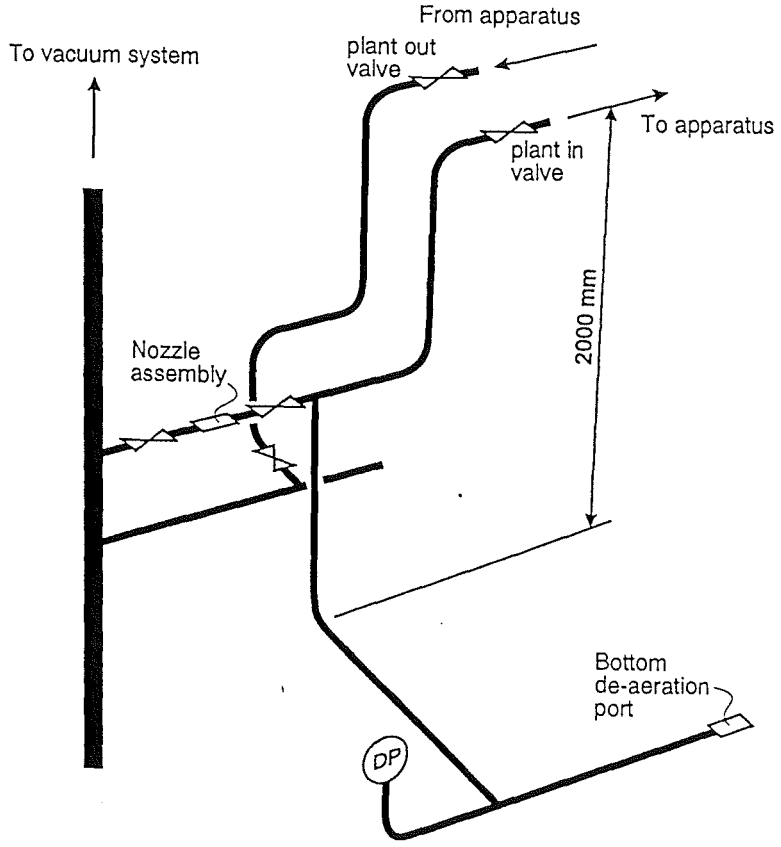

Figure 7.3: Physical Location of NCG Apparatus with Respect to Third Evaporator (Graphics by Garnett Davy, NZDRI).

7.3 List of Components

The components were as follows:

For Section 7.1 Item (1)

(a) A surface mounted platinum resistance bulb was mounted on each of the de-aeration lines prior to the sonic nozzle.

(b) For each de-aeration line, the standard orifice plate was removed and replaced by a nozzle assembly (see Figure 7.1b).

For Section 7.1 Item (2)

(c) Differential pressure transmitters were mounted on the Third Evaporator de-aeration line entry sections.

For Section 7.1 Items (3), (4), (5), (6) and (7)

(d) One process line was welded to each of the de-aeration lines upstream of the sonic nozzle, with shut-off ball valve and Quick Connect full flow female fitting (Swagelock Co, Solon, Ohio, USA) .

(e) Tubing with one male and one female Quick Connect full flow fittings to connect items (d) with item (g), and item (g) with items (f).

(f) Process line welded onto top or side of line to research evaporator's condenser with shut-off ball valve and Quick Connect full flow female fitting. One was required at tower roof level and one at the bottom of the calandria.

(g) A vessel (see Figure 7.1) with three process line connections with shut off valves and female Quick Connect fittings. The vessel had a septum port with a vacuum tight cap. The vessel was designed as a flow-through cell but with all fittings at top to allow immersion.

(h) A vacuum pump (SpeedVac2, Edwards High Vacuum, Crawley, England) which was capable of drawing down to 0.013 kPa absolute.

(i) A pressure transmitter (Rosemount 1151AP4E22B1, Rosemount Inc., Eden Prairie, Minnesota, USA) ranged at 0-7 kPa absolute with an accuracy of $\pm$ 0.25% of range ($\pm$ 0.0175 kPa).

(j) One pressure transmitter (Rosemount 1151AP5E22B1) ranged at 0-114 kPa (absolute).

(k) A cold trap was used prior to the vacuum pump fitting.

(l) A heated jacket (see Figure 7.1) for vessel (g) with temperature regulation.

(m) An insulated bucket for immersing vessel (g) in dry ice.

(n) A supply of dry ice.

(o) A portable temperature probe to check hot water temperature.

(p) Lines to connect the vessel to pressure gauges, helium bottle and dry ice trap. These include Quick-connect male fittings and a shut off valve at both ends plus side lines to two AP pressure transmitters and a side line with shut-off valve and female Quick Connect fitting for connection to the helium bottle. A drain valve was installed at the lowest point of the plumbing (underneath the absolute pressure sensors).

(q) A small helium bottle with gauge and regulator and a flexible line to a male Quick Connect fitting.

(r) A line between the vessel and the fitting on the line to the condenser with a male Quick Connect fitting to connect it to the vessel and a female fitting to connect it to the line to the condenser. The line had a nozzle mounted in-line. The nozzle assembly was designed to allow ready access, for changing nozzle size.

For Section 7.1 Item (8)

(s) A Gas Chromatograph (GC-9A, Shimadzu, Kyoto Japan) was set up to measure the following gases; CO_2, O_2 and N_2.

(t) A hypodermic syringe was used to extract samples from vessel (g) and inject them into the GC column.

The experimental procedure and results obtained using this apparatus is presented in Chapters 35-36.

8 MATERIALS

8.1 Water

The condenser cooling water was treated water and thus could be assumed to be equivalent to 'tap' water. All water which came in contact with the evaporator internal heating surfaces was soft water, except of course for the natural water content of the milk. Samples of soft water were taken from the plant during the first water experiment (Experiment Wa1) and from the soft water supply regularly during the 1991-92 season. The analysis results are presented in Appendix C.

8.2 Sucrose

The sucrose used was standard granulated 1A sugar (New Zealand Sugar Company, Auckland). The sucrose was dissolved in hot soft water to make up the desired sugar solutions. The solutions were stored in the 'Special' CIP tank.

8.3 Skim Milk

The milk used for Experiments Sk0 and Sk2 came from the seasonal supply of Tui Co-operative Dairy Company. The milk for Experiment Sk1 came from the town milk supply of Tui CDC. The pre-treatment of the milk is described in Chapter 29.

8.4 CIP Chemicals

Bulk caustic soda and nitric acid were used for CIP at a strength of 1% v/v. A dairy sanitiser (Klenz Iodophor, Economics Laboratory, Hamilton) was occasionally used after CIP.

8.5 Antifoam

Antifoam (Foamnox HC, Economics Laboratory, Hamilton) was added to the skim milk during Experiments Sk0 and Sk1 to reduce foam levels in the product transfer pump suction line. Antifoam was also added to the caustic supply on occasions to reduce foaming during CIP. However, it was not added to the caustic used during the skim milk trials.

8.6 NCG Measurement Chemicals

Ethylene glycol was extracted from a refrigeration plant to use as a cooling medium for the NCG measurement work. Liquid nitrogen and dry ice (CO_2) were used for cooling the NCG apparatus. The dry ice was also used to cool the glycol. Bottled helium (balloon gas grade) was used to increase the pressure in the sample vessel to above atmospheric pressure before extracting a sample for the GC.

8.7 GC Test Gases

To calibrate the Gas Chromatograph (GC) before analysing samples extracted from the de-aeration lines, a test gas (NZ Industrial Gases, Lower Hutt) with the molecular composition; $15.4 \pm 0.2\%$ CO_2, $2.54 \pm 0.05\%$ O_2 and balance N_2 was used. This was not ideal, given the much smaller amounts of all three gases expected in the extracted samples (due to helium addition) but the desired test gas (molecular composition $0.51 \pm 0.01\%$ CO_2, $0.54 \pm 0.01\%$ O_2, $1.97 \pm 0.04\%$ N_2, balance He) did not arrive in time for the trial work.

PART III: HEAT TRANSFER

9 CONDENSATION THEORY

This chapter first discusses the two mechanisms by which condensation occurs, and then looks at the theory and numerical correlations for film condensation.

9.1 Condensation Mechanisms

There are two mechanisms by which a vapour will condense on a vertical surface, *drop-wise* and *film* condensation.

In *drop-wise* condensation, the vapour condenses as droplets which grow until they are large enough to run down the surface. The droplets only cover part of the surface at any time and thus there is little resistance to heat transfer. To maintain *drop-wise* condensation, the surface needs to be treated to ensure the condensing vapour does not wet the surface. Silicones, Teflon, waxes and fatty acids have been used (Incropera & DeWitt, 1990, p610) to inhibit surface wetting. The coatings, however, lose their effectiveness with time due to oxidation, fouling or removal. The presence of superheat and non-condensable gases tends to promote film condensation (Incropera & DeWitt, 1990). It has been suggested (Jebson, 1992) that milkfat carried over into the steam-side could form a layer on the tubes, and thus promote drop-wise condensation. The author suspects, however, that the carry over of CIP chemicals (caustic soda and nitric acid solutions) during cleaning would prevent the formation of an effective fat layer. The author has observed film condensation occurring at the bottom of commercial evaporator tubes. To observe the condensation mechanism at the top of the tubes, would require calandria modification (perhaps a temporary modification to a top de-aeration port). The actual condensation mechanism at the top of commercial milk evaporators has yet to be verified.

Film condensation is the expected mode on clean surfaces. The steam-side of the Research Evaporator calandrias were cleaned with caustic soda and nitric acid solutions several times during the experimental program to ensure film condensation occurred. The vapour condenses as a film (see Figure 9.1) which thickens as it travels down the tube. At the top of the film the flow is laminar, then waves start appearing on the surface which introduce a small amount of mixing and also disturb the vapour boundary layer. Eventually the film will become turbulent. In commercial milk evaporators, the condensate film only experiences laminar and wavy-laminar conditions (see Appendix D).

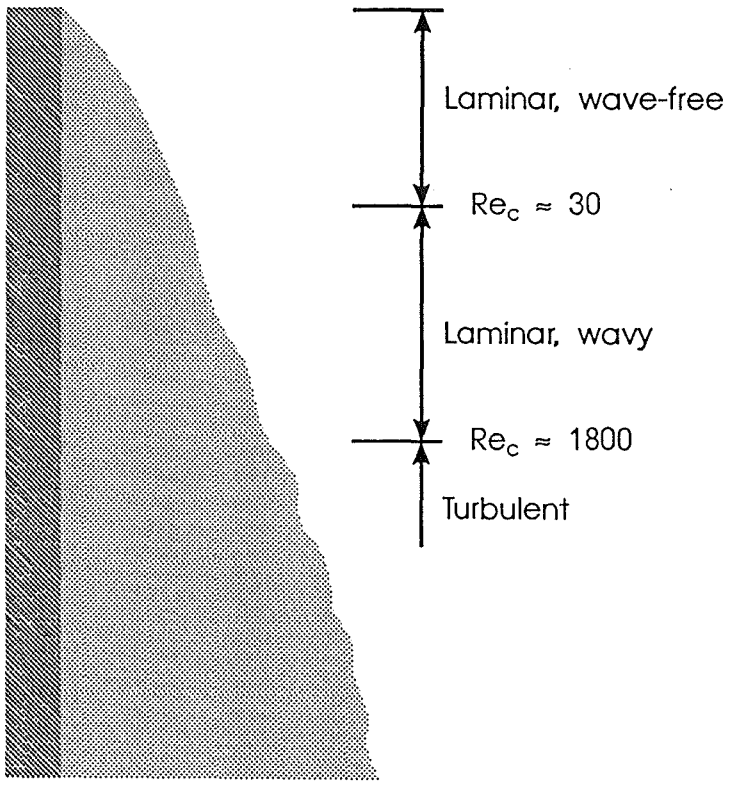

Figure 9.1: Film Condensation on a Vertical Surface (Adapted from Incropera & DeWitt, 1990, p616).

Superheated vapour has to be brought down to its saturation temperature before it will condense. The additional heat generated is usually insignificant. In MVR evaporators that use compressors, a small amount of hot condensate is sprayed into the steam, after the compressor, to remove the superheat. At the top of the tubes, the condensate film coverage will be very thin and possibly incomplete. The presence of superheat in this region, in conjunction with poor liquid distribution, may cause localised hot spots leading to rapid fouling. Other variables which affect the condensation process are the vapour velocity and the concentration of non-condensable gases. The effect of the steam-side vapour phase conditions on heat transfer is discussed in Chapter 33.

9.2 Film Condensation Theory

Nusselt (1916) proposed a theory for laminar film condensation on a vertical surface. His theory was based on a number of simplifying assumptions:

1. Constant properties and laminar flow are assumed for the liquid film.
2. The gas phase is assumed to be at constant temperature over the full length of the condensing surface. The gas phase is a pure vapour at its saturation temperature.
3. The shear stress acting at the vapour-liquid interface is assumed to be negligible.
4. Heat transfer through the film occurs by conduction alone.

The normal forms in which Nusselt's theory is presented are:

$$\delta(z) = \left[\frac{4 k_c \mu_c \left(T_{steam} - T_{w_{OD}}\right) z}{g \rho_c \left(\rho_c - \rho_v\right) \lambda_c} \right]^{1/4} \tag{9.1a}$$

and

$$\bar{\alpha}_c = 0.943 \left[\frac{g \rho_c \left(\rho_c - \rho_{steam}\right) k_c^3 \lambda_c}{\mu_c \left(T_{steam} - T_{w_{OD}}\right) L} \right]^{1/4} \tag{9.1b}$$

To take account of thermal advection it was proposed by Nusselt that λ_c is replaced by:

$$\lambda_c' = \lambda_c + 0.68 C_{p_c} \left(T_{steam} - T_{w_{OD}}\right) \tag{9.2}$$

For condensing steam with a ΔT_c of 1°C, λ'_c is only 0.13% larger than λ_c and therefore λ_c was used in all calculations.

Nusselt's theory can also be expressed in terms of the modified Nusselt number:

$$\bar{Nu}_c = 1.47\, Re_{c_\perp}^{-1/3} \tag{9.3}$$

This holds well for $Re_c \leq 30$. Above about $Re_c = 30$, waves begin to form on the surface. Various equations have been proposed to fit experimental data in the laminar-wavy and turbulent zones. A comprehensive evaluation of these has been done by Chun & Kim (1990). The existing equation which best fitted the previously published experimental data for *laminar flow* ($Re_c < 1800$) was the Zazuli correction of Nusselt's equation:

$$\begin{aligned} \bar{Nu}_c &= 0.687\, Re_{c_\perp}^{0.11} \times 1.47\, Re_{c_\perp}^{-1/3} \\ &= 1.01\, Re_{c_\perp}^{-0.22} \end{aligned} \tag{9.4}$$

Chun & Kim (1990) proposed the following equation:

$$\bar{Nu}_c = 1.33\, Re_{c_\perp}^{-1/3} + 9.56\times10^{-6}\, Re_{c_\perp}^{0.89}\, Pr_c^{0.94} + 8.22\times10^{-2} \tag{9.5}$$

$$\text{For } 10 < Re_{c_\perp} < 3.1\times10^4$$

The above three equations are plotted in Figure 9.2.

Nusselt's theory (Equation 9.3) can be expressed in terms of ΔT_c (Wassner, 1981) as follows:

$$\bar{Nu}_c = 0.94\left[\frac{C_{p_c} L\, \Delta T_c}{\lambda_c\, Pr_c \left(\frac{\nu_c^2}{g}\right)^{1/3}}\right]^{-1/4} \tag{9.6}$$

And the Zazuli correction (Equation 9.4) can likewise be expressed as follows:

$$\bar{Nu}_c = 0.785\left[\frac{C_{p_c} L\, \Delta T_c}{\lambda_c\, Pr_c \left(\frac{\nu_c^2}{g}\right)^{1/3}}\right]^{-0.18} \tag{9.7}$$

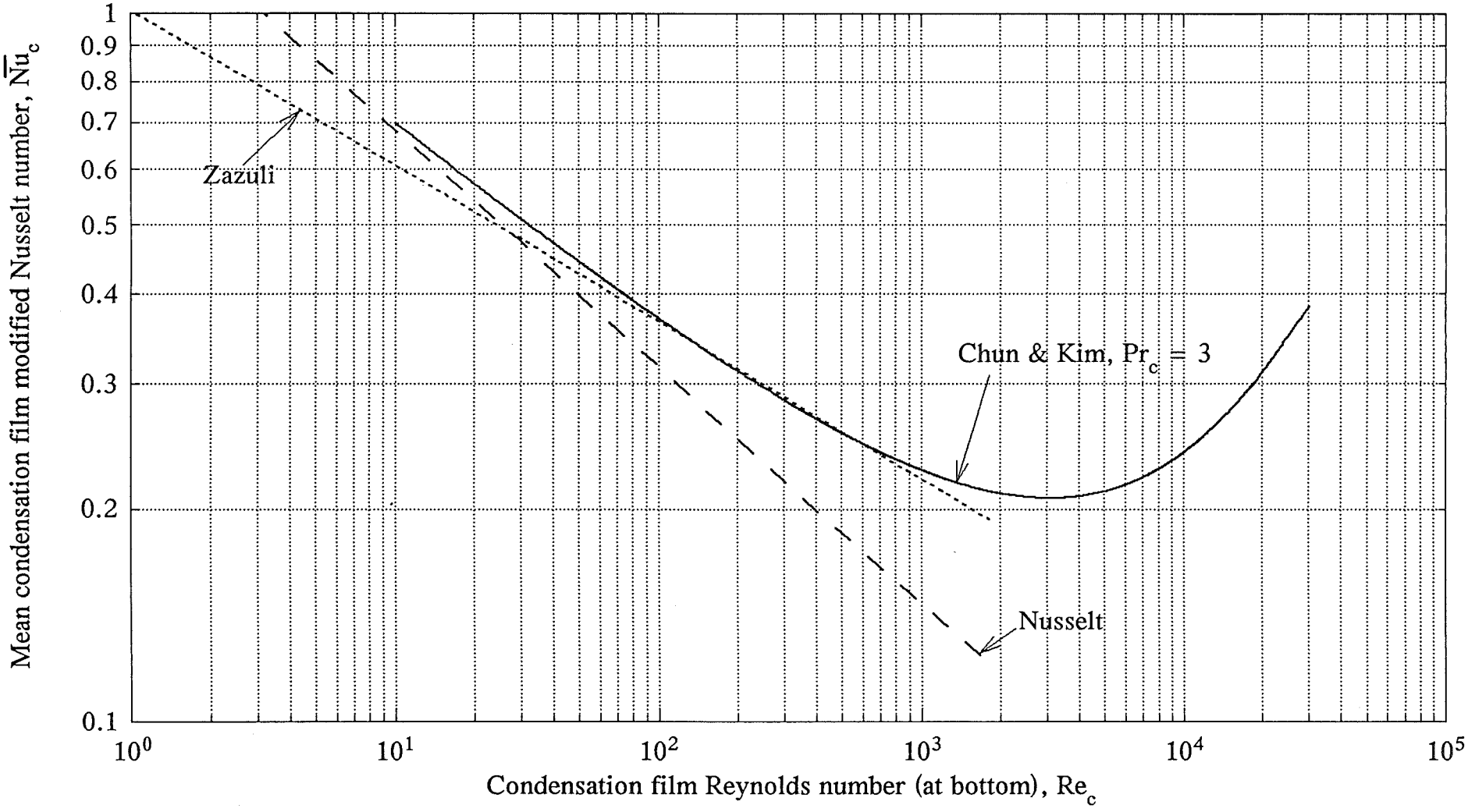

Figure 9.2: Mean Condensation Nusselt Number Correlations.

The Chun & Kim correlation (Equation 9.5) can be expressed in a similar form but can only be solved by iteration:

$$\bar{Nu}_c = \frac{0.588\,\lambda_c\,Pr_c\left(\frac{\nu_c^2}{g}\right)^{1/3}}{C_p L\,\Delta T_c\left[\bar{Nu}_c - 9.56\times10^{-6}\,Re_c^{0.89}\,Pr_c^{0.94} - 0.0822\right]^3} \tag{9.8}$$

The derivation of Equations 9.6, 9.7 & 9.8 is outlined in Appendix E. As the condensate Reynolds number did not exceed 1000, the Zuzuli correction form (Equation 9.7) was used (for simplicity) to determine predictive overall transfer coefficients (see Chapter 11 for method) to compare with experimental values from the differential pressure experiments (see Chapter 19) and the boiling temperature experiments (see Chapter 20).

10 BOILING-SIDE THEORY

This chapter discusses the various boiling modes, and means of estimating film thickness. Heat transfer correlations of Linke, Chun & Seban, and, Billet are presented.

10.1 Boiling Modes

For pool boiling, the Nukiyama boiling curve (see Figure 10.1) is the traditional representation used to illustrate the different boiling modes. The boiling modes of interest for falling film evaporation are the free (or forced) convection regime ($\Delta T_e \leq 5°C$)[1] and the *isolated bubble* nucleate boiling regime ($5 \leq \Delta T_e \leq 10°C$). The effect of liquid flow over the heated surface is to increase the heat transfer rate in the forced convection regime, and to extend the ΔT_e range for forced convection (Müller-Steinhagen, 1989). Billet (1989, p139) reports that vapour bubbles may not form on the tube wall in *trickled-film*[2] evaporators until $\Delta T_e = 7°C$. Houšová (1970) presented experimental data of α_e and q/A for falling film evaporation of water in a 3 m long tube for a boiling temperature range of 50-74°C. The data indicates that the change to nucleate boiling takes place above a ΔT_e of 10°C. Therefore, falling film evaporators in the dairy industry should operate solely under the forced (or free) convection boiling regime (see Appendix D).

Bouman et al (1993) claim that the change to nucleate boiling for skim (and whole) milk occurs at a ΔT_e of 0.5°C. This conflicts with previous work, but could explain why measured overall heat transfer coefficients (Mackereth, 1987) are normally greater than predicted by convection boiling heat transfer models. However, the presence of waves and their interaction with the flowing vapour (Jebson & Iyer, 1991) could also explain the high heat transfer coefficients. The results of Bouman et al suggest that foam formation initiates nucleate boiling at lower ΔT_e than occur on non-foaming liquid streams (eg water and sucrose solutions).

Further work is required to verify the boiling regime for skim milk under normal evaporation conditions.

---

[1] For water.

[2] Falling film evaporation with negligible boiling-side vapour velocities.

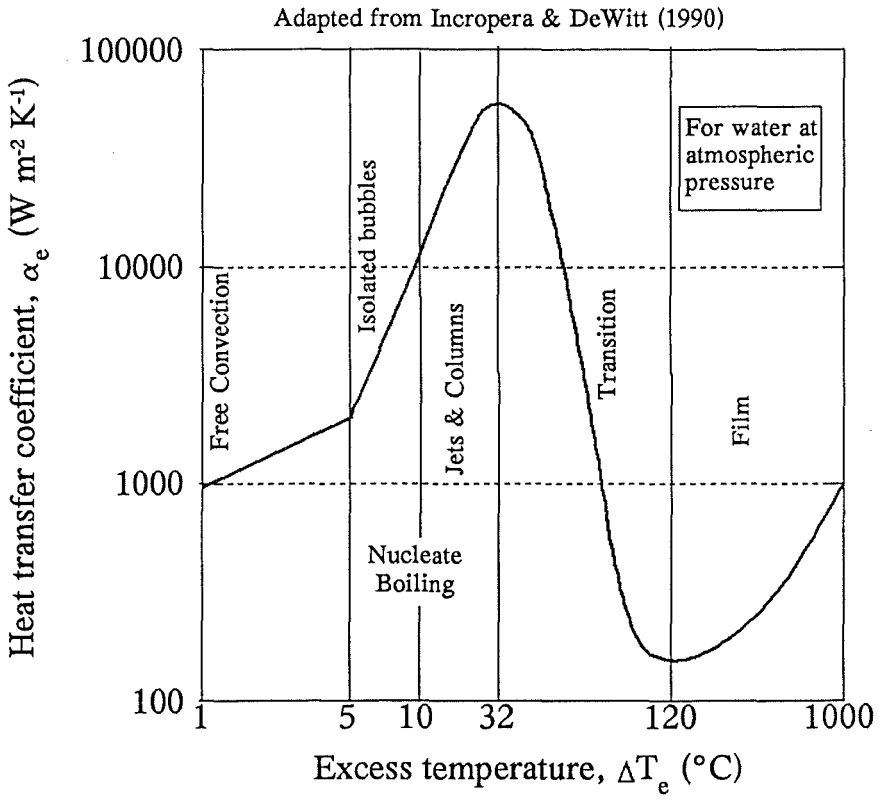

Figure 10.1: Nukiyama Boiling Curve for Pool Boiling.

10.2 Boiling Film Thickness

For laminar flow of a film undergoing convective heat transfer (and ignoring radial, shear and entrance effects) the film thickness at point z, is given by the *Hagen-Poiseuille* law (Billet, 1989, p137):

$$\delta_e(z) = \sqrt[3]{\frac{3\,\mu_e\,\Gamma_e(z)}{\rho_e^2\,g}} \tag{10.1}$$

Billet (1989, p138) gives the following for turbulent flow.

$$\delta_e = 0.369\left(\frac{3\,\mu_e^2}{\rho_e^2\,g}\right)^{\frac{1}{3}}\left(\frac{\Gamma_e}{\mu_e}\right)^{\frac{1}{2}} \tag{10.2}$$

The thickness of the boiling film over the range of operating conditions used in this work is discussed in Section 38.2.

10.3 Linke and Chun & Seban Models

For laminar flow of pure liquids, Linke (1953) derived the following relationship for α_e:

$$\overline{\alpha}_e = \frac{g\,\lambda_e\,\rho_e^2}{3\,\mu_e\,\Delta T_e\,L}\left(\delta_{e_\tau}^3 - \delta_{e_\perp}^3\right) \tag{10.3}$$

Where the change in film thickness over the tube length (cf Equation 9.1a) is:

$$\delta_{e_{top}} - \delta_{e_{bottom}} = \left[\frac{4\,k_e\,\mu_e\,\Delta T_e\,L}{g\,\lambda_e\,\rho_e^2}\right]^{1/4} \tag{10.4}$$

The above equations are based on a similarity principle. That is that the local film heat transfer coefficient is the same for film condensation and for evaporation by surface (convection) boiling from a falling film. The condensing film has a zero mass flow rate at the top of the tube and increases to the tube condensation rate at the bottom of the tube. The boiling liquid film starts at an initial mass flow rate, and leaves the bottom of the tube at a reduced flow rate. As the exit flow rate is not zero, the various models for average film condensation heat transfer can not be applied directly. Thus, determination of an average boiling-side heat transfer coefficient requires integration of local heat transfer coefficients over the length of the tube.

Chun & Seban (1971) applied the same similarity principle to determine α_e for films whose range of Reynolds numbers were in the laminar and/or turbulent zones. For

wavy-laminar flow[3] they used a local Nusselt number which is consistent with Equation 9.4:

$$Nu_e = 0.822\, Re_e^{-0.22} \tag{10.5}$$

Chun & Seban proposed the following for turbulent flow:

$$Nu_e = 3.8\times10^{-3}\, Re_e^{0.4}\, Pr_e^{0.65} \tag{10.6}$$

Now Chun & Seban present two different $Re_{lam\rightarrow tur}$
Either:

$$Re_{lam\text{-}tur} = 5800\, Pr_e^{-1.06} \tag{10.7}$$

Or

$$Re_{lam\text{-}tur} = 2460\, Pr_e^{-0.65} \tag{10.8}$$

To avoid a step change in Nusselt number at the transition point, a third $Re_{lam\rightarrow tur}$ was determined by setting Equation 10.4 equal to Equation 10.5 and solving for Re_e:

$$Re_{lam\text{-}tur} = 5838 Pr_e^{-1.05} \tag{10.9}$$

Equations 10.7, 10.8 and 10.9 are plotted in Figure 10.2. Chun & Seban's Nu_e versus Re_e curves for a range of Pr_e numbers (see Figure 10.3) were determined using Equation 10.9 to determine $Re_{lam\rightarrow tur}$. The correlations of Chun & Seban are compared with experimental data for water in Chapters 17, 19-22, for sucrose solutions in Chapters 25-27, and, skim milk in Chapter 31.

10.4 Correlations Presented by Billet

Billet (1989, p138) presented the following equations[4] for local Nusselt numbers for trickled film surface evaporation:

---

[3] Chun & Seban (1972) had an equation for purely laminar flow, but found that, due to the low Reynolds number at which waves form, the wavy-laminar equation could be used for all laminar flow. The transition from laminar to wavy-laminar flow at 60°C occurs at Reynolds numbers of 30 for water and 5 for 45% w/w skim milk concentrate.

[4] Equations 10.10-10.12 have been modified to meet the definition of Re used in this thesis.

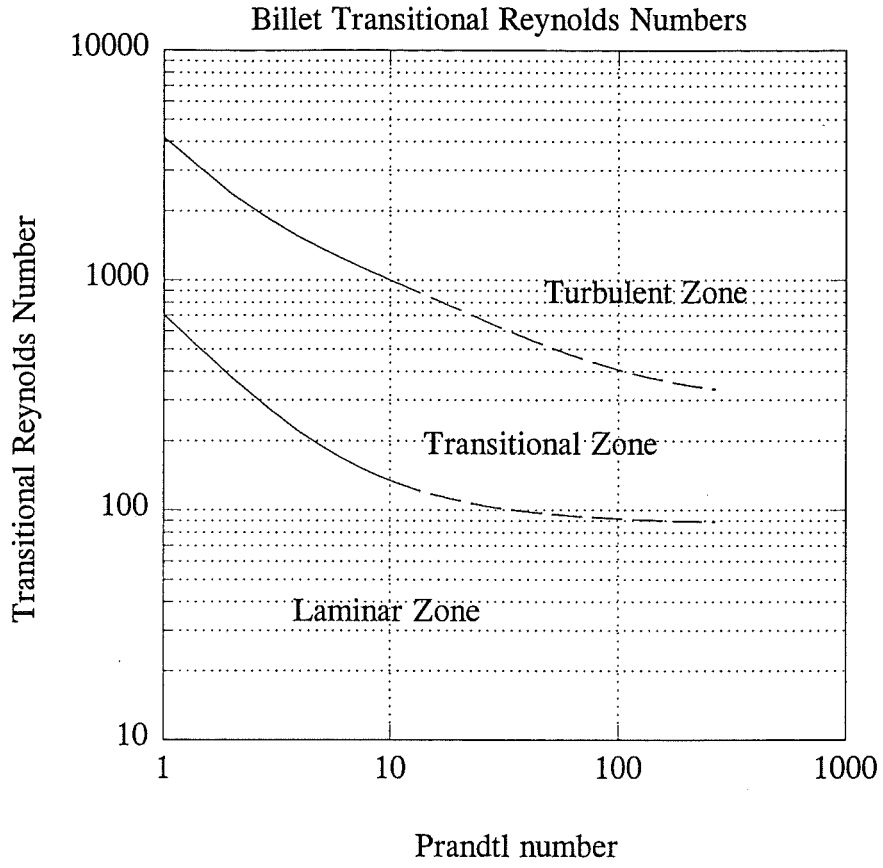

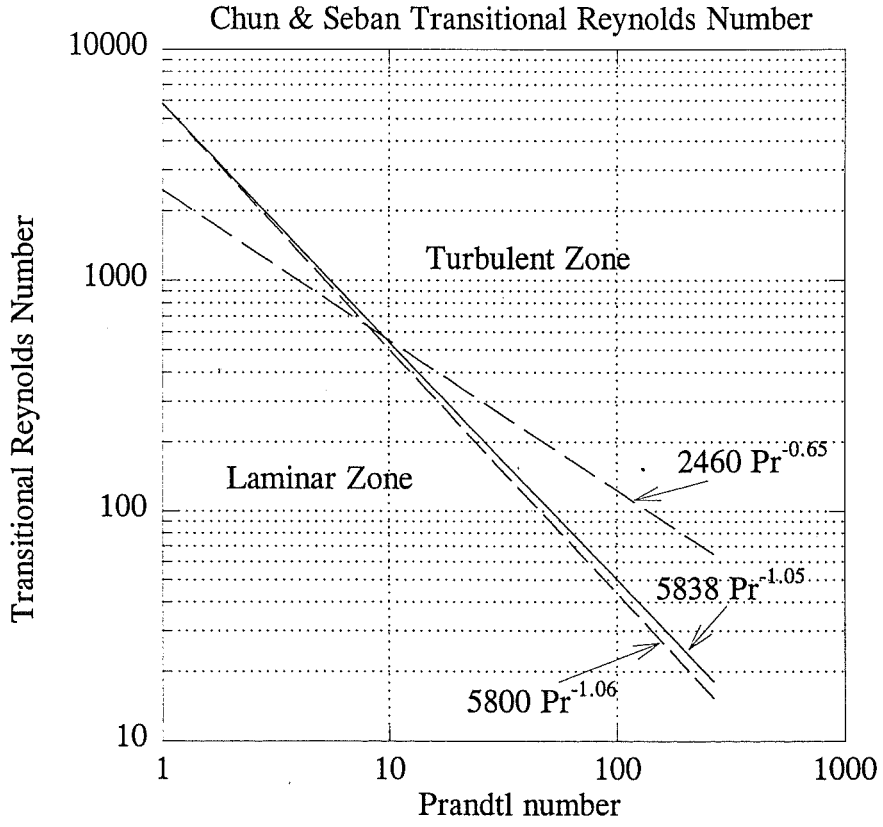

Figure 10.2: Points of Transition in Re_e for Billet (1989) and Chun & Seban (1971) Nu_e Correlations as a Function of Pr_e.

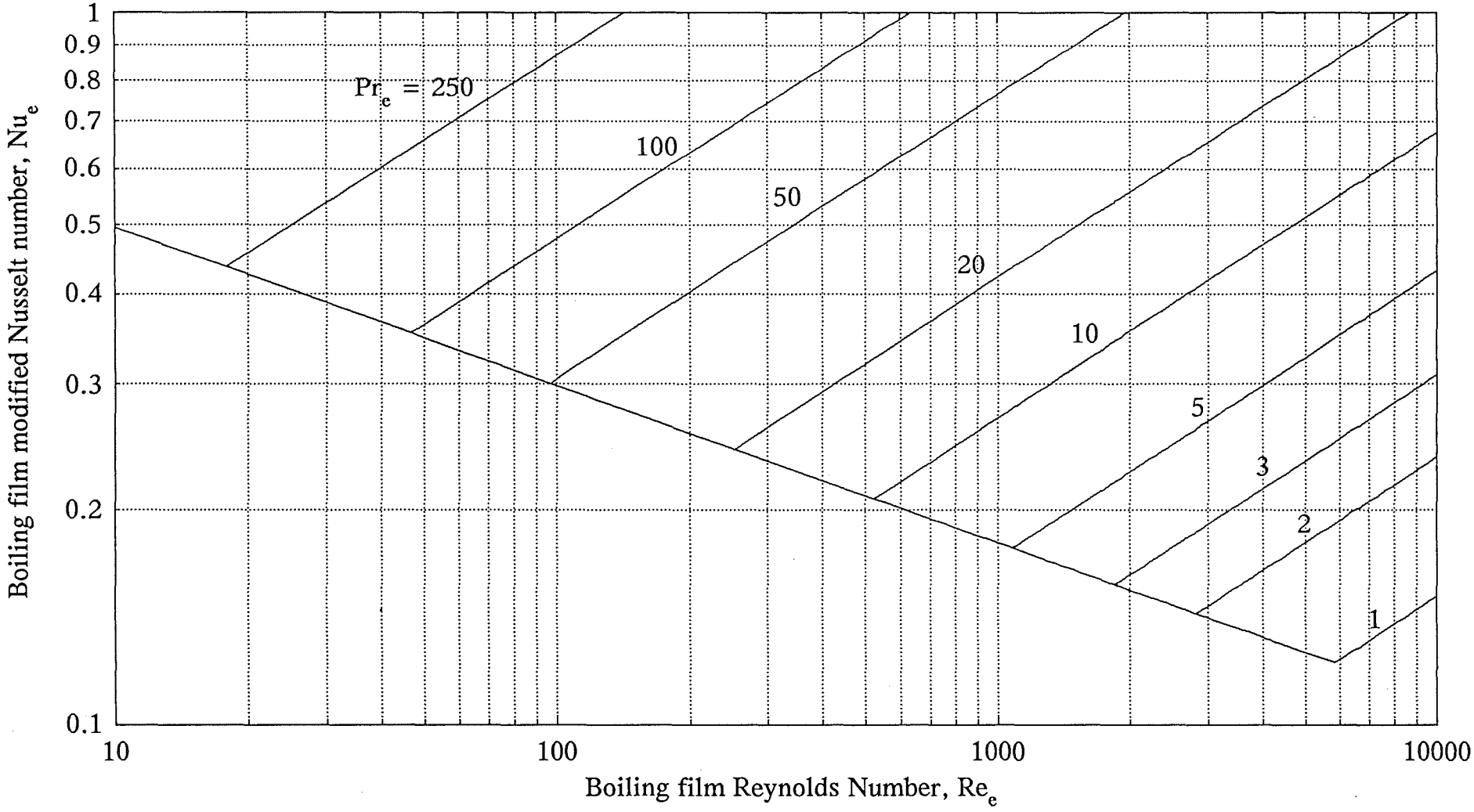

Figure 10.3: Chun & Seban (1971) Nu_e versus Re_e Curves for a Range of Pr_e ($Re_{lam-tur}$ Determined Using Equation 10.8).

For wavy-laminar flow:

$$Nu_e = 1.43\, Re_e^{-\frac{1}{3}} \tag{10.10}$$

For transitional flow:

$$Nu_e = 0.176\left(\frac{Re_e}{4}\right)^{\left(0.196 - \frac{0.844}{Pr_e + 2.95}\right)} \tag{10.11}$$

For turbulent flow:

$$Nu_e = \left(0.110 - \frac{0.565}{Pr_e + 5.47}\right) Re_e^{0.231} \tag{10.12}$$

The equations were fitted to experimental data and verified for $1 \leq Pr_e \leq 10$ (Billet, 1989, p138). The points of transition from wavy-laminar to transitional flow and from transitional to turbulent flow were not given directly for the above equations. However, by assuming that there is no step change at the transition points, the transition points can be determined as follows:

$$Re_{lam\text{-}tra} = \left(8.125 \times 4^{n_B}\right)^{\frac{1}{n_B + \frac{1}{3}}} \tag{10.13}$$

and

$$Re_{tra\text{-}tur} = \left[\left(0.625 - \frac{3.21}{Pr_e + 5.47}\right) 4^{n_B}\right]^{\frac{1}{n_B - 0.231}} \tag{10.14}$$

where the transitional power term, n_B is defined as:

$$n_B = 0.196 - \frac{0.844}{Pr_e + 2.95} \tag{10.15}$$

The effect of Pr_e on the two transitional points, $Re_{lam\rightarrow tra}$ and $Re_{tra\rightarrow tur}$ is shown in Figure 10.2. Billet's combined local Nusselt number versus Re_e curves for a range of Pr_e are plotted in Figure 10.4.

The correlations of Billet are compared with experimental data for water in Chapters 17, 19-22 and for sucrose solutions in Chapters 25-26.

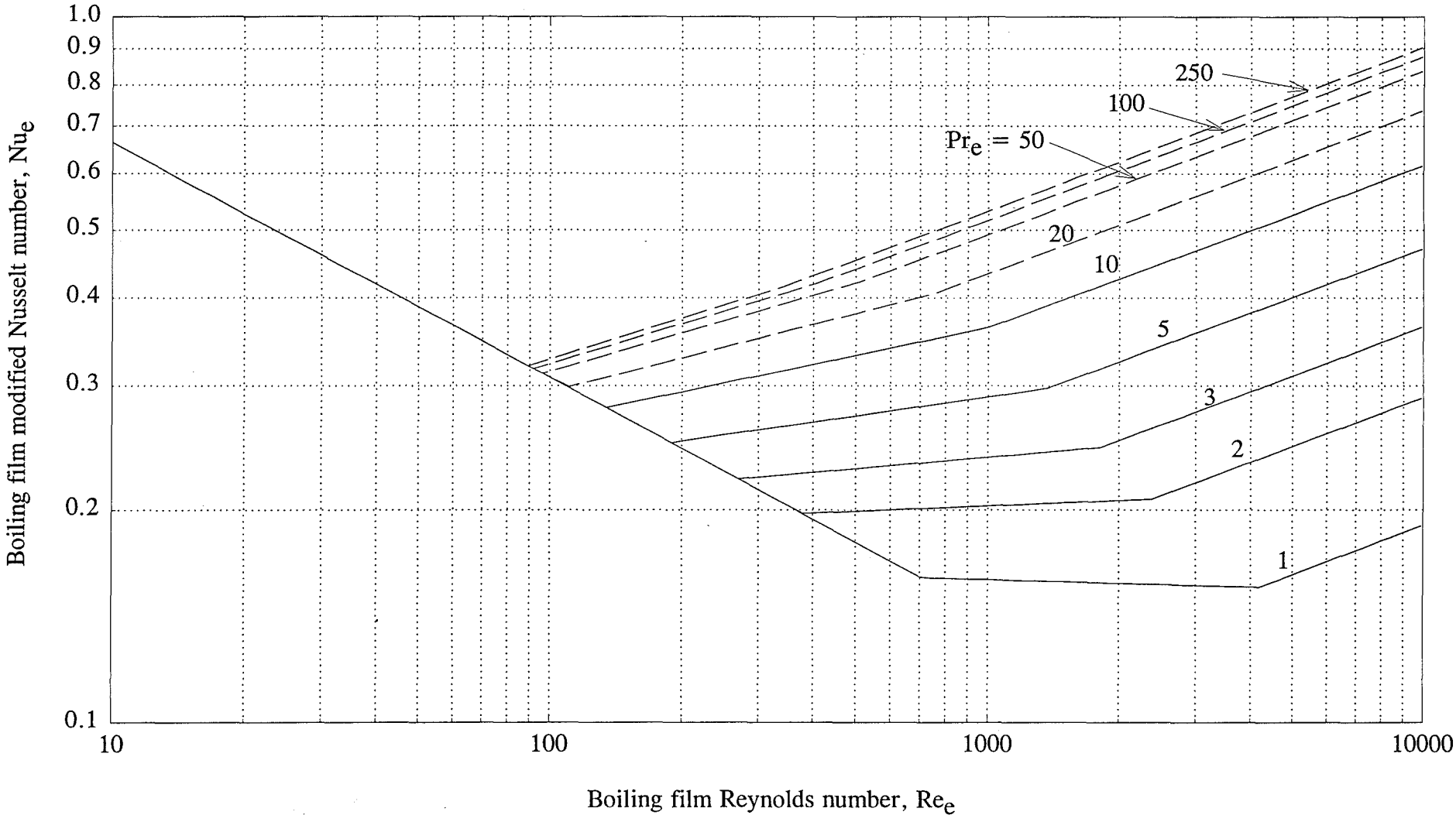

Figure 10.4: Billet (1989) Nu_e versus Re_e Curves for a Range of Pr_e.

11 OVERALL HEAT TRANSFER THEORY

Baloh (1984) presented local temperature profiles over the length of a 4 m long tube (see Figure 11.1) for the surface evaporation from a turbulent film of water. The exit vapour velocity was low (3 m s^{-1}) so the pressure drop over the tube length would be negligible. The temperature profiles show that more evaporation occurs at the top of the tube, because of the thinner condensate film. The measured temperature profile starts about 0.25 m down the tube, thus apparently avoiding measurement where entrance effects could be significant. The boiling film is turbulent, and therefore the boiling-side heat transfer coefficient would also be higher at the top of the tube. The effective dimensionless driving force, $\Delta T_e/\Delta T_U$ is lowest at the bottom of the tube.

In practice, the temperature profiles over the length of the tube will depend on the sum of the following effects.

1. The change in boiling-side fluid properties (μ, k, Cp, BPE, Γ) over the length of the tube due to concentration.
2. The local vapour velocities on both sides of the tube wall.
3. The local concentration of non-condensable gases (see Chapter 33) at the condensate-steam interface.

The measurement of local temperatures over the length of the evaporator tube was not feasible on the Research Evaporator, so only average heat transfer coefficients were determined.

Wassner (1981) has proposed a simple method (see Appendix F for derivation) for calculating the average overall heat transfer coefficient, using dimensionless parameters. It involves solving the following equations simultaneously:

$$\frac{\Delta T_c}{\Delta T_U} = \frac{x \dfrac{\bar{Nu}_e}{\bar{Nu}_c}}{\left(1 + x \dfrac{\bar{Nu}_e}{\bar{Nu}_c} + y \bar{Nu}_e\right)} \tag{11.1}$$

$$\frac{\Delta T_e}{\Delta T_U} = \frac{1}{\left(1 + x \dfrac{\bar{Nu}_e}{\bar{Nu}_c} + y \bar{Nu}_e\right)} \tag{11.2}$$

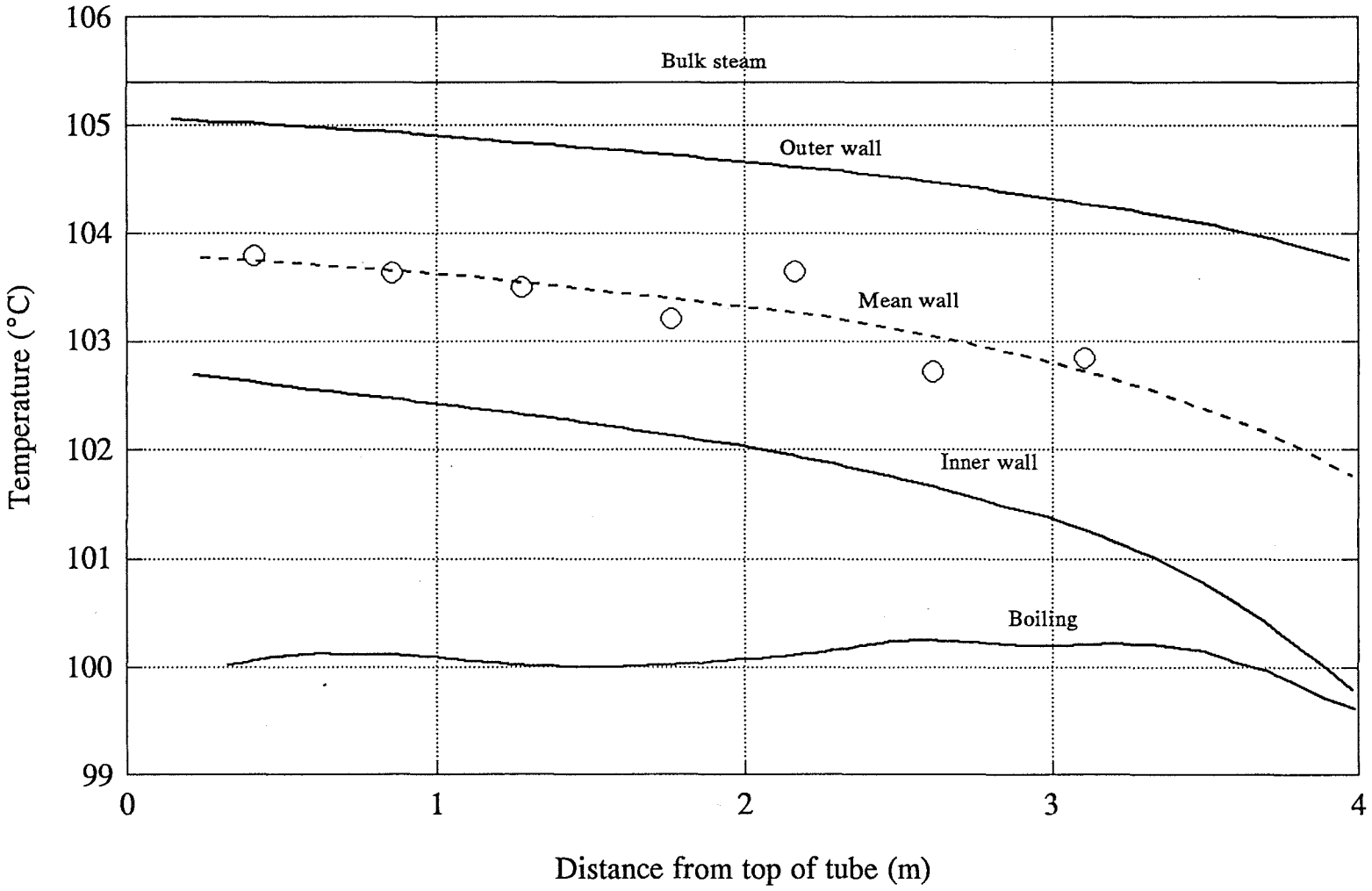

Figure 11.1: Local Temperature Profiles During Evaporation of a Turbulent Falling Film of Water (Adapted from Baloh (1984)).

The most practical application of this method is to determine the evaporation rate per tube, given that the following information is known.

1. The boiling-side Nusselt number as a function of fluid properties.
2. The condensate and boiling-side average fluid properties:
   viscosity, thermal conductivity, specific heat, boiling point elevation (BPE), and, latent heat.
3. The tube parameters:
   length, diameter, wall thickness, and, thermal conductivity.
4. The effective overall temperature driving force, ΔT_U - BPE.

Wassner used Nusselt's analysis (Equation 9.6) to determine the average condensation Nusselt number. To eliminate the unknown, ΔT_c, Equation 11.1 was used, giving the following relationship:

$$\bar{Nu}_c^4 Z^* = 0.79\left(1 + \frac{1 + y\bar{Nu}_e}{x\bar{Nu}_e}\bar{Nu}_c\right) \tag{11.3}$$

where x, y and Z^* are dimensionless groups.

This equation can be solved graphically (Wassner 1981) or by iteration. Equation 11.3 must be satisfied in addition to Equations 11.1 & 11.2. To allow for ripples in the condensate film, it is possible to use Zazuli's correction (Equation 9.7) or Chun & Kim's correlation (Equation 9.8) instead of Equation 9.6.

Wassner's method was used to determine predictive overall transfer coefficients to compare with experimental values from the differential pressure experiments (see Chapter 19) and the boiling temperature experiments (see Chapter 20).

12 DATA ANALYSIS

This chapter sets out the procedure used for calculating the experimental overall heat transfer coefficients and film parameters from measurements made on the Third and Fifth Evaporators.

12.1 Known Parameters

Tube length, L	10, 15 m
Tube inner diameter, d_{ID}	22.6, 39.7, 48.1 mm
Tube outer diameter, d_{OD}	24.6, 41.7, 50.1 mm
Tube wall material	316 Stainless Steel
Acceleration due to gravity, g	9.81 m s^{-2}

12.2 Experimental Measurements

For all boiling-side fluids

Feed flow rate, m_{feed}

Concentrate flow rate, m_{out}

Boiling Pressure, p_{boil}

Pressure difference across tube wall, Δp

Feed temperature, T_{feed}

For sucrose and skim milk

Feed density meter output, ρ_{MM}

Temperature in feed density meter, T_ρ

Product temperature, T_{prod}

Steam temperature, T_{steam}

Temperature of viscosity measurement[1], T_μ

Viscometer pressure drop, Δp_μ

For skim milk only

Feed total solids, S_{feed}

Concentrate total solids, $S_\perp$

---

[1] Temperature of density meter tube, mounted in concentrate line just before viscometer.

12.2

12.3 Calculated Constants

Wall thickness, s

$$s = \frac{d_{OD} - d_{ID}}{2}$$

Heat transfer surface areas, A_{ID}, A_{OD}, A_m

$$A_{ID} = \pi d_{ID} L$$
$$A_{OD} = \pi d_{OD} L$$
$$A_m = \frac{(A_{OD} - A_{ID})}{\ln\left(\frac{A_{OD}}{A_{ID}}\right)}$$

12.4 Calculated Variables

The actual correlations used to determine various physical properties in terms of known properties are described in Appendix G.

Feed density correction (See Appendix B)

For sucrose and skim milk

$$\rho_{feed} = \rho_{MM} + 1.1935 + 0.0422 T_\rho - 0.00162 T_\rho^2$$

Feed total solids

For sucrose

$$S_{feed} = S_{sugar}(\rho_{feed}, T_\rho)$$

For skim milk

$$S_{feed}|_{calc} = S_{skim}(\rho_{feed}, T_\rho)$$

Concentrate total solids

For sucrose and skim milk

$$S_{\perp} = S_{feed}\left(\frac{m_{feed}}{m_{\perp}}\right)$$

Steam-side pressure

$$p_{steam} = p_{boil} + \Delta p$$

Boiling-side saturation temperature

$$T_{boil} = \mathrm{T_{sat}}\left(p_{boil}\right)$$

Steam-side saturation temperature[2]

If $\Delta p < 20$ kPa then

$$T_{sat\ steam} = \mathrm{T_{sat}}\left(p_{steam}\right)$$

Else

$$T_{sat\ steam} = T_{steam} + 0.5$$

End If

Thermal conductivity of 316 Stainless Steel

$$k_w = \mathrm{k_{SS316}}\left(T_{sat\ steam}\right)$$

Temperature driving force

$$\Delta T = T_{sat\ steam} - T_{boil}$$

---

[2] There was usually a 0.5°C difference between the measured steam temperature (surface probe) and the saturation temperature determined from the differential pressure measurement. Therefore, when the differential pressure sensor was out of range, a corrected steam temperature was used instead.

Gross Evaporation rate

$$E_{gross} = m_{feed} - m_{\perp}$$

Flash Evaporation rate

For water

$$E_{flash} = \frac{\left(\mathrm{h}_{\mathrm{water}}\left(T_{feed}\right) - \mathrm{h}_{\mathrm{water}}\left(T_{boil}\right)\right) m_{feed}}{\lambda_{\mathrm{steam}}\left(T_{boil}\right)}$$

For sucrose

$$E_{net\ flash} = \frac{\left(\mathrm{h}_{\mathrm{sugar}}\left(S_{feed}, T_{feed}\right) - \mathrm{h}_{\mathrm{sugar}}\left(S_{\perp}, T_{prod}\right)\right) m_{feed}}{\lambda_{\mathrm{steam}}\left(T_{boil}\right)}$$

For skim milk

$$E_{flash} \approx \frac{m_{feed}\ \mathrm{C}_{\mathrm{p}_{60^{\circ}\mathrm{C}}}\left(S_{feed}\right)\left[T_{feed} - T_{boil} - \mathrm{BPE}_{\mathrm{skim}}\left(S_{feed}\right)\right]}{\lambda_{\mathrm{steam}}\left(T_{boil}\right)}$$

Net Evaporation rate

$$E_{net} = E_{gross} - E_{flash}$$

Total solids after flash

For sucrose it was determined by iteration of the following equations:

$$\begin{aligned}
S_{\tau} &= S_{guess} \\
BPE_{\tau} &= \mathrm{BPE}_{\mathrm{sugar}}\left(S_{\tau}\right) \\
T_{\tau} &= T_{boil} + BPE_{\tau} \\
h_{\tau} &= \mathrm{h}_{\mathrm{sugar}}\left(S_{\tau}, T_{\tau}\right) \\
E_{flash_{\tau}} &= m_{feed}\frac{\left(h_{feed} - h_{\tau}\right)}{\left(h_{steam} - h_{\tau}\right)} \\
S_{guess} &= \frac{S_{feed}\, m_{feed}}{\left(m_{feed} - E_{flash_{\tau}}\right)}
\end{aligned}$$

For skim

$$S_{\tau} = S_{feed}\left(\frac{m_{feed}}{m_{feed} - E_{flash}}\right)$$

Boiling point elevation

For water

$$BPE = 0$$

For sucrose

$$\begin{aligned} BPE_{\tau} &= \mathrm{BPE}_{\mathrm{sugar}}(S_{\tau}) \\ BPE_{\perp} &= \mathrm{BPE}_{\mathrm{sugar}}(S_{\perp}) \\ \overline{BPE}_{e} &= \left(\frac{BPE_{\tau} - BPE_{\perp}}{\ln\left(\frac{BPE_{\tau}}{BPE_{\perp}}\right)}\right) \end{aligned}$$

For skim milk

$$\begin{aligned} BPE_{\tau} &= \mathrm{BPE}_{\mathrm{skim}}(S_{\tau}) \\ BPE_{\perp} &= \mathrm{BPE}_{\mathrm{skim}}(S_{\perp}) \\ \overline{BPE}_{e} &= \left(\frac{BPE_{\tau} - BPE_{\perp}}{\ln\left(\frac{BPE_{\tau}}{BPE_{\perp}}\right)}\right) \end{aligned}$$

Mean boiling-side film temperatures

$$T_{film_{\tau}} \approx \frac{(T_{boil} + BPE_{\tau}) + (T_{steam} - 0.5)}{2}$$

$$T_{film_{\perp}} \approx \frac{(T_{boil} + BPE_{\perp}) + (T_{steam} - 1.5)}{2}$$

Boiling-side thermal conductivities

For water

$$k_{e} = \mathrm{k}_{\mathrm{water}}(T_{boil})$$

For sucrose

$$k_{\top} = k_{sugar}\left(S_{\top}, T_{film_{\top}}\right)$$
$$k_{\perp} = k_{sugar}\left(S_{\perp}, T_{film_{\perp}}\right)$$
$$\bar{k}_e = \left(\frac{k_{\top} + k_{\perp}}{2}\right)$$

For skim milk

$$k_{\top} = k_{skim}\left(S_{\top}, T_{film_{\top}}\right)$$
$$k_{\perp} = k_{skim}\left(S_{\perp}, T_{film_{\perp}}\right)$$
$$\bar{k}_e = \left(\frac{k_{\top} + k_{\perp}}{2}\right)$$

Boiling-side viscosities

Calculated viscosities

For water

$$\bar{\mu}_e = \mu_e = \mu_{water}\left(T_{boil}\right)$$

For sugar

$$\mu_{\top} = \mu_{sugar}\left(S_{\top}, T_{film_{\top}}\right)$$
$$\mu_{\perp} = \mu_{sugar}\left(S_{\perp}, T_{film_{\perp}}\right)$$
$$\bar{\mu}_e = \left(\frac{\mu_{\top} - \mu_{\perp}}{\ln\left(\frac{\mu_{\top}}{\mu_{\perp}}\right)}\right)$$

For skim milk

$$\mu_{\top} = \mu_{skim}\left(S_{\top}, T_{film_{\top}}\right)$$
$$\mu_{\perp} = \mu_{skim}\left(S_{\perp}, T_{film_{\perp}}\right)$$
$$\bar{\mu}_e = \left(\frac{\mu_{\top} - \mu_{\perp}}{\ln\left(\frac{\mu_{\top}}{\mu_{\perp}}\right)}\right)$$

Measured concentrate viscosity

For sucrose and skim milk (assuming flow behaviour is approximately Newtonian)

$$\mu = \frac{\pi\, d_{\mu}^4\, \Delta p_{\mu}\, \rho_{\perp}}{128\, L_{\mu}\, m_{\perp}}$$

Provided that the flow is laminar, *i.e.*

$$\mu > \mu_{min} = \frac{m_{\perp}}{525\,\pi\,d_{\mu}}$$

Where

$d_{\mu} = 0.0061$ m

$L_{\mu} = 0.730$ m

Boiling-side specific heat capacities

For water

$$C_{p_e} = C_{p_{water}}(T_{boil})$$

For sucrose

$$C_{p_{\tau}} = C_{p_{sugar}}(S_{\tau}, T_{film_{\tau}})$$
$$C_{p_{\perp}} = C_{p_{sugar}}(S_{\perp}, T_{film_{\perp}})$$
$$\bar{C}_{p_e} = \left(\frac{C_{p_{\tau}} + C_{p_{\perp}}}{2}\right)$$

For skim milk

$$C_{p_{\tau}} = C_{p_{skim_{60°C}}}(S_{\tau})$$
$$C_{p_{\perp}} = C_{p_{skim_{60°C}}}(S_{\perp})$$
$$\bar{C}_{p_e} = \left(\frac{C_{p_{\tau}} + C_{p_{\perp}}}{2}\right)$$

Boiling-side Prandtl numbers

For water

$$Pr_e \frac{C_{p_e}\mu_e}{k_e}$$

For sucrose and skim milk

$$Pr_{\top} = \frac{C_{p_{\top}} \mu_{\top}}{k_{\top}}$$

$$Pr_{\perp} = \frac{C_{p_{\perp}} \mu_{\perp}}{k_{\perp}}$$

$$\overline{Pr}_e = \frac{\overline{C}_{p_e} \overline{\mu}_e}{\overline{k}_e}$$

Boiling-side densities

For sucrose

$$\rho_{\top} = \rho_{\text{sugar}}\left(S_{\top}, T_{film_{\top}}\right)$$

$$\rho_{\perp} = \rho_{\text{sugar}}\left(S_{\perp}, T_{film_{\perp}}\right)$$

$$\overline{\rho}_e = \left(\frac{\rho_{\top} + \rho_{\perp}}{2}\right)$$

For skim milk

$$\rho_{\top} = \rho_{\text{skim}}\left(S_{\top}, T_{film_{\top}}\right)$$

$$\rho_{\perp} = \rho_{\text{skim}}\left(S_{\perp}, T_{film_{\perp}}\right)$$

$$\overline{\rho}_e = \left(\frac{\rho_{\top} + \rho_{\perp}}{2}\right)$$

Boiling-side kinematic viscosity

For water

$$\nu_e = \left(\frac{\mu_e}{\rho_e}\right)$$

For sucrose and skim milk

$$\overline{\nu}_e = \left(\frac{\overline{\mu}_e}{\overline{\rho}_e}\right)$$

Boiling-side latent heat of vaporisation

$$\lambda_e = \lambda_{\text{water}}(T_{boil})$$

Condensate film properties

$$\begin{aligned}
\rho_c &= \rho_{\text{water}}(T_{sat\ steam}) \\
\mu_c &= \mu_{\text{water}}(T_{sat\ steam}) \\
C_{p_c} &= C_{p_{\text{water}}}(T_{sat\ steam}) \\
k_c &= k_{\text{water}}(T_{sat\ steam}) \\
\lambda_c &= \lambda_{\text{water}}(T_{sat\ steam}) \\
\nu_c &= \frac{\mu_c}{\rho_c} \quad , \quad Pr_c = \frac{C_{p_c}\,\mu_c}{k_c}
\end{aligned}$$

Condensate flow rate and wetting factor

$$m_c \approx E_{net}\frac{\lambda_e}{\lambda_c} \quad , \quad \Gamma_c = \frac{m_c}{\pi\, d_{OD}}$$

Condensate Reynolds number

$$Re_c = \frac{4\,\Gamma_c}{\mu_c}$$

Boiling-side wetting factors

$$\Gamma_e\big|_{top} = \frac{m_{feed} - E_{flash}}{\pi\, d_{ID}} \quad , \quad \Gamma_e\big|_{bottom} = \frac{m_{feed} - E_{gross}}{\pi\, d_{ID}}$$

$$\bar{\Gamma}_e = \frac{\Gamma_e\big|_{\top} + \Gamma_e\big|_{\perp}}{2}$$

Boiling-side Reynolds numbers

$$Re_e\big|_{\top} = \frac{4\,\Gamma_e\big|_{\top}}{\mu_e\big|_{\top}} \quad , \quad Re_e\big|_{\perp} = \frac{4\,\Gamma_e\big|_{\perp}}{\mu_e\big|_{\perp}} \quad , \quad \bar{Re}_e = \frac{4\,\bar{\Gamma}_e}{\bar{\mu}_e}$$

12.10

Heat transferred through tube wall

$$q = m_c \lambda_c$$

Overall heat transfer coefficient

$$U = \frac{q}{A_{ID} \Delta T}$$

Steam-side Nusselt number using Chun & Kim (1990) correlation

$$\bar{Nu}_c = 1.33 Re_{c_\perp}^{-\frac{1}{3}} + 9.56 \times 10^{-6} Re_{c_\perp}^{0.89} Pr_c^{0.94} + 0.0822$$

Steam-side heat transfer coefficient

$$\bar{\alpha}_c = \frac{\bar{Nu}_c \, k_c}{\left(\frac{\nu_c^2}{g} \right)^{\frac{1}{3}}}$$

Temperature drop across condensate film and tube wall

$$\Delta T_c = \frac{q}{A_{OD} \bar{\alpha}_c} \quad , \quad \Delta T_w = \frac{q s}{A_m k_w}$$

Temperature drop across boiling film

$$\Delta T_e = \Delta T_U - \Delta T_w - \Delta T_c - B\bar{P}E$$

Boiling-side heat transfer coefficient

$$\bar{\alpha}_e = \frac{q}{A_{ID} \Delta T_e}$$

Boiling-side Nusselt number

$$\bar{Nu}_e = \frac{\bar{\alpha}_e}{k_e}\left(\frac{\nu_e^2}{g}\right)^{\frac{1}{3}}$$

Modified Jacob number

$$Ja^* = \frac{\bar{C}_{p_e}\Delta T_U}{\lambda_{\text{steam}}(T_{boil})}$$

Vapour/liquid loading ratio

$$N_{\Gamma_v/\Gamma_e} = \frac{\bar{\Gamma}_v}{\bar{\Gamma}_e}$$

Tube aspect ratio

$$N_{L/d} = \frac{L}{d_{ID}}$$

Modified boiling point elevation number

$$N^*_{BPE} = \frac{\Delta T_U - \bar{BPE}}{\Delta T_U}$$

12.5 Comparison with Previous Boiling-side Models

Hagen-Poiseuille laminar film thickness

Calculate film thickness at top and bottom using Equation 10.1.

Chun & Seban local Nu_e number

Using the mean Re_e and Pr_e numbers, calculate $Re_{lam\rightarrow tur}$ using equation 10.9 and then use either Equation 10.5 or 10.6, as appropriate, to determine Nu_e.

Billet's local Nu_e number

Using the mean Re_e and Pr_e numbers, calculate the Reynolds number transition points using equations 10.14 and 10.15. Nu_e is then determined from the appropriate selection of Equations 10.10, 10.11 and 10.12.

12.6 Integration of Local Nusselt Number Correlations over the Tube Length

The local Nusselt equations presented by Billet (1989) and Chun & Seban (1971) were numerically integrated over the length of the tube to determine more accurate mean Re_e and Pr_e numbers for the sucrose experiments. In addition, the predicted mean Nu_e numbers based on Billet and Chun & Seban local Nu_e correlations were determined. The integration procedure is outlined in Appendix H.

12.7 Predicted Overall Heat Transfer Coefficient using Wassner (1981) Method

For several of the water experiments, predicted overall HTC were calculated based on Chun & Seban (1971) and Billet (1989) Nu_e correlations as follows:

(1) A predicted Nu_e was calculated using the appropriate correlation,

(2) A predicted Nu_c was calculated using Wassner's method (see Appendix F) with the Zazuli correction,

(3) A predicted U was calculated using the following equation:

$$\frac{1}{U} = \left[\frac{\left(\frac{\nu_e^2}{g}\right)^{\frac{1}{3}}}{Nu_e k_e} + \frac{s}{k_w} + \frac{\left(\frac{\nu_c^2}{g}\right)^{\frac{1}{3}}}{Nu_c k_c} \right] \left(\frac{\Delta T_U}{\Delta T_U - B\bar{P}E} \right)$$

13 EXPERIMENTAL DESIGN - WATER

The experimental design of all the experiments on water (except the NCG experiments) are presented below. The experimental procedure is covered in Chapter 14, and the results and discussion of the water experiments are found in Chapters 15-22.

13.1 Standard Operating Conditions

The standard operating conditions for all experiments unless expressly stated were:

Evaporator	Third
Tube length	15 m
Tube inner diameter	48.1 mm
Feed type	soft water
Feed flow rate	110 kg h^{-1}
Feed temperature	61.5°C
Boiling temperature	60°C
Temperature driving force	3°C
De-aeration nozzle diameter	3.2 mm

13.2 Order of Experimental Runs

The experimental run order was randomised, except for additional centre-point replicates which were deliberately placed at the beginning, end and at regular intervals through the experiments. Where all experimental points were replicated, the sets of replicates were blocked, so that if a plant failure prevented completion of second (or third) block, completed blocks could still be statistically analyzed (if desired). The blocking also allowed checking for non-cyclic time trends. The randomisation was done prior to writing the operating procedures and sequences (see Section 6.5) for each experiment design. Thus, when an experiment design was repeated several times, the run order remained the same throughout.

13.3 Steady State

Three steady-state runs were carried out (Experiments Wa2, 3-4 September 1991; Wa8, 14-15 October 1991 and Wa15, 7-8 November 1991) to determine the effect of ambient conditions, steam supply variations and other disturbances on the overall heat transfer coefficient (HTC). The results are presented in Chapter 15.

13.4 Boiling Temperature, Temperature Driving Force and Concentrate Flow Rate

A 3^3 factorial experiment with four centre point replicates (31 runs) was conducted to determine the effect on the overall HTC of boiling temperature, temperature driving force, and concentrate flow rate (liquid loading) The experimental design allowed the determination of any significant interactions between the variables. The feed temperature was varied in conjunction with the boiling temperature to keep the flash temperature difference constant.

The levels used in Experiment Wa1 (30 Oct 1990 - 1 Nov 1990) were:

Boiling temperature	55, 62.5, 70°C
(Feed temperature	56.5, 64, 71.5°C)
Delta temperature	2, 3, 4°C
Concentrate flow rate	18, 90, 162 kg h^{-1}

This experiment was repeated twice (Experiment Wa3, 4-5 September 1991; Experiment Wa6, 11-13 October 1991). The levels used in Experiments Wa3 and Wa6 were:

Boiling temperature	55, 60, 65°C
(Feed temperature	56.5, 61.5, 66.5°C)
Delta temperature	2, 3, 4°C
Concentrate flow rate	18, 90, 162 kg h^{-1}

The results for Experiments Wa1, Wa3 and Wa6 are presented in Chapter 16.

13.5 Liquid Loading (Feed Flow Rate)

The effect of feed flow rate (liquid loading) was investigated using three experimental designs. The first was a replicated 9^1 factorial (2 blocks) with 4 additional replicates of the centre-point (22 runs). The levels were:

Feed flow rate	30, 50, 70, 90, 110, 130, 150, 170, 190 kg h^{-1}

The results (Experiment Wa7, 13-14 October 1991) are presented in Section 17.1.

The second experimental design was used to further investigate the transition between laminar and transitional flow. The design was a twice replicated 5^1 factorial (3 blocks, 15 runs) with feed flow rate levels of:

35, 40, 45, 50, 55 kg h^{-1}

This experiment was carried out five times as follows:

Experiment Wa9, 15 October 1991; (first four runs only)

Experiment Wa10, 16-17 October 1991

Experiment Wa11, 18-19 October 1991;

De-aeration nozzle SS0002 (diameter 0.99 mm)

Experiment Wa12, 21-22 October 1991;

De-aeration nozzle SS0002

Experiment Wa13, 22-23 October 1991;

De-aeration nozzle SS0002,

Air bleed nozzle SS000009 (diameter 0.2 mm)

The results for Experiments Wa9 and Wa10 are found in Section 17.1. The results for Experiments Wa11, Wa12 and Wa13 are found in Section 36.3. Because of the complex effect liquid loading has on heat transfer, a third design was developed to fully explore the laminar to early turbulent flow region. The third design was a replicated 20^1 factorial (2 blocks) with three replicates of the 110 kg h^{-1} feed flow rate run (43 runs). The feed flow rate levels were:

35, 37.5, 40, 42.5, 45, 50, 60, 70, 80, 90, 100, 110, 120, 130, 140, 150, 160, 170, 180, 190 kg h^{-1}

This experiment was carried out four times:

Experiment Wa19, 12-13 November 1991 (Runs 1-14 only)

Experiment Wa20, 13-14 November 1991 (Runs 1-22 only)

Experiment Wa21, 14-15 November 1991 (Runs 22-43 only)

Experiment Wa22, 15-17 November 1991

The experimental results for Experiments Wa19-Wa22 are presented in Section 17.1.

13.6 Flash Temperature Difference

Three experimental designs were used to determine the effect of feed temperature on evaporative heat transfer. The first was a replicated 7^1 factorial experiment with three extra centre-point replicates (17 runs) with 'flash' temperature differences (feed temperature - product temperature) of:

-4.5, -3, -1.5, 0, 1.5, 3, 4.5 °C

The concentrate flow rate was kept constant at 90 kg/h by varying the feed flow rate. The experiment was carried out once (Experiment Wa4, 5-6 September 1991).

The second experimental design used is shown in Table 13.1. The feed flow rate is a co-variant of the degree of flash. The concentrate flow rate was included as a variable so the effect of a small change in liquid loading could be determined independently. This experiment was carried out once (Experiment Wa5, 10-11 October 1991).

Table 13.1: Second Flash Experiment Levels and Replicates			
Flash Temperature Difference, °C	Concentrate flow rate kg h^{-1}		
	80	90	100
-12	2	-	2
-8	1	-	1
-4	1	-	1
0	2	4	2
4	1	-	1
8	1	-	1
12	2	-	2

The third experiment was a replicated 19^1 factorial (two blocks) with three additional centre-point replicates (41 runs). The flash temperature difference levels were:

-12, -10, -8, -6, -5, -4, -3, -2, -1,

0, 1, 2, 3, 4, 5, 6, 8, 10, 12°C

This experiment was carried out three times as follows:

Experiment Wa16, 8-9 November 1991 (Runs 1-17 only)

Experiment Wa17, 9-11 November 1991

Experiment Wa18, 11-12 November 1991 (Runs 1-21 only)

The results for Experiments Wa4, Wa5 and Wa16-Wa18 are presented in Chapter 18.

13.7 Differential Pressure

Two experimental designs were used to investigate the effect of the saturated temperature difference across the tube wall, that is the steam saturated temperature minus the vapour saturated temperature. The first design was a twice replicated (3 blocks) 6^1 factorial (18 runs) with differential pressure levels of 1, 2, 3, 4, 5 and 6 kPa. This experiment was carried out once (Experiment Wa14, 24-25 October 1991) using 0.99 mm diameter de-aeration nozzles.

The second design was a twice replicated (three blocks) 12^1 factorial (36 runs) with differential pressure levels of:

0.5, 1, 1.5, 2, 2.5, 3, 3.5, 4, 4.5, 5, 5.5, 6 kPa

This experiment was carried out once (Experiment Wa23, 17-20 November 1991) using 3.2 mm de-aeration nozzles. The results for Experiments Wa14 and Wa23 are presented in Chapter 19.

13.8 Boiling Temperature

The effect of boiling temperature was investigated with a constant temperature driving force (3 °C) and a constant flash temperature difference (1 °C). The experimental design was a twice replicated (three blocks) 9^1 factorial (27 runs) with boiling temperature levels of: 45, 47.5, 50, 52.5, 55, 57.5, 60, 62.5, 65 °C.

This experiment was carried out once (Experiment Wa24, 20-21 November 1991) and the results are presented in Chapter 20.

13.9 Tube Diameter, Differential Pressure and Flash

To evaluate the effect of tube diameter, a 3^2 factorial design with three centre-point replicates (12 runs) with differential pressures levels of 3, 6 and 9 kPa and flash temperature difference levels of 5, 10 and 15 °C was used. This factorial was carried out on each tube in the Fifth Evaporator (tube length 10 m). The entry liquid loading after flash was fixed for all tubes at 0.73 kg h^{-1} mm^{-1} (0.203 kg m^{-1} s^{-1}). The de-superheating of the steam was not effective during Experiments Wa25-Wa28 so a larger de-superheating water nozzle was installed prior to Experiments Wa29-Wa32. The experiments carried out are tabulated in Table 13.2, and their results are presented in Chapter 21.

Table 13.2: Fifth Evaporator Water Experiments

Experiment Code	Date	Tube Diameter mm
Wa25	22 Feb 1992	48.14
Wa26	22 Feb 1992	22.56
Wa27	23 Feb 1992	39.71
Wa28	23 Feb 1992	48.14
Wa29	24 Feb 1992	48.14
Wa30	25 Feb 1992	22.56
Wa31	25-26 Feb 1992	39.71
Wa32	26 Feb 1992	39.71

14 EXPERIMENTAL PROCEDURE - WATER

The procedure used for the water experiments is outlined below. Each step in the procedure (unless otherwise noted) were carried out automatically using sequencers provided in the operating program.

1. The evaporator was manually assembled in the correct configuration. If the plant had been used for skim milk or sucrose previously, it was cleaned using the CIP program. An acid clean of the steam-side of the calandria was carried out prior to the start of the water experimental programme to remove any scale deposits.
2. All solenoid and control valves were set to a desired condition and the position of certain critical valves was monitored.
3. Soft water was supplied to the feed balance tank to maintain the level within a desired range.
4. The feed and concentrate pumps were turned on using a procedure which first checked that liquid was available to the pumps, and then after starting the pumps, checked that the pumps were functioning correctly.
5. The vacuum pump was started.
6. When the condenser pressure was less than 10 kPa absolute, the third effect steam valve was opened to 50% to warm up the calandria. Steam was also supplied to the plate heat exchanger to preheat the feed to 60°C.
7. Five minutes later the plant controllers were set at the default set-points and put on automatic.
8. The low pressure side of the differential pressure lines were manually bled to remove water from the lines.
9. Once the process variables were within the set limits around the set-point, the plant was switched to the first run's operating conditions and held for a minimum of three hours.
10. The plant was maintained at steady state for a 30-min period[1] which was deemed to be the sampling period for the run. The data, presented in Appendix A, are mean values for the steady state period.
11. The conditions were then switched to the next run conditions and held for 30 min prior to switching back to step 10.
12. When all the runs were completed, the plant was automatically shutdown.

The status of the plant was monitored during the run and if any abnormal event occurred, the operating computer was programmed to take appropriate action.

---

[1]For all Fifth Evaporator experiments (Wa25-Wa32 & Su6-Su11) the steady state period was 15 min.

15 WATER STEADY STATE EXPERIMENTS

The standard operating conditions for the steady state runs are found in Section 13.1.

15.1 Results

The plant was left running at steady state overnight on several occasions. Figure 15.1 shows the effect of variations in the steam supply quality and ambient conditions on the evaporation rate for Experiment Wa2. Likewise Figures 15.2 and 15.3 show the variations experienced during Experiment Wa8 and Experiment Wa15 respectively.

15.2 Discussion

The purpose of the steady state trials was to determine the likely variation in evaporation due to background load changes. Figure 15.1 shows the environmental conditions before an effort was made to minimise disturbances. In early September the control of main steam pressure was poor due to large fluctuations in load. With the assistance of the boiler operator, some of these load fluctuations were removed or reduced. The steam pressure and quality were dependent on the source of the steam, the main boiler or the steam generator. The main boiler was generally used only during the day, five days a week. The main uncontrollable fluctuations in steam load also occurred during this period. Thus it was decided to do the water experiments either during the night or over weekends, when the steam supply pressure and quality was reasonably constant.

The steam supplied to the evaporator passed through a pressure regulator which reduced the pressure to 650 kPa gauge to reduce the pressure fluctuations. This steam was used directly by the DSI unit. The steam pressure was reduced further to 200 kPa gauge before entering the steam header. The steam supply to the calandria was drawn from the header. This ensured reasonable pressure control except after a boiler failure (see Figure 15.2) but did not ensure a constant steam quality.

The ambient air temperatures at the top, bottom and middle (steam entry) of the calandria were monitored during all experiments. For Experiment Wa2 the ventilation fans for the tower were automatically switched off at 2200 h which caused the air temperature at the steam entry section to rise. The fans control system was modified to ensure that the ventilation remained on overnight before Experiment Wa8. However, the fans were

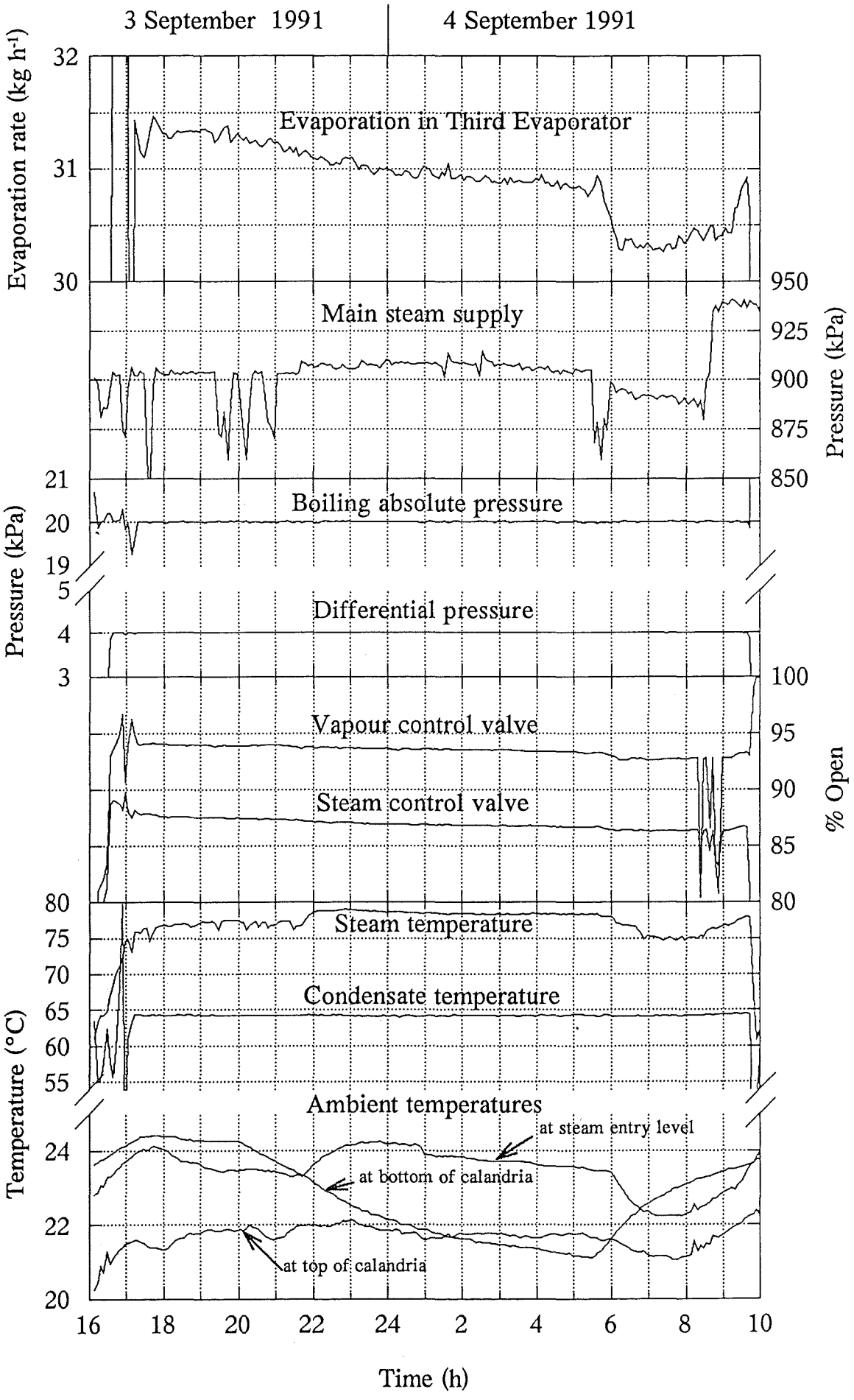

Figure 15.1: Steady State Experiment Wa2 Results.

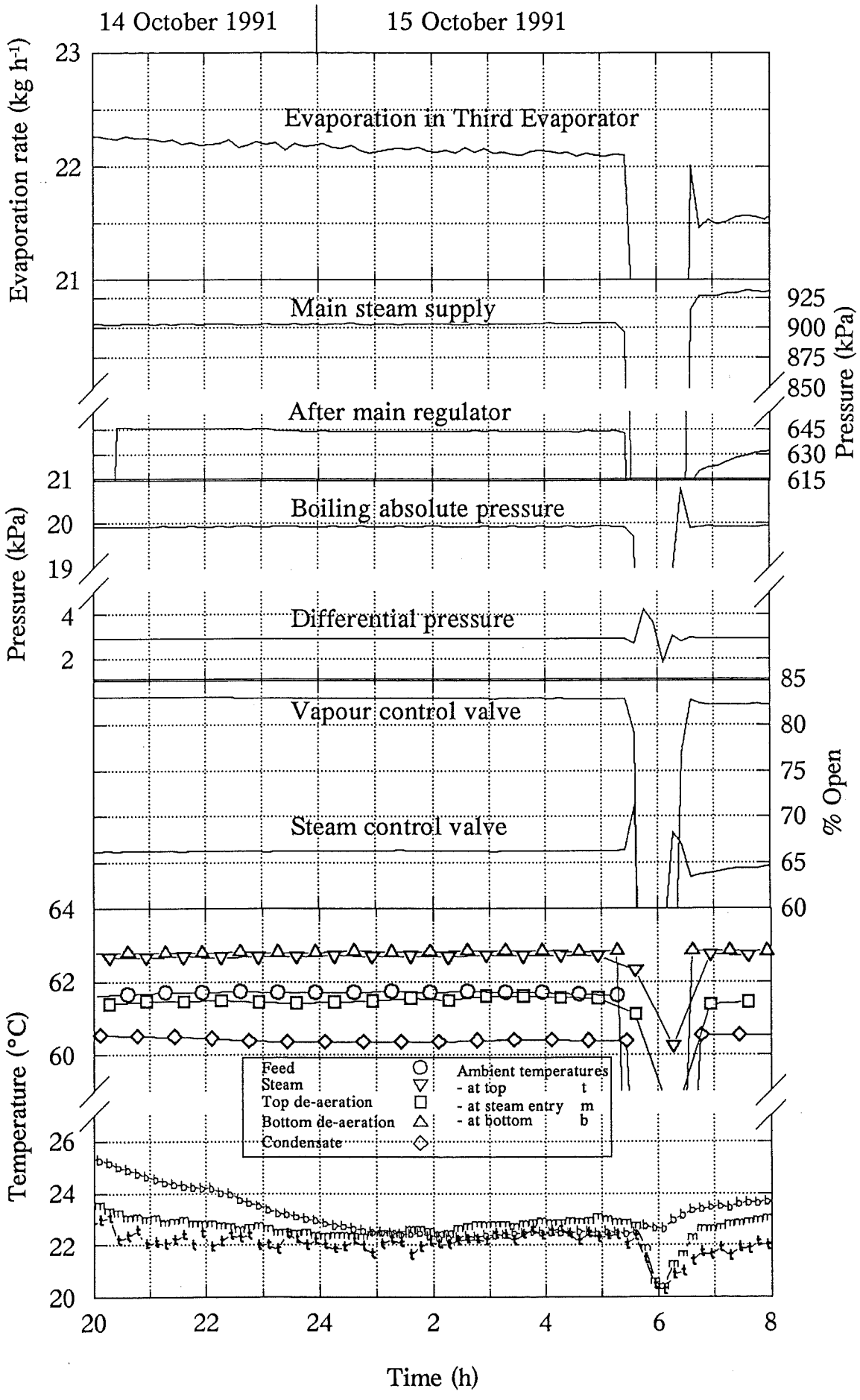

Figure 15.2: Steady State Experiment Wa8 Results.

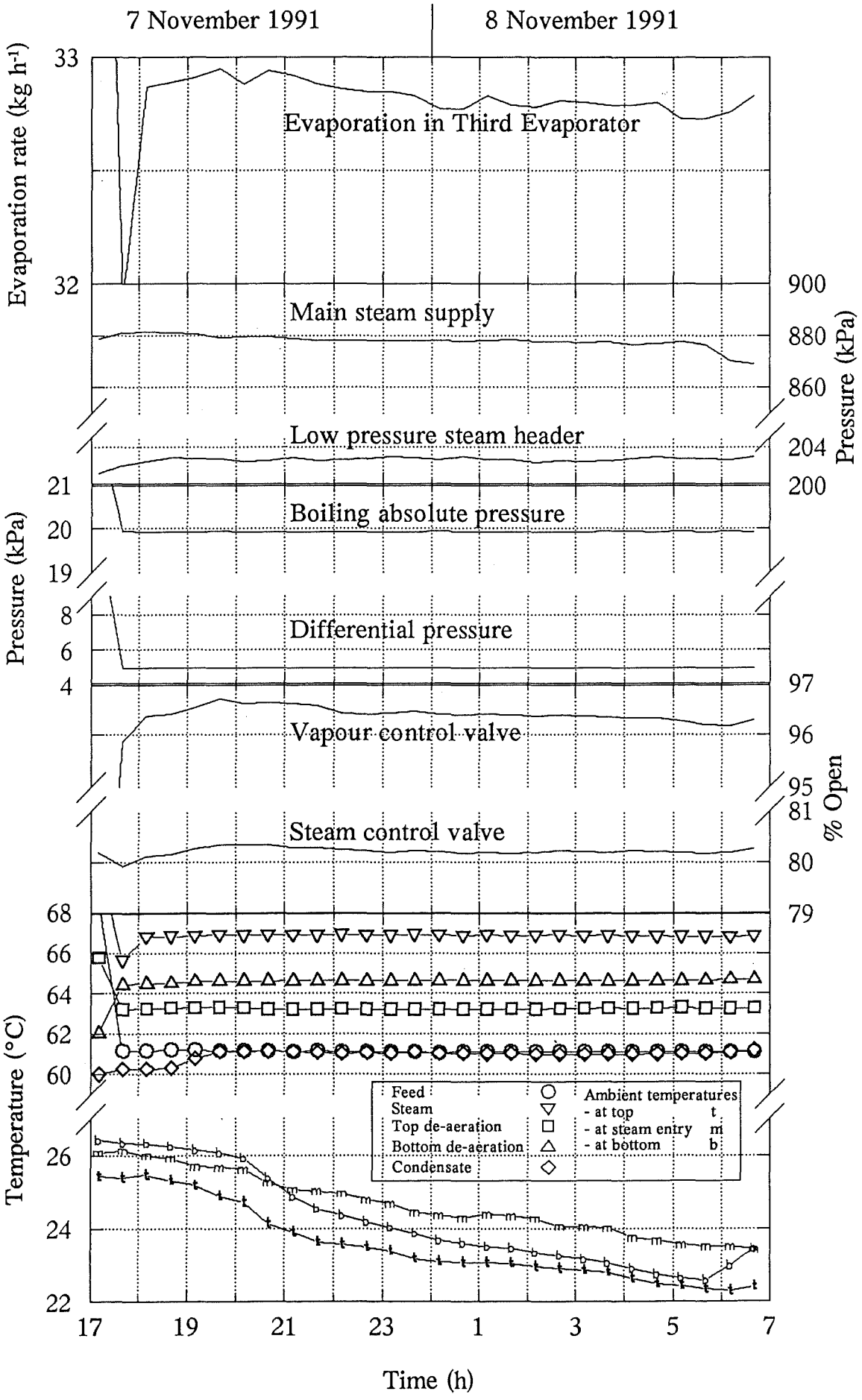

Figure 15.3: Steady State Experiment Wa15 Results.

sometimes manually switched off at the end of the working day so not all water experiments after this date had continuous tower ventilation.

Modifications were made to the steam de-superheat system in early October 1991 (before Experiment Wa5) to reduce the superheat. In September 1991 (see Figure 15.1) the superheat was $>10°C$, whereas in November 1991 the superheat was $<2°C$ (see Figure 15.3). The differential pressure measurement method was changed in late September 1991. The new transmitters had vertical "free draining" lines running down to the plant tapping point. When the plant pressure was increased rapidly, water was sucked up the suction-side line and remained there. When the vacuum was drawn, the water drained very slowly from the lines. To speed up the process, a pulse of air was bled into the suction leg at the transmitter end to blow out the water. This was done at the start of all experiments. The effect of the air pulse can be seen in Figure 15.3.

The condensate temperature was about 2°C lower than the bottom de-aeration temperature. This is probably due to a combination of the following factors. First, the mean condensate film temperature will be lower than the steam temperature. Second, there was a small level of concentrate (50 mm) at the bottom of the calandria, which would be cooled (slightly) by heat transfer to the boiling film. Third, the surface temperature probe was attached to the calandria shell about 20 mm above a large flange. Heat loss from this flange may have reduced the surface temperature measured by the probe.

The uncertainty of the overall HTC values calculated from the measured parameters was determined to be $\pm$ 100 W m^{-2} K^{-1} (see Appendix B) for Experiment Wa2 and $\pm$ 75 W m^{-2} K^{-1} for Experiment Wa8 and Wa15. The variation in evaporation rate during Experiment Wa15 (ignoring the first hour) was 0.25 kg h^{-1}, which corresponds to variation in overall HTC of approximately $\pm$ 15 W m^{-2} K^{-1}. Given the replication carried out within each experiment, the effects of ambient temperature and steam supply conditions are unlikely to affect the accuracy of the conclusions drawn in this work.

A steady state run on skim milk is reported in Chapter 30.

16 WATER 3^3 FACTORIAL EXPERIMENTS

The experimental design and standard operating conditions for these experiments are found in Chapter 13.

16.1 Results

The raw data for the 3^3 factorial experiments (Wa1, Wa3 and Wa6) are tabulated in Appendix I. The overall HTC in terms of the independent variables for Experiment Wa6 is plotted in Figure 16.1. A stepwise multiple linear regression analysis of the data from Experiment Wa6 using SAS (VMS SAS Production Release 5.18. SAS Institute Inc., Cary, North Carolina, USA) revealed that the following variables were significant:

Variable	Confidence Level
ΔT_U	0.0003
T_{boil}	0.0001
Γ_e	0.0001
ΔT_U^2	0.0021
Γ_e^2	0.0001

There were no significant interactions between the independent variables.

16.2 Discussion

Experiments Wa1 and Wa3 were carried out before the instrumentation of the Third Evaporator was complete. In Experiment Wa1 the feed temperature was measured immediately after the plate heat exchanger, and thus the feed line temperature drop was not allowed for. Before Experiment Wa6, the differential pressure measurement was upgraded (see Section 4.12) and the level measurement system modified. The results obtained confirmed that all the independent variables were significant and that the response with respect to liquid loading and possibly temperature driving force was non-linear. The effect of each of the three variables was investigated independently (see Chapters 17, 19 and 20).

This type of experiment is useful in determined what variables are significant and the magnitude of the effect. However, the danger in fitting a response curve to data from a statistical experiment of this type, is demonstrated by the complex effect of liquid loading (see Chapter 17).

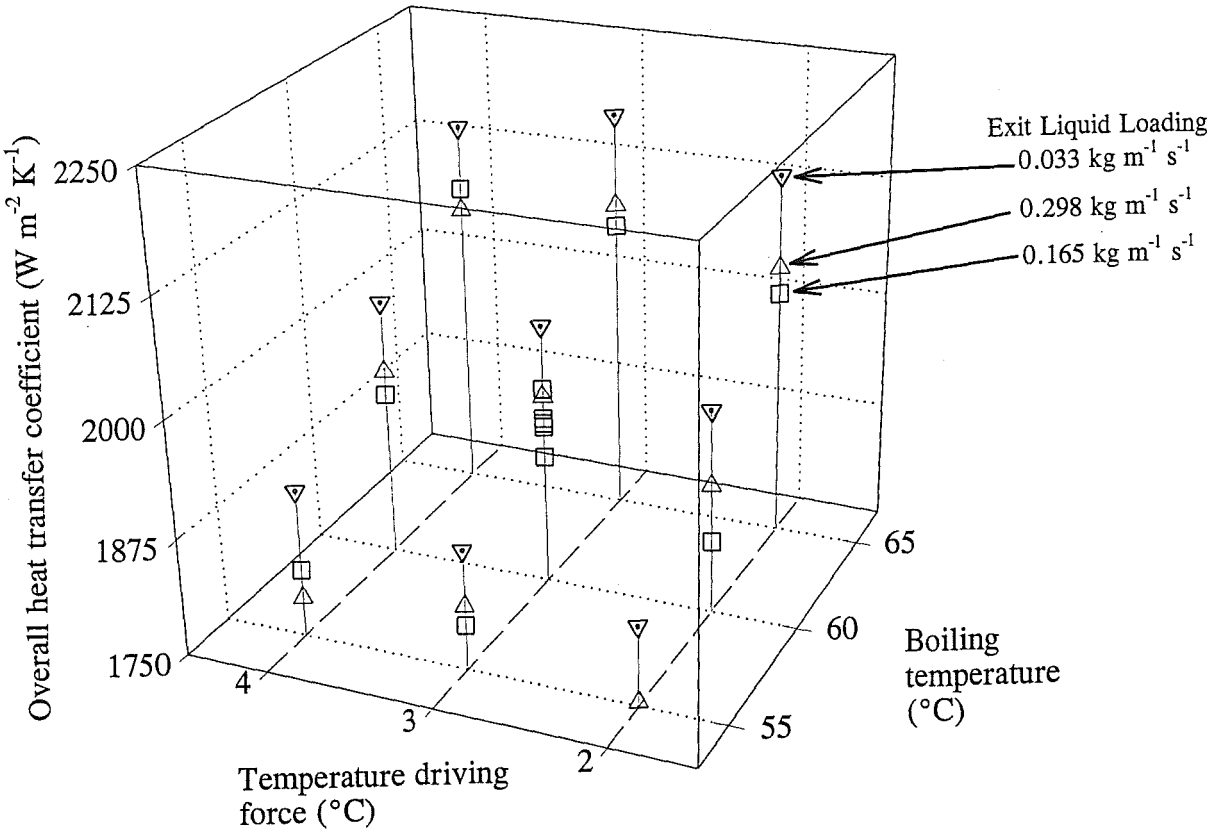

Figure 16.1: 33 Factorial Experiment Wa6 Results.

17 WATER LIQUID LOADING EXPERIMENTS

The experimental design and standard operating conditions for these experiments are found in Chapter 13.

17.1 Results

The raw data for the liquid loading experiments (Wa7, Wa9-10 and Wa19-22) are tabulated in Appendix I. The overall HTC in terms of entry liquid loading is shown in Figure 17.1. The boiling film modified Nusselt number, $\bar{Nu}_e$ is plotted against $\bar{Re}_e$[2], (which coincides with the liquid loading) for Experiments Wa9-Wa10 and Experiments Wa19-Wa22 in Figure 17.2 along with a fitted curve which has a r^2 of 0.866:

$$\bar{Nu}_e = c_0 + c_1\bar{Re}_e + c_2\bar{Re}_e^2 + c_3\bar{Re}_e^3 + c_4\bar{Re}_e^4 + c_5\bar{Re}_e^5 + c_6\bar{Re}_e^6 + c_7\bar{Re}_e^7 + c_8\bar{Re}_e^8 \qquad (17.1)$$

Where $c_0 = 0.3453$, $c_1 = -0.0009214$, $c_2 = 2.1281\times10^{-6}$, $c_3 = -2.8252\times10^{-9}$, $c_4 = 2.3450\times10^{-12}$, $c_5 = -1.2319\times10^{-15}$, $c_6 = 3.9502\times10^{-19}$, $c_7 = -7.0101\times10^{-23}$, $c_8 = 5.2525\times10^{-27}$

This equation was used only to smooth and average the data to permit comparison with theory in Chapter 10. The Experiment Wa7 data was omitted as it produced abnormally low HTCs. The de-aeration temperatures indicate that there was no difference in the air concentration in the steam, and the plant was cleaned with nitric acid before the run. The plant was cleaned again after Experiment Wa7 and the evaporation achieved in Experiment Wa8 (see Figure 15.2) was similar to that found in Experiment Wa9. The second half of Experiment Wa22 data ('g' points on Figure 17.2) were lower than those obtained during the first half ('f' points) for some unknown reason. Further experiments carried out at lower de-aeration rates and with deliberate air addition are discussed in Section 36.2.

17.2 Discussion

The predicted curves of Billet (see Section 10.4) and Chun & Seban (see Section 10.3) are shown on Figure 17.3. The Billet curves, sourced from Struve (1969), do not fit the experiment data well. The shape of the plot of the Struve data for refrigerant R11 (see Figure 17.4) does bear a remarkable resemblance to the plot obtained on water.

---

[2]Arithmetic mean of end-point values

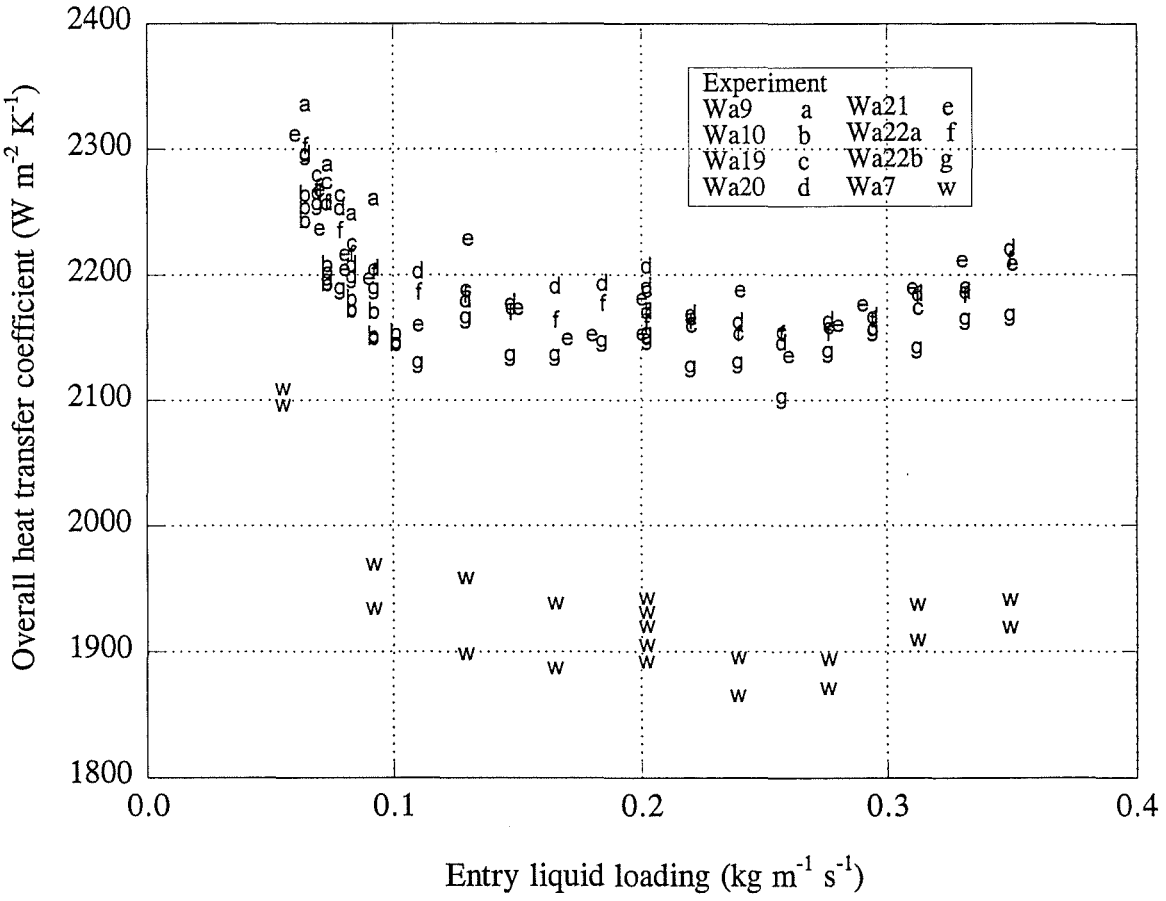

Figure 17.1: Overall Heat Transfer Coefficients for Liquid Loading Experiments.

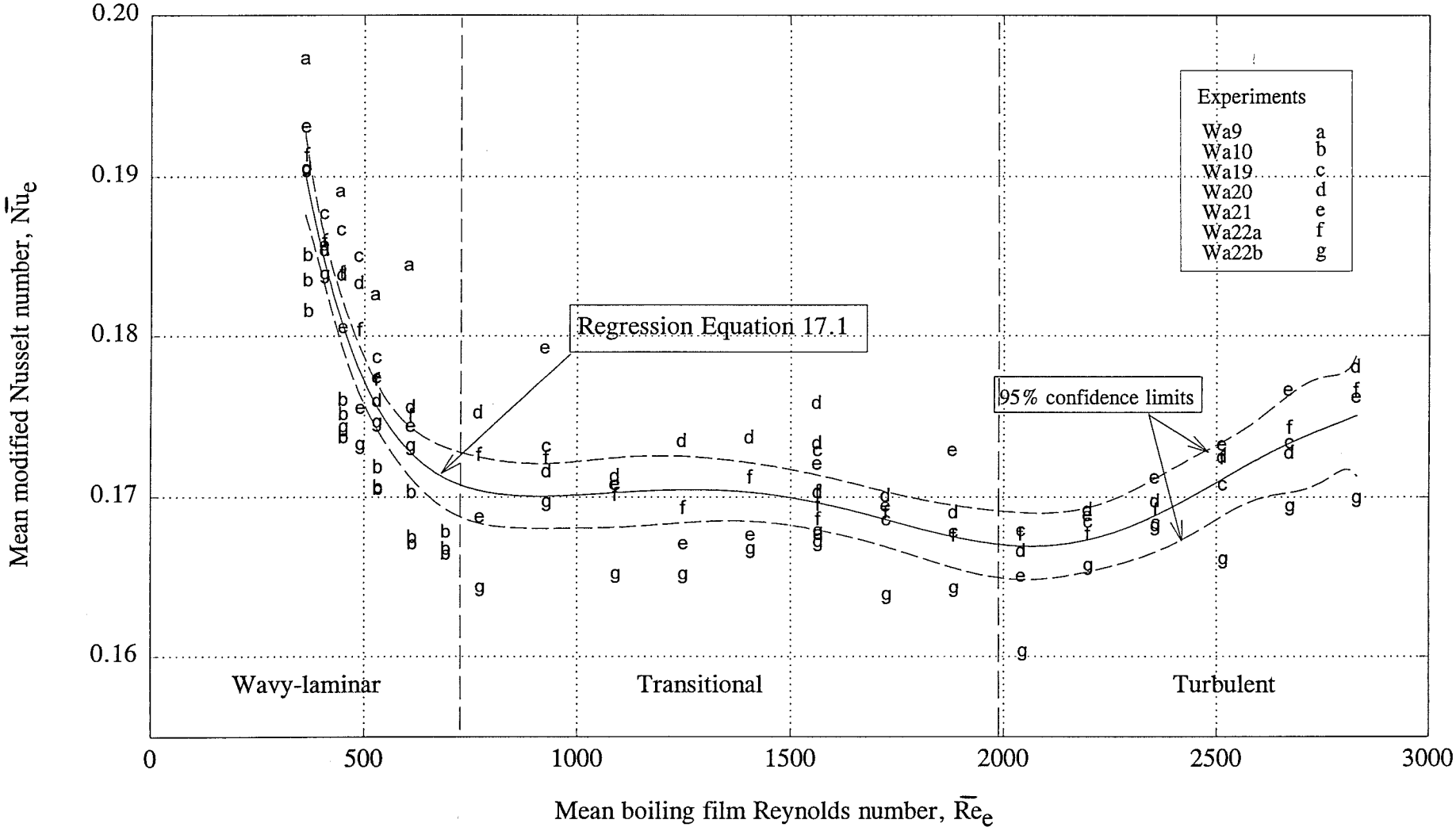

Figure 17.2: Boiling Side Modified Nusselt Numbers for the Liquid Loading Experiments.

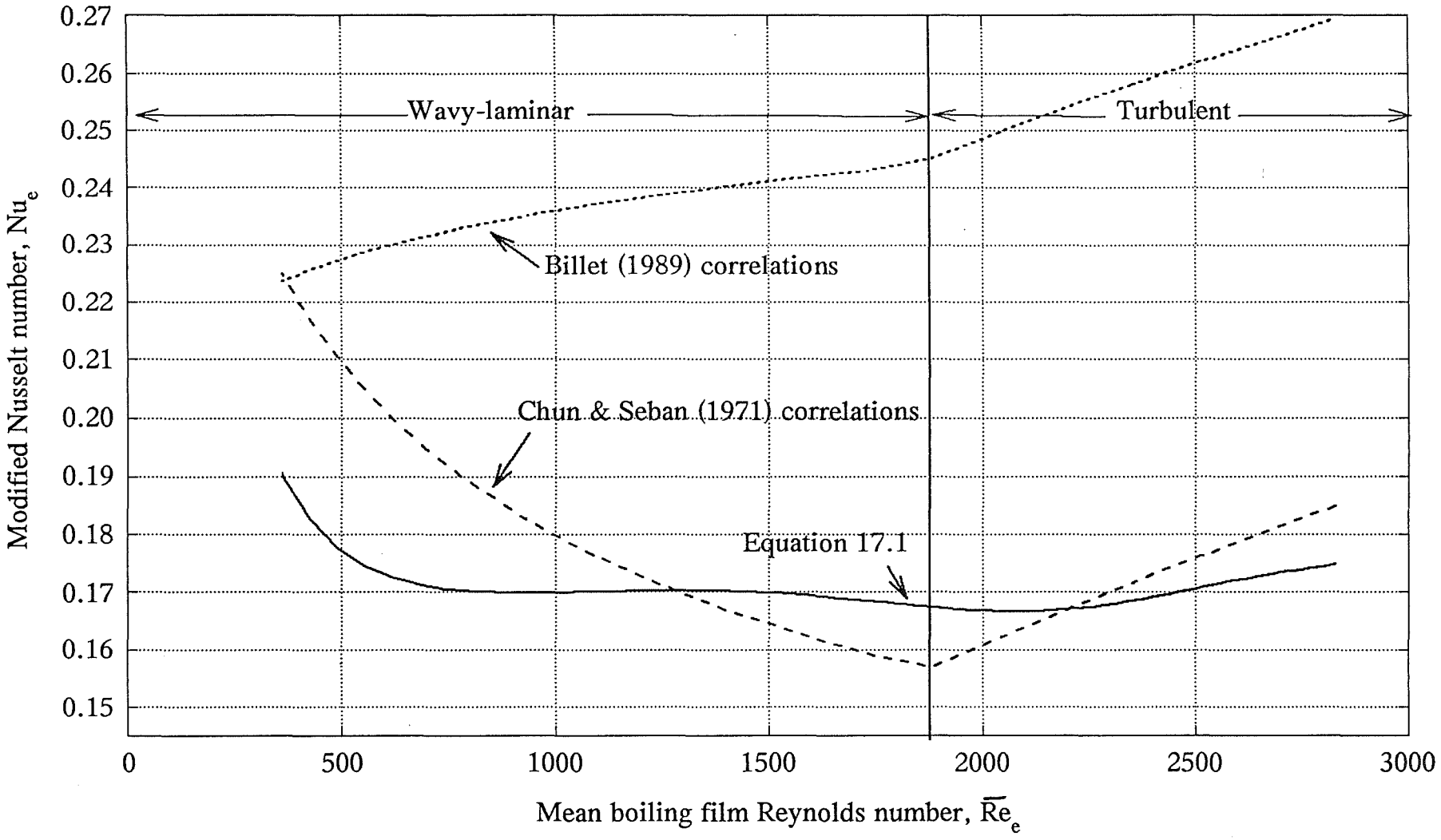

Figure 17.3: Comparison of Billet (1989) and Chun & Seban (1971) Nu_e Correlations with Equation 17.1.

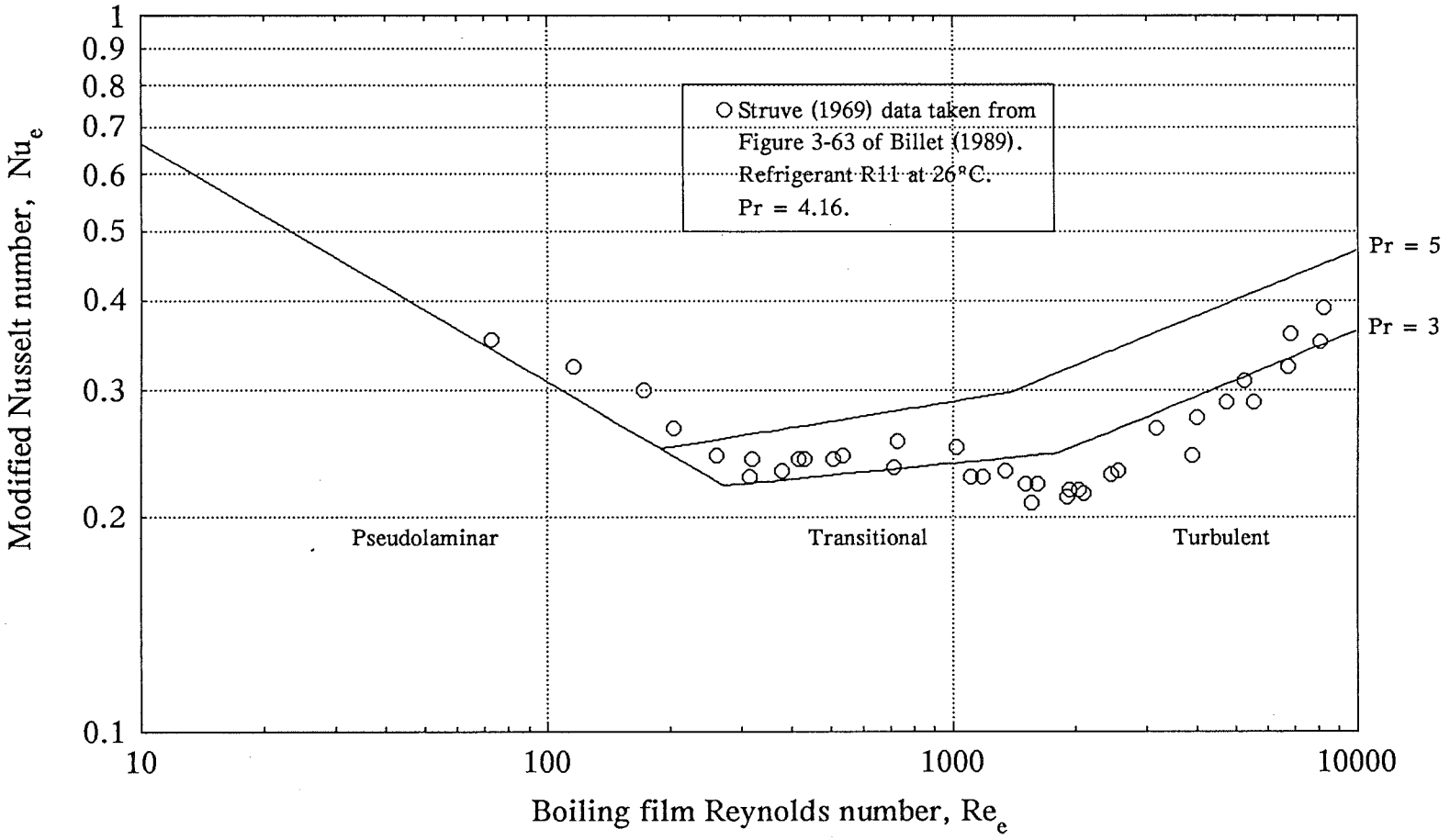

Figure 17.4: Comparison of Refrigerant R11 Data (Struve, 1969) with Billet (1989) Correlations.

Åsblad & Berntsson (1990) commented on the lack of agreement between Struve's data and the equation Struve recommended for turbulent flow. To the author's knowledge, the local maximum observed both in this work and in Struve's data has not been noted previously. The reason for the local maximum is not fully understood at present, but could be due to ripples. Houšová (1970) presented data for the boiling-side HTC for varying feed flow rates but the range of flow rates did not extend as far as the local maximum. Both Struve's data (point values at 1.00 - 1.25 m down a tube) and the mean values obtained here on a 15 m tube exhibit a similarly shaped curve. The reason for Struve's local maximum being at a lower Reynolds number than that obtained in this work, is due to the difference in Prandtl number. Struve also demonstrated the entry effects when adding the fluid to the outside of a tube were dissipated within 1 m. Thus, for the 15 m tube with the assistance of a vapour core, the entrance effects are likely to be insignificant. This is an area for further work, especially when considering viscous non-Newtonian fluids.

As waves start appearing above a film Reynolds number of 30, the boiling film, ignore entrance region effects, only experiences wavy-laminar or turbulent flow (see Figure 17.3). However the experimental data demonstrates that there is a transition zone in the $\overline{Re}_e$ range 700 to 1800. This is recognised by Billet (1989) but the correlation chosen does not fit the data well. The transition appears to indicate a mixture of flow regimes caused by the formation of ripples. The expected steady reduction in Nusselt number in this zone due to increasing laminar film thickness, appears to be balanced by turbulent-like behaviour. The size and mixing action of the ripples appears to dependent on the $\overline{Re}_e$ in a complex way, so that the Nusselt number first increases from the first minimum, and then decreases again to a second minimum point. In practice, the Zazuli correlation used by Chun & Seban (1971) which ignores the transitional zone behaviour, fits the data better than Billet's correlation.

18 WATER FLASH EXPERIMENTS

The experimental design and standard operating conditions for these experiments are found in Chapter 13.

18.1 Results

The raw data for the flash experiments (Wa4, Wa5, Wa16, Wa17 and Wa18) are tabulated in Appendix I. The gross and net evaporation rates in terms of degree of flash (Experiments Wa16, Wa17 and Wa18) are shown in Figure 18.1. The effect of liquid loading and degree of flash on the evaporation rate (Experiment Wa5) is shown in Figure 18.2.

While the mass flow rate leaving the tube was kept constant, the feed flow rate varied during the run. The variation in mean liquid loading with respect to the degree of flash for Experiment Wa17 is shown in Figure 18.3. The steam header pressure was high during Experiment Wa16 (due to a faulty pressure regulating valve) but did not have a significant effect on HTC. The vapour temperature probe mounted above the liquid distributor plate is in contact with the liquid feed and therefore measures the temperature of the feed after flashing (see Figure 18.4).

18.2 Discussion

The gross evaporation rate represents the combined heat transferred to the vapour phase from flashing and from heat transfer through the tube wall. Thus, the gross evaporation rate (see Figure 18.1) increases with increasing degree of flash. For positive degrees of flash, the calculated "net" evaporation rate was determined by subtracting the flash evaporation rate from the gross evaporation rate. For negative degrees of flash, the quantity of steam required to heat the feed to the boiling temperature was added to the gross evaporation rate to obtain the "net" evaporation rate. The "net" evaporation rate is a measure of the heat transferred through the tube wall. Thus, the difference between the gross and net evaporation curves was due to the sensible heat load (for negative degrees of flash) and the flash evaporation (for positive degrees of flash). For positive degrees of flash (up to 12°C), the net evaporation rate was effectively constant, indicating that the change in vapour velocity was not sufficient to affect the heat transfer process.

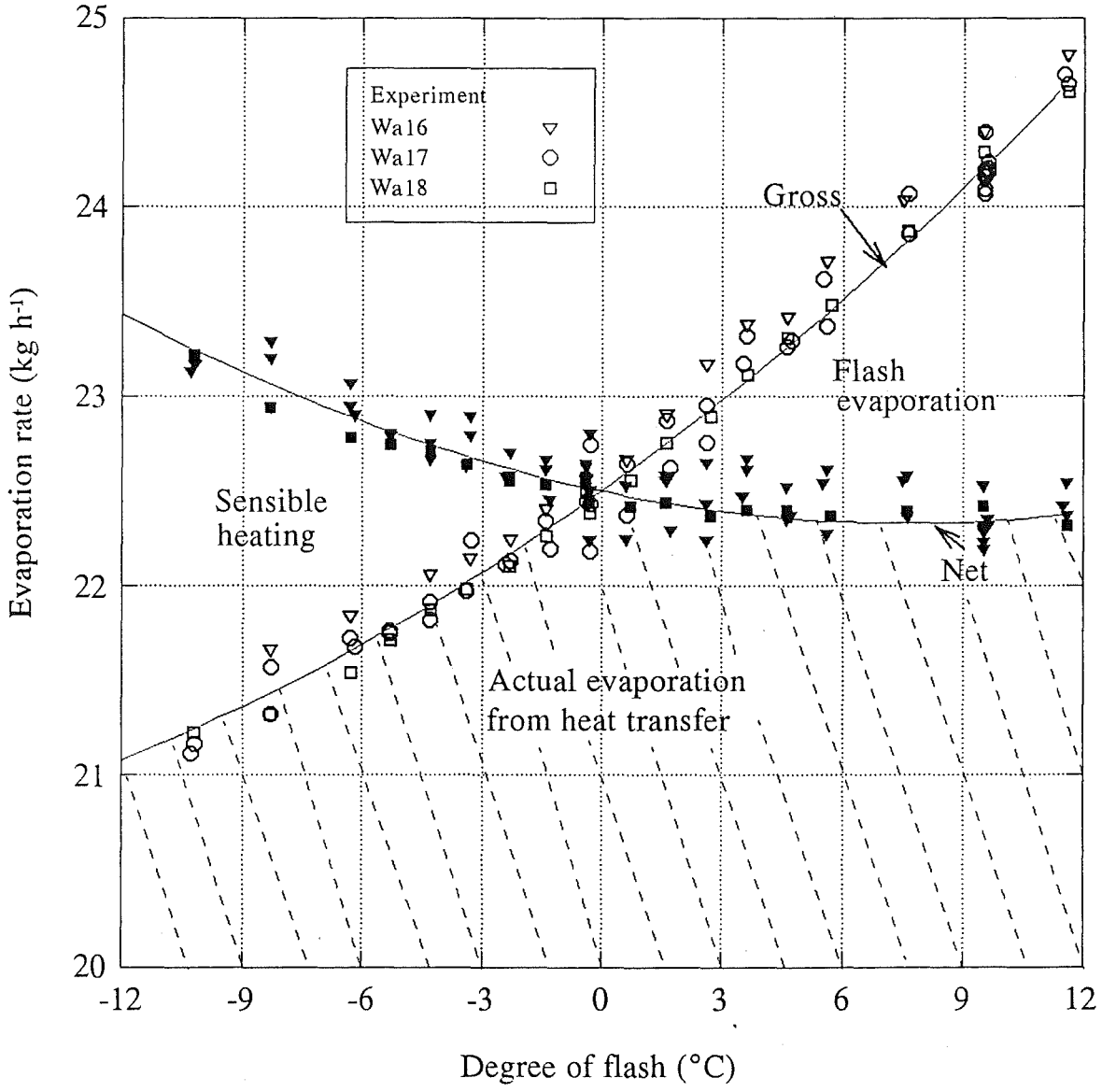

Figure 18.1: Effect of Degree of Flash on Evaporation Rate.

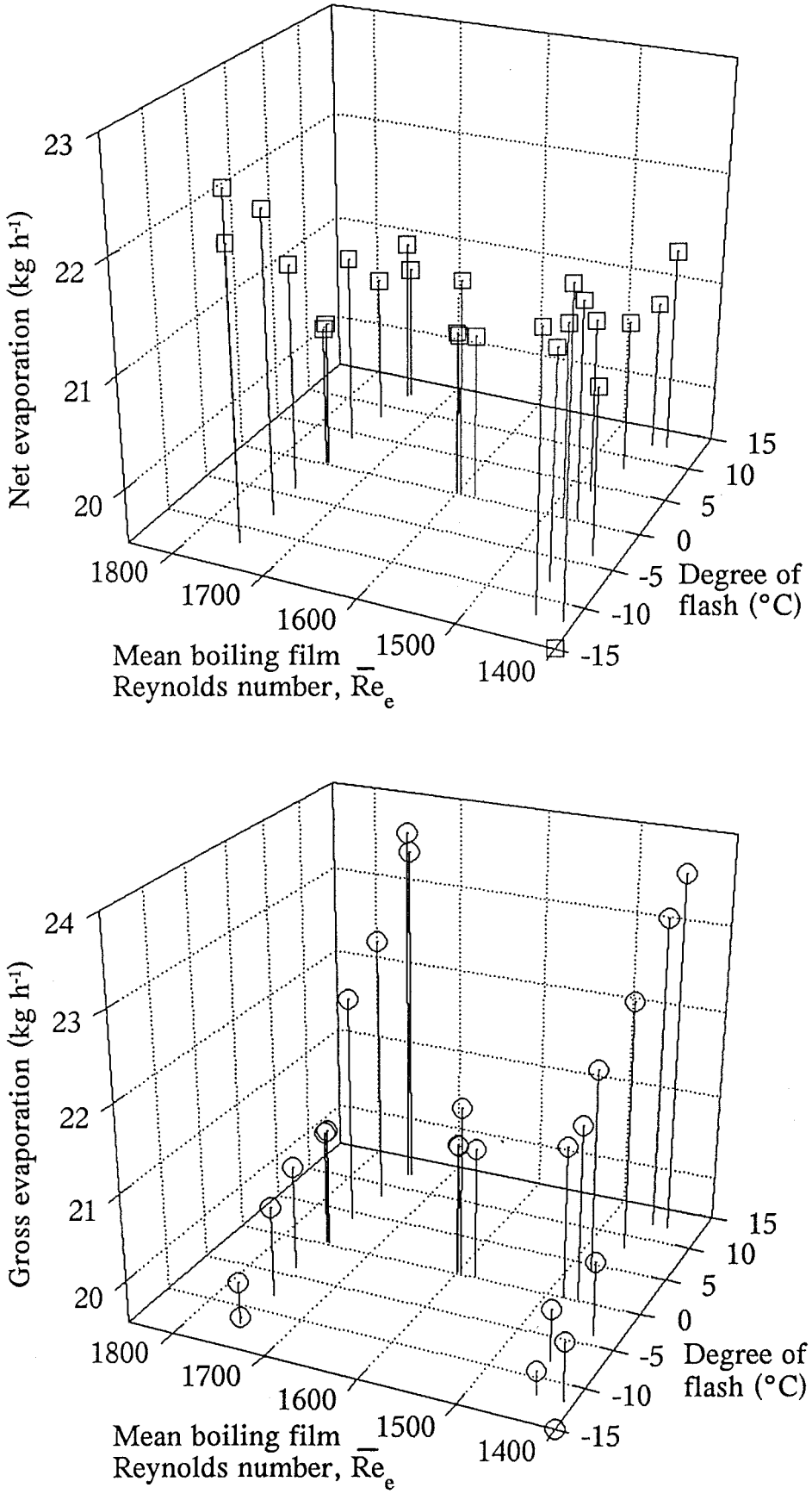

Figure 18.2: Experiment Wa5 Results.

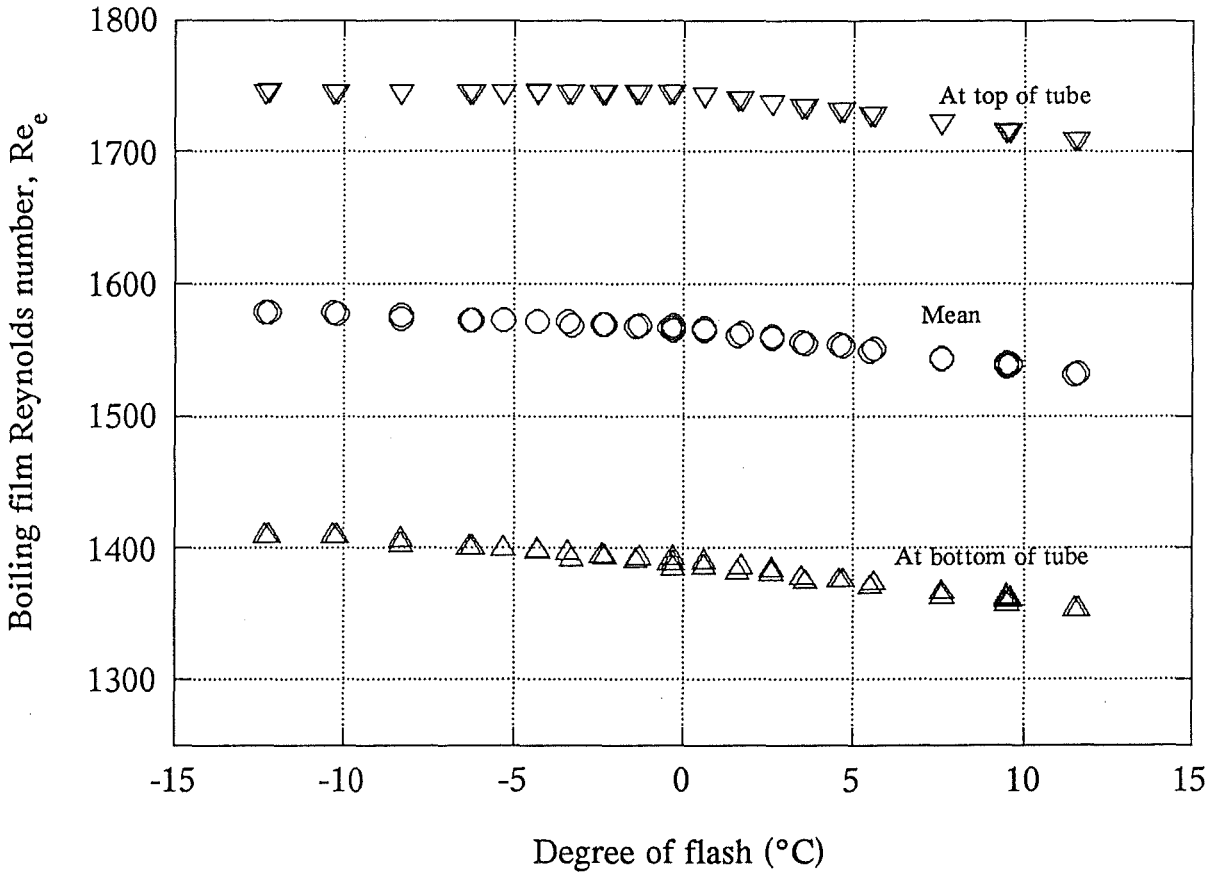

Figure 18.3: Dependence of Boiling Film Reynolds Number on Degree of Flash (Data from Experiment Wa17).

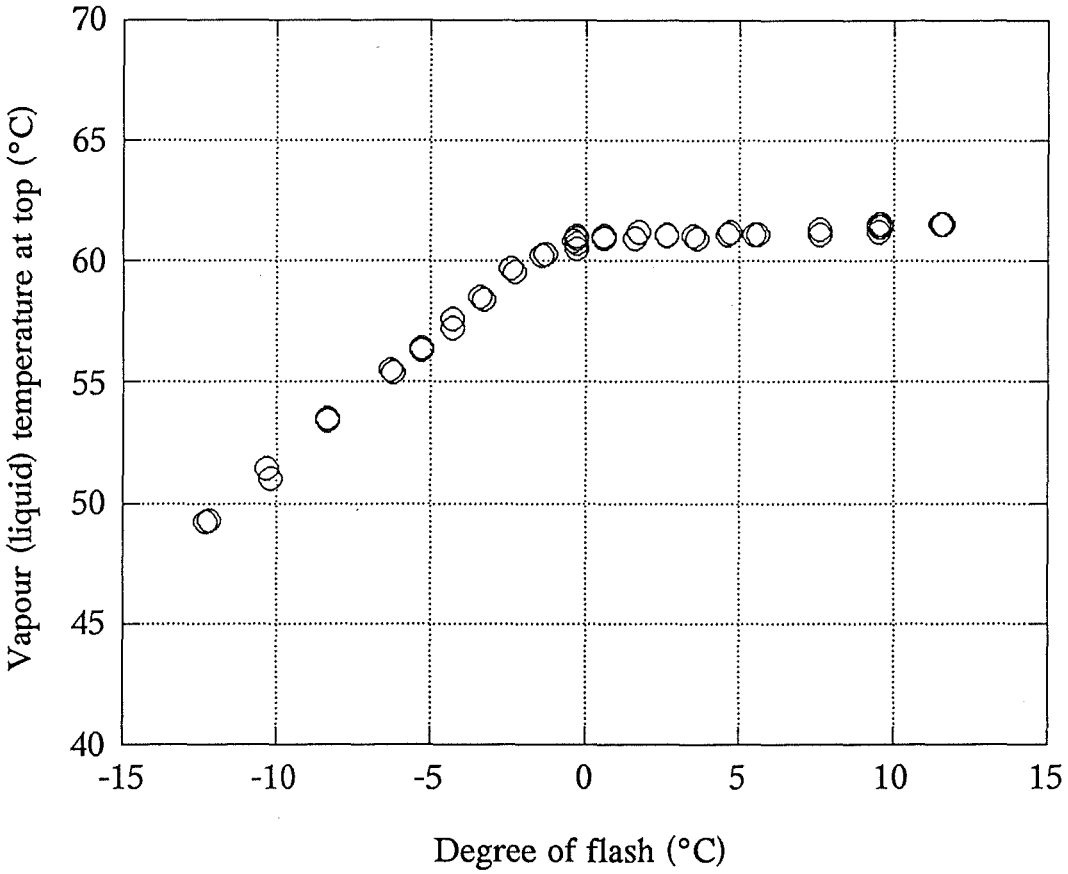

Figure 18.4: Effect of Degree of Flash on Vapour (Liquid) Temperature At Top of Tube (Data from Experiment Wa17).

The effect of vapour velocity on the heat transfer process is discussed further in Chapter 21 where degrees of flash of up to 25°C were investigated. In the sensible heating region (i.e. negative degree of flash) the net evaporation rate increased as the feed temperature dropped. This was due to the increase in the local temperature driving force at the top of the tube as indicated by the measured liquid/vapour temperature (see Figure 18.4) at the top of the tube.

The variation in $\bar{Re}_e$ in Experiments Wa4 and Wa16-Wa18 was slight (see Figure 18.3) and would have an insignificant effect (see Figure 17.2) on the evaporation rate. The average net evaporation rates for each of the concentrate flow rates in Experiment Wa5 were:

Concentrate flow rate, kg h^{-1}	80	90	100
Net evaporation rate, kg h^{-1}	21.36	21.09	21.38

This indicates that there was little change in HTC over the $\bar{Re}_e$ range of 1450 to 1850. This is at variance with Equation 17.1 which predicted that the evaporation rate would rise and then drop as $\bar{Re}_e$ increased from 1450 to 1850. However, the difference is slight and within the expected variation due to ambient and instrument repeatability (see Chapter 15) .

19 WATER DIFFERENTIAL PRESSURE EXPERIMENTS

The experimental design and standard operating conditions for these experiments are found in Chapter 13.

19.1 Results

The raw data for the differential pressure experiments (Wa14 and Wa23) are tabulated in Appendix I. The effect of differential pressure (essentially the temperature driving force) on the evaporation rate is shown in Figure 19.1. As the feed flow rate was fixed, $\bar{Re}_e$ varied with differential pressure (see Figure 19.2) because of the change in concentrate flow rate. The overall heat transfer results from Experiments Wa14 and Wa23 were compared (see Figure 19.3) with values calculated using the Wassner (1981) method (see Appendix F). The Zazuli correction was used to determine $\bar{Nu}_c$. The liquid loading experiment correlation (Equation 17.1) and those of Billet (1989) and Chun & Seban (1971) were used to determine three different predictions of $\bar{Nu}_e$. The de-aeration (venting) rates at each level of differential pressure are shown in Figure 19.4. An estimate[1] of the air concentration entering and leaving the calandria shell is shown in Figure 19.5.

19.2 Discussion

The results obtained at a differential pressure of 6 kPa were high because the boiling pressure for these runs was higher (20.44 - 20.76 kPa absolute) than the desired set-point (20 kPa absolute) due to the limited capacity of the vapour control valve. There was a slight drop in the overall HTC from Experiment Wa23 (see Figure 19.3) as the differential pressure increased from 2.5 kPa to 5.5 kPa followed by a small rise at 6 kPa. This change in slope can be explained solely by the increase in boiling pressure (see Chapter 20) so there was no evidence to support a change to the nucleate boiling regime.

The large variation in the results obtained at a differential pressure of 0.5 kPa was probably due to the increasing inaccuracy ($\pm$19% at 5 kg h^{-1}) of the calculated evaporation rate (determined by difference from the feed and concentrate flow rates).

---

[1] Based on an assumed air leakage rate of 0.018 kg h^{-1} (see Appendix R) and assuming no non-condensable gases in steam supply.

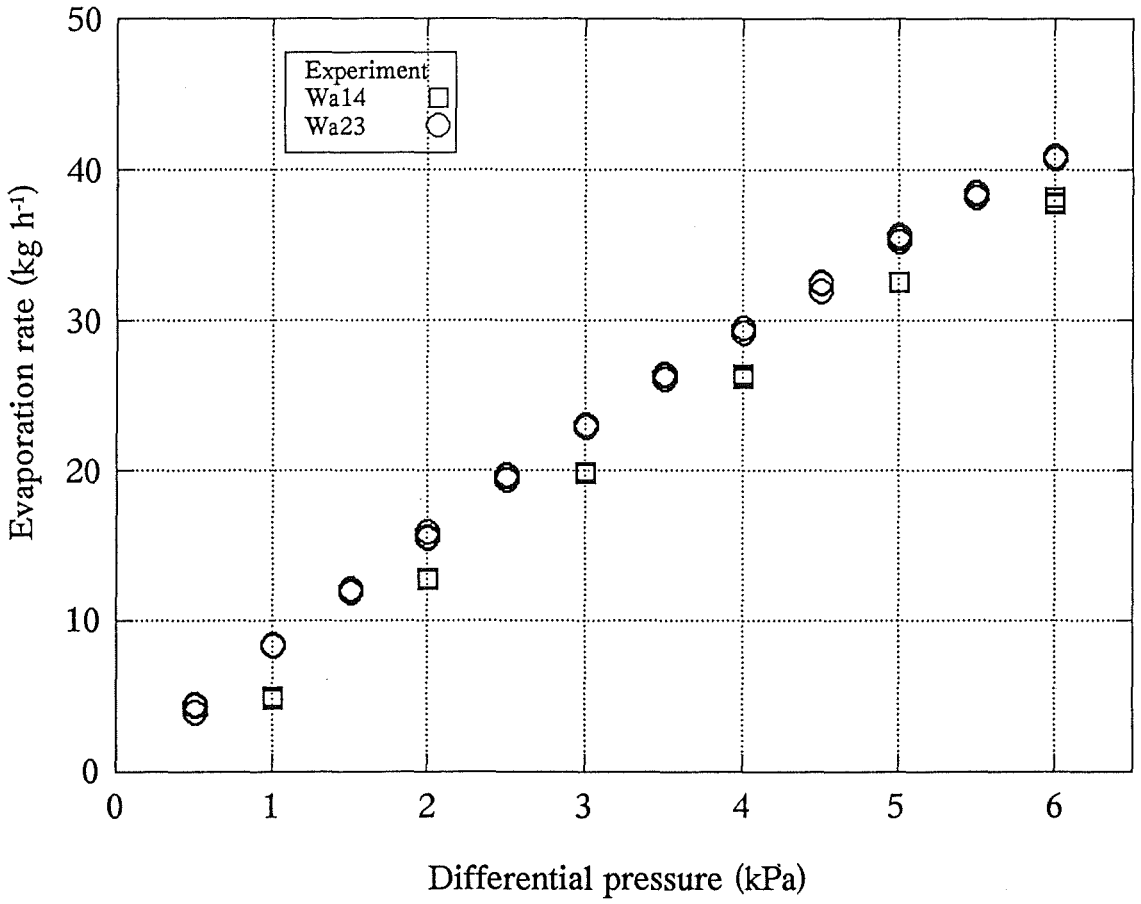

Figure 19.1: Effect of Differential Pressure on the Evaporation Rate.

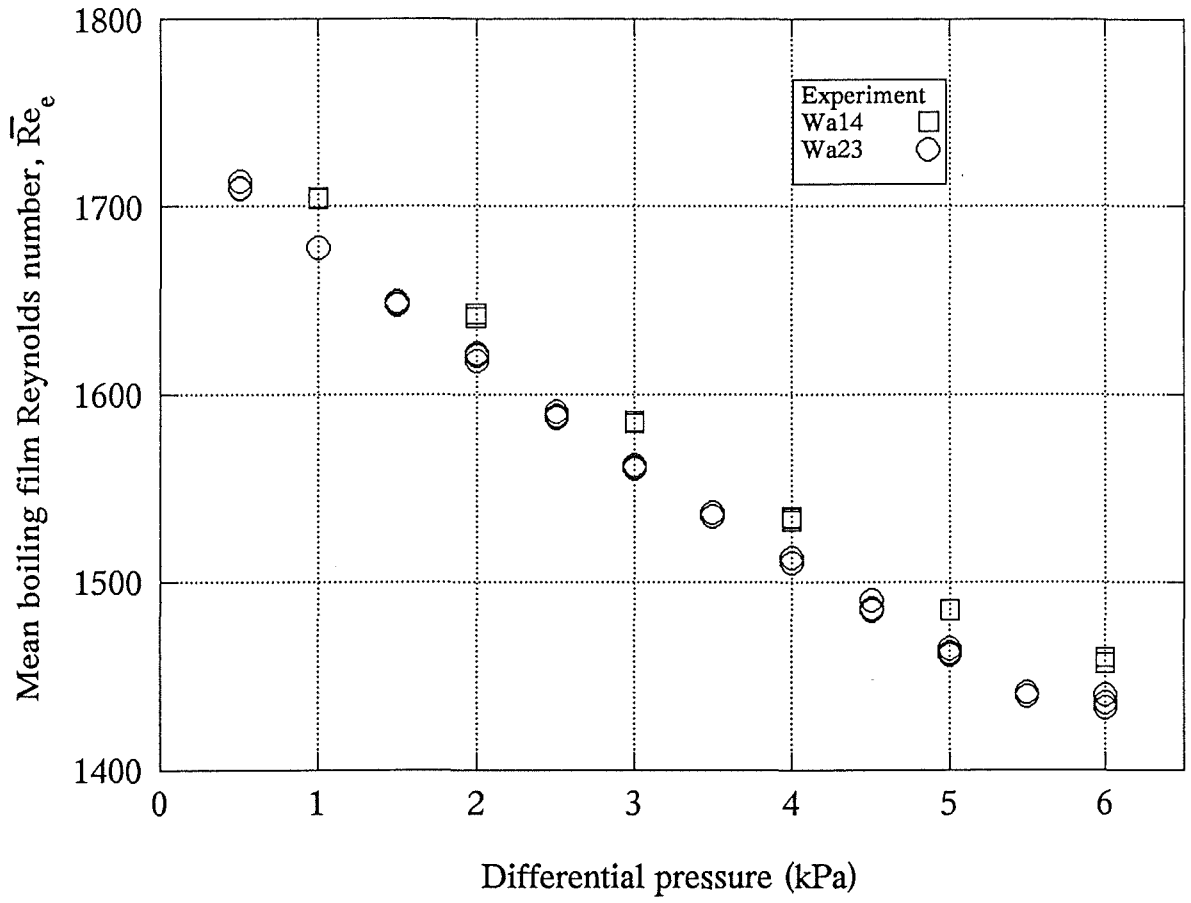

Figure 19.2: Inter-relationship between Differential Pressure and Mean Boiling Film Reynolds Number.

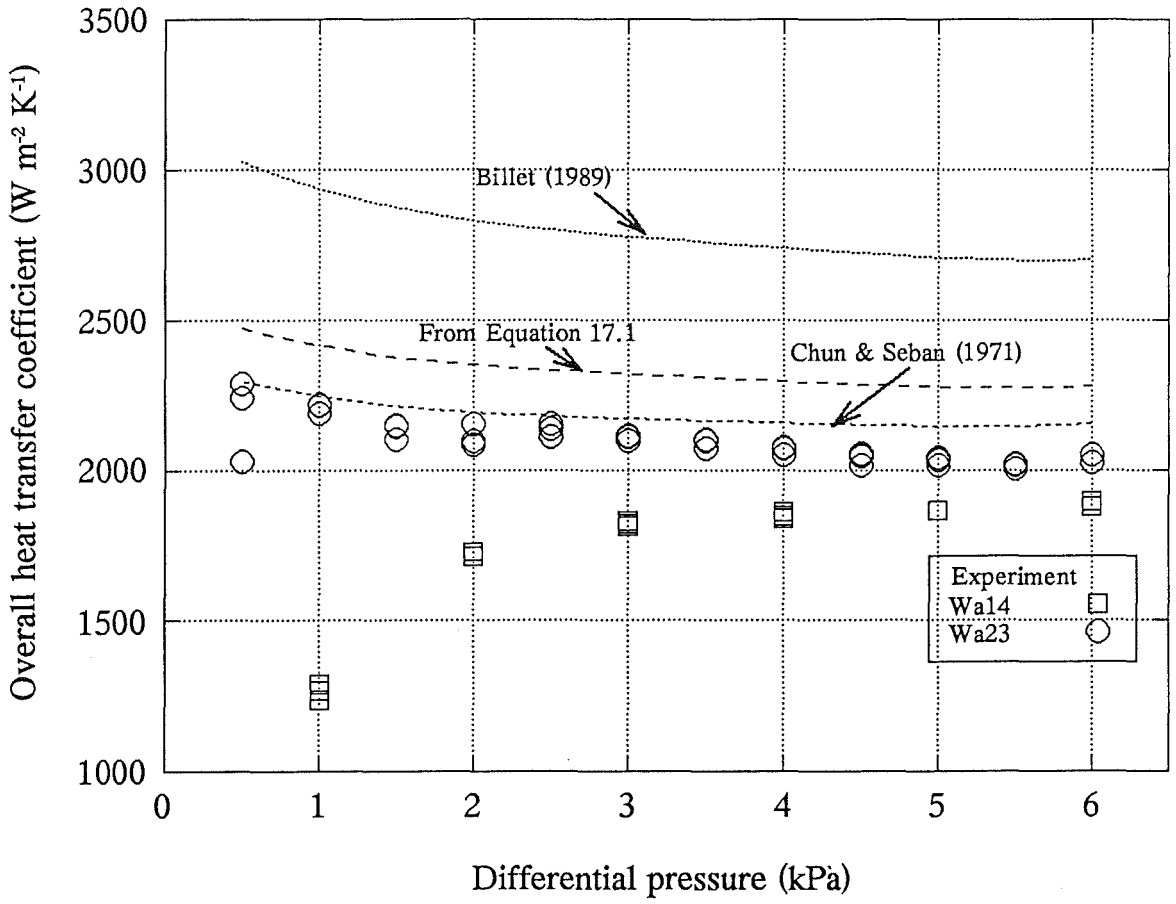

Figure 19.3: Comparison of Differential Pressure Results with the Wetting Factor Curve and the Correlations of Billet (1989) and Chun & Seban (1971).

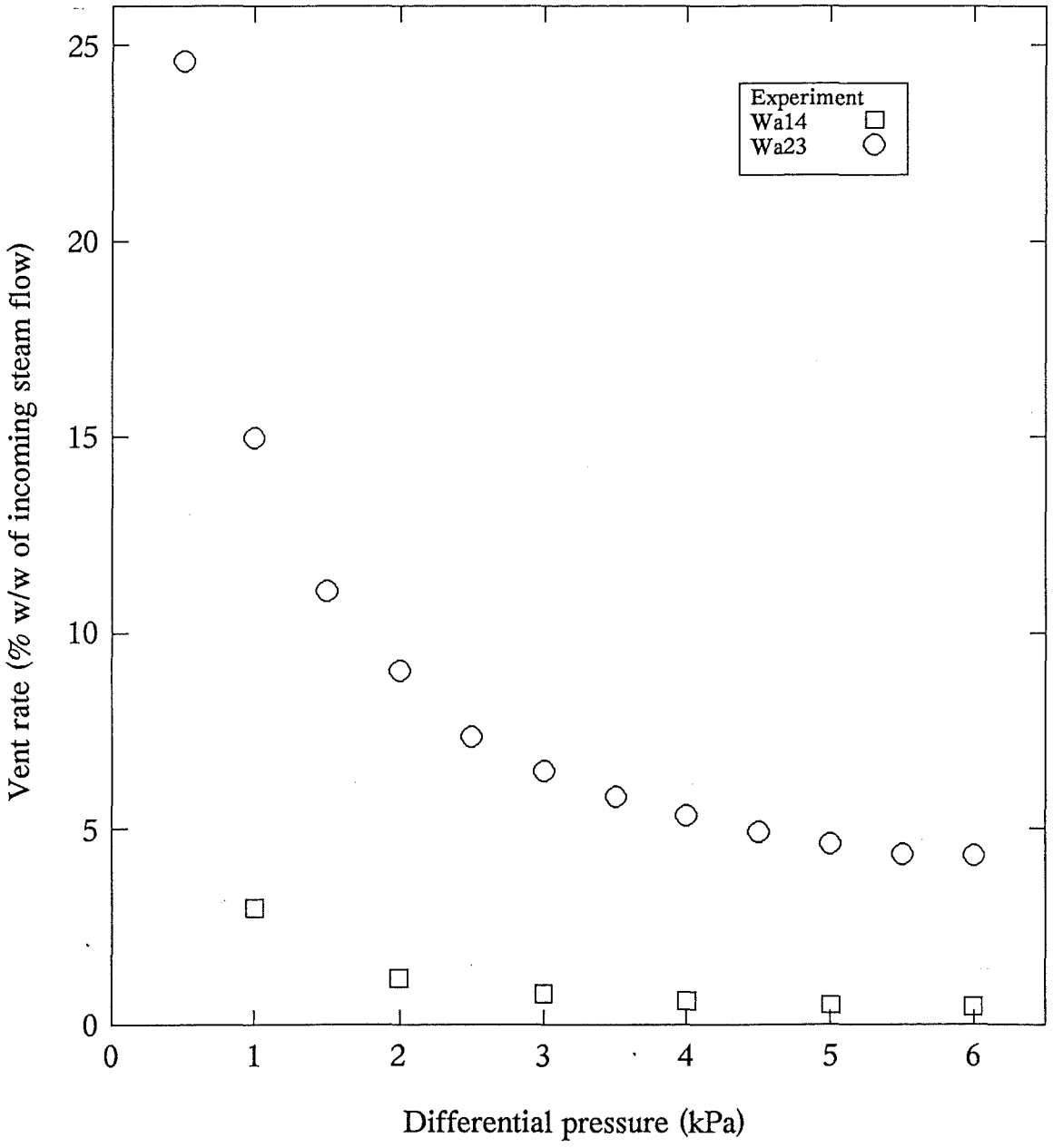

Figure 19.4: Venting rates for Differential Pressure Experiments.

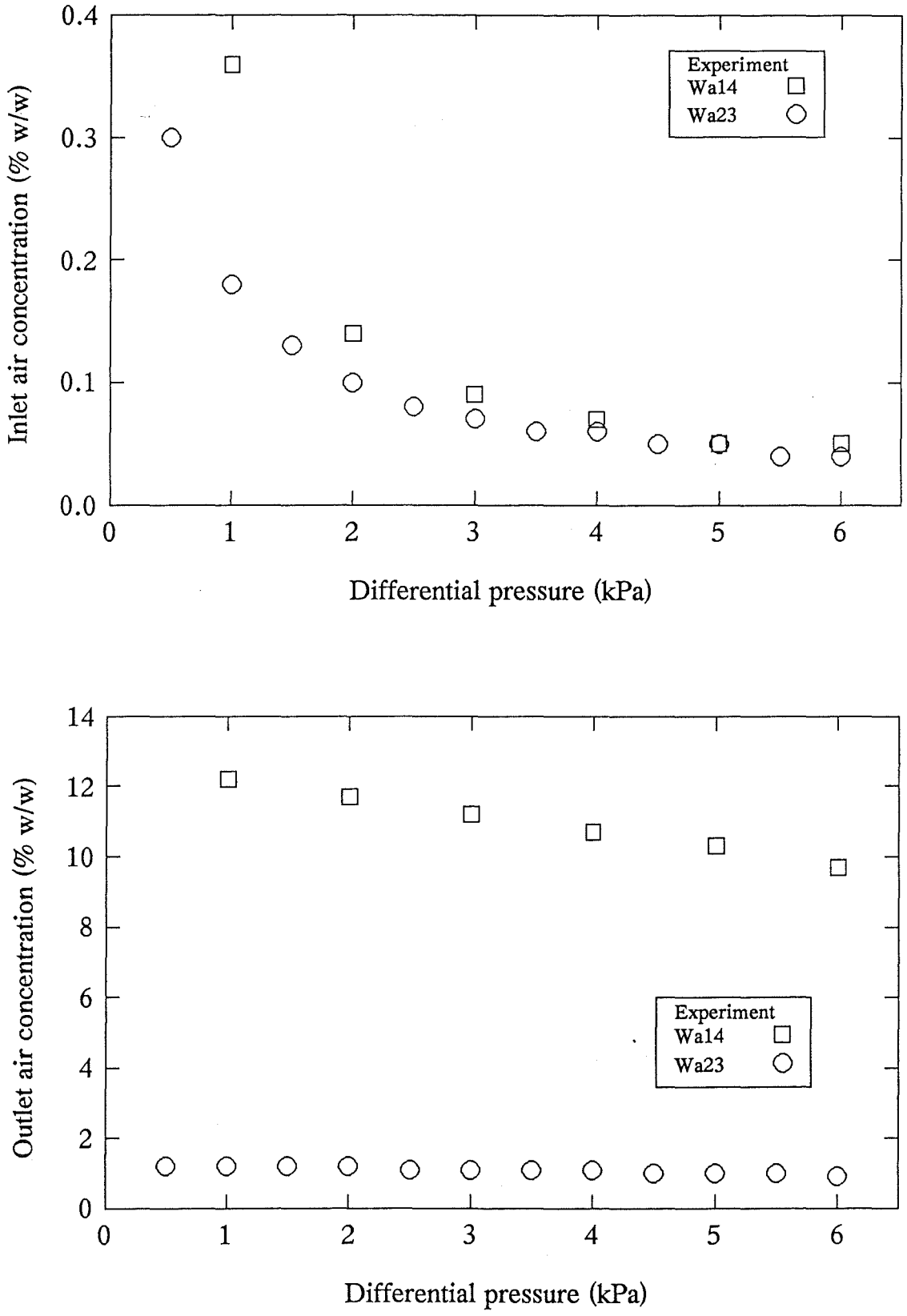

Figure 19.5: Air Concentration in Steam Entering and Leaving Calandria Shell.

The marked difference between the results of Wa14 and Wa23 demonstrated that the de-aeration rate has a major effect on heat transfer at low differential pressures.

Experiment Wa23

For Experiment Wa23, the overall heat transfer coefficient dropped slowly with increasing differential pressure due to the increasing thickness of the condensate film. This was because the change in venting rate (see Figure 19.4) with differential pressure ensured that the outlet air concentration remained steady at about 1% w/w (see Figure 19.5) even when the inlet air concentration decreased from 0.3 to 0.04% w/w. The $\bar{Re}_e$ dropped from 1700 to 1450 over the differential pressure range 0.5 kPa to 6 kPa. Figure 17.2 indicates that $\bar{Nu}_e$ goes through a maximum point in this $\bar{Re}_e$ range which could explain the slight changes in slope at differential pressures of 1.5 kPa and 2.5 kPa. This is not reflected by Equation 17.1 which predicts a gradual decrease in Nusselt number. Chun & Seban predict a decrease and Billet predicts an increase in $\bar{Nu}_e$ (see Figure 17.3) over the same range which explains the slight differences in the slopes of their curves (see Figure 19.3). The difference between the curve generated from Equation 17.1 and the Experiment Wa23 data indicates that perhaps the air leakage rate was about 0.1% w/w higher in Experiment Wa23.

For Experiment Wa23, at differential pressures above 4.5 kPa, the steam was superheated (up to 5°C at 6 kPa). The lack of any sudden change in HTC (see Figure 19.3) at 4.5°C indicates that the presence of superheat had no significant effect on the heat transfer rate.

Experiment Wa14

In Experiment Wa14, with the smaller de-aeration nozzles, the venting rate again decreased (see Figure 19.4) as the differential pressure increased due to the increase in steam pressure. The outlet air concentration (see Figure 19.5) was approximately ten times the level experienced in Experiment Wa23, and steadily decreased with increasing differential pressure. The inlet air concentration at low differential pressures was higher than in Experiment Wa23 due to the reduction in steam flow through the de-aeration ports. The effect of air concentration on heat transfer is discussed in depth in Part IV. Essentially, an air rich boundary layer forms at the condensate film surface, and reduces the steam temperature at the interface. At low differential pressures, this reduction in steam temperature can drastically reduce the overall HTC (see Figure 19.3).

The overall HTC from Experiment Wa14 increased with differential pressure indicating that even at high differential pressures the presence of air was more significant than the condensate film thickness.

20 WATER BOILING TEMPERATURE EXPERIMENT

The experimental design and standard operating conditions for this experiment are found in Chapter 13.

20.1 Results

The raw data for the boiling temperature experiment (Wa24) are tabulated in Appendix I. The overall heat transfer results for Experiment Wa24 are shown in Figure 20.1. The results were compared with values calculated using the Wassner (1981) method (see Appendix F). The Zazuli correlation for condensation was used to determine $\bar{Nu}_c$. The liquid loading experiment correlation (Equation 17.1) and those of Billet (1989) and Chun & Seban (1971) were used to determine three different predictions of $\bar{Nu}_e$.

20.2 Discussion

The overall HTC was found to increase with boiling temperature. This was expected because as the temperature of the water increases, the thermal conductivity increases and the viscosity decreases. These factors clearly out weigh the potential increase in film thickness due to a reduction in liquid density.

The measured HTC data were lower than predicted by Equation 17.1 which suggests that the air ingress rate was about 0.1% w/w higher for Experiment Wa24. The measured data had a steeper slope with respect to boiling temperature than predicted by any of the curves. This was probably due to three factors.

- The greater effect of non-condensable gases at lower pressures due to the non-linear relationship between saturated steam pressure and temperature (see Table J1, Appendix J). That is, the presence of a fixed molar percentage of non-condensable gas in steam will drop the saturated steam temperature more at a lower total pressure.
- An increased air leakage rate at lower pressures. While the flow through any leakage point will be sonic, the orifice coefficient will vary as the pressure ratio changes (see Appendix K) and, in addition, as the pressure drop increases the cross-sectional area of leakage points could increase.
- The effect of the boiling film Reynolds number. The $\bar{Re}_e$ increased linearly from 1230 to 1650 as the temperature increased from 45°C to 65°C. The variation in

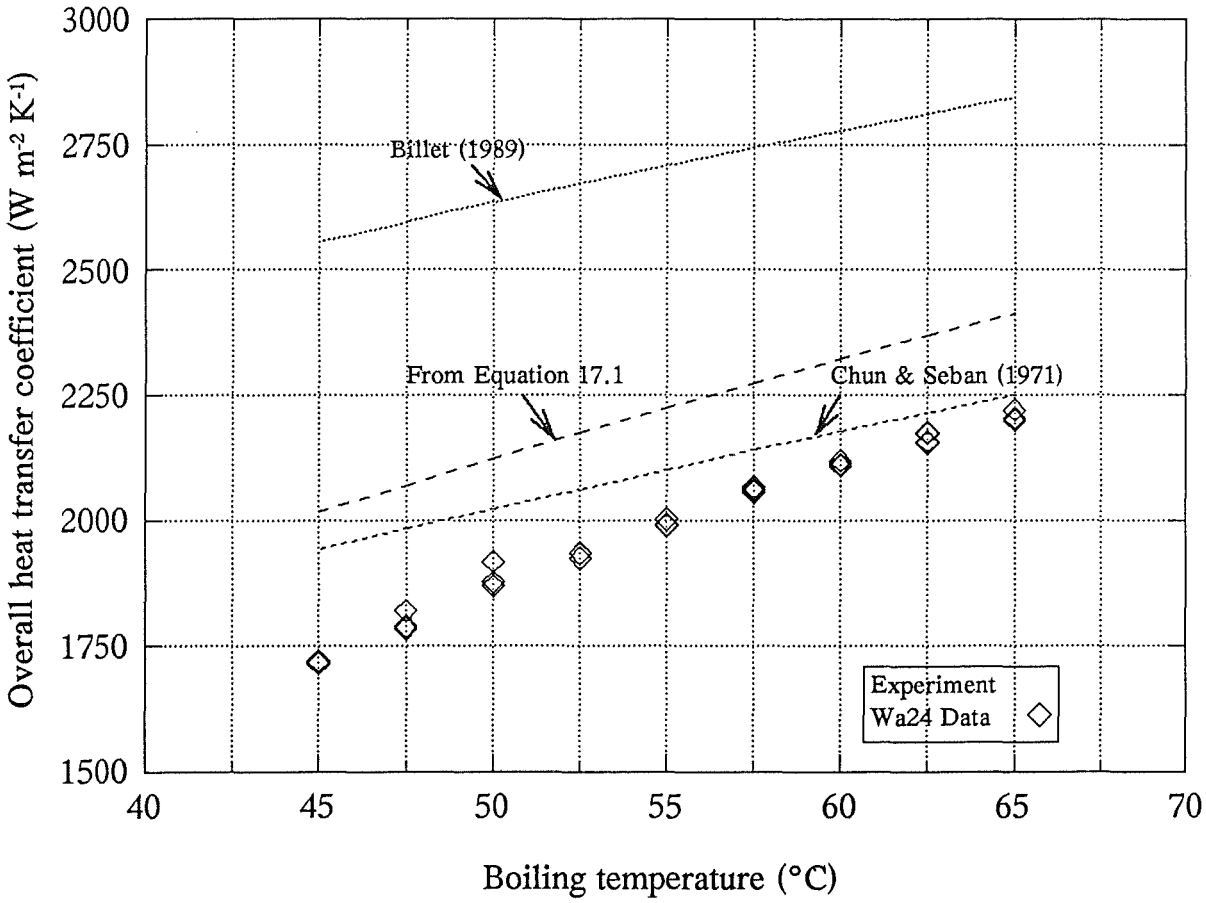

Figure 20.1: Effect of Boiling Temperature on the Overall Heat Transfer Coefficient.

the slope of the curve from Equation 17.1 and the Chun & Seban and Billet correlations is due to the way in which they predict $\bar{Nu}_e$ will change over this range (see Section 19.2).

A possible factor considered was an increased pressure drop over the tube length at lower pressures. However, the difference between the vapour temperature at the top of the tube and the boiling temperature was essentially constant for the experiment.

21 TUBE DIAMETER EXPERIMENTS

The experimental design and standard operating conditions for these experiments are found in Chapter 13.

21.1 Results

The raw data for the tube diameter experiments (Wa25-Wa32) are tabulated in Appendix I. The entry vapour velocity was dependent (see Figure 21.1) on the degree of flash (DOF) and the tube diameter. The exit vapour velocity (see Figure 21.2) and overall HTC (see Figures 21.3 and 21.4) were dependent on the DOF, temperature driving force and the tube diameter. The relationship between the mean vapour velocity and overall HTC is shown in Figure 21.5. The degree of superheat was high during Experiments Wa25-Wa28 and Experiment Wa31 was not completed. Therefore, only the results of Experiments Wa29, Wa30 and Wa32 are presented here.

21.2 Discussion

This experiment was designed to investigate the effect of tube diameter on heat transfer under a range of operating conditions. Increasing the temperature driving force from 3°C to 8.3°C (see Figure 21.3) reduced the overall HTC as expected. There was no clear trend in overall HTC (see Figure 21.4) when the DOF was varied from 5°C to 25°C.

The tube liquid loading after flash was fixed so that the film thickness on entry was fixed. Thus the feed flow rate and the quantity of flash was proportional to the tube diameter (or strictly the tube circumference). The vapour velocity was proportional to the square of the tube diameter whereas the heat transfer area was proportional to the tube diameter. Thus both the entry vapour velocity (see Figure 21.1) and the exit vapour velocity (see Figure 21.2) were inversely proportional to the tube diameter. Thus, by varying the tube diameter, the effect of vapour momentum on heat transfer could be determined.

Jebson & Iyer (1991) gave a regression equation for the overall HTC of milk concentrate in terms of temperature driving force, viscosity and vapour momentum:

$$U = 2288 - 349\,\Delta T_U + 1.8\,\Delta T_U\,\mu + 82\,\Delta T_U\,M - 2\,\Delta T_U\,\mu\,M \qquad (21.1)$$

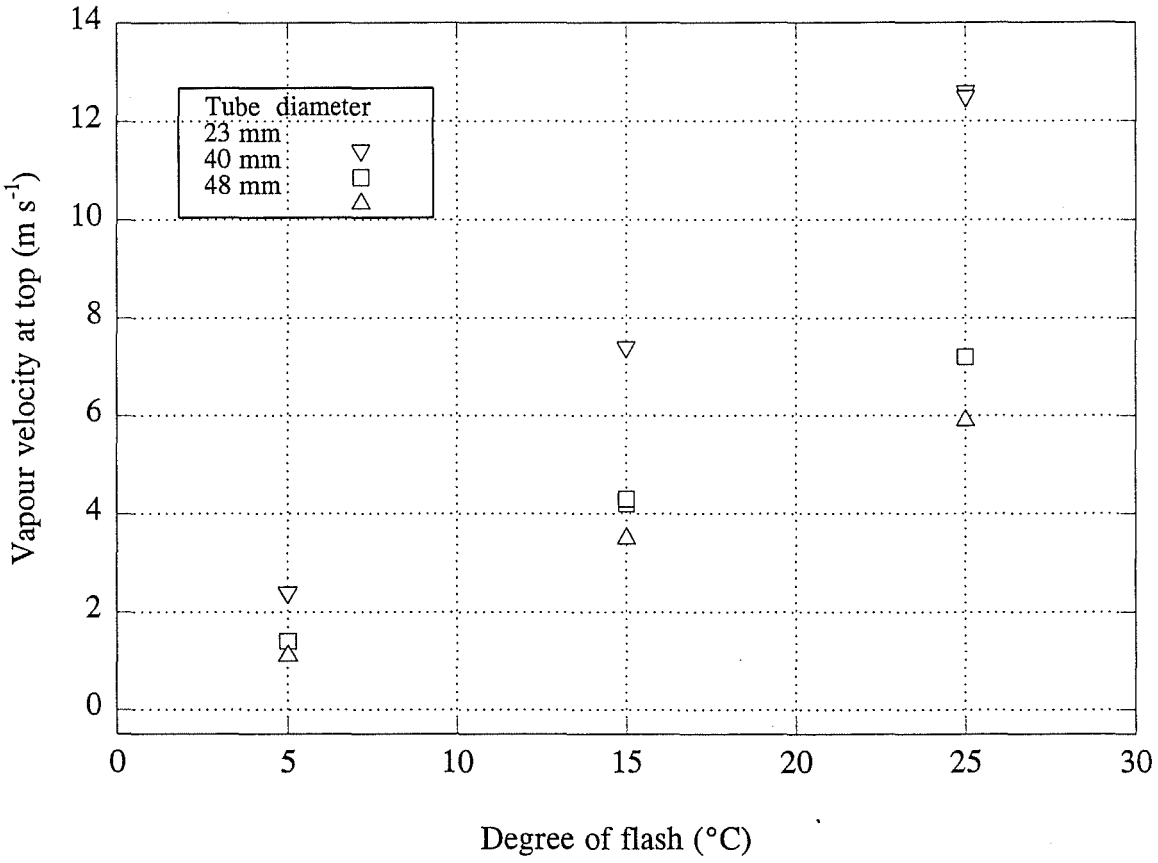

Figure 21.1: Tube Entry Velocities (Data from Experiments Wa29, Wa30 and Wa32).

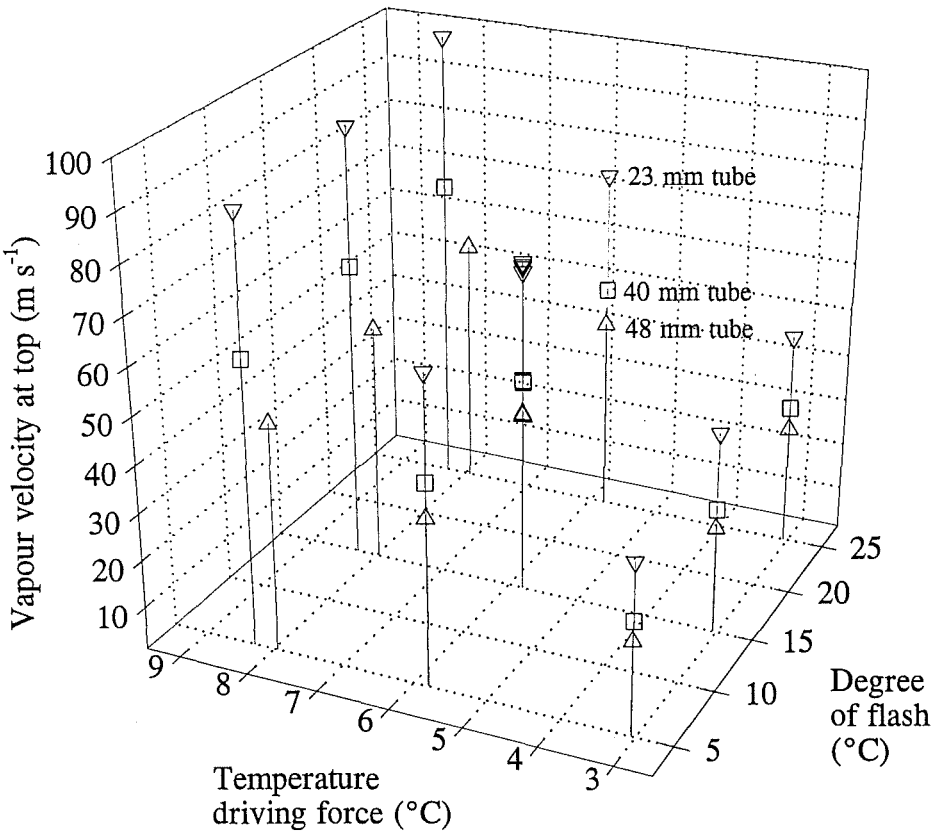

Figure 21.2: Tube Exit Vapour Velocities (Data from Experiments Wa29, Wa30 and Wa32).

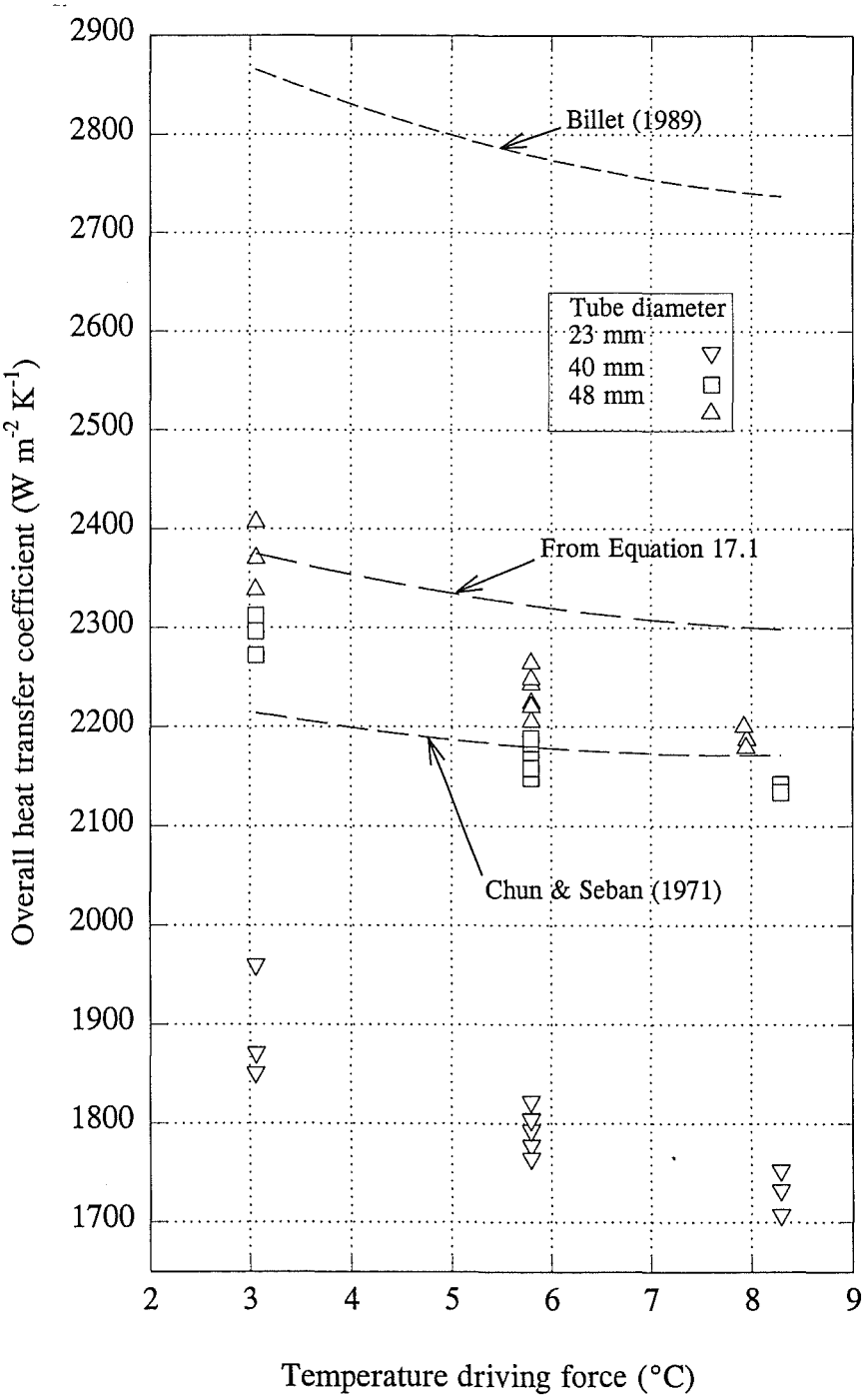

Figure 21.3: Overall Heat Transfer Coefficients Plotted Against Temperature Driving Force (Data from Experiments Wa29, Wa30 and Wa32).

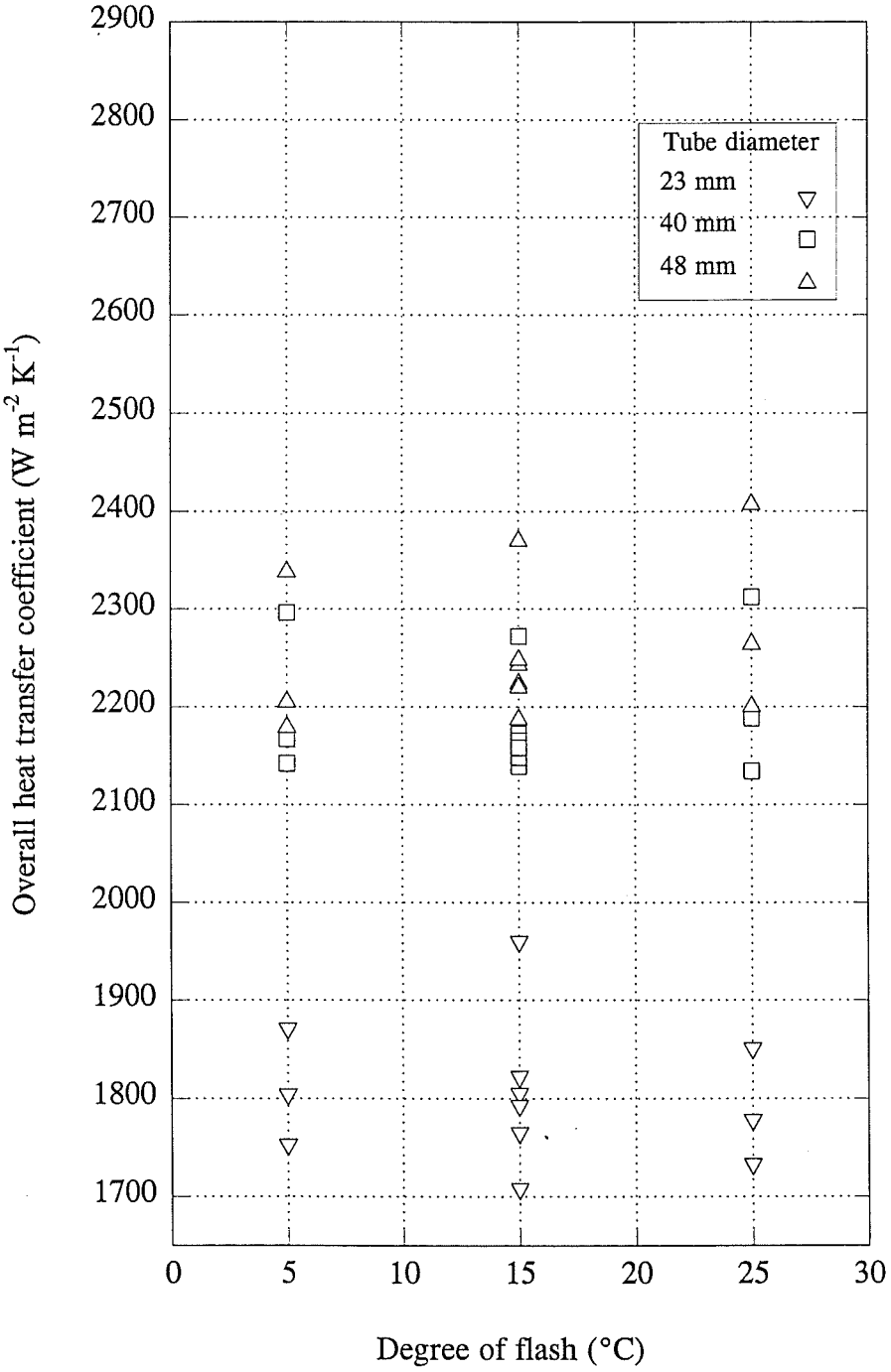

Figure 21.4: Overall Heat Transfer Coefficients Plotted Against Degree of Flash (Data from Experiments Wa 29, Wa 30 and Wa32).

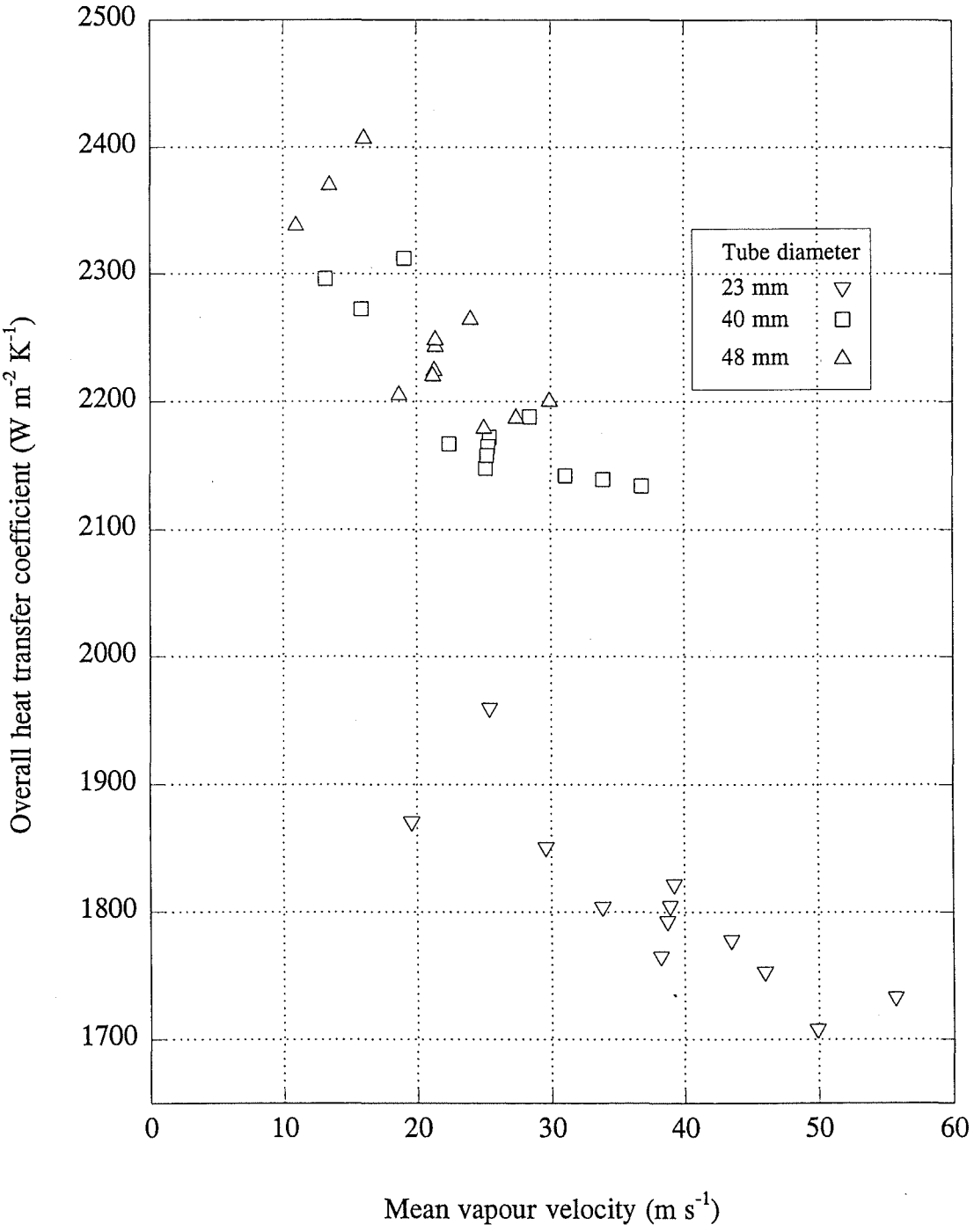

Figure 21.5: Overall Heat Transfer Coefficients Plotted Against Mean Vapour Velocity (Data from Experiments Wa 29, Wa30 and Wa 32).

where the momentum, M was defined as mass (kg) times the vapour velocity (m s^{-1}) per tube circumference (m). The regression equation was based on data collected from a 7-effect DSE evaporator, and therefore, the effect of concentration or viscosity had a co-variant, boiling temperature. The mass was apparently per unit volume (Jebson, 1992) and thus essentially was the vapour density. Therefore, as the boiling temperature and viscosity were constant in Experiments Wa29, Wa30 and Wa31, Equation 21.1 can be reduced to:

$$HTC \propto k_1 + k_2 \Delta T_U + k_3 \Delta T_U \frac{\bar{u}}{d_{i_e}} \tag{21.2}$$

The mean velocity divided by the diameter can be considered to be roughly proportional to the shear rate at the boiling film liquid-vapour interface. The overall HTC is plotted against the mean vapour velocity per tube diameter in Figure 21.6. The first order regression equation with a regression coefficient, r^2 of 0.95 is:

$$U = 2382 - 0.32\left(\frac{\bar{u}}{d_{i_e}}\right) \tag{21.3}$$

The second order regression equation with a regression coefficient, r^2 of 0.97 is:

$$U = 2515 - 0.64\left(\frac{\bar{u}}{d_{i_e}}\right) + 1.3\times10^{-4}\left(\frac{\bar{u}}{d_{i_e}}\right)^2 \tag{21.4}$$

There were, however, several potential co-variants which may have contributed to the observed effect of tube diameter.

1. The de-aeration lines had a fixed nozzle size, so the percentage of steam passing through the de-aeration lines was inversely proportional to the steam condensation rate and hence to the tube diameter.
2. Assuming the non-condensable gas was sourced from vacuum leaks, the percentage of air in the steam was also inversely proportional to the condensation rate.
3. Another possibility is that there was a layer of scale on the outside of the 23 mm diameter tube. This is possible due to the greater usage of the 23 mm tube. However the usage was not extensive since the steam side was cleaned with caustic and acid on 27 August 1990.

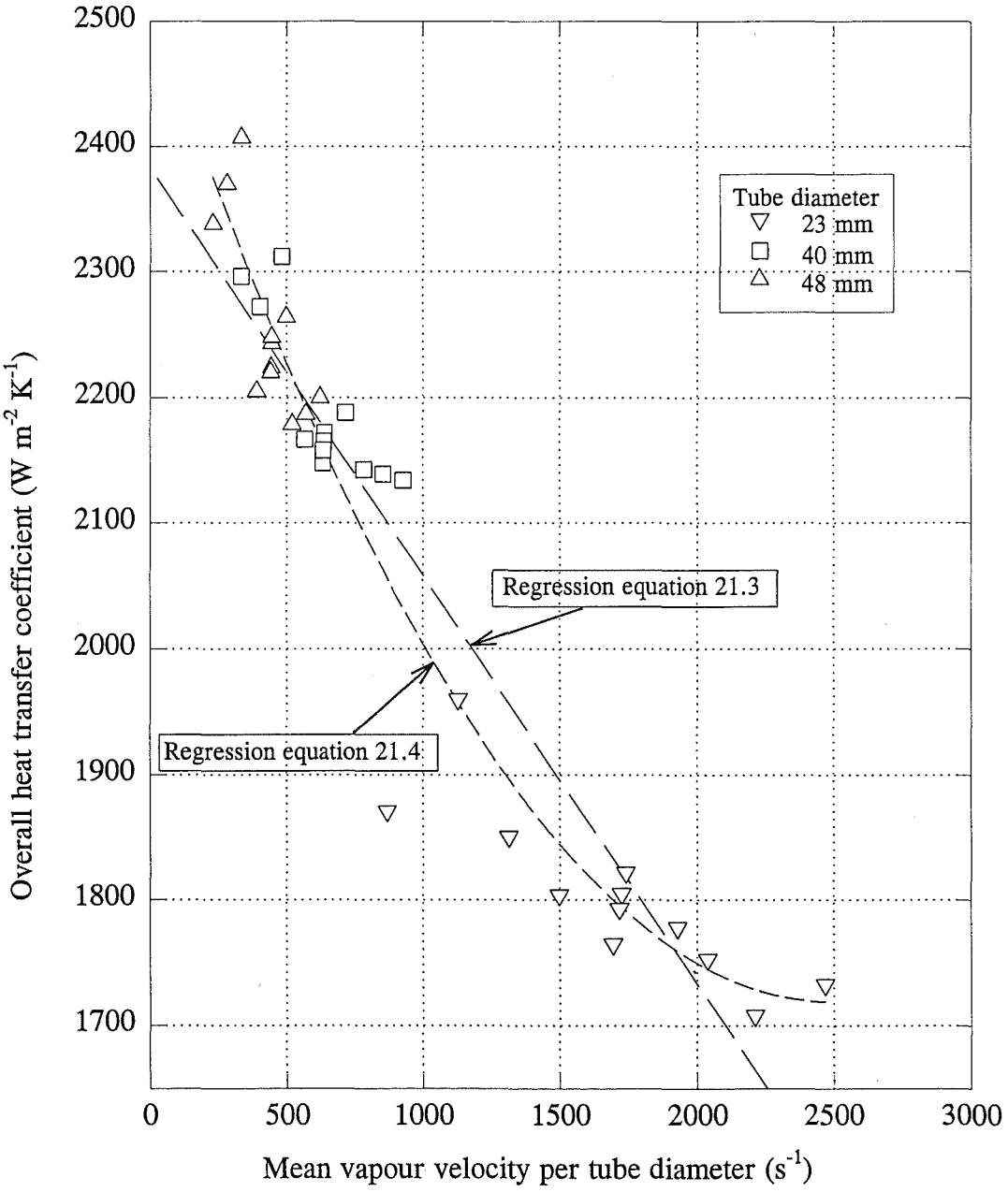

Figure 21.6: Relationship Between Mean Vapour Velocity and Overall Heat Transfer Coefficient (Data from Experiments Wa29, Wa30 and Wa32).

4. The degree of superheat varied directly with the steam flow rate. The maximum quantity of superheat (at the maximum temperature driving force of ≈ 8°C) for the three tube diameters were:

Tube diameter (mm)	23	40	48
Superheat (°C)	-0.5	3.5	3.6

The above values are for Experiments Wa28, Wa29 and Wa31. Before the de-superheat nozzle was changed superheat levels of up to 8°C were obtained on the 48 mm diameter tube.

5. The pressure drop over the length of the tube. The range of vapour temperature probe measurements obtained on each tube were:

Tube diameter (mm)	23	40	48
Vapour temperature (°C)	60.6-65.7	60.3-62.2	59.8-61.9
- corrected[1] (°C)	60.6-65.7	60.3-62.2	60.2-62.3

This shows that the pressure drop was significantly greater for the 23 mm tube (at high temperature driving forces) than for the other tubes. No evaporation would have occurred at the top of the 23 mm tube on some of the runs.

The first two co-variants should cancel each other out to a certain extent, and the small quantity of superheat should be insignificant. The insignificance of low levels of superheat can be confirmed by comparing data from Experiment Wa25 and Wa29 (see Table 21.1). There was no superheat present in either experiment for runs with a differential pressure of 3 kPa. However, superheat was present for runs with differential pressures of 6 or 9 kPa. The increase in HTC between Experiment Wa25 and Wa29 was 2.5% for the 3 kPa runs and 1.6% for the 6-9 kPa runs. The slight difference (1.6% versus 2.5%) in HTC is not significant given the accuracy of the measurements. Therefore, the reduction in the degree of superheat from 8 to 2.6°C did not have a significant effect on the heat transfer rate.

There was a significant reduction in pressure drop as the tube diameter increased. The high pressure drop obtained in the 23 mm tube would have contributed to the reduced overall HTC values achieved on that tube. Bouman et al (1993) used an average of the temperature driving force at the top and bottom of the tube, when calculating the overall

---

[1] The calibration of the 48 mm tube probe was suspect (see Appendix B). A check on the relative readings of the three vapour temperature probes during CIP (of all three tubes simultaneously) revealed that the 48 mm tube probe read 0.4°C lower than the 23 mm and 40 mm tube probes.

HTC. This may partially explain why they found that vapour velocity had no significant effect on heat transfer.

The scatter in the data collected using the 23 mm tube shows the inaccuracy of the flow measurement at low flow rates and low evaporation rates. For this reason alone, there is no justification to use the second order equation (Equation 21.4).

Table 21.1 Comparison of heat transfer coefficients from Experiments Wa25 & Wa29.

Experiment	Wa25	Wa29
Mean values for runs with differential pressure of 3 kPa		
Degree of superheat (°C)	0	0
Heat transfer coefficient (W m^{-2} K^{-1})	2315	2372
Mean values for runs with differential pressures of 6 or 9 kPa		
Degree of superheat (°C)	8	2.6
Heat transfer coefficient (W m^{-2} K^{-1})	2183	2219

Dimensional analysis model

The following equation form[2] was fitted to the data from Experiments Wa29, Wa30 and Wa32:

$$U = a\left[Re_e^{1.05}\, Pr_e^{0.65}\right]\left(Ja_e^*\right)^d \left(N_{\Gamma_v/\Gamma_e}\right)^e \left[\left(N_{BPE}^*\right)^1\right]\left(N_{L/d}\right)^g \qquad (21.5)$$

to determine the values of a, d, e and g. The resultant equation was:

$$U = 2.78\left[\bar{Re}_e^{1.05}\, Pr_e^{0.65}\right]\left(\bar{Ja}_e^*\right)^{0.016} \left(\bar{N}_{\Gamma_v/\Gamma_e}\right)^{0.031} \left[\left(N_{BPE}^*\right)^1\right]\left(N_{L/d}\right)^{-0.32} \qquad (21.6)$$

The fit of Equation 21.6 to the experimental data is shown in Figure 21.7. A regression line fitted to the data in Figure 21.7 gave a r^2 of 0.98. The background and significance of the model is discussed in Chapter 26.

---

[2] The exponent for Re_e was obtained from Figure 25.14 and the exponent for Pr_e from Equation 10.5.

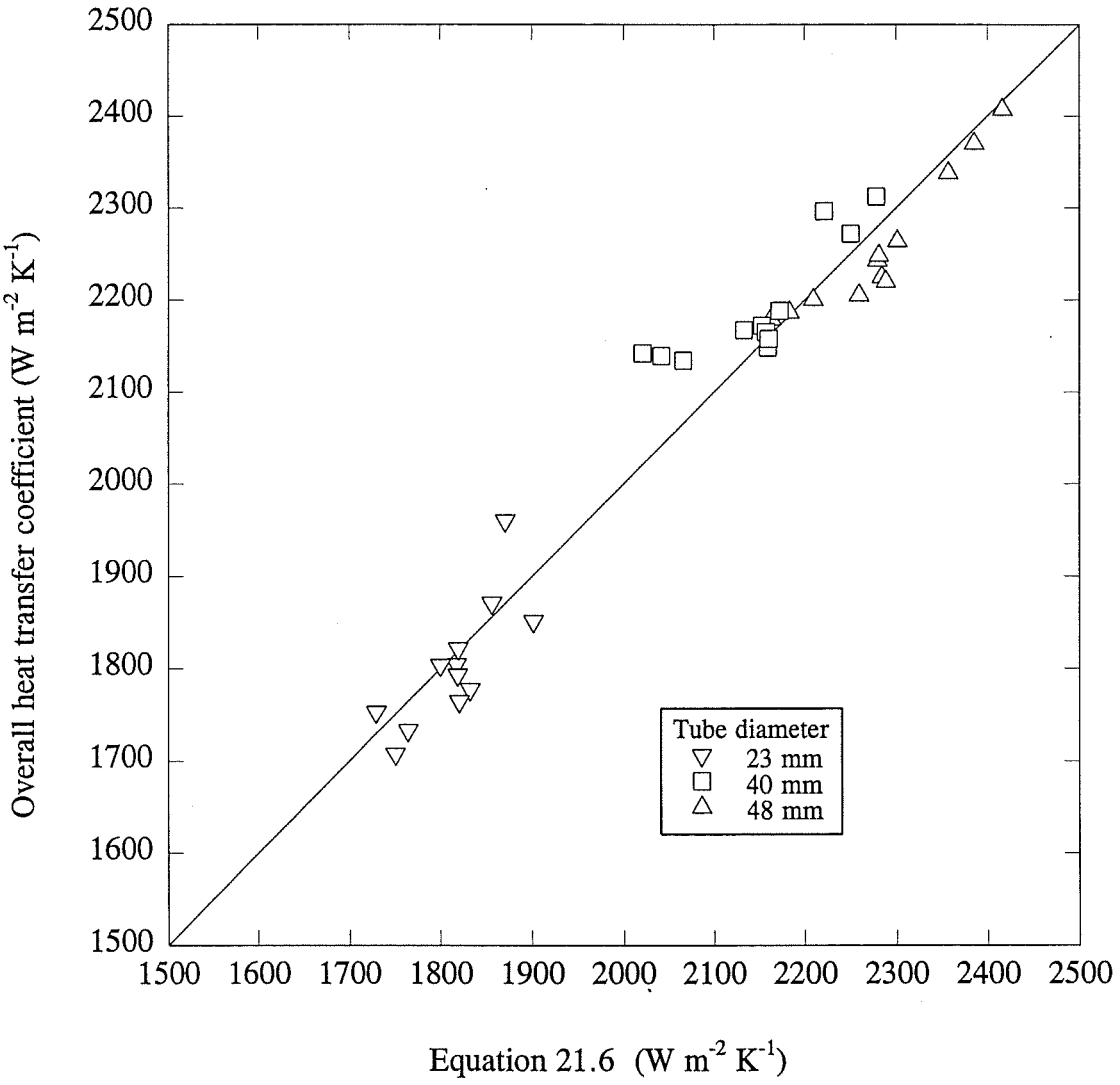

Figure 21.7: Fit of Equation 21.6 to Data from Experiments Wa29, Wa30 and Wa32.

22 DISCUSSION - WATER EXPERIMENTS

The 3^3 factorial experiments (see Chapter 16) confirmed that boiling temperature, temperature driving force and liquid loading all had an significant effect on the overall HTC.

The diameter of the de-aeration nozzles used in the experiments presented in Chapters 15-21 with the exception of Experiment Wa14 (see Chapter 19) was fixed at 3.2 mm. Thus the sonic volumetric flow through the nozzles was essentially constant (see Appendix K for qualifications). The mass flow rate was dependent on the steam pressure and thus the boiling temperature and/or temperature driving force. The mass de-aeration rate therefore varied during the experiments as a co-variant of boiling temperature and temperature driving force. In commercial practice the de-aeration rate is usually fixed relative to the steam condensation rate in the effect, ˥ . The value of ˥ varied during these experiments and was inversely proportional to the evaporation rate. Thus, the boiling temperature and temperature driving force were confounded with respect to ˥ .

The liquid loading experiments (see Chapter 17) confirmed that there were (at least) three flow regimes (wavy-laminar, transitional and turbulent) and revealed the presence of a local maximum in the Nusselt number within the transitional zone. The boiling side Nusselt numbers, calculated from the experimental data, were within 15% of the values predicted by the correlations of Chun & Seban (1971). The correlations presented by Billet (1989) however predicted values up to 50% higher than the experimental data. Experimental data obtained on refrigerant R11 (Struve, 1969) presented by Billet also displays a local maximum in the transitional zone as observed in the liquid loadings experiments. No explanation was given, but it appears to be a real effect. The boiling side Nusselt numbers presented here are the mean values over the tube length. Further work is required to determine local Nu_e values over the same range of Re_e and to establish the significance of the liquid entry transition region.

The degree of flash was found to have little or no effect on the overall HTC (see Chapters 18 and 21). Sub-cooling the feed did reduce the evaporation rate as expected.

The effect of differential pressure or temperature driving force was non-linear (see Chapter 19), due to two competing factors. These are the increased condensate film thickness with increasing temperature driving force which reduces the overall HTC and the presence of non-condensable

gases in the steam which affects the overall HTC especially at low temperature driving forces.

The tube diameter experiments (See Chapter 21) revealed that the overall HTC is highly dependent on the tube diameter. This appears to be due to the adverse effects of high vapour velocities in small diameter tubes, in particular an increase in pressure drop over the tube length which reduces the effective temperature driving force. Therefore the use of tubes smaller than 40 mm in diameter should be avoided.

The effect of tube length on the overall HTC was not investigated during these experiments due to the difficulties encountered in controlling and, in particular, measuring non-condensable gases levels, which made comparison between different calandrias suspect. However, a comparison of Figure 17.1 (with $\Gamma_e = 0.2$ kg m^{-1} s^{-1}) and Figure 21.3 (with $\Delta T_U = 3°C$) shows that the effect of increasing the tube length from 10 to 15 m reduces overall HTC from 2350 to 2150 W m^{-2} K^{-1}. A reduction was expected due to the increase in average condensate film thickness.

23 EXPERIMENTAL DESIGN - SUCROSE

23.1 Standard Operating Conditions

The standard operating conditions for all experiments unless expressly stated were as described in Section 13.1 except for:

Feed type	sucrose solution

The experimental run order was determined as described in Section 13.2.

23.2 Third Evaporator Experiments

A 3^2 factorial experiment with three centre point replicates (12 runs) was conducted to investigate the effect of feed flow rate and boiling temperature on the overall heat transfer coefficient. The levels used were:

Feed flow rate	110, 150, 190 kg h^{-1}
Boiling pressure	15.75, 19.96, 25.01 kPa absolute
(Feed temperature	59.5, 64.5, 69.5°C)

This experiment was repeated with a number of feed concentrations (see Table 23.1) and the results are presented in Chapter 25.

Table 23.1 Third Evaporator Sucrose Experiments

Experiment	Date	Feed Concentration (% w/w)
Su1	19-20 Dec 1991	40
Su2	06-07 Jan 1992	60
Su3	07-08 Jan 1992	50
Su4	08-09 Jan 1992	55
Su5	09-10 Jan 1992	40

23.3 Fifth Evaporator Experiments

To evaluate the effect of tube diameter, a 3^2 factorial design with three centre-point replicates (12 runs), with differential pressures levels of 3, 6 and 9 kPa and feed temperature levels of 65, 75 and 85°C, was used. This factorial was carried out on each tube in the Fifth Evaporator (tube length 10 m) at two feed concentrations (40 and

50% w/w). The entry wetting factor after flash was fixed for all tubes at 0.73 kg h^{-1} mm^{-1} (0.203 kg m^{-1} s^{-1}). The experiments carried out are listed in Table 23.2 and their results are presented in Chapter 26.

Table 23.2: Fifth Evaporator Sucrose Experiments

Experiment Code	Date	Feed Concentration (% w/w)	Tube Diameter, (mm)
Su6	28-29 Feb 1992	40	22.56
Su7	29 Feb 1992	40	39.71
Su8	29 Feb - 1 Mar 1992	40	48.14
Su9	1-2 Mar 1992	50	39.71
Su10	2 Mar 1992	50	48.14
Su11	2-3 Mar 1992	50	22.56

24 EXPERIMENTAL PROCEDURE - SUCROSE

The procedure used for the sucrose experiments was the same as used for the water experiments (see Chapter 14) except for the following:

1. The balance tank was filled with the appropriate sucrose solution and the sucrose solution was pumped through the evaporator and recirculated to the feed tank. The level in the feed tank (and therefore the feed concentration) was maintained by the addition of soft water. To minimise the vertical concentration gradient in the feed balance tank an Ultra-Turrix T50 mixer (Janke & Kundel, Funkenstört, Germany) was installed in the feed balance tank.
2. Samples of the sucrose solution in the feed tank and ex-evaporator were taken and analyzed for total solids using a vacuum oven method (Mojonnier & Troy, 1925).

25 SUCROSE THIRD EVAPORATOR EXPERIMENTS

The experimental design and procedure for these experiments are covered in Chapters 23-24.

25.1 Experiments Su1-Su5 Results

The raw data for Experiments Su1-Su5 are tabulated in Appendix I.

Effect of experimental design variables

The overall HTCs are plotted with respect to feed flow rate and boiling (vapour) temperature for Experiment Su2 (60% w/w feed concentration) in Figure 25.1 and for Experiment Su5 (40% w/w feed concentration) in Figure 25.2.

Boiling Point Elevation

The boiling point elevation, BPE (see Figure 25.3) of the product leaving the tube was determined from the boiling-side absolute pressure and the product temperature. The following curve was fitted to the data and used to determine the BPE where S is the sucrose concentration (% w/w) leaving the effect.

$$BPE = e^{(-0.09 - 0.033S + 8.1\times10^{-4}S^2)} \qquad (25.1)$$

Equation 27.1 was fitted for S ranging from 43 to 75% w/w. The temperature measurement point is 0.4 m below the tube exit, and the liquid free falls from the tube and then flows over the bottom section of an uninsulated duct before flowing over the surface probe. Therefore, any superheat due to the temperature gradient across the evaporating film should have dissipated through flashing and convective cooling before temperature measurement. A theoretical boiling point elevation curve determined using Equation 2.1 is also shown in Figure 25.3. Equation 2.1 assumes the solution is ideal, and the difference between the curve and the data indicates that sucrose solutions are non-ideal at high concentrations due to solute component interactions (Jebson, 1994).

Example of numerical integration procedure results

The local values of α_c, α_e and α_U for a selected experimental run (Experiment Su2, Run 11) using the local Nu_e correlations given by both Chun & Seban (1971) and Billet (1989) are presented in Figure 25.4. For this same run, the temperature profiles (see Figure 25.5), the boiling film property profiles (see Figure 25.6) and the vapour velocity

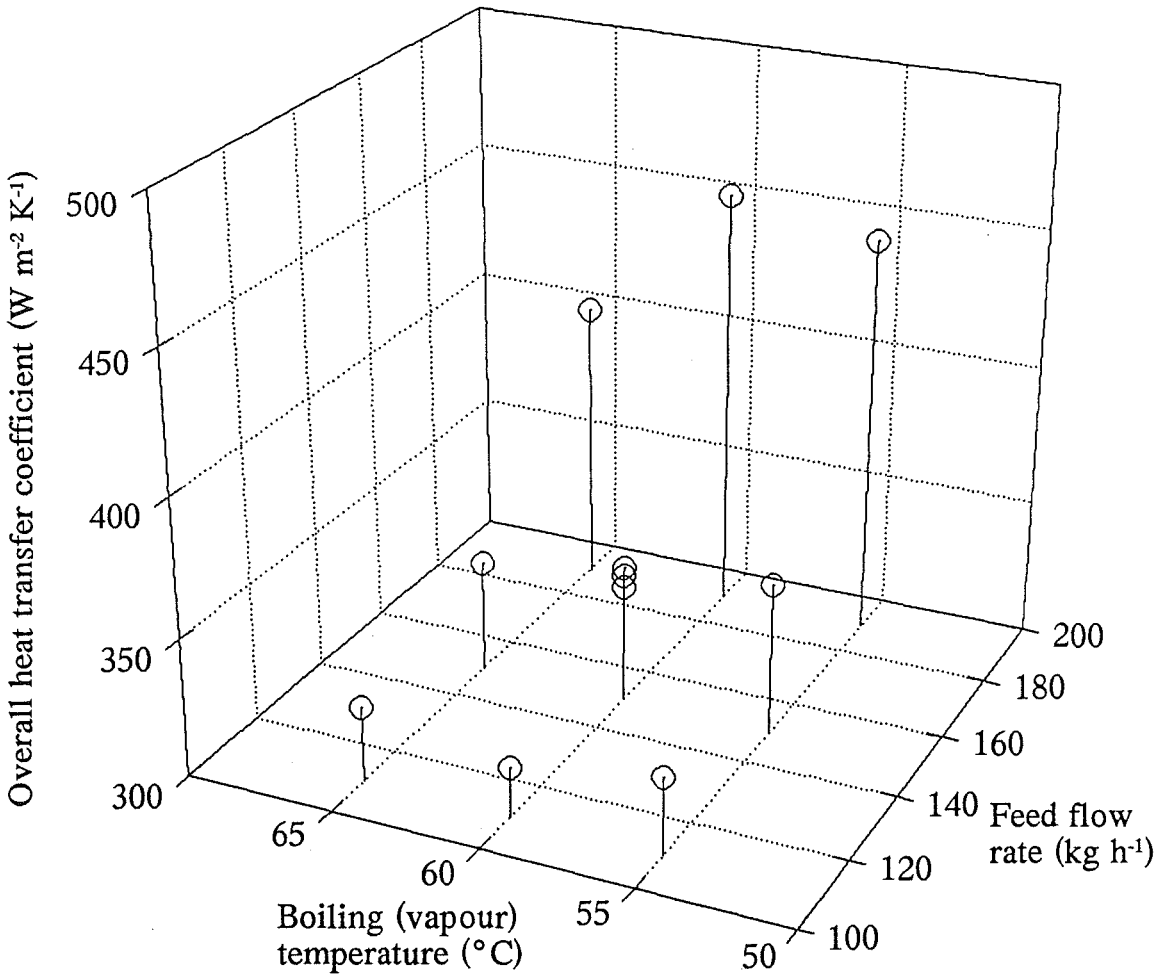

Figure 25.1: Overall Heat Transfer Coefficients for Sucrose with a Feed Concentration of 60% w/w (Experiment Su2).

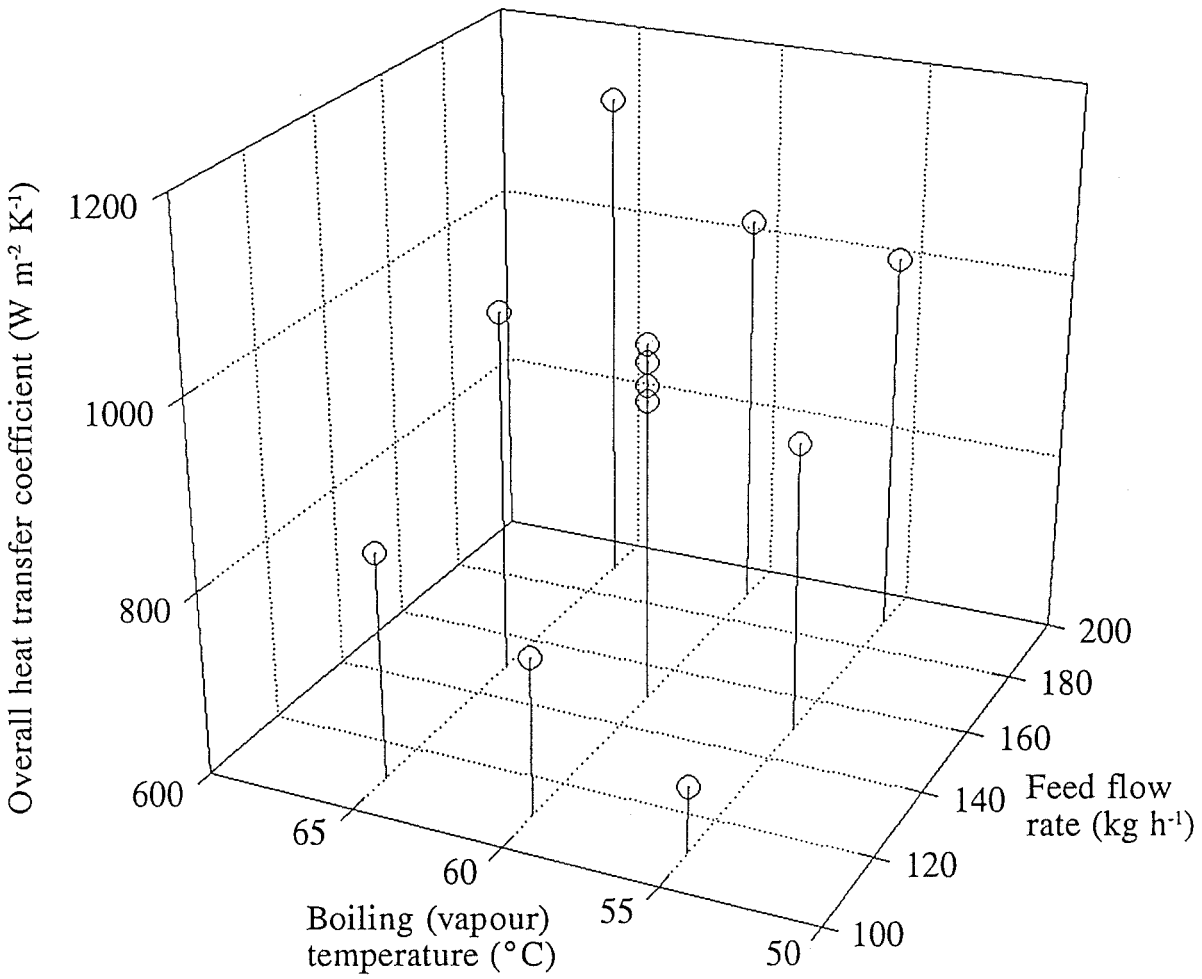

Figure 25.2: Overall Heat Transfer Coefficients for Sucrose with a Feed Concentration of 40% w/w (Experiment Su5).

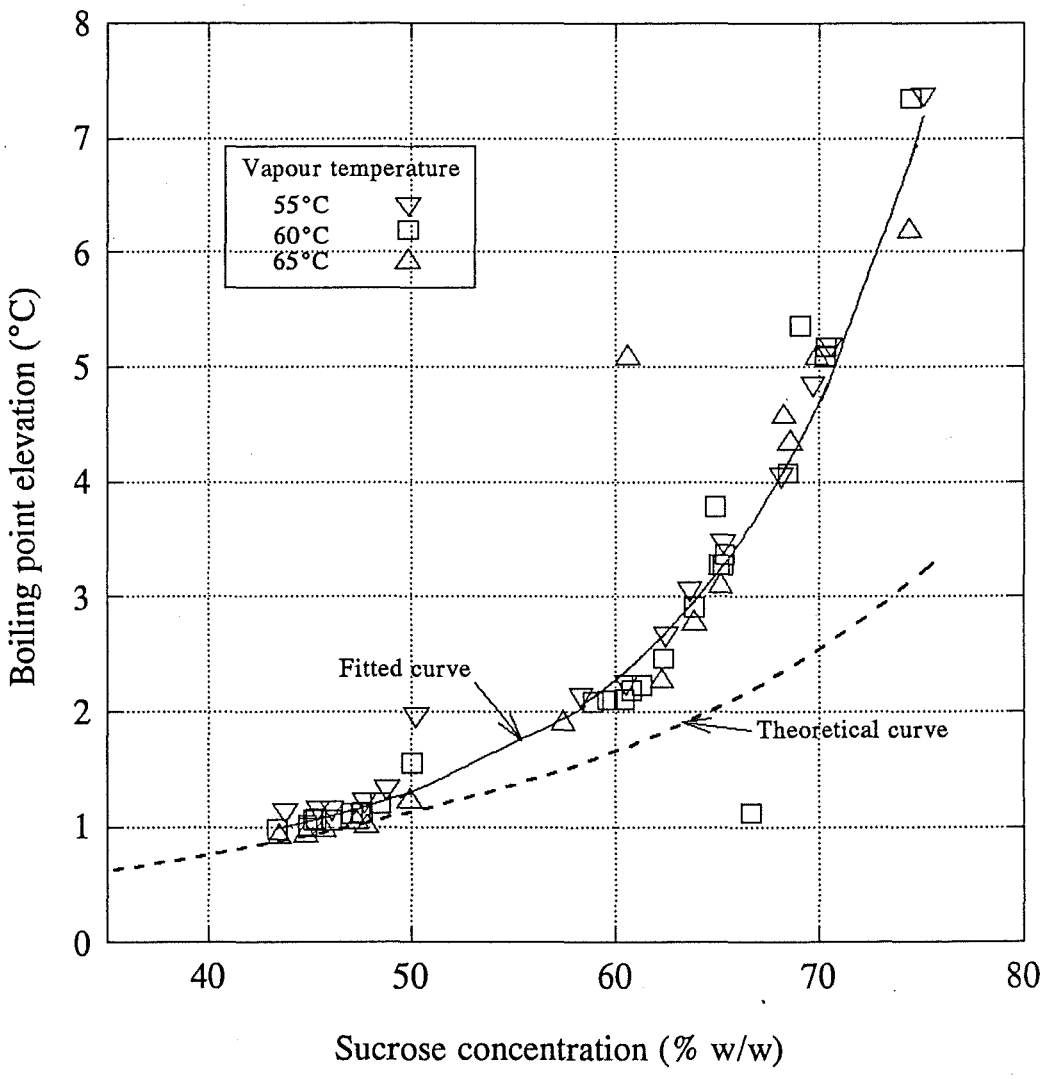

Figure 25.3: Boiling Point Elevation Measurements from Experiments Su1-Su5.

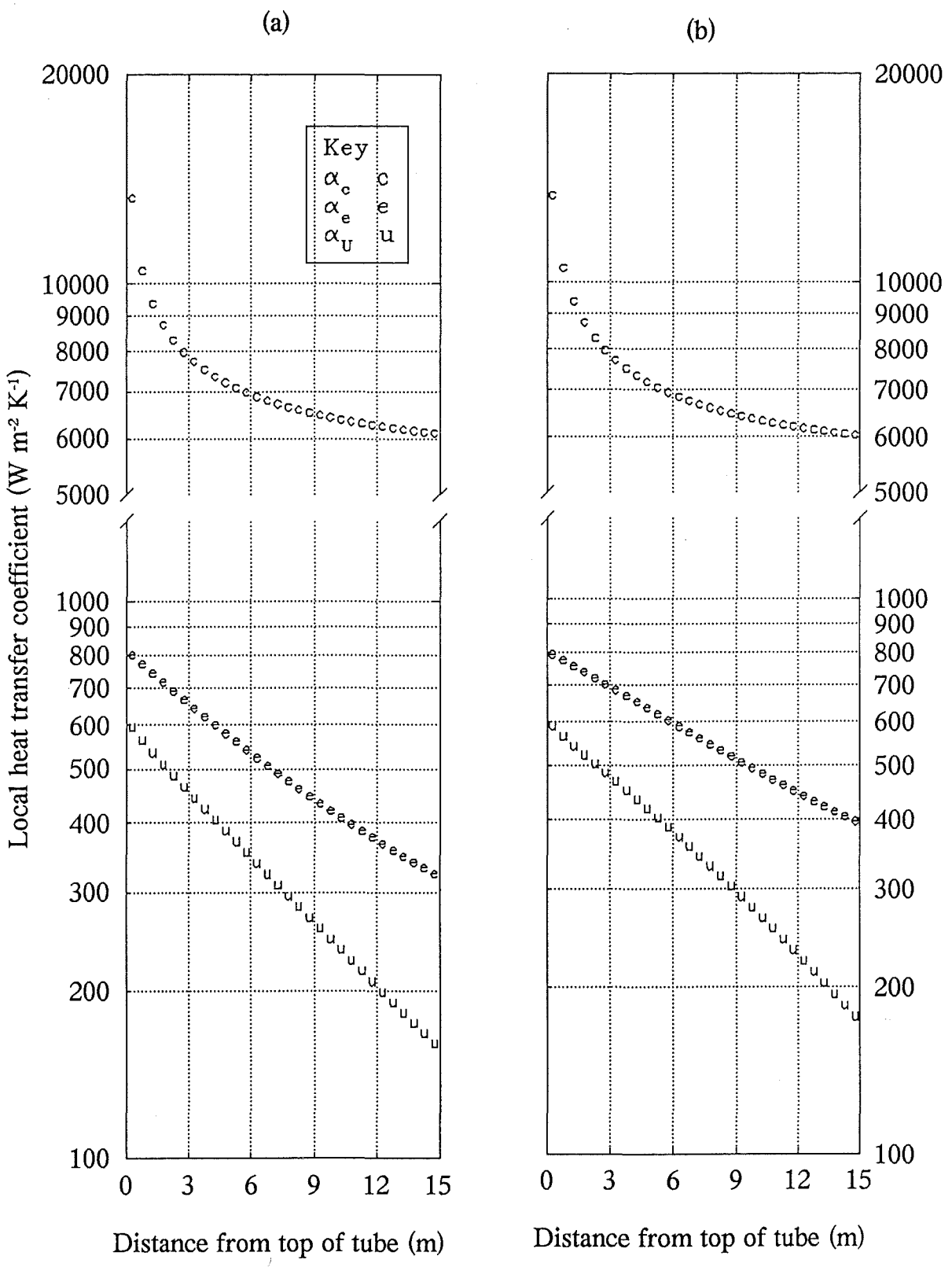

Figure 25.4: Local Heat Transfer Coefficients for Experiment Su2, Run 11.
(a) Using Chun & Seban (1971) Nu_e (Turbulent Flow).
(b) Using Billet (1989) Nu_e (Laminar Flow).

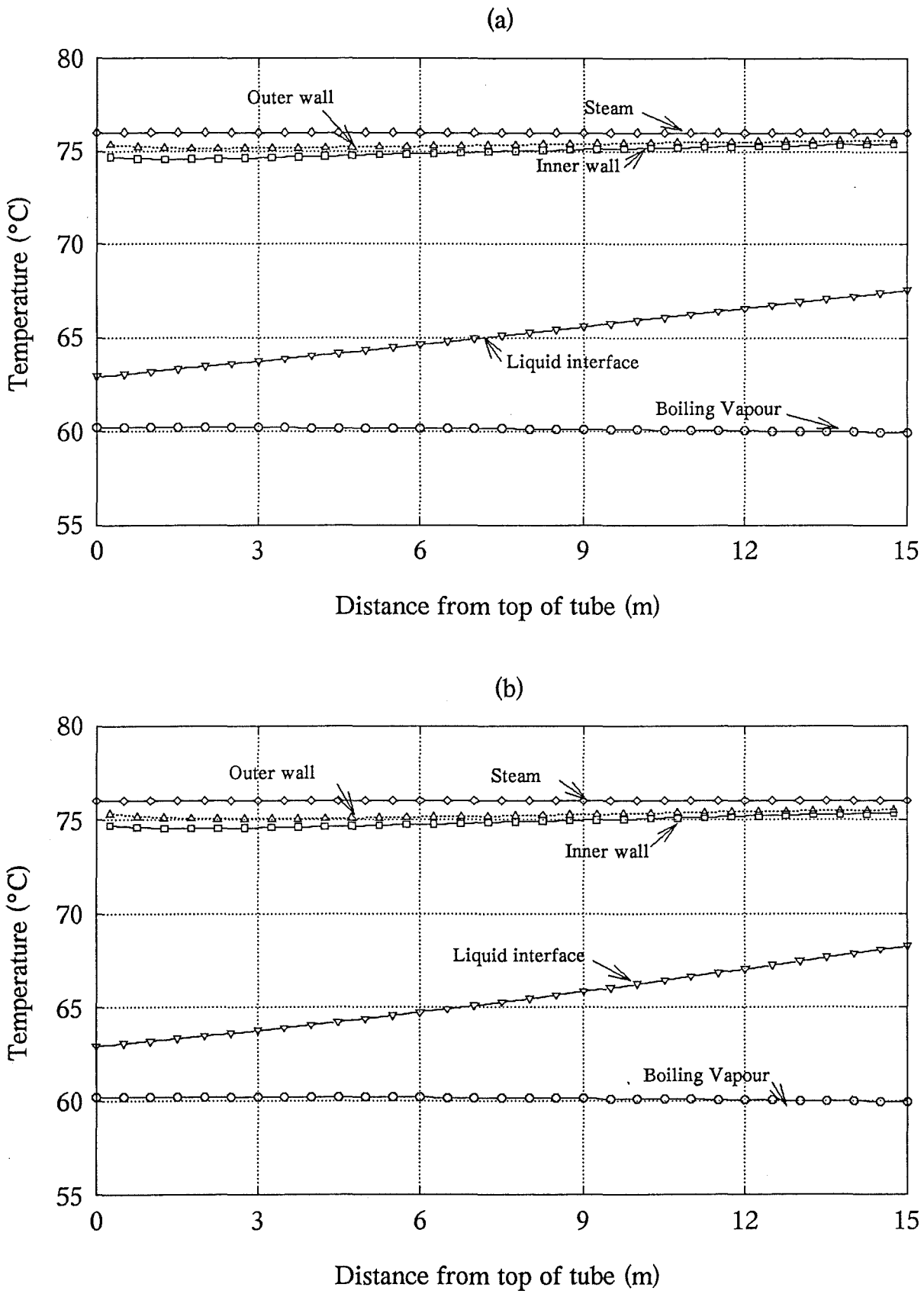

Figure 25.5: Temperature Profiles for Experiment Su2, Run 11.
(a) Using Chun & Seban (1971) Nu_e (Turbulent Flow).
(b) Using Billet (1989) Nu_e (Laminar Flow).

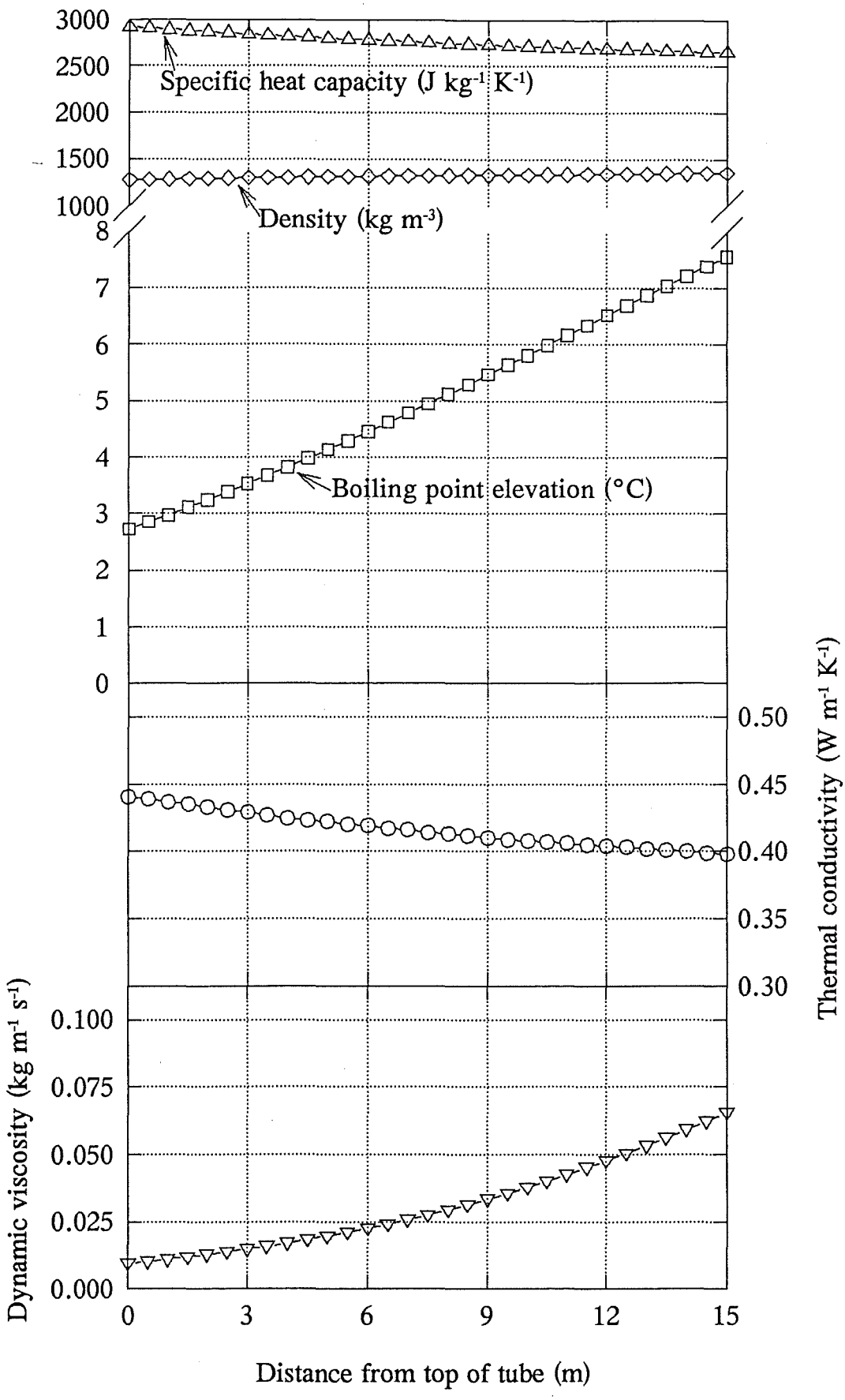

Figure 25.6: Local Boiling Film Properties for Experiment Su2, Run 11 (Using the Chun & Seban (1971) Nu_e Correlation).

profiles (see Figure 25.7) are also presented. The Re_e and Pr_e profiles are shown in Figure 25.8.

Mean values for dimensionless groups

Experimental values for $\overline{Re}_e$ and $\overline{Pr}_e$ were determined for each experimental point by two methods. Firstly, using an arithmetic or logarithmic average (see Chapter 12) of the end-point values (*i.e.* values at the top and bottom of the tube) of $C_{p,e}$, μ_e, k_e and Γ_e. Secondly, values of $\overline{Re}_e$ and $\overline{Pr}_e$ were determined, by numerical integration (see Appendix H) of the local Nu_e correlations of Chun & Seban (1971). A comparison of the mean values obtained by each method (see Figures 25.9 and 25.10) demonstrated that for $\overline{Pr}_e$ there was little difference ($\leq 5\%$) but for $\overline{Re}_e < 100$, the differences exceed 10%. However, to avoid any possibility of circularity, the mean values determined from the end-point values were used in all further data analysis.

Mean values for boiling point elevation

Due to the major effect of boiling point elevation on the overall HTC, it was important to get a good estimate of $\overline{BPE}$. The logarithmic mean of the end-point values was expected to be inaccurate at high sucrose concentrations due to the high concentration ratio. However, for the highest mean sucrose concentration (Experiment Su2, Run 11), the difference was only 5%. So the logarithmic mean of the end-point values was used in all further data analysis.

Correlations between dimensionless groups

The combinations of $\overline{Re}_e$ and $\overline{Pr}_e$ used in experiments Su1-Su5 are shown in Figure 25.11. The three lines of data points on the log-log plot represent the three feed flow rates used in the experiment.

Overall heat transfer coefficient results

The overall HTCs from Experiments Su1-Su5 are plotted with respect to $\overline{Re}_e$ and $\overline{Pr}_e$ in Figure 25.12. The overall HTCs determined from the integration procedure using Chun & Seban (1971) and Billet (1989) local Nu_e correlations are plotted against the experimental overall HTCs in Figure 25.13. The correlations of Chun & Seban (1971) were used for Nu_c. To compare the data with Chun & Seban's turbulent Nu_e correlation (Equation 10.5), $U * \overline{Pr}_e^{-0.65}$ and $\overline{Nu}_e * \overline{Pr}_e^{-0.65}$ have been plotted (see Figure 25.14) against $\overline{Re}_e$.

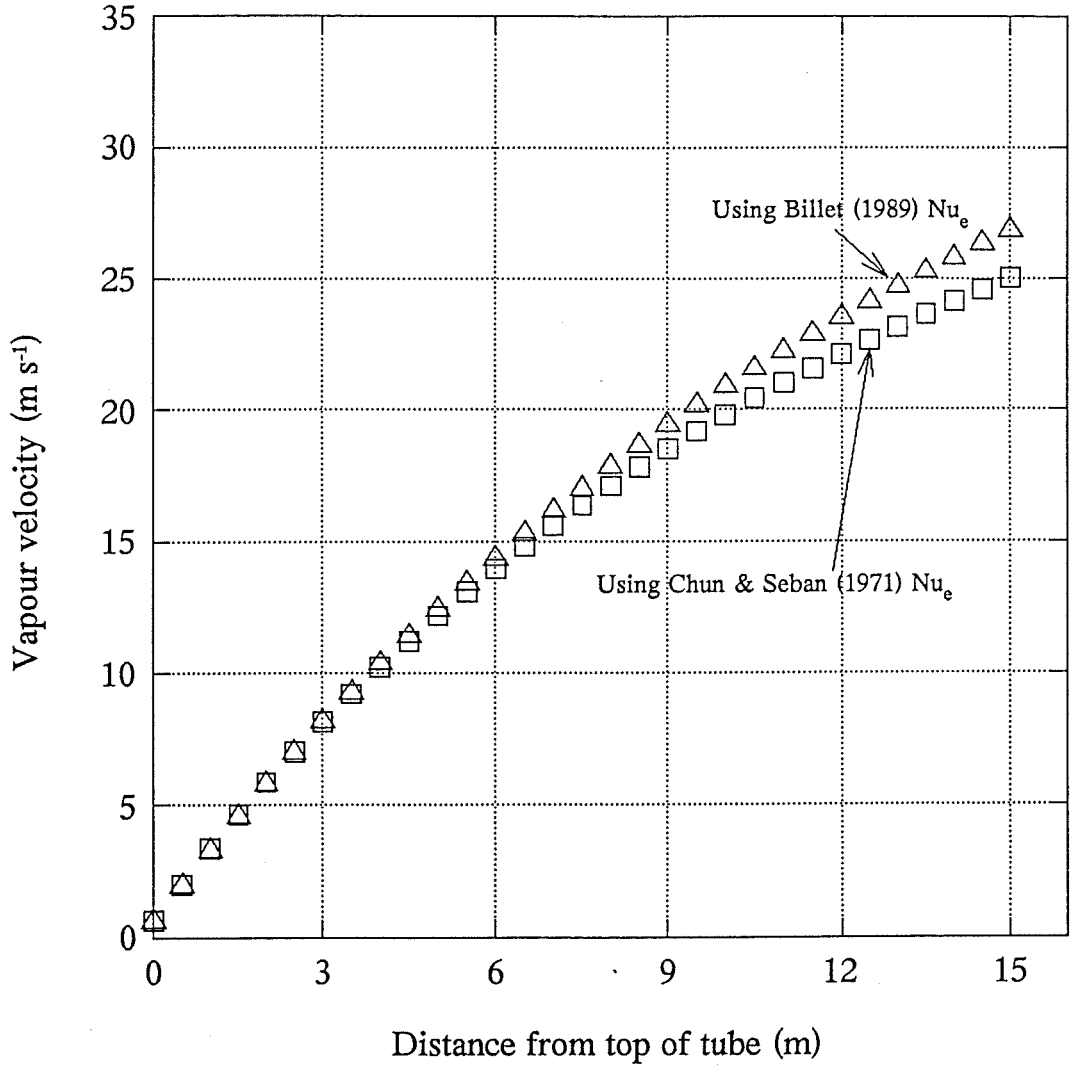

Figure 25.7: Vapour Velocity Profiles for Experiment Su2, Run 11.

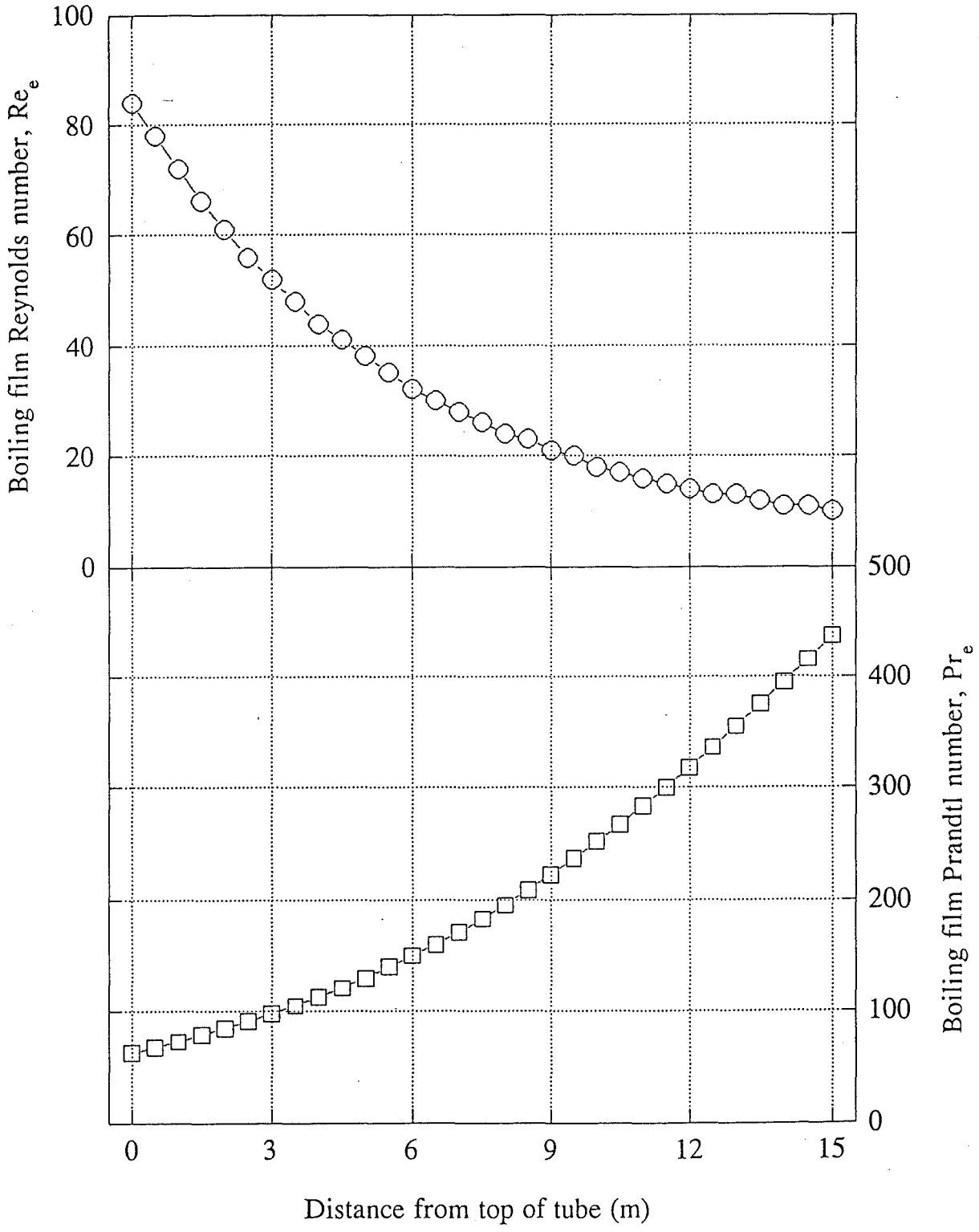

Figure 25.8: Profiles of Re_e and Pr_e for Experiment Su2, Run 11 (Using the Chun & Seban (1971) Nu_e Correlation).

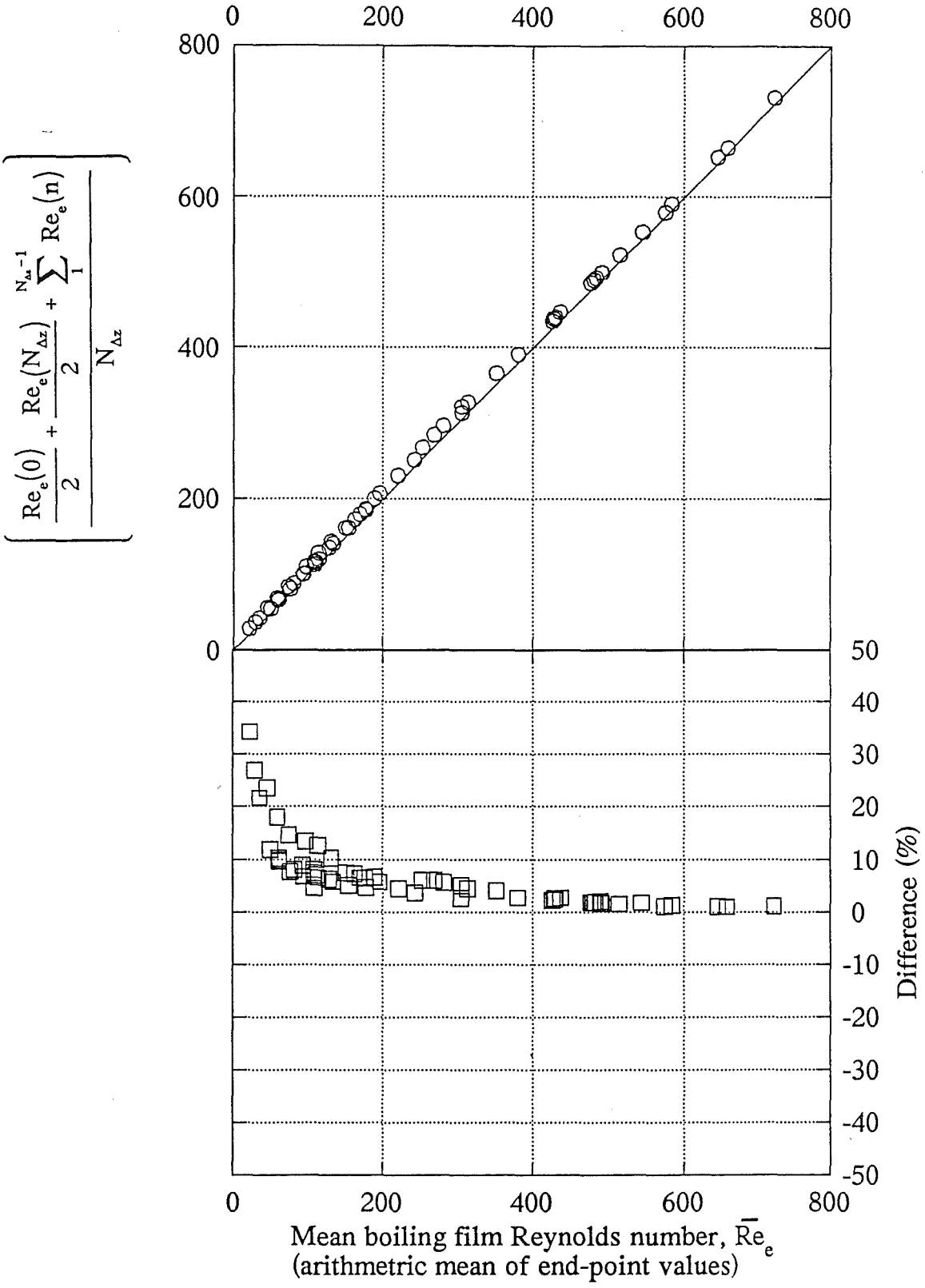

Figure 25.9: Comparison of Methods for Determining the Mean Boiling Film Reynolds Number.

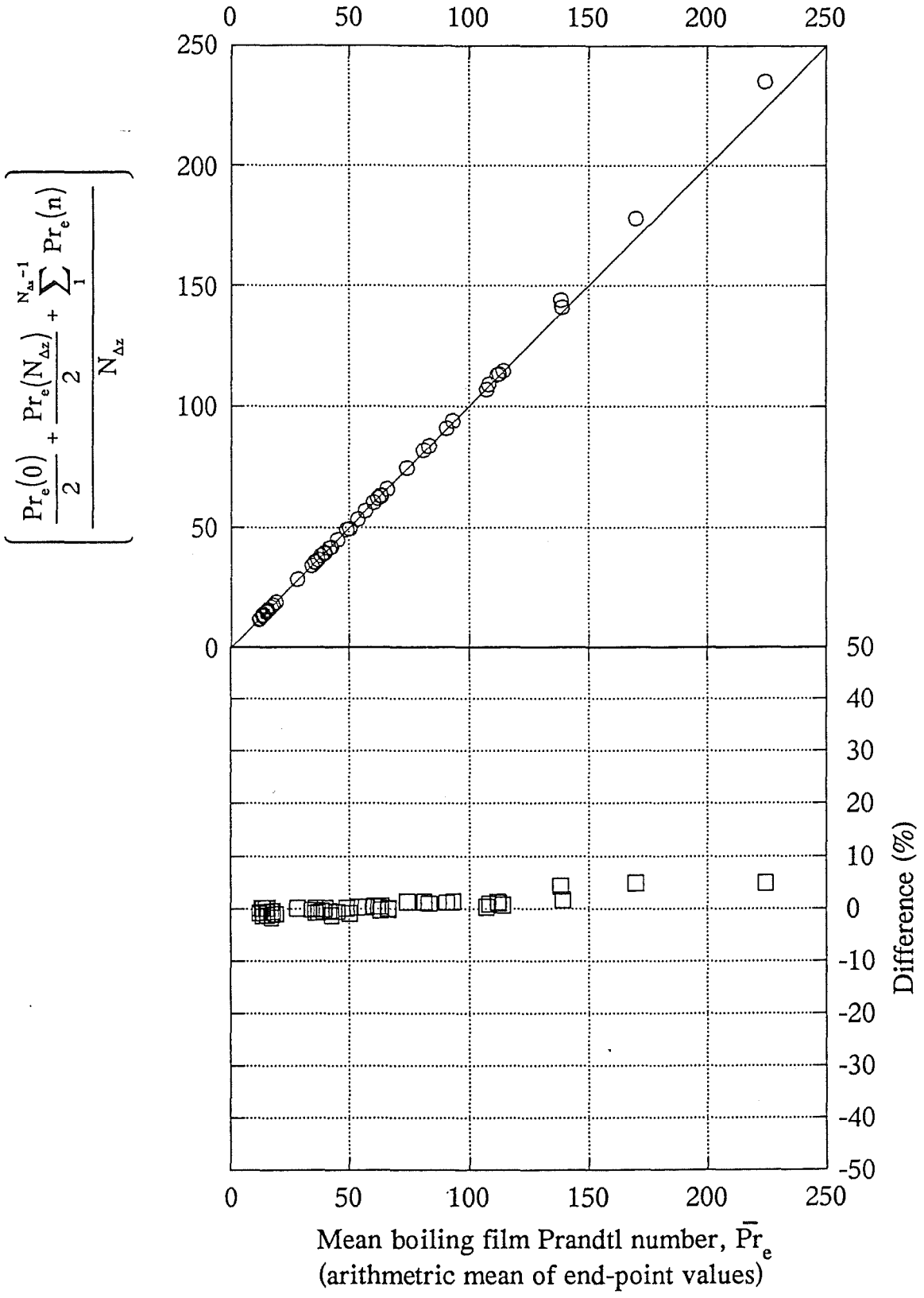

Figure 25.10: Comparison of Methods of Determining the Mean Boiling Film Prandtl Number.

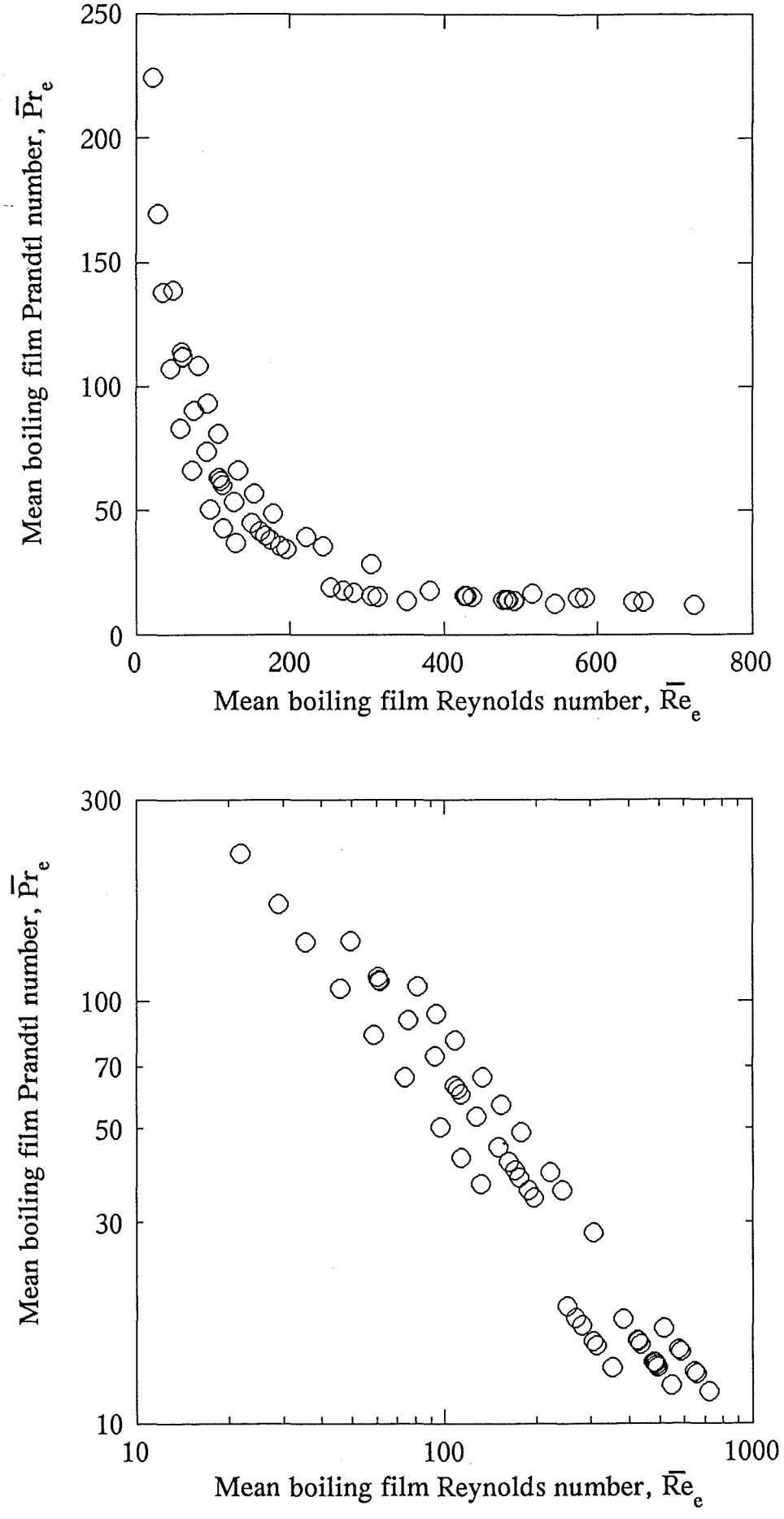

Figure 25.11: Combinations of $\bar{Re}_e$ and $\bar{Pr}_e$ Used in Experiments Su1-Su5.

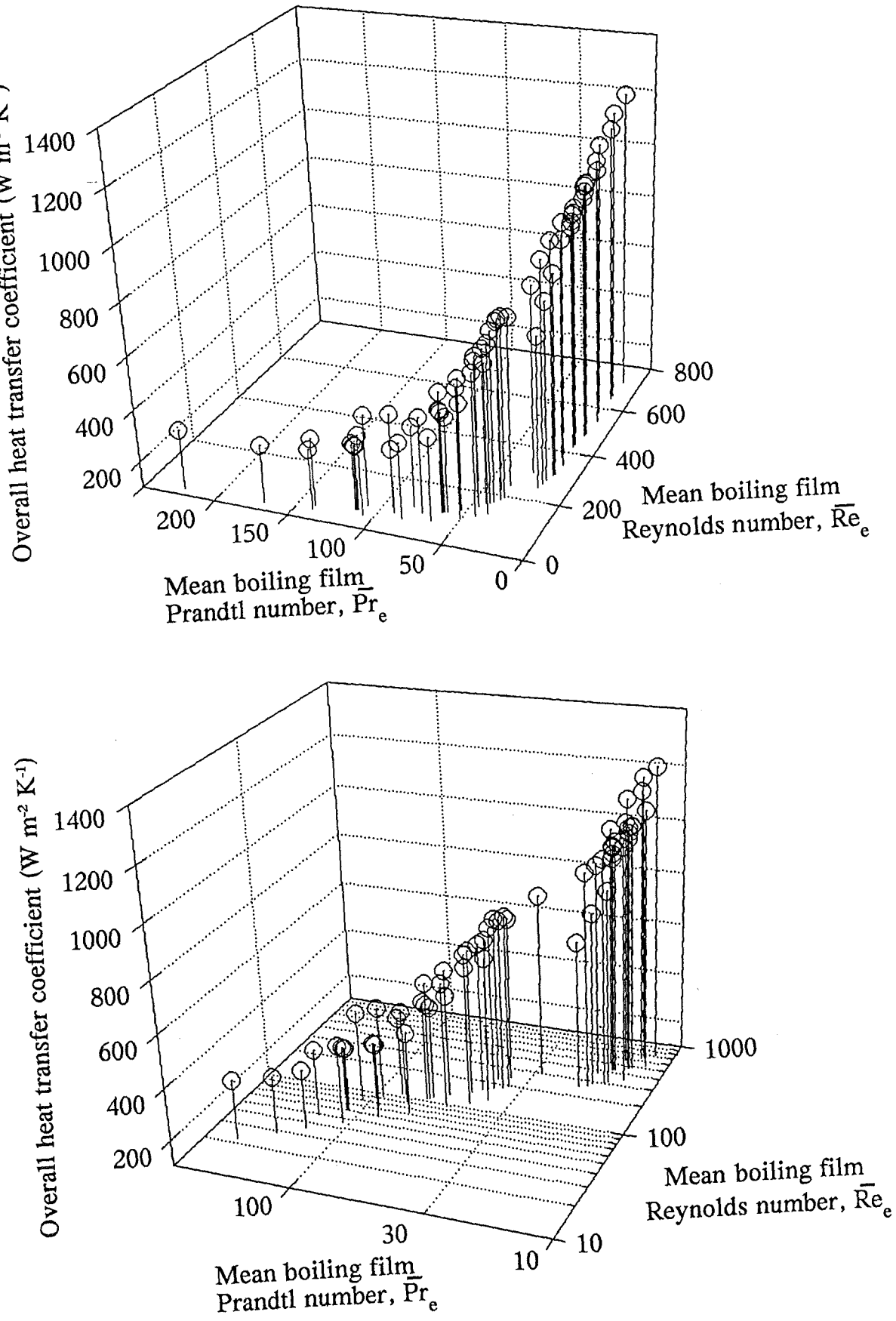

Figure 25.12: Overall Heat Transfer Coefficients in Terms of Re_e and Pr_e (Data from Experiments Su1-Su5).

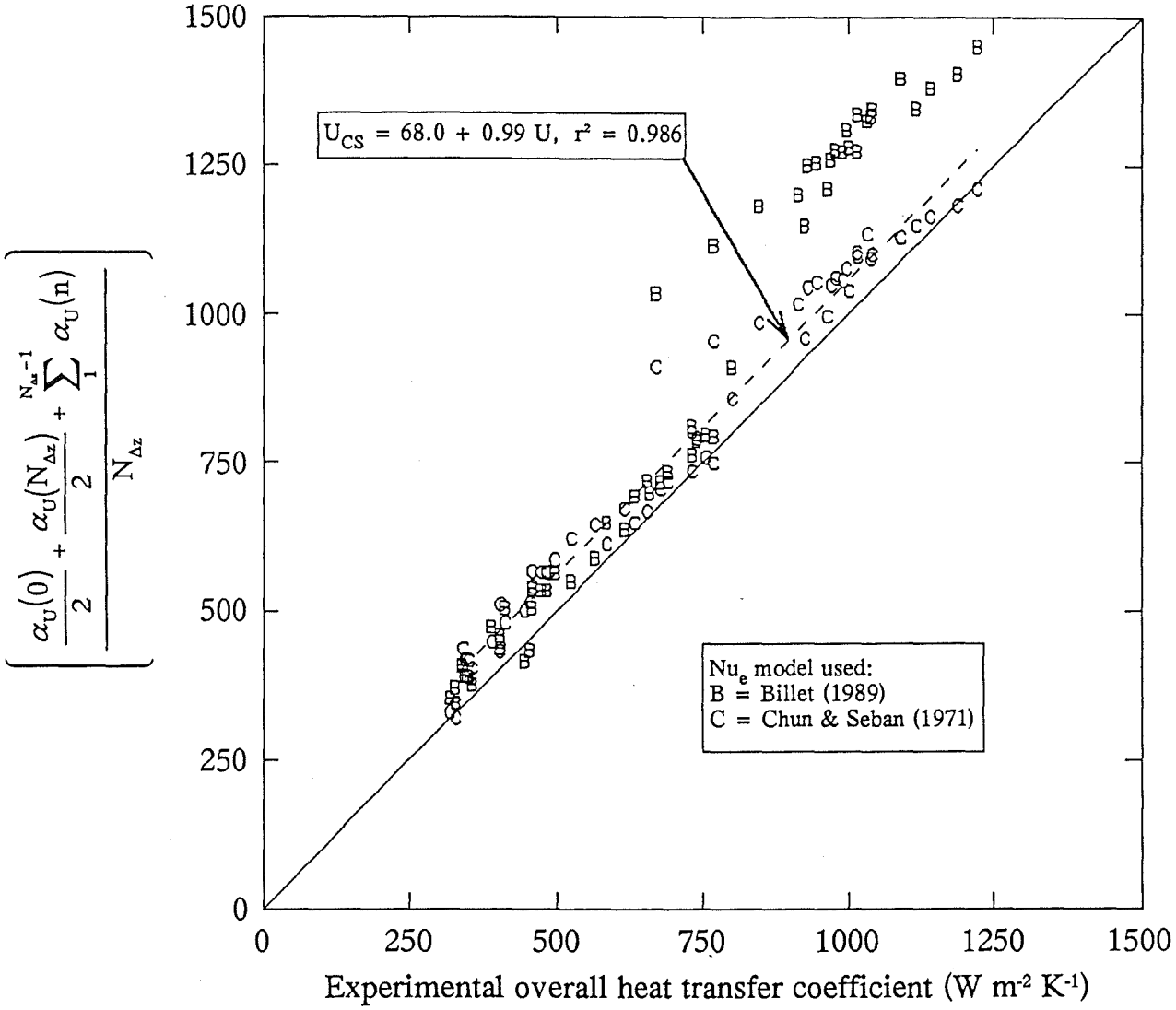

Figure 25.13: Comparison of the Experimental Overall Heat Transfer Coefficients with the Numerical Integration Results (Data from Experiments Su1-Su5).

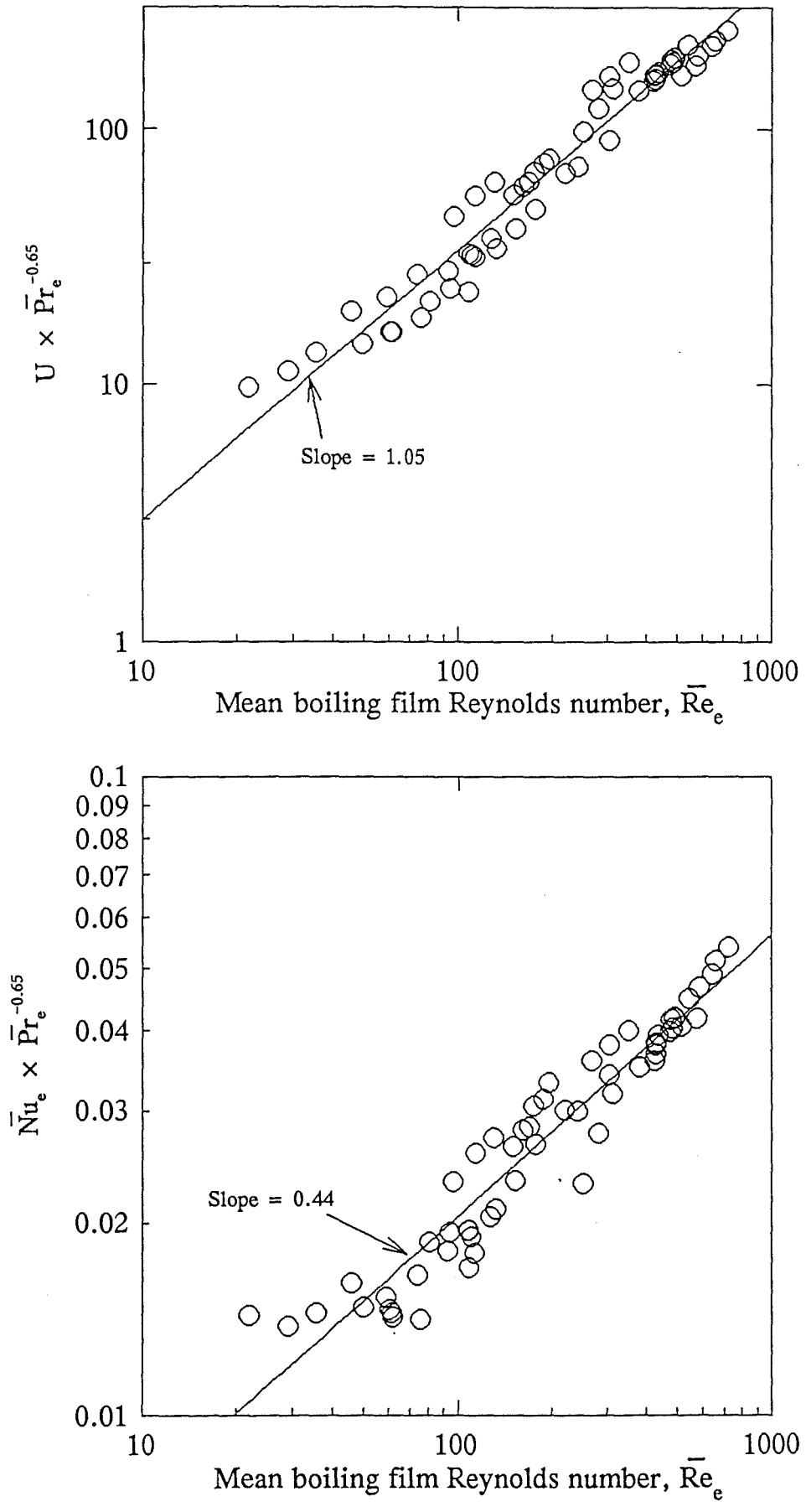

Figure 25.14: Determination of Fit of Chun & Seban's Turbulent Nu_e Correlation to Data from Experiments Su1-Su5.
(Using Means of End-point Values for Re_e and Pr_e.)

25.2 Discussion

Check on sucrose concentration

The feed density meter was calibrated (see Appendix B) using sucrose solutions prior to the sugar experiments, by assuming the correlation between density and concentration at a known temperature (see Section G13). The samples were taken from the balance tank during the sucrose experiments to confirm that there was no drift in the calibration. The laboratory total solids (concentration) results (see Table I30) had a mean value of 48.64% w/w which was 0.27% lower than the mean predicted concentration (48.91% w/w) calculated from the feed density and temperature. The accuracy of the laboratory total solids method is reflected in part by the allowable difference between the two replicates (0.3% w/w). Due to the recirculation of concentrate, there were visible variations in concentration in the top layer of the sucrose solution in the feed balance tank which made obtaining a representative sample difficult. The contents of the tank were agitated to reduce the large vertical concentration gradient observed previously, but the agitation was not severe enough to completely eliminate the vertical concentration gradient. These three factors could clearly account for the observed differences and thus there is no reason to suspect the calibration of the feed density meter.

Effect of experimental design variables

The effect of increasing the feed flow rate is to increase the overall HTC (see Figures 25.1 and 25.2). This can be partially attributed to an increase in turbulence, but is more likely due to the reduction in the mean concentration over the length of the tube (due to the lower concentration ratio) and thus a reduction in $\overline{BPE}$ and $\overline{\mu}_e$ (reduced film thickness) and an increase in $\overline{k}_e$. Another factor was the reduced vertical concentration gradient in the feed balance tank at high feed flow rates (due to a shorter residence time) which led to lower feed concentrations for the high flow rate runs.

The effect of increasing boiling pressure (or vapour temperature) on the overall HTC is less clear, with a slight negative (if any) effect at high sugar concentrations (see Figure 25.1) and a moderate positive effect at low sugar concentrations (see Figure 25.2). The reduction in $\overline{\mu}_e$ and the increase in $\overline{k}_e$, with increasing boiling pressure, would be expected to improve the overall HTC and this effect should be greatest at high concentrations due to massive changes in $\overline{Pr}_e$. However, the vapour velocity decreases with increasing boiling pressure, and the results indicate that it may

be a significant factor, at high concentrations, in improving heat transfer.

Differences between centre point replicates

The centre point replicates for Experiment Su2 (see Figure 25.1) were all within 2% of each other. A wider variation (10%) was obtained for Experiment Su5 (see Figure 25.2). The difference appears to be due to a greater variation in actual feed concentration in Experiment Su5 (40.2-40.7% w/w) than for Experiment Su2 (62.2-62.4% w/w). This was a contributing factor in the decision to present the results in terms of $\bar{Re}_e$ and $\bar{Pr}_e$ rather than in terms of the experimental design variables; feed concentration, feed flow rate, and, boiling pressure.

Measurement of boiling point elevation

The values obtained for BPE (see Figure 25.3) appear to be reasonably independent of boiling pressure, although there was some suggestion (particularly at lower concentrations) that BPE decreased as the boiling pressure increased. This conflicts with previous work (Nicol, 1968) and theory (Equation 2.1) which show that BPE increases with temperature. Thus, as the range of vapour temperatures was only 10°C for the sucrose experiments, the curve fitted to the BPE data (Equation 25.1) was based solely on sucrose concentration.

Integration of local Nu_e correlations with respect to z

The integration of local Nu_e revealed that the HTC dropped drastically over the length of the tube (see Figure 25.4) due mainly to a rapid increase in BPE and μ_e (which increased the boiling film thickness) and a reduction in k_e (see Figure 25.6). The temperature profiles (see Figure 25.5) demonstrate that the boiling-side film provides the main resistance to heat transfer to solutions and that the BPE can drastically reduce the effective temperature driving force. The integration procedure does not take the vapour velocity conditions into account. High vapour velocities would tend to increase the film surface velocity and flatten the film against the wall, leading to an increased HTC. The vapour velocity is greatest at the bottom of the tube (see Figure 25.7) so there would be more evaporation at the bottom of the tube, than the integration procedure predicts.

Determination of $\bar{Re}_e$ and $\bar{Pr}_e$

The determination of $\bar{Re}_e$ and $\bar{Pr}_e$ is difficult when local conditions over the length of the tube are unknown. When end-point values are known, an approximation of the mean

can be arrived at using *eg* either an arithmetic or logarithmic mean of the end points. However, this does involve an assumption concerning the way in which the fluid property changes with length. If local property correlations are available, an integration procedure can be used to determine the change of the fluid property with respect to length. Depending on the assumptions made, this should offer a better approximation of the mean value. However, the distinction between an experimental data point and a theoretical or predicted data point can be become blurred, leading to arguments regarding circularity. Therefore, as the difference between the means derived from end-point values and from integration was usually small (see Figures 25.9 and 25.10), and that in practice the integrated results are not readily available, the mean of the end-point values was used. The effect of this on the exponents obtained for $\overline{Re}_e$ and $\overline{Pr}_e$ is discussed below.

Applicability of dimensionless group models

The heat transfer to a boiling falling film can be described using dimensional analysis (see Appendix L). For this experiment the most important dimensional groups were found to be $\overline{Re}_e$ and $\overline{Pr}_e$. When using only one solute (*i.e.* sucrose) it is impossible to avoid some correlation between the experimental values of $\overline{Re}_e$ and $\overline{Pr}_e$. In these experiments, there was a high correlation between the two dimensionless groups (see Figure 25.11) and thus any model fitted would be of limited value. However, there was a clear trend (see Figure 25.12) that the overall HTC increased as the ratio of $\overline{Re}_e$ over $\overline{Pr}_e$ increased.

$\overline{Nu}_e$ correlations

The experimental overall HTC values were compared (see Figure 25.13) with the predicted values obtained by integration with respect to distance from the top of the tube using both Chun & Seban (1971) and Billet (1989) local Nu_e correlations. There was good agreement with both for U values below 700 W m^{-2} K^{-1} (high $\overline{Pr}_e$, low $\overline{Re}_e$). For high U values, Billet's correlations overestimate by 20-40% due to the poor fit of Billet's transitional Nu_e correlation. Chun & Seban's correlations give good predictions for overall HTC values over 900 W m^{-2} K^{-1}. For overall HTC values between 700 and 900 W m^{-2} K^{-1} there were three experimental points which gave lower values than expected, which may to due to a change in flow behaviour in the film. It was not due to a change in Nu_e correlation as for all the experimental points the local Re_e was within

Chun & Seban's turbulent zone over the full length of the tube.

When U * $\bar{Pr}_e^{-0.65}$ is plotted against $\bar{Re}_e$ on a log-log plot (see Figure 25.14), the slope of the line gives the exponent (b) and the intercept gives the coefficient (a) in the following equation[1]:

$$U = a \bar{Re}_e^{\,b} \bar{Pr}_e^{0.65} \tag{25.2}$$

The slope was 1.05 and the y axis intercept was -0.58, so the data can be described by:

$$U = 0.264 \bar{Re}_e^{1.05} \bar{Pr}_e^{0.65} \tag{25.3}$$

with a regression coefficient, r^2 of 0.98.

If the 'experimental' $\bar{Nu}_e$ (see Chapter 12 for calculation method) is used instead of U (see Figure 25.14) the following equation is obtained with a regression coefficient, r^2 of 0.96:

$$\bar{Nu}_e = 0.00269 \bar{Re}_e^{0.44} \bar{Pr}_e^{0.65} \tag{25.4}$$

The exponent 0.44 compares well with the 0.4 exponent of Chun & Seban (1971). The difference between the exponent on Re for the U and $\bar{Nu}_e$ correlations can be attributed to the effect of $\bar{BPE}$ which decreased as $\bar{Re}_e$ increased in this experiment. The apparent change in slope at $\bar{Re}_e$ of about 50 (see Figure 25.14) may be due to the film exhibiting laminar or early transitional behaviour in this region.

If the experimental values of $\bar{Re}_e$ and $\bar{Pr}_e$ are determined from the integration procedure, then the $\bar{Re}_e$ exponents are 1.13 and 0.48 for U and $\bar{Nu}_e$ respectively and the regression coefficients improve slightly (see Figure 25.15). The difference in the slope of the $\bar{Nu}_e$ * $\bar{Pr}_e^{-0.65}$ against $\bar{Re}_e$ line can be attributed mainly to the large change in position of the three lowest $\bar{Re}_e$ points.

---

[1] The exponent of 0.65 for the Prandtl number comes from the Chun & Seban (1971) correlation for turbulent flow.

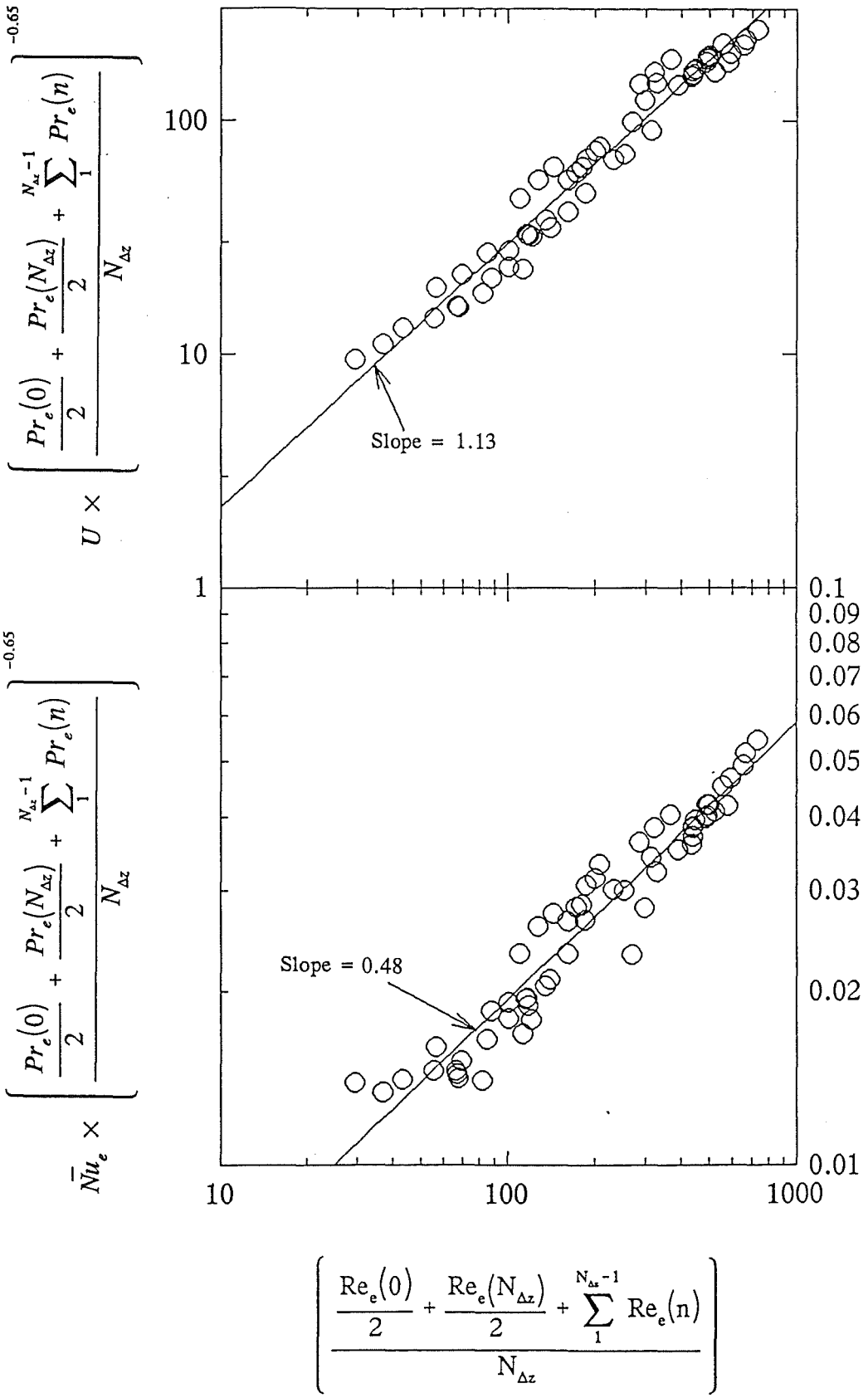

Figure 25.15: Determination of Fit of Chun & Seban's Turbulent Nu_e Correlation to Data from Experiments Su1-Su5. (Using Means Determined by Integration for Re_e and Pr_e.)

26 SUCROSE FIFTH EVAPORATOR EXPERIMENTS

The experimental design and procedure for these experiments are covered in Chapters 23-24.

26.1 Experiments Su6-Su10 Results

The raw data for Experiments Su6-Su11 are tabulated in Appendix I.

Effect of independent variables on the overall HTC

The effects of temperature driving force, degree of flash, and, tube diameter on the overall HTC are shown for each feed concentration in Figures 26.1 and 26.2.

Mean values for independent variables

A dimensional analysis of boiling side heat transfer (See Appendix L) demonstrated that the system could be described in terms of Re_e, Pr_e, Ja_e, $N_{\Gamma v/\Gamma e}$ and $N_{L/d}$. When boiling point elevation is significant an additional dimensionless group is required:

$$N_{BPE} = \frac{(\Delta T_e - BPE)}{\Delta T_e} \qquad (26.1)$$

N_{BPE} can be viewed as a normalised effective boiling film temperature driving force. As ΔT_e is unknown, it was replaced by ΔT_U, to obtain Ja_e^* and N_{BPE}^*. Values for $\bar{Re}_e$, $\bar{Pr}_e$, $\bar{Ja}_e^*$, $\bar{N}_{\Gamma_v/\Gamma_e}$ and $\bar{N}_{BPE}^*$ were determined for each experimental point by taking either an arithmetic or logarithmic average (see Chapter 12) of the values at the top and bottom of the tube.

Correlations between dimensionless groups

The combinations of $\bar{Re}_e$, $\bar{Pr}_e$, $\bar{Ja}_e^*$, $\bar{N}_{\Gamma_v/\Gamma_e}$, $\bar{N}_{BPE}^*$ and $N_{L/d}$ used in Experiments Su6-Su11 are shown in Figure 26.3.

Experimental overall heat transfer coefficients

The overall HTCs determined from the integration procedure (see Appendix H) using Chun & Seban (1971) and Billet (1989) local Nu_e correlations are plotted against the experimental overall HTC values in Figure 26.4. The Chun & Seban predicted values were closer to the experimental values than those of Billet. The slope of 0.63 for the Chun & Seban predicted values is partially an artifact of the strong tube diameter effect, which neither Chun & Seban or Billet account for. If correlations are fitted to the data

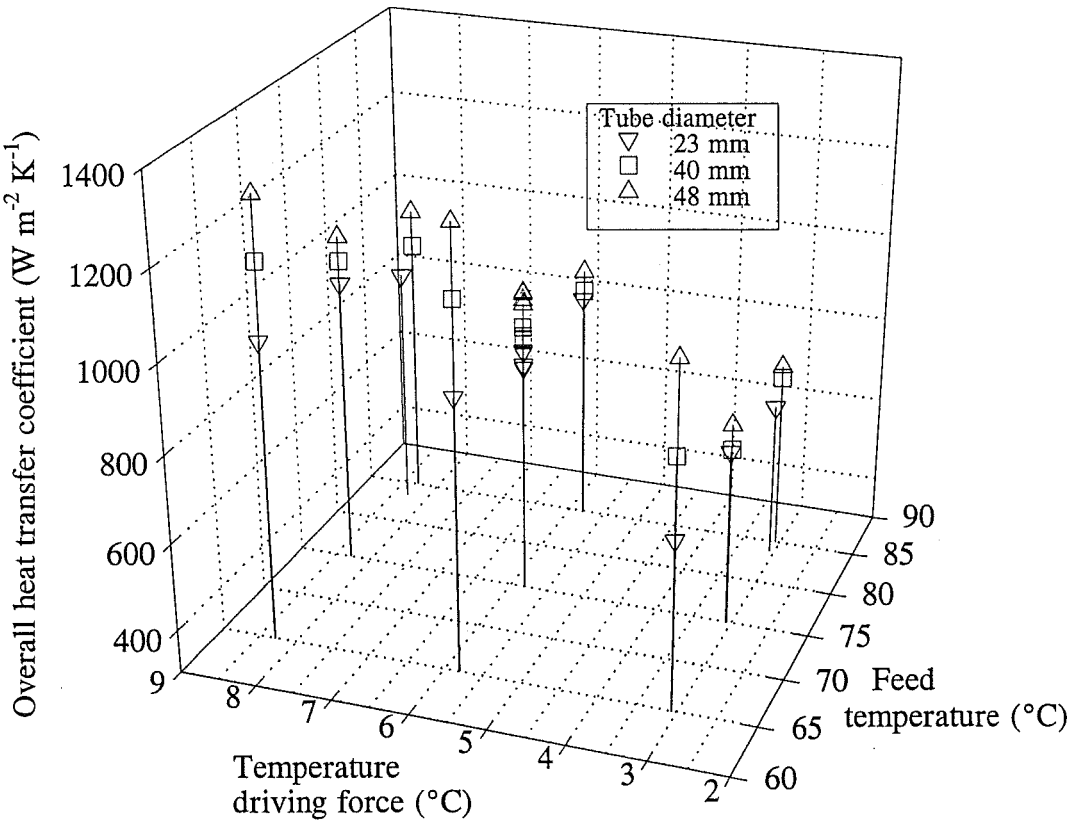

Figure 26.1: Overall Heat Transfer Coefficients for a Sucrose Feed Concentration of 40% w/w (Data from Experiments Su6-Su8).

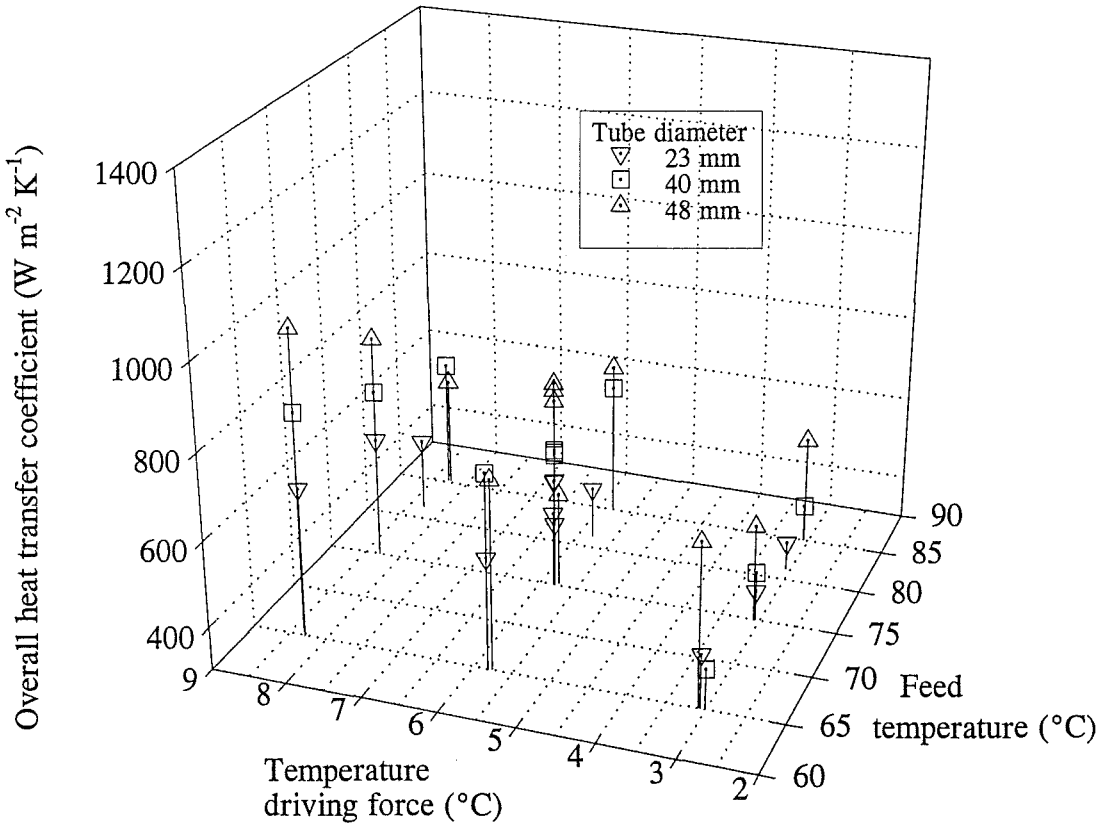

Figure 26.2: Overall Heat Transfer Coefficients for a Sucrose Feed Concentration of 50% w/w (Data from Experiments Su9-Su11).

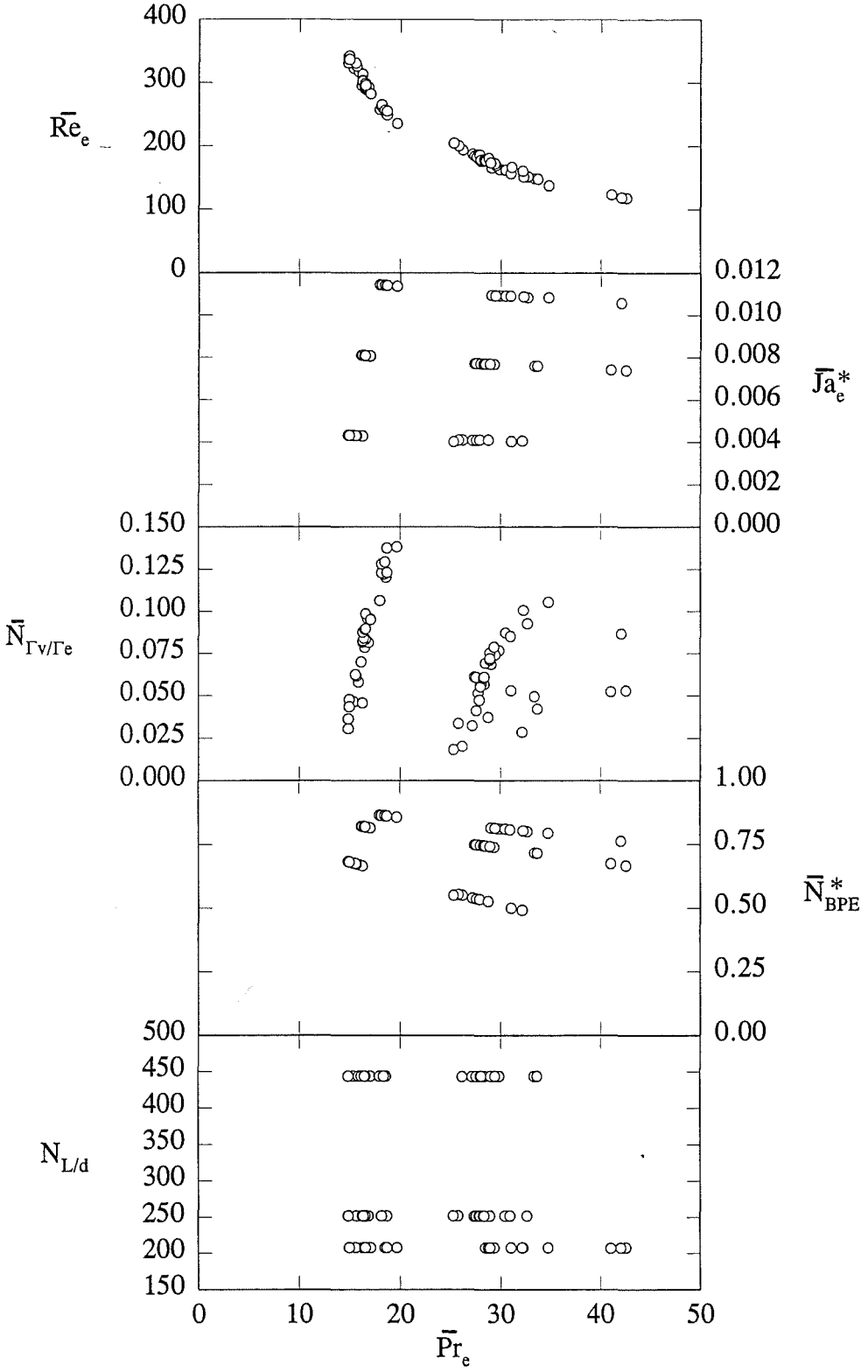

Figure 26.3: Correlations between the Dimensionless Groups for Experiments Su6-Su11.

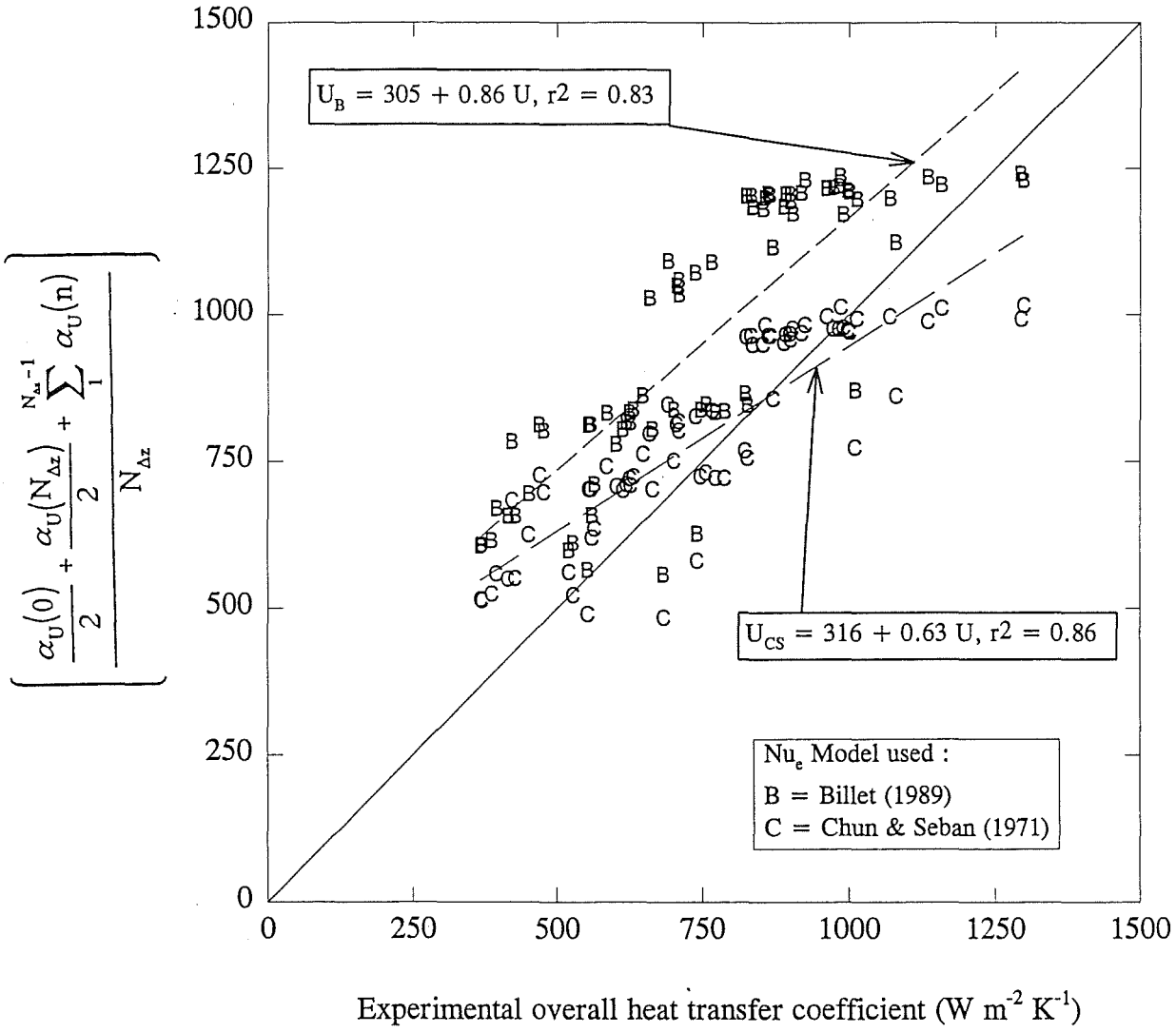

Figure 26.4: Comparison of the Experimental Overall Heat Transfer Coefficients with the Numerical Integration Results (Data from Experiments Su6-Su11).

from each tube independently, then the slope ranged from 0.7 (40 & 48 mm tubes) to 0.8 (23 mm tube).

The following equation form was fitted (using SigmaPlot Version 5.0, Jandel Scientific, USA) to the data from Experiments Su6-Su11:

$$U = a\,Re_e^{\,b}\,Pr_e^{\,c}\left(Ja_e^{*}\right)^{d}\left(N_{\Gamma_v/\Gamma_e}\right)^{e}\left(N_{BPE}^{*}\right)^{f}\left(N_{Ld}\right)^{g} \tag{26.1}$$

to obtain the exponents shown below:

$$U = 183\,\bar{Re}_e^{\,0.68}\,\bar{Pr}_e^{\,0.18}\left(\bar{Ja}_e^{*}\right)^{-0.16}\left(\bar{N}_{\Gamma_v/\Gamma_e}\right)^{0.14}\left(\bar{N}_{BPE}^{*}\right)^{0.56}\left(N_{Ld}\right)^{-0.27} \tag{26.2}$$

The fit of Equation 26.2 is shown in Figure 26.5. A regression line fitted to the points on Figure 26.5 gave a r^2 of 0.87. In addition, Equation 26.1 (with fixed exponents of 1.05 and 0.65 for $\bar{Re}_e$ and $\bar{Pr}_e$ respectively) was fitted to allow comparison with the Third Evaporator sucrose experimental results (presented in Chapter 25). Fitting the above equation to the data, the following coefficients were obtained:

$$U = 3.8\left[\bar{Re}_e^{\,1.05}\,\bar{Pr}_e^{\,0.65}\right]\left(\bar{Ja}_e^{*}\right)^{0.03}\left(\bar{N}_{\Gamma_v/\Gamma_e}\right)^{0.19}\left(\bar{N}_{BPE}^{*}\right)^{0.86}\left(N_{Ld}\right)^{-0.26} \tag{26.3}$$

The fit of Equation 26.3 is shown in Figure 26.6. A regression line fitted to the points on Figure 26.6 gave a r^2 of 0.87. To increase the range of Re_e and Pr_e the Fifth Evaporator water experimental data (from Experiments Wa29, Wa30 and Wa32) was included and the above two equation forms fitted. The two equations obtained were as follows:

$$U = 114\,\bar{Re}_e^{\,0.63}\,\bar{Pr}_e^{\,0.24}\left(\bar{Ja}_e^{*}\right)^{0.02}\left(\bar{N}_{\Gamma_v/\Gamma_e}^{*}\right)^{-0.02}\left(\bar{N}_{BPE}^{*}\right)^{1.4}\left(N_{Ld}\right)^{-0.32} \tag{26.4}$$

$$U = 12\left[\bar{Re}_e^{\,1.05}\,\bar{Pr}_e^{\,0.65}\right]\left(\bar{Ja}_e^{*}\right)^{0.15}\left(\bar{N}_{\Gamma_v/\Gamma_e}\right)^{-0.1}\left(\bar{N}_{BPE}^{*}\right)^{1.24}\left(N_{Ld}\right)^{-0.35} \tag{26.5}$$

The fit of each of Equations 26.4 and 26.5 to the data is shown in Figures 26.7 and 26.8 respectively. Regression lines fitted to the data in both figures each had a r^2 of 0.98.

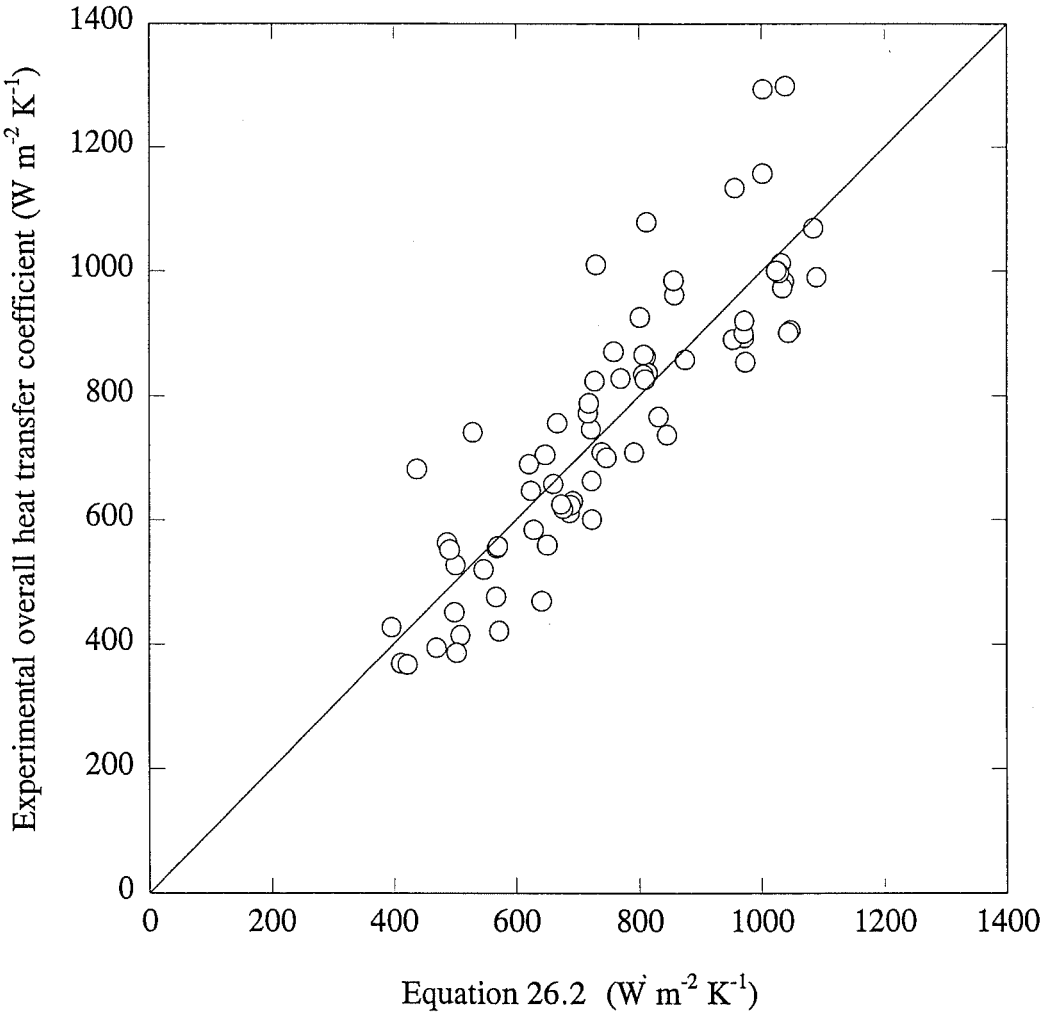

Figure 26.5 Fit of Equation 26.2 to Data from Experiments Su6-Su11.

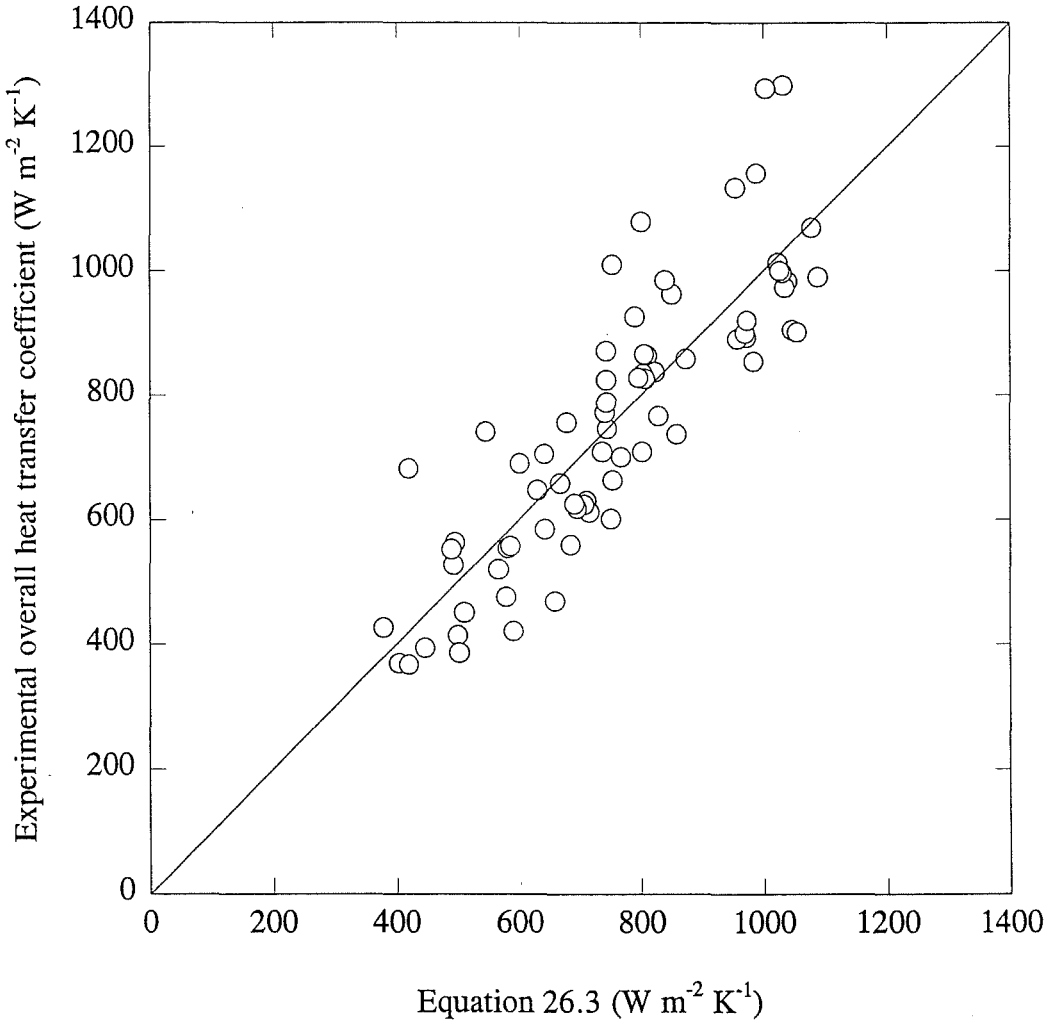

Figure 26.6: Fit of Equation 26.3 to Data from Experiments Su6-Su11.

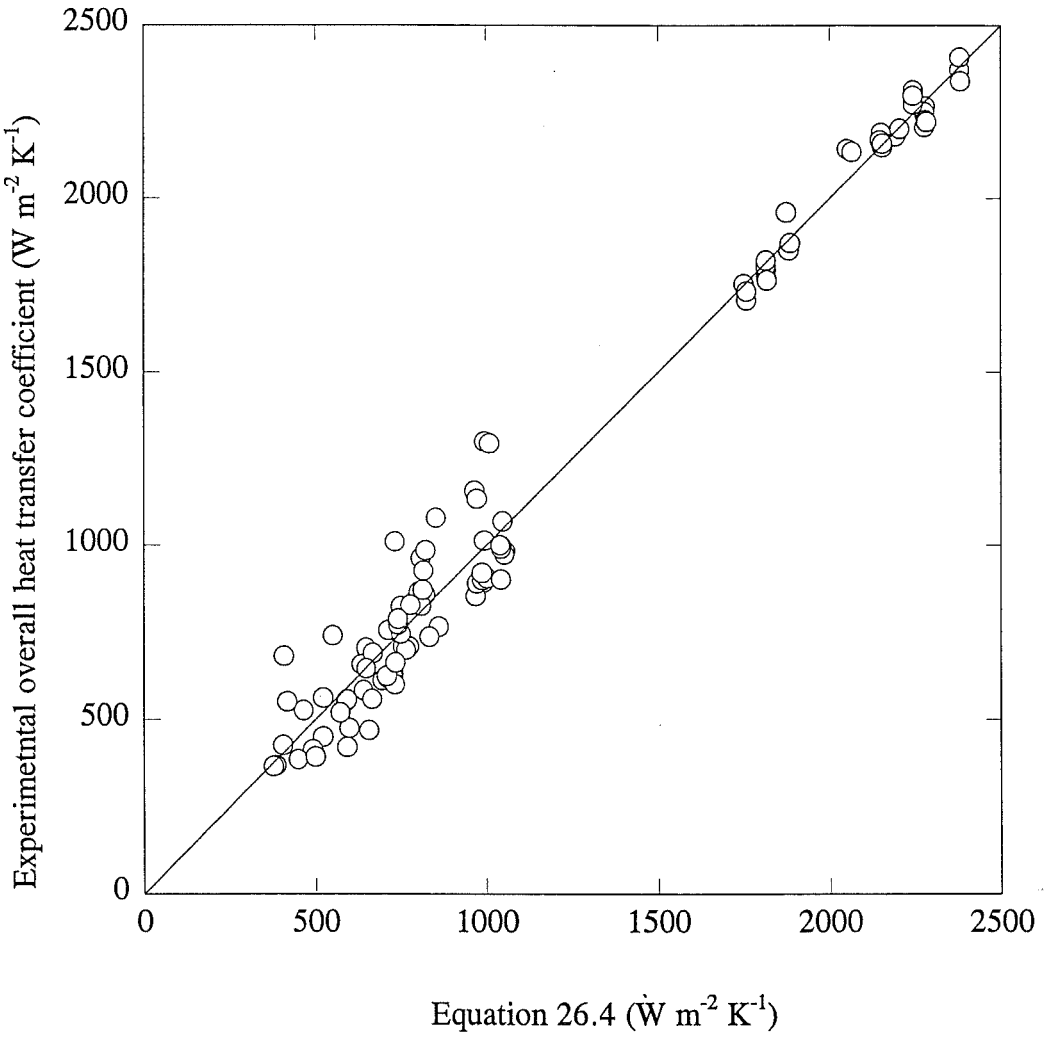

Figure 26.7: Fit of Equation 26.4 to Data from Experiments Su6-Su11, Wa29, Wa30 & Wa32.

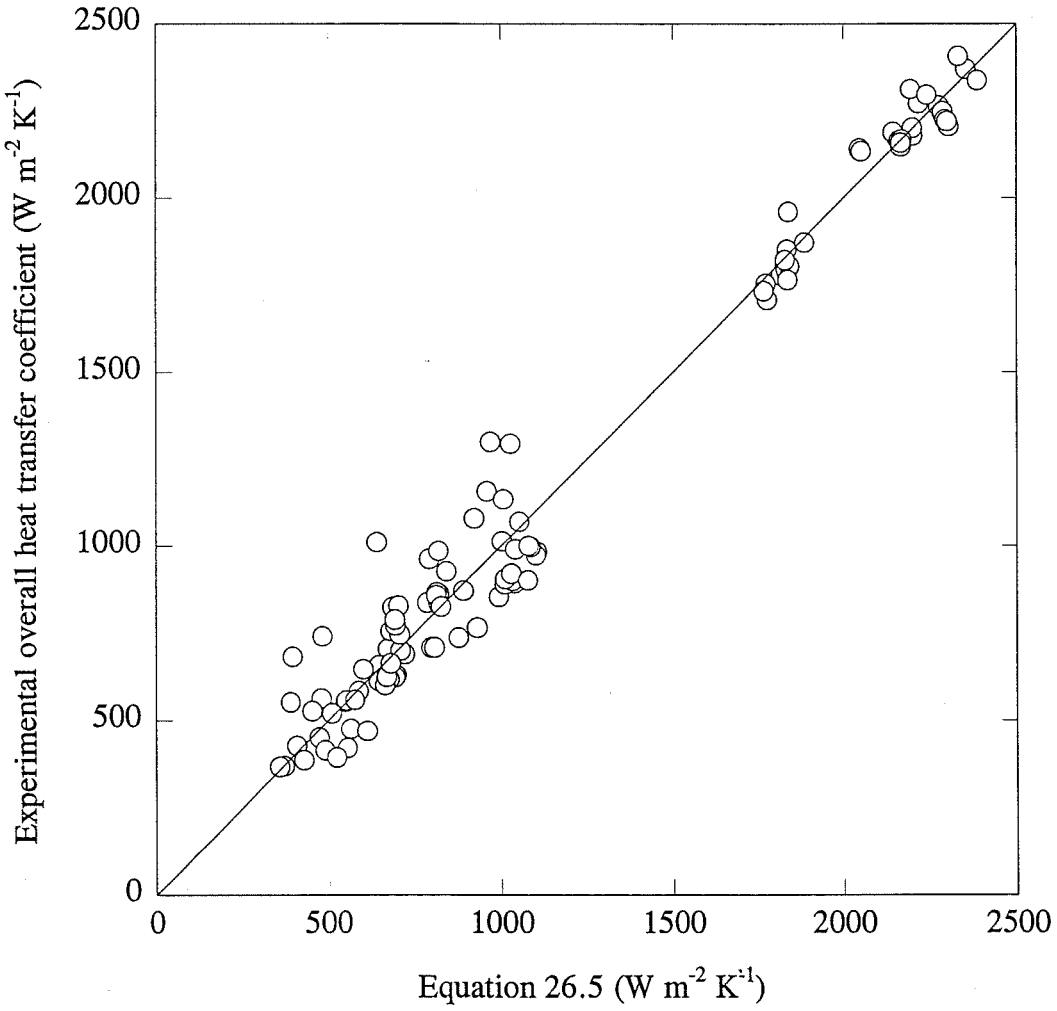

Figure 26.8 Fit of Equation 26.5 to Data from Experiments Su6-Su11, Wa29, Wa30 & Wa32.

26.2 Discussion

Comments on issues discussed in Chapter 25

The measurement of sucrose concentration, the determination of BPE, the integration of local Nu_e with respect to length and the choice of a method for determining experimental $\bar{Re}_e$ and $\bar{Pr}_e$ values have been discussed in Section 25.2.

The range of $\bar{Re}_e$ and $\bar{Pr}_e$ used in Experiments Su6-Su11 was well within the range used in Experiments Su1-Su5 so the mean of end-point values was also used for data analysis here. The accuracy of the absolute pressure (AP) measurement on the Fifth Evaporator was slightly suspect, and therefore the Third Evaporator AP sensor was also mounted on the Fifth effect to give an independent reading. The Third Evaporator AP sensor gave readings that were 0.75 kPa lower but some of this could have been due to the difference in location of the remote diaphragm seal. The product temperature on water (see Table I22) indicates that the absolute pressure should be 0.5 kPa lower than indicated by the Fifth Evaporator AP measurements. The Fifth Evaporator AP readings were used for data analysis purposes, but due to the uncertainty, the BPE figures from Experiments Su6-Su11 were not used in determining the sucrose BPE correlation presented in Section G19.

Change in colour of sucrose solution

The same sucrose solution (with some addition of sucrose) was used for Experiments Su6-Su11. As the experiments proceeded the solution changed from almost clear (very light golden) to dark brown in colour. Colour development is dependent on several factors including temperature, storage time and presence of traces of reducing sugars and coloured non-sugars (Pancoast & Junk, 1980, p52). The reason for the rapid increase in colour observed could be due to keeping the sugar at temperatures between 45-95°C over several days in which case there is unlikely to be any changes in fluid transport properties. However, the high preheat temperatures used (in excess of 95°C immediately after the PHE) could have caused caramelization of the sugar which may change the fluid transport properties.

Effect of experimental design variables

The tube diameter was found to have a dramatic positive effect on the overall HTC for the water experiments (see Chapter 23) and the effect was greater on sucrose solutions (see Figures 26.1 and 26.2). The effect of increasing the temperature driving force was positive which is expected, as the increased film temperature would improve fluid

transport properties and increase the effective temperature driving force ($\bar{N}^{*}_{BPE}$). The negative effect of an increased condensate film thickness was insignificant. The effect of increasing the feed temperature had a negative effect on the overall HTC, due to the increase in concentration (after flash).

Nu_e correlations

The comparison (see Figure 26.4) of the experimental U values with the predicted values obtained by integration with respect to z showed considerable scatter, indicating the predicted models clearly did not account for all variables, in particular, tube diameter.

Experimental correlations between dimensionless groups

There was a high experimental correlation between $\bar{Re}_e$ and $\bar{Pr}_e$ (see Figure 26.3) in Experiments Su6-Su11. However there was a reasonable spread when $\bar{Pr}_e$ was compared with the other dimensionless groups ($\bar{Ja}^{*}_{e}$, $\bar{N}_{\Gamma_v/\Gamma_e}$, $\bar{N}^{*}_{BPE}$ and $N_{L/d}$) so dimensional models were fitted to the data.

Dimensional group model

The exponents of $\bar{Re}_e$ and $\bar{Pr}_e$ in Equations 26.2 and 26.4 are significantly different to those found during the Third Evaporator experiments (see Chapter 25). Given the high correlation between $\bar{Re}_e$ and $\bar{Pr}_e$, their exponents were fixed at values determined during the Third Evaporator experiments. This enabled the effect of the other variables to be ascertained.

The effect of $\bar{Ja}^{*}_{e}$ was insignificant for the water data (Equation 21.6) and for the sucrose data (Equation 26.3), but there was a small positive effect for the combined water and sucrose data (Equation 26.5). This is reasonable, given the competing effects of a higher effective temperature driving force and a thicker condensate film as the temperature driving force increases (see Chapter 19). $\bar{N}_{\Gamma_v/\Gamma_e}$ had a positive effect for the sucrose data alone, but was insignificant for the water data and combined water-sucrose data. $N_{L/d}$ had a small negative effect. $N_{L/d}$ and $\bar{N}_{\Gamma_v/\Gamma_e}$ are highly correlated which would explain the differences between the exponents in Equations 21.5, 26.3 and 26.5. The possible causes of the observed tube diameter effect have been discussed in depth in Chapter 21. $\bar{N}^{*}_{BPE}$ had a large positive effect as expected given that it is a normalized effective temperature driving force.

27 DISCUSSION - SUCROSE EXPERIMENTS

The experiments on sucrose solutions were carried out for several reasons. The physical properties of sucrose were reasonably well known and it was cheap, non-corrosive, not heat sensitive (at boiling temperatures of 55-65°C) and readily available. Sucrose solutions exhibit Newtonian behaviour and are thus considered to be "ideal" solutions for determining the effect of concentration on heat transfer. The BPE of sucrose solutions is much higher than that of skim milk at the same total solids concentration, which meant that the $\overline{BPE}$ has a dominant effect on the heat transfer rate.

The change in concentration over the length of the tube presents difficulties when trying to determine local heat transfer rates. Chun & Seban (1972) presented an integration procedure for the evaporation of a pure liquid. This work presents the results of a numerical integration procedure for the evaporation of solutions. The procedure accounts for the change in fluid properties due to concentration over the length of the tube. The concentration gradient across the film was ignored in this work for simplicity. Thus, the integration procedure underestimates the sucrose concentration at the liquid-vapour interface, and so the effect of BPE is underestimated. The effect of NCG in the steam was also not included in the model, due to the high de-aeration rates used for the experiments. The incorporation of the effect of the vertical gradient in NCG concentration is simple, but horizontal gradients would be more difficult. Modelling of NCG concentration profiles in the steam is discussed in Chapter 34.

The physical properties of sucrose were readily available with the exception of BPE and enthalpy. An enthalpy diagram (see Figure 27.1) was determined based on heat of solution and heat of dilution data sourced from Pancoast & Junk (1980) and referenced to water (infinite dilution) at 0.01°C. The resultant equation can be found in Section G3.4. The available BPE correlations (Nicol, 1968) were in the wrong form, so a curve fitted to the experimental data from Experiments Su1-Su5 was used.

It is virtually impossible to obtain correlations of the effects of Re_e and Pr_e independently of α_e or U under conditions of common practice in dairy evaporators. The long tube length means that there are significant concentration ratios for the range of practical flow rates and also Re_e and Pr_e are strongly correlated. To evaluate the effect of Pr_e independently of Re_e would require a range of pure liquids, few of which would be acceptable in a dairy factory due to hygiene requirements.

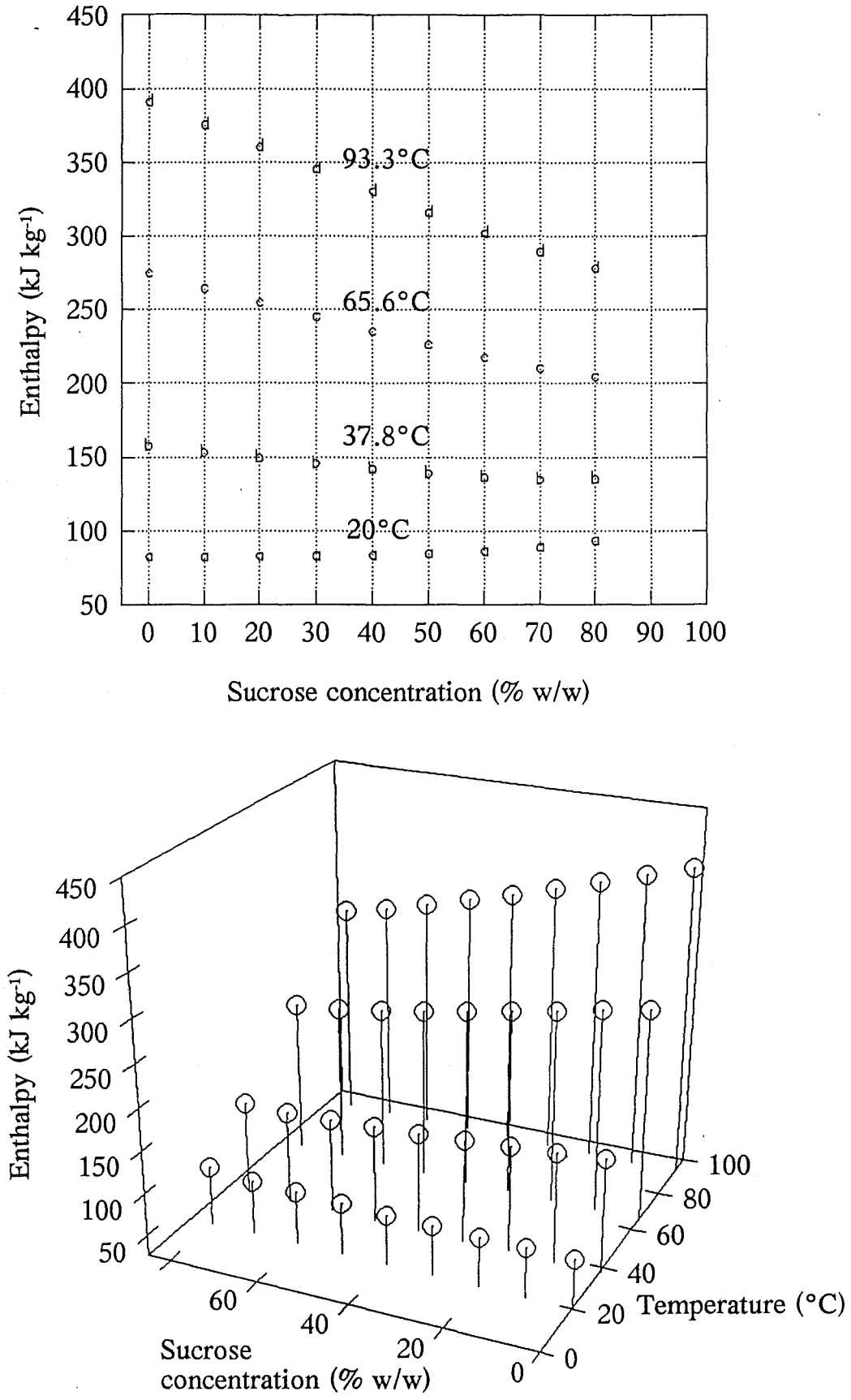

Figure 27.1: Enthalpy Diagrams for Sucrose Solutions.

28 EXPERIMENTAL DESIGN - SKIM MILK

28.1 Standard Operating Conditions

The standard operating conditions for all experiments unless expressly stated were as described in Section 13.1 except for:

Feed type skim milk (with a range of solids concentrations and preheat treatments)

28.2 Run Order

The nature of the experiments made full randomisation logistically difficult. This was because the low concentration feed stocks were obtained by diluting the high concentration feed stocks and there were only a limited number of tanks available. For Experiments Sk1 and Sk2, the centre-points were placed at regular intervals throughout the experiment to determine any time trends. The runs at each concentration were blocked and randomised within the blocks. In Experiment Sk2 where two levels of feed rate were used for each run, the feed flow rate order was randomized.

28.3 Skim Milk Experiments

The three experiments carried out are listed in Table 28.1.

Table 28.1 Skim Milk Experiments

Experiment	Date	Experimental Variables
Sk0	14-16 Jan 1991	Fresh versus Reconstituted Feed
Sk1	21-24 Jan 1992	Preheat treatment & Feed Concentration
Sk2	02-06 Mar 1992	Preheat treatment, Feed Concentration, Feed flow rate, Steam valve position

The objective of the first experiment was to determine whether reconstituted milk behaved like fresh milk during evaporation. If the behaviour was similar, then experimental work could have been done using one batch of commercial powder, thus eliminating variations in milk composition between runs. Experiment Sk0 was to be two

20-h steady state runs using milk which had been given a high preheat treatment (120°C for 180 s). The first run used skim milk concentrate which had been diluted to approximately 30% w/w. The second run was to use powder reconstituted to 30% w/w. The Research Evaporator feed flow rate was set at 70 kg h^{-1}.

The second experiment (Experiment Sk1) was a 3^2 factorial experiment with 3 centre-point replicates (12 runs) with the variables being preheat treatment and feed concentration. The design levels for preheat treatment were 100°C/1 s (low heat), 95°C/20 s (medium heat) and 120°C/180 s (high heat). The design levels for feed concentration were 15, 22.5 and 30% w/w. The steam valve was fixed at 70% open for all runs, so that the evaporation rate would remain reasonably constant and so that the delta pressure would be the main response variable. The runs for Experiment Sk1 are listed in Table 28.2.

Table 28.2: Experimental design for Experiment Sk1 showing run order.

Feed Concentration (% w/w)	Preheat Treatment		
	Low (100°C, 1 s)	Medium (95°C, 20 s)	High (120°C, 180 s)
15	K	J	I
22.5	F	A, E, H, L	G
30	D	C	B

The third experiment (Experiment Sk2) was a repeat of Experiment Sk1 but with two feed flow rates (55 and 110 kg h^{-1}) and two steam valve positions (70 and 80%) being used at each 3^2 factorial point. Each run was three hours long, with one hour at each of the following operating conditions:

S m_{feed} = 110 kg h^{-1}, steam value 70%

HS m_{feed} = 110 kg h^{-1}, steam value 80%

LF m_{feed} = 55 kg h^{-1}, steam value 70%

The run order for Experiment Sk2 was identical to that of Experiment Sk1. The order in which the operating conditions were used for each run are shown in Table 28.3.

Table 28.3: Operating condition order for Experiment Sk2 runs.

Run Number	Operating Condition		
	S (110 kg h^{-1}, 70%)	HS (110 kg h^{-1}, 80%)	LF (55 kg h^{-1}, 70%)
A	3	2	1
B	2	3	1
C	3	1	2
D	2	1	3
E	3	1	2
F	3	2	1
G	2	1	3
H	3	1	2
I	1 {3}	3 {2}	2 {1}
J	3 {2}	1 {3}	2 {1}
K	3 {3}	2 {1}	1 {2}
L	1	2	3
{M}	{1}	-	-

Figures in {} indicate actual run order where it differed from experimental design. The reason for the change in order for runs I-K was that a computer breakdown restarted the order sequence at Run A conditions. Run M was an extra run using the milk left over from Run C.

29 EXPERIMENTAL PROCEDURE - SKIM MILK

The Milk Powders and Drying Processing "Run Sheets" have been included in Appendix M. These give a detailed description of the order of events during the trials. The "Experimental Procedure" section of the run sheets have been annotated with the actual times and observations made during the experiments. The following is a summary of the procedures used.

29.1 Preparation of Feed and Concentrate Disposal

1. For Experiments Sk0 and Sk2, whole milk supplied by Tui Co-operative Dairy Company (Tui CDC) was brought in and separated at 55°C. The skim milk was pasteurised at 72.3°C for 15 s, chilled to 14°C and placed in a 20 m^3 refrigerated silo where it was chilled to 3°C overnight. For Experiment Sk1, pasteurized skim milk was brought in from Tui CDC.
2. The skim milk was then drawn at 1.8 m^3 h^{-1} from the silo to a triple effect falling film evaporator (GEA Wiegand Gmb, Ettlingen, Germany) heated by direct steam expansion. The milk was heated to 70°C indirectly, heated using direct steam injection (DSI) to the desired preheat treatment and held for the desired holding time, and then flashed down to 65.5°C. The milk was then concentrated to 45% w/w under the following boiling temperature regime:

First effect, 1 pass	66°C
Second effect, 1 pass	57°C
Third effect, 3 passes	45°C

   The total residence time during concentration in the evaporator was approximately 5 min (1 min per pass).
3. The concentrate was cooled using a PHE, placed in a refrigerated tank and agitated. A sample was taken for total solid analysis and, when the result was known, chilled soft water at 3°C was added to reduce the concentration to 30% w/w. For Experiments Sk1 and Sk2, once the 30% w/w concentration experimental runs were complete, water was added to the concentrate to reduce the concentration to 22.5% w/w and later to 15% w/w.

3B. During Experiment Sk0, some of the 44% w/w concentrate was spray dried on a tall form drier (DeLaval Co., Ploughkeepsie, New York, USA) with nozzle atomization. The powder produced was to be reconstituted at a concentration of 30% w/w. The reconstitution process was to blow the powder into an tank half

full with warm water. The tank contents were agitated and the mixture was drawn from the bottom of the tank, through a centrifugal pump, and recirculated back to the tank while the powder was being added.

4. The feed stock was then gravity fed to the Research Evaporator feed balance tank. The balance tank level was maintained between reasonable limits using a solenoid valve at the end of the gravity feed line.
5. The milk was concentrated in the third evaporator, diluted with soft water to approximately 20% w/w and stored in the refrigerated tank, prior to being collected by a local pig farmer.

29.2 Research Evaporator Operating Procedure

1. The Research Evaporator was cleaned-in-place using caustic and acid and rinsed thoroughly prior to each experiment (see Section 29.4).
2. Steps 1-9 of Chapter 14 were then carried out.

For Experiment Sk0

3A. Skim milk was then supplied to the balance tank and the plant was run at steady state for a 20-h period.

For Experiment Sk1

3B. Skim milk was then supplied to the balance tank and the plant was run at steady state for 1.5 h with the final 30-min period taken to be the steady state run period. Reduced steady state run periods (see Appendix I) were used for some runs where a major disturbance occurred.

For Experiment Sk2

3C. Skim milk was then supplied to the balance tank and the plant was run at steady state for 1 h with the final 30-min period taken to be the steady state run period. The feed flow rate and/or the steam valve position was then adjusted and the plant was run for another hour with the final 30-min period taken to be the second steady state run period. The feed flow rate and/or the steam valve position was then adjusted and the plant was run for another hour with the final 30-min period taken to be the third steady state run period. Reduced steady state run periods were used (see Appendix I) for some runs where a major disturbance occurred.

For Experiments Sk1 and Sk2

4. The plant was rinsed on water and then cleaned-in-place and rinsed again.
5. Steps 3 and 4 were repeated until all the experimental runs were completed

29.3 Sampling and Analysis

The laboratory analysis methods used are described in Appendix N.

Chemical and Physical Property Analysis

A sample of the skim milk was taken from the silo and analyzed for total solids, titratable acidity and whey protein nitrogen index, WPNI. A concentrate sample was taken ex-Wiegand evaporator for each batch for total solids analysis. A sample of powder produced during Experiment Sk0, Run 2 was analyzed for gross composition (Ash, Lactose, Protein (Total Nitrogen (TN)), Fat, Moisture). For Experiments Sk1 and Sk2, a sample taken from the skim milk silo and analyzed for gross composition (Ash, Lactose, Protein (TN), Casein (TN-NCN), Whey Proteins (NCN-NPN), Fat, Total Solids). For each run a sample of the Research evaporator feed was taken from the batch tank and analyzed for total solids and WPNI (when appropriate). Likewise, a sample of the concentrate leaving the Research evaporator was taken mid way through the 30 min steady state run period and analyzed for total solids and, when appropriate, WPNI.

Microbiological Analysis

Liquid samples were taken aseptically using Vacutainer evacuated blood collection tubes and needles from the following points during the trial.

1. Skim milk silo (Port in door)
2. Wiegand evaporator feed balance tank
3. Wiegand evaporator concentrate line
4. Research evaporator feed balance tank
5. Research evaporator concentrate line

These were analyzed by the Starters & Microbiology Section, NZDRI for the following:

For samples from points 1-3: Standard plate count (SPC), Coliform, Mesophilic spore formers Thermophilic spore formers, Sulphite reducing clostridia and Yeast & Mould (Y&M).

For samples from points 4-5: SPC, Thermophiles, Y&M.

29.4 CIP Procedure used between Runs for Experiments Sk1 & Sk2

1. The milk supply to the feed balance tank was stopped, and the level in the balance was allowed to drop to less than 1 kg (from 5-10 kg) before water was added to the tank. The feed line was then manually disconnected and rinsed, and the feed valve was pulsed and rinsed.
2. After 10 min rinsing, the spray ball in the separator was activated in short pulses over a 5 min period. During each pulse, the feed pump was placed on manual to give a flow rate of >500 kg h^{-1}
3. The third effect suction-side level was then monitored until the level had dropped back to normal and was stable for 1 min.
4. The plant was then maintained at steady state for 15 min, to enable the overall HTC on water (with the dirty plant) to be determined at the previous run operating conditions.
5. After checking the concentrate density was less than 1000 kg m^{-3}, the feed balance tank was drained, and caustic soda solution (1 %w/v) was added to the balance tank and controlled at a level of 20 kg. The feed flow rate was increased to 150 kg h^{-1}.
6. After 5 min, the separator spray-ball was pulse activated over a 5-min period.
7. Repeat of Step 3 above.
8. The concentrate was recirculated to the feed balance tank. The CIP solution supply to the balance tank was stopped and water was added to maintain the balance tank level between 19.5-20.5 kg.
9. After 30 min the recirculation was stopped and the feed balance tank drained to less than 1 kg.
10. The plant was then rinsed for 10 min at a feed flow rate of 250 kg h^{-1}.
11. Steps 2 & 3 were then repeated.
12. The CIP return line to the feed balance tank was then flushed with water for 30 s.
13. The feed flow rate was dropped to 150 kg h^{-1}. After checking the concentrate density was less than 1000 kg h^{-1}, the feed balance tank was then drained to less than 1 kg, and nitric acid solution (1% w/v) was added to the balance tank and the level maintained at 20 kg.
14. Steps 6-13 were then repeated for acid, except that the time for Step 9 was 15 min.
15. The above CIP procedure usually took 2.5 h, so the plant ran on water at 250 kg h^{-1} for a further 30 min before the start of the next run.

30 SKIM MILK STEADY STATE EXPERIMENT

The experimental design and procedure for this experiment are covered in Chapters 28-29.

30.1 Experiment Sk0 Results

Observations

During Run 1, the concentrate pump suction side level control was very poor due to the formation of a stable foam. The foam was visible in the sight glass at the bottom of the differential pressure level measurement section at 1100 h on 15 January 1992. The foam affected the level measurement which led to huge variations in concentrate flow rate, and finally caused a suction-side blockage which shut the plant down. The reconstitution of the powder proved to be a dismal failure, with most of the powder forming a large lump. In addition, after Run 1, the Research Evaporator level control system malfunctioned causing several plant shut downs, so Run 2 was abandoned.

Physical, Chemical and Microbiological Analysis Results

The laboratory analysis results are included in Appendix I. The feed concentration for Run 1 was 28.4% w/w and a concentrate sample taken at 0826 h, 15 January 1992 had a concentration of 42.1% w/w. The microbiological quality of samples taken from throughout the process was good.

Changes in operating conditions during the trial

The variation in operating conditions during Run 1 are shown in Figure 30.1, and the variation in overall HTC in Figure 30.2.

30.2 Experiment Sk0 Discussion

This experiment was undertaken to determine the effect of reconstitution on the behaviour of milk during evaporation. If there had been little or no difference in behaviour between reconstituted and fresh milk, there would be an opportunity to do a large number of 20-h runs using commercial powder with uniform composition (*i.e.* made from one mixed silo of milk). The powder could be mixed up when required which would avoid the problems of change in milk quality with age of the milk. As the reconstitution process failed, further work is required, using a better reconstitution procedure, to determine the differences (in terms of evaporation heat transfer and fouling) between

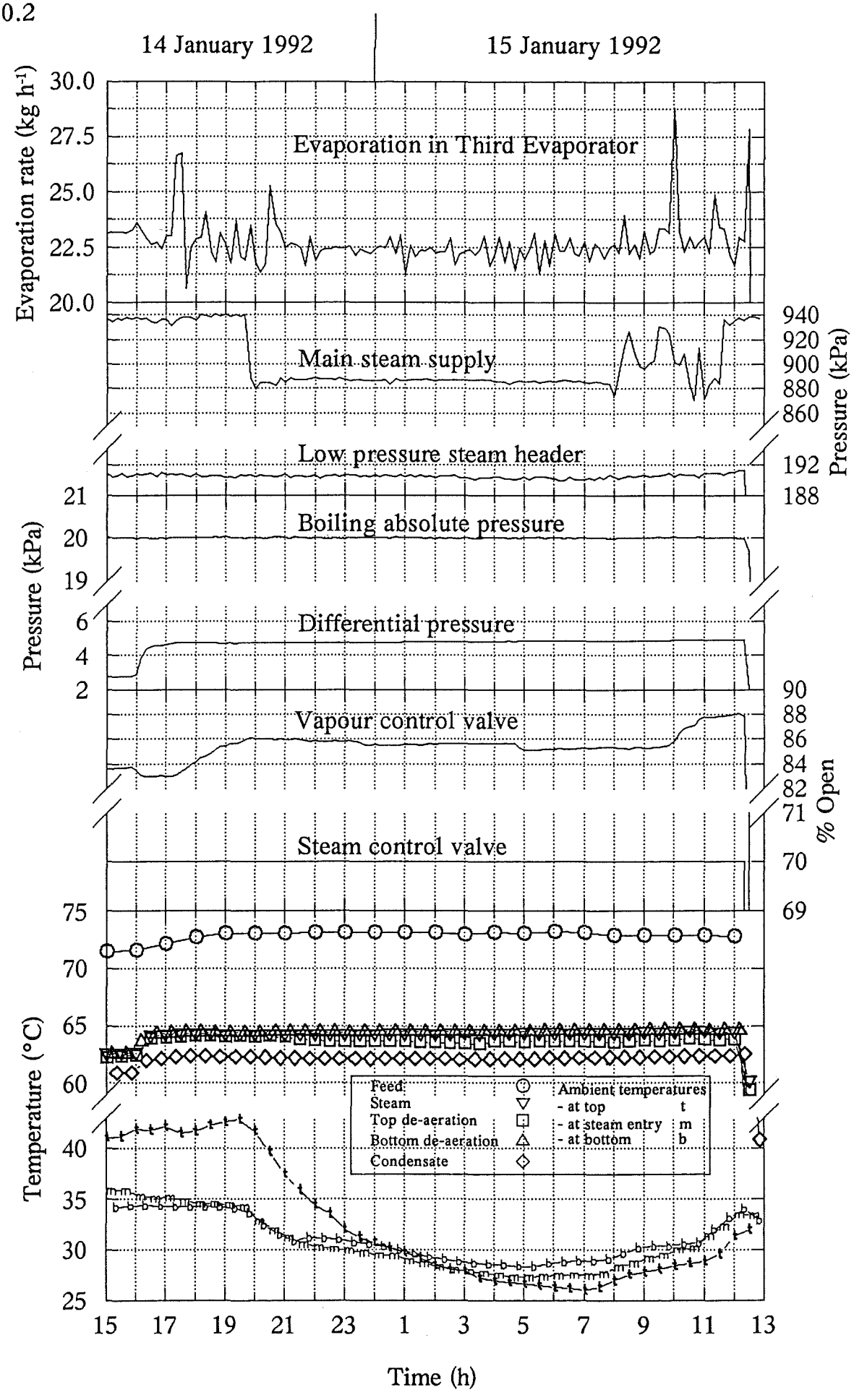

Figure 30.1: Operating Condition Trends for Experiment Sk0, Run 1.

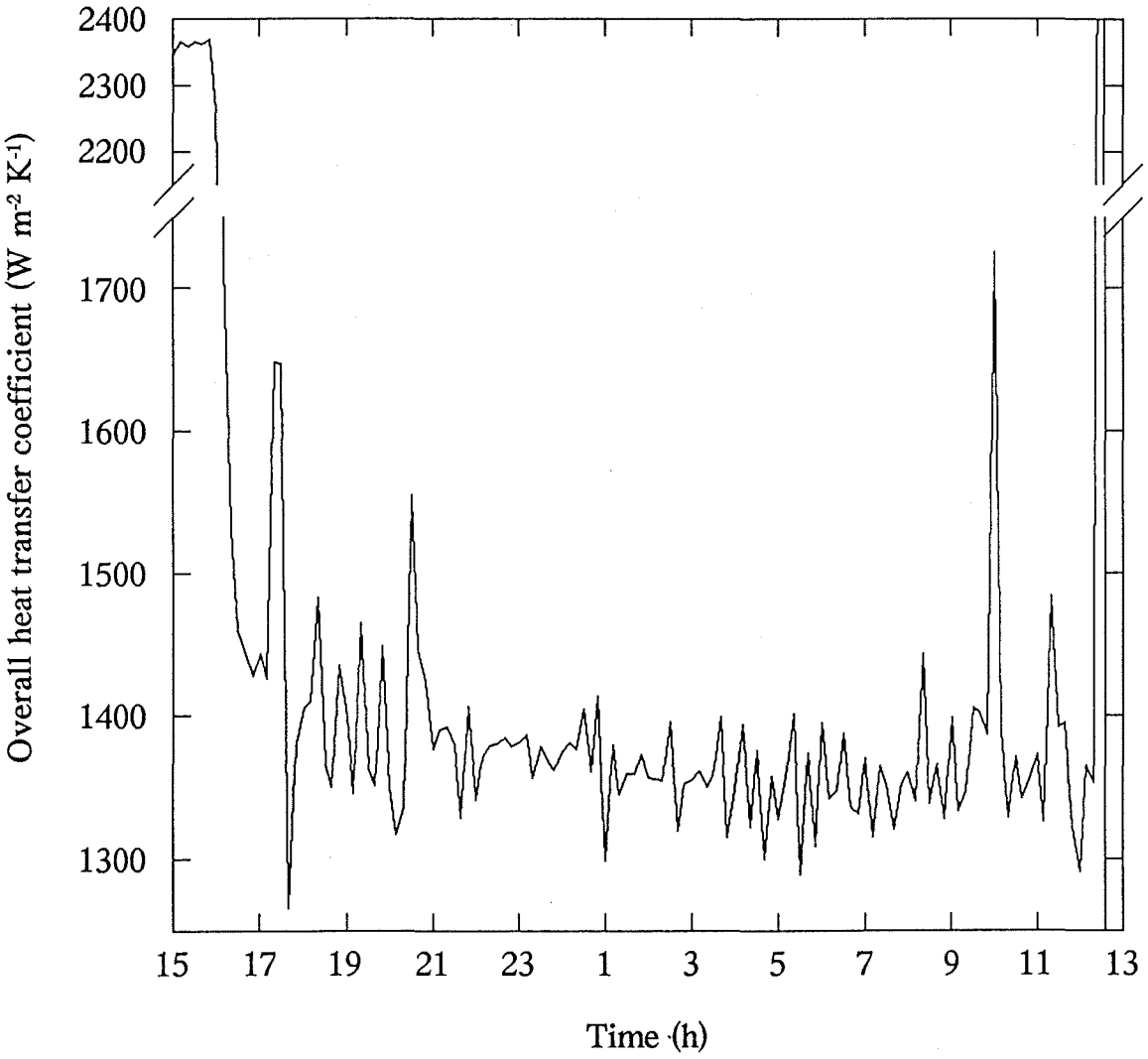

Figure 30.2: Overall Heat Transfer Coefficient Trend for Experiment Sk0, Run 1.

reconstituted and fresh milk. One important factor for reconstitution is to minimise the formation of foam.

The 20-h run on fresh concentrated skim milk (28.45% w/w) was very unstable as even the 10-min average values show (see Figure 30.1). For this run, no antifoam was added to the milk, and foam affected the level measurement. Foam could be seen in the sight glass located at the bottom of the differential pressure level measurement section, even when the level measurement output was greater than 50%. The concentrate pump speed was controlled to maintain the suction side level and, due to the difference between the flow behaviour of the liquid and the foam, the level control system was unstable. The evaporation rate was determined by difference from the feed and concentrate mass flow rates, and thus reflects the noise generated by poor level control.

The run finished abruptly when the plant monitoring system observed low flow through the concentrate pump. This probably occurred because the concentrate pump ran dry due to a false level indication caused by the foam, and a failure of the non return valve allowed air to flow backwards through the pump. This air bleed back may also explain why, at approximately 1000 h on 15 January 1992, the vapour valve opened by about 3%, to maintain the boiling side pressure. This was unlikely to be due to an increase in evaporation and was more likely to be due to two-phase flow of foam and vapour.

In comparison with the steady state water runs (compare Figures 17.1, 17.2, 17.3 and 30.1) there was also a much greater variation in ambient air temperatures due to the operation of Wiegand evaporator and Delaval drier. The main steam pressure was stable for most of the run, but was extremely variable near the end which would have affected the steam quality. The measured condensate temperature was around 2°C lower than the steam condensing temperature. The reasons for this are discussed in Chapter 17.

The steam control valve was run on manual for this run, and as it acts as a sonic orifice, the steam flow rate varied linearly with upstream pressure. The upstream pressure was stable during the run, so that the slight increase in the differential pressure across the tube, can be attributed to an increase in resistance to heat transfer. As the ambient temperatures dropped during the run, it can not have been due to a reduction in heat losses through the calandria shell and from the steam supply line. Therefore, the slight increase in differential pressure can be attributed to the fouling of the heat transfer surfaces.

The amount of heat transferred through the wall does not stay constant as the differential pressure increases, due to a number of competing factors;

- reduction in the latent heat of vaporization,
- increased de-aeration flow rates,
- increased heat losses,
- reduction in sonic steam flow rate through valve due to increase in downstream pressure (changes area of the *vena contracta*), and,
- increase in condensate temperature leading to increased thermal conductivity and reduced viscosity.

However, these factors do not prevent the differential pressure being used as a good indicator of overall HTC. Thus, using the differential pressure trend, it is apparent that the overall HTC slowly dropped over the length of the run. A similar trend can be deduced from the calculated overall HTC values (see Figure 30.2). Fouling of the tube inner surface by the milk is expected to be the reason for the gradual reduction in HTC.

31 SKIM MILK 3^2 FACTORIAL EXPERIMENTS

The experimental design and procedure for these experiments are covered in Chapters 28-29.

31.1 Experiments Sk1 & Sk2 Results

Observations

The detailed observations made during the trial are included as comments on the run sheets in Appendix M.

Experiment Sk1

The Wiegand preheat temperature probe failed at the beginning of the high heat run, which allowed a small amount of milk to pass though with only a preheat treatment of 73°C for 3 min. The DSI unit was run on manual for the remainder of the high heat run and the low heat run, and the temperature was monitored using a hand held temperature probe.

During Run A, antifoam was added to the separator, in an attempt to reduce the foam to a manageable level. The antifoam was added intermittently during Run A, but did not even temporarily improve the level control. Antifoam was subsequently added to the balance tank during Run A and to the feed stocks for all the remaining runs.

The concentrate flow was unstable during most of the runs and caused a plant shutdown during Run C. Reasonable steady state periods were selected over which to determine the HTC. These varied from 18 min to 2 h except for Run C (4 min) and Run G (none).

Experiment Sk2

During the hydraulic test just prior to this experiment, a leak was discovered on the union fitting between the third evaporator calandria and the vapour duct. Attempts to rectify this, reduced the leak to a drip (during a repeat hydraulic test), but did not eliminate it.

No antifoam was added during this experiment and the concentrate pump was run at a fixed speed.

The differential pressure gauge mounted on the bottom de-aeration line gave erroneous readings during this experiment due to the blockage of one or both its lines with protein type deposits.

Physical, Chemical and Microbiological Analysis Results

The laboratory analysis results are included in Appendix I along with the raw data from the data logger.

Boiling Point Elevation

The BPE was determined experimentally, (during Experiment Sk1 only) for the concentrate, by comparing the product temperature with the saturation temperature calculated from the absolute pressure. The difference on water varied from -0.07 to 0°C (average -0.036°C). The BPE figures for skim milk were adjusted to account for this offset. The corrected figures are shown in Figure 31.1 along with a theoretical curve (described in Section 2.1). The data indicates that the actual molality of the skim used in Experiment Sk1 is lower than that used for the theoretical prediction. This could either be due to differences in composition, or perhaps due to association of molecules (Jebson, 1994). The regression equation fitted to the data[1] had a regression coefficient, r^2 of 0.985:

$$BPE_{skim} = 0.0028\, S_{skim} + 0.00029\, S_{skim}^2 \qquad (31.1)$$

Concentrate viscosity measurements

The low pressure drop across the viscometer, the uncertainty concerning concentrate density and actual temperature during measurement, and, the wild fluctuations in concentrate flow rate made detailed analysis of doubtful benefit. Assuming Newtonian flow properties, the measured viscosities have been plotted against predicted viscosity (see Appendix G) in Figure 31.2. The data from some runs were omitted because the flow through the viscometer was turbulent. The results confirm that the predicted viscosity correlation can be used with a reasonable degree of confidence.

Fouling and CIP effectiveness

After 30-45 minutes on water rinse, the plant was maintained at steady state for 15 min to determine the HTC on the "dirty" plant. The plant was also on water for a period of 30 min after the CIP (and prior to the next run) to determine the clean HTC. The differential pressure readings for a steady state portion of each of the above two periods are shown in Figure 31.3.

---

[1] The concentration values were calculated from the feed concentration and the concentration ratio.

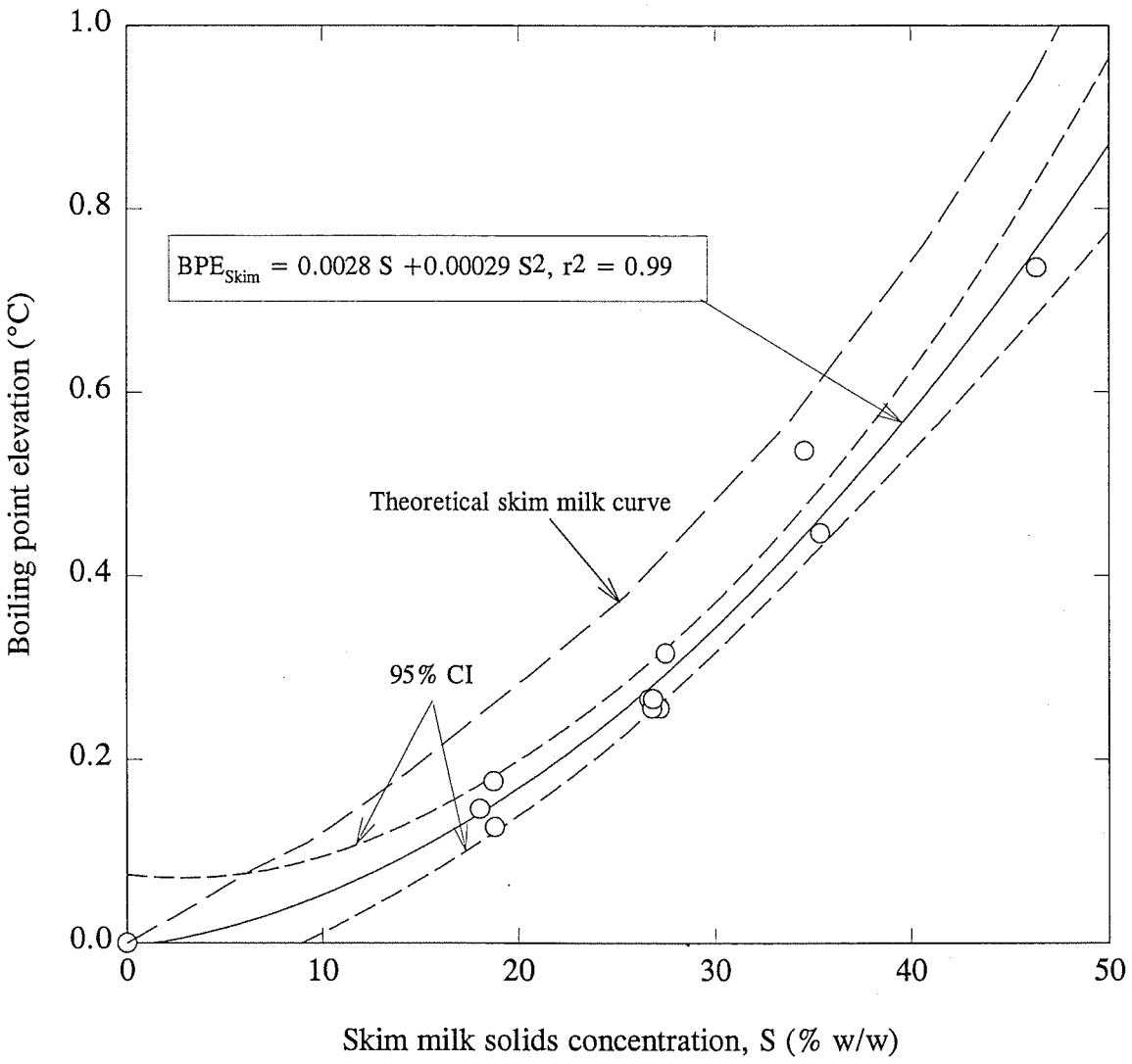

Figure 31.1: Boiling Point Elevation Data from Experiment Sk1.

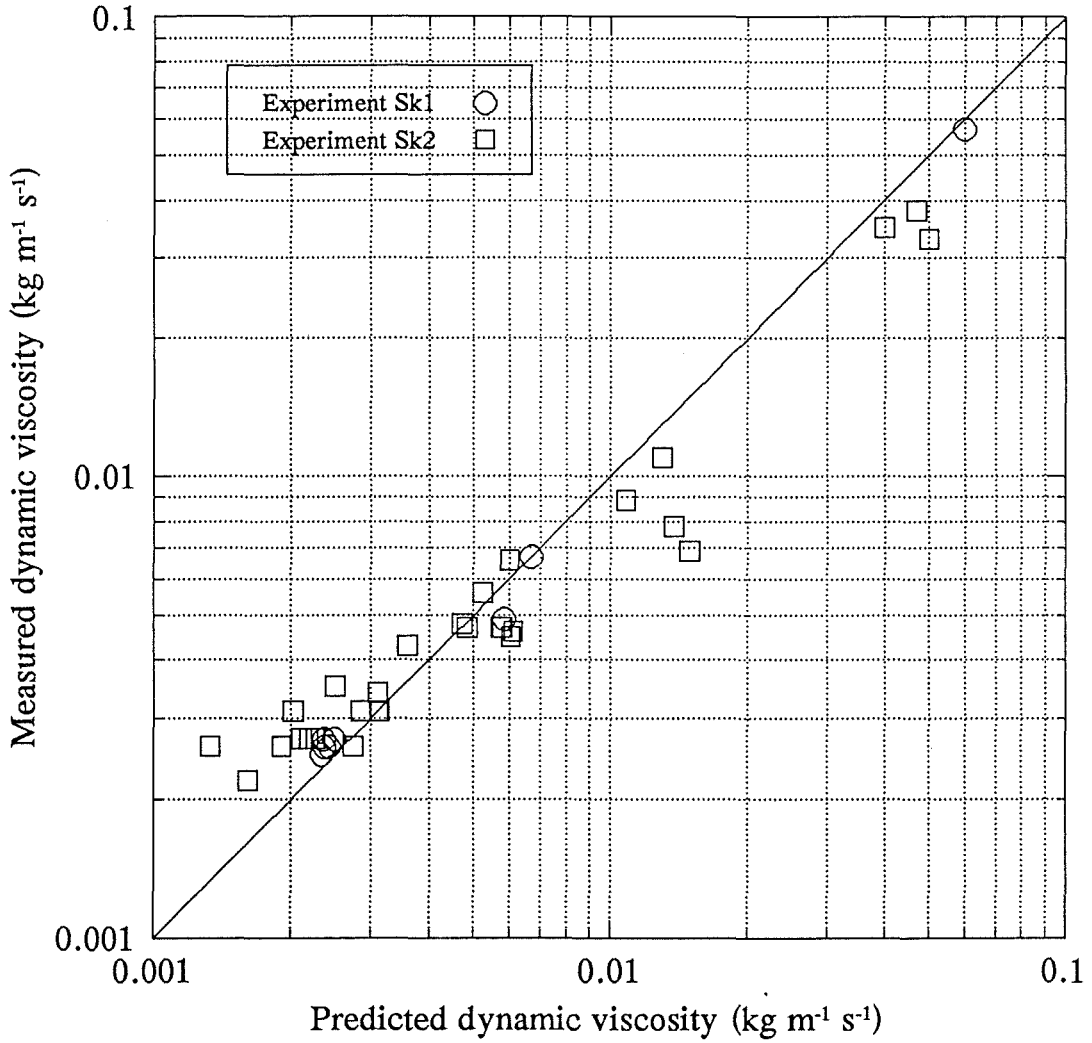

Figure 31.2: Comparison of Measured Viscosity Data with Predicted Viscosity.

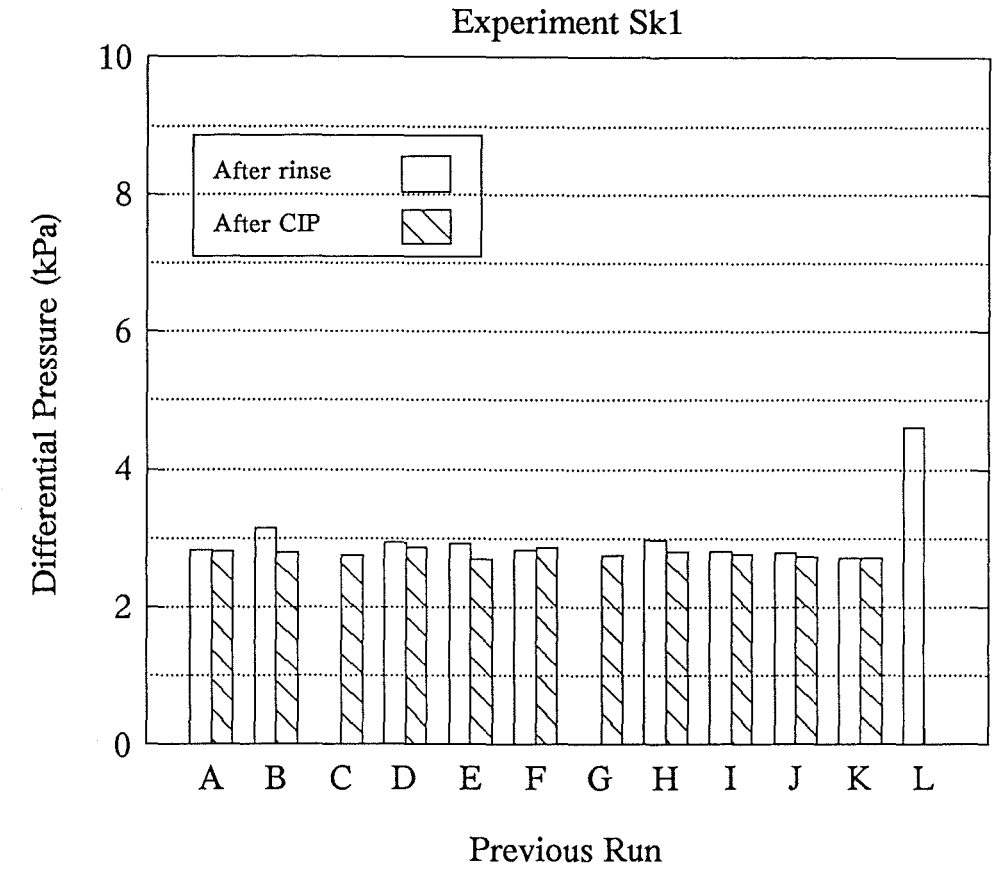

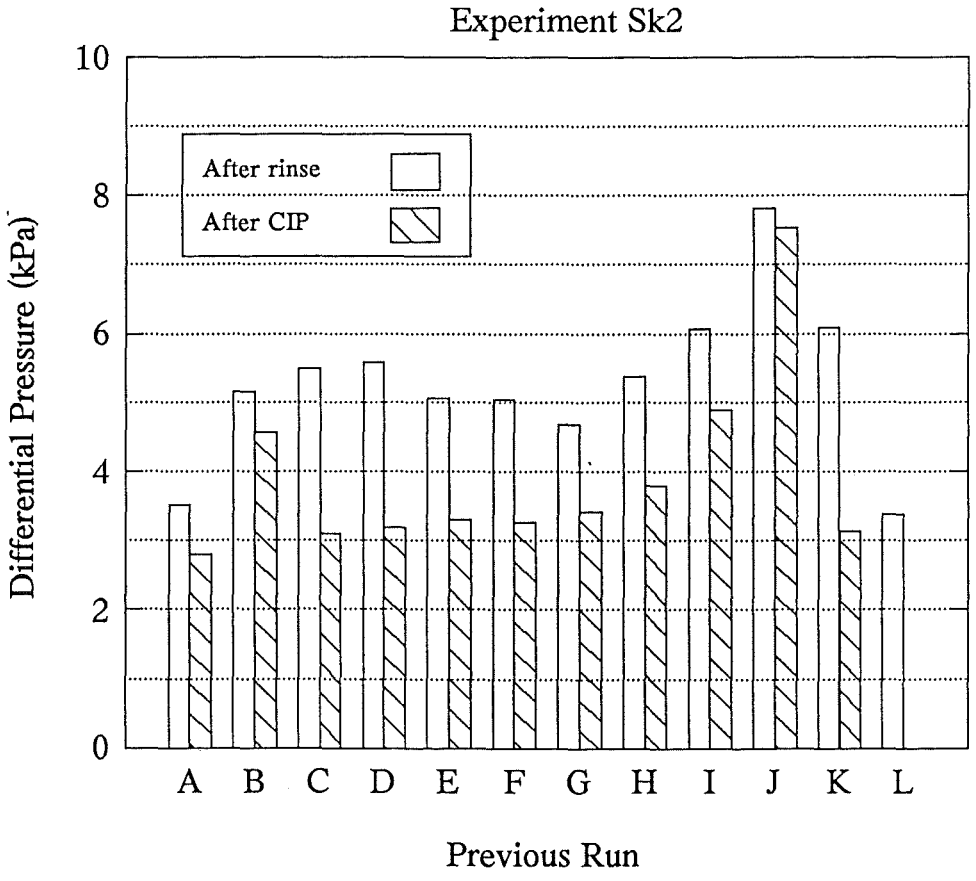

Figure 31.3: Monitoring of Plant Fouling Levels After Rinsing and After CIP.

Overall heat transfer coefficients

The overall HTC values for Experiments Sk1 and Sk2 are shown with respect to run order in Figures 31.4 and 31.5 respectively. The width of the bars on Figure 31.4 is roughly proportional to the length of the steady state period over which the overall HTC value was calculated. The overall HTCs for Experiments Sk1 and Sk2 are plotted with respect to feed concentration in Figure 31.6.

The combinations of $\overline{Re}_e$ and $\overline{Pr}_e$ used in Experiments Sk1 and Sk2 are shown in Figure 31.7. The comparison of overall HTCs determined by integration of the local Nu_e values of Chun & Seban (1971) with the Experiment Sk1 overall HTCs is shown in Figure 31.8. The flow regime predicted by Chun & Seban is indicated for each point on Figure 31.8. Where the flow regime changes from turbulent to laminar over the length of the tube, the percentage of the integration grid points at which the flow is turbulent is noted. The fit of the Chun & Seban turbulent local Nu_e correlation to the Experiment Sk1 data is shown in Figure 31.9.

31.2 Discussion for Experiments Sk1 and Sk2

Age of milk

For both Experiments Sk1 and Sk2, one tanker load of milk was brought in, processed and stored in one silo prior to evaporation. This ensured that the composition of the milk throughout the experiment was constant. However, it did mean that the age of the milk varied during the trial which could have affected the behaviour of the milk during evaporation. The milk and the feed stocks produced were kept chilled to minimise any microbiological growth. While the measured microbiological quality varied considerably during the experiments (see below), the overall HTC values for Experiment Sk1 centre-point runs were consistent throughout the four day period (see Runs A, E, H and L on Figure 31.4), which indicates that it is feasible to hold milk for that period for experimental purposes.

Microbiological quality

The microbiological quality of samples taken from throughout the process (see Appendix I) varied tremendously. The trends mainly suggest the variation was due to sampling location and contamination during sampling rather than due to microbial growth in the bulk. Some of the Research Evaporator concentrate samples were mistakenly taken from the concentrate balance tank which explains the few high counts obtained. The levels, while excessive in some cases in terms of food quality, are not considered

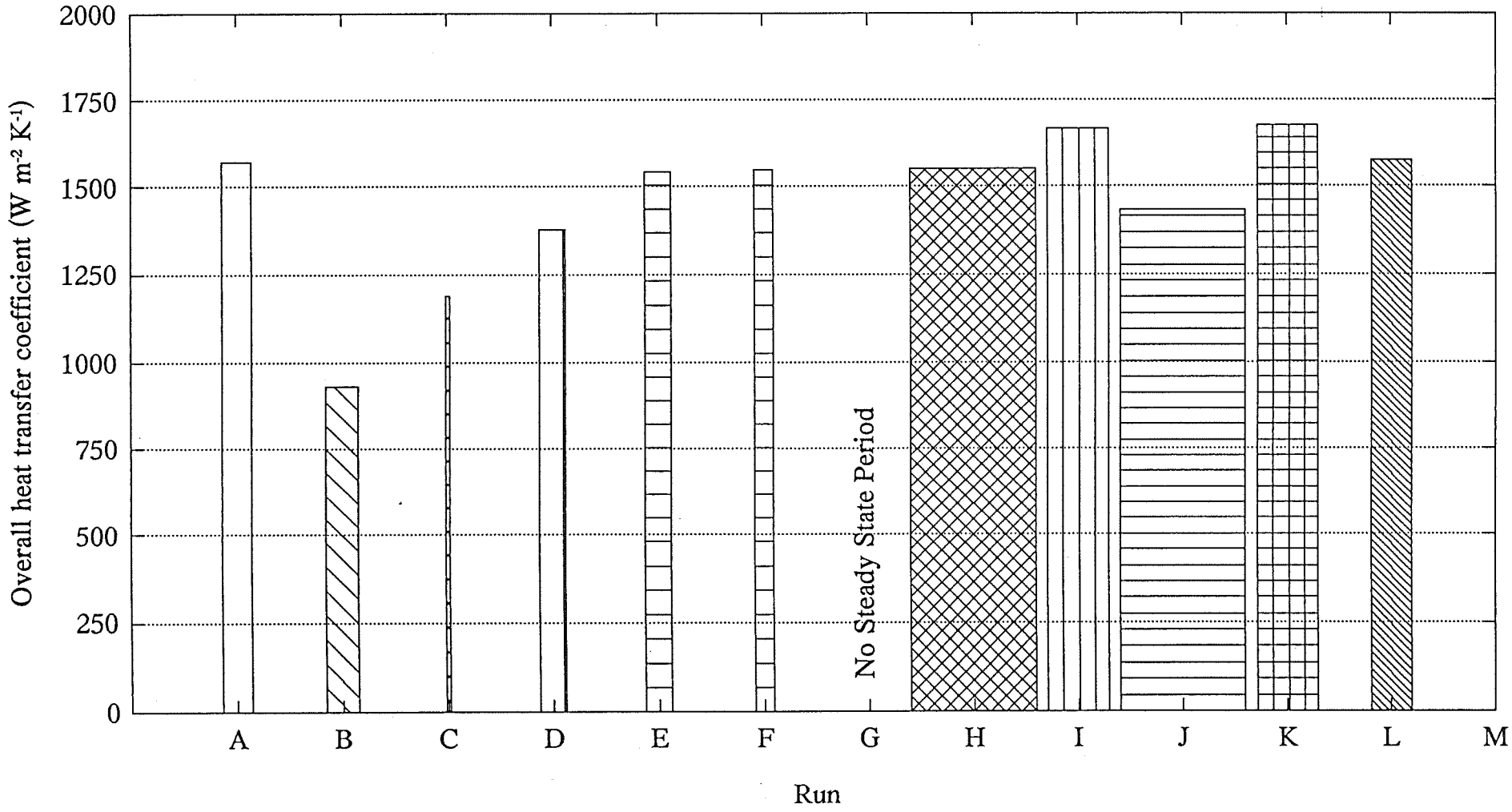

Figure 31.4: Overall Heat Transfer Coefficient with Respect to Run Order for Experiment Sk1. (Width of bar indicates relative length of steady state period.)

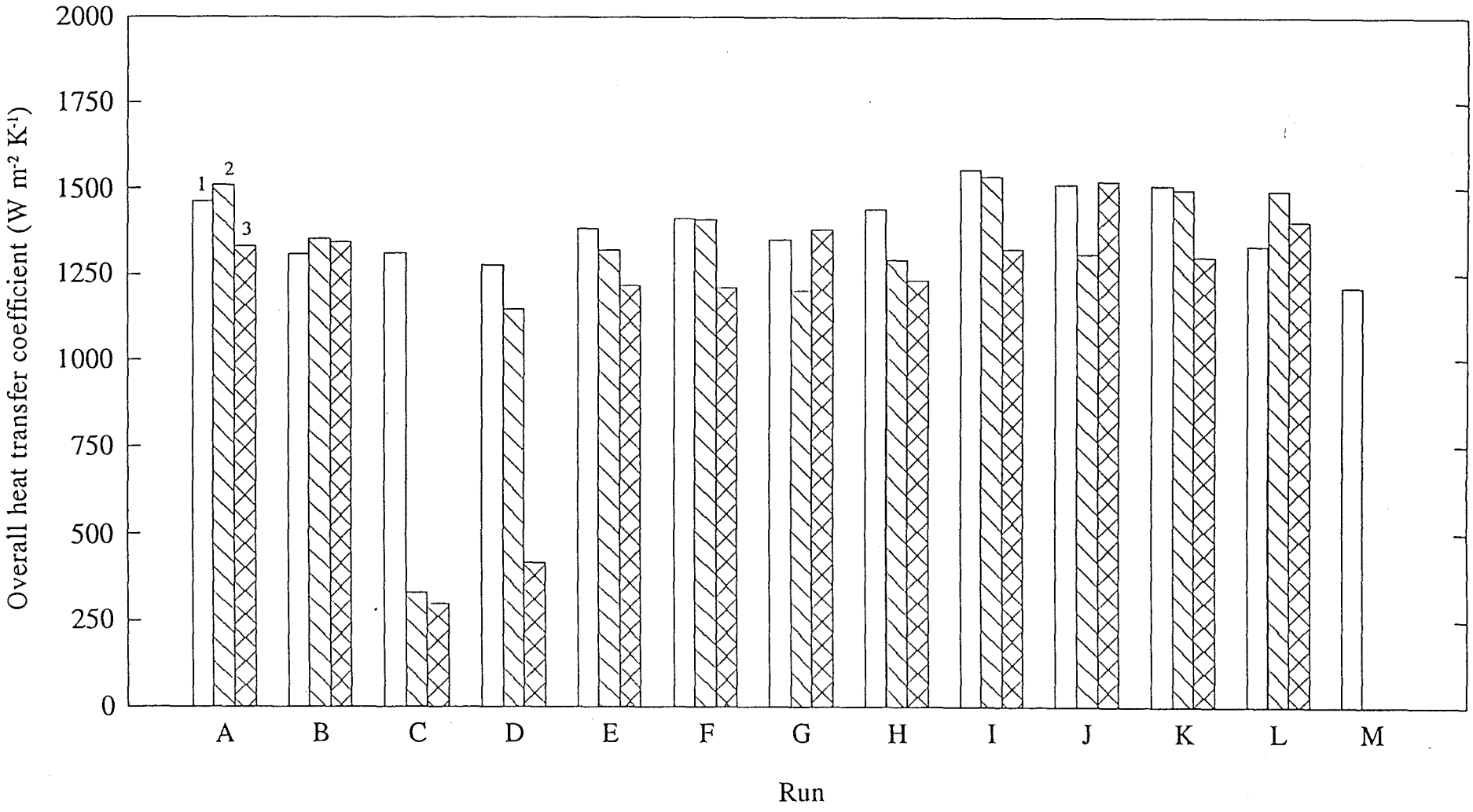

Figure 31.5: Overall Heat Transfer Coefficient with Respect to Run (and Operating Condition) Order for Experiment Sk2.

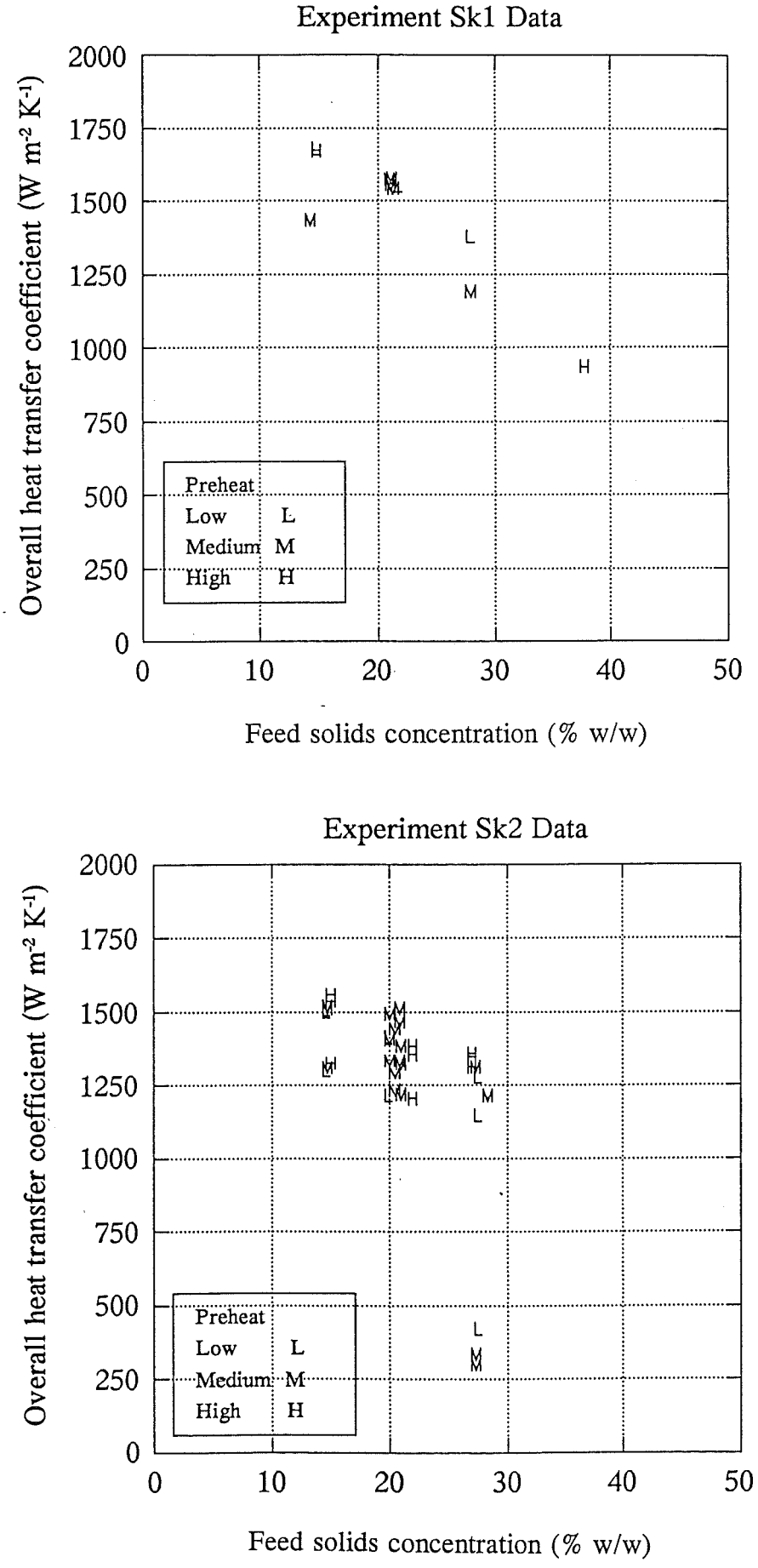

Figure 31.6: Overall Heat Transfer Coefficients with Respect to Feed Concentration.

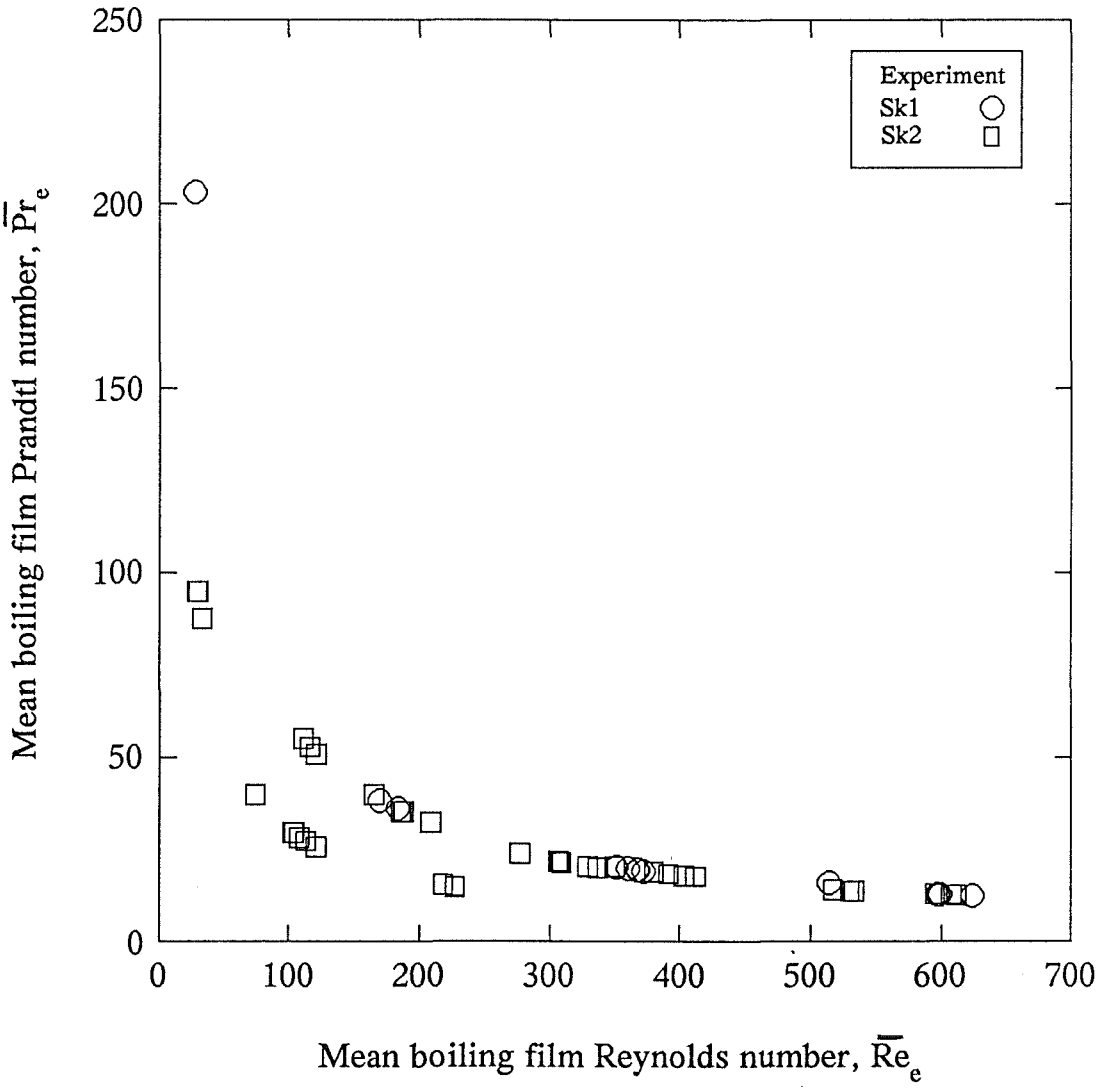

Figure 31.7: Combinations of $\overline{Re}_e$ and $\overline{Pr}_e$ for Skim Milk Experiments.

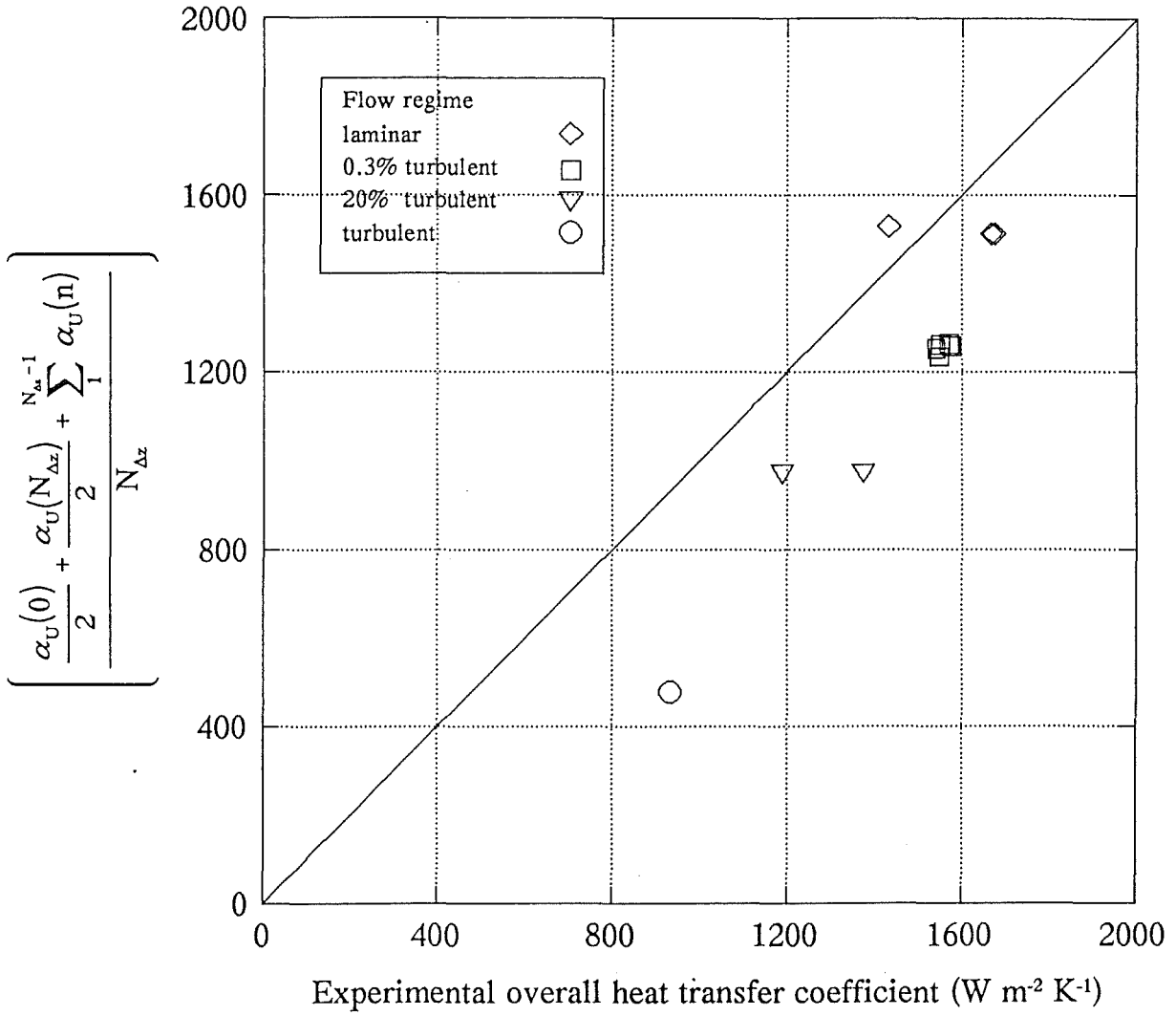

Figure 31.8: Comparison of the Experiment Sk1 Overall Heat Transfer Coefficients with Values Determined by Integration Using Chun & Seban (1971) Nu_e Correlations.

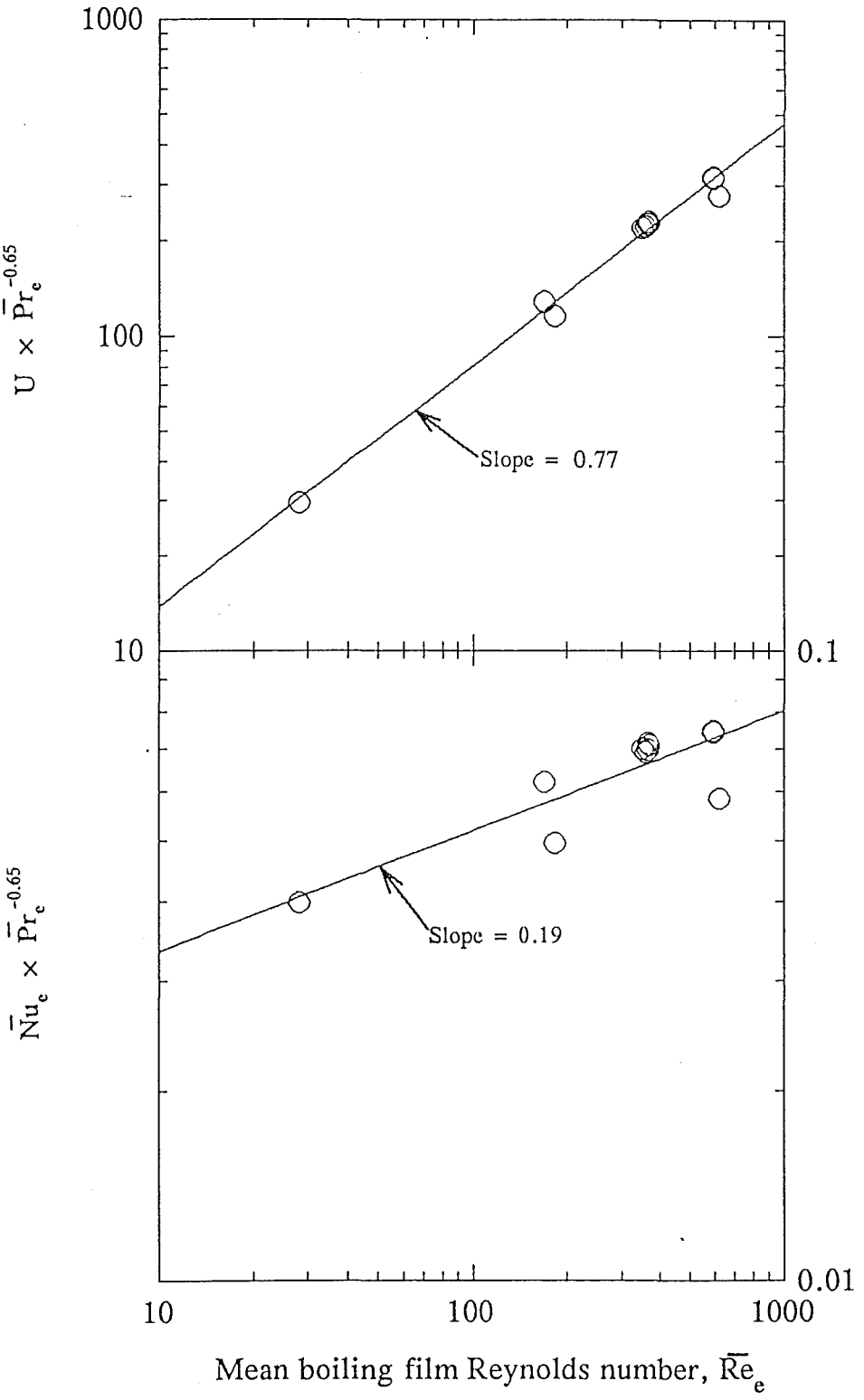

Figure 31.9: Determination of Fit of the Chun & Seban (1971) Turbulent Nu_e Correlation to Experiment Sk1 Data Using End-point Means of Re_e and Pr_e.

high enough to cause the acid production required to significantly affect the HTC results. Standard plate counts of ≥500,000 would be required for acid production (Hill, 1993).

Apparent viscosity

Milk is claimed to be a pseudoplastic fluid (Liu *et al*, 1991) and therefore the apparent viscosity is actually dependent on the shear rate. At concentrations above about 40% w/w, milk is also thixotropic (Wood, 1982) which means that after a change in shear rate, the apparent viscosity takes time to reach its final value at the new shear rate. These non-Newtonian characteristics of milk mean that the equation (see Section 12.4) given for calculating the viscosity does not strictly apply. The non-Newtonian properties of milk are the subject of a programme of work recently started at the NZDRI. The effect of the non-Newtonian properties on heat transfer may be investigated as part of this study. For the purposes of determining an apparent viscosity to use in heat transfer calculations, the values presented by Buckingham (1973) were used (see Appendix G).

Total solids results

The actual feed total solids results were used in the calculations, because the samples were taken from the bulk feed stock and were thus likely to be representative. The concentrate total solids results were not used as they were spot samples taken, in some cases, outside the steady state period used for calculating HTCs. The concentrate total solids used in the calculations was determined by a balance of the milk solids component across the evaporator.

Air leak into separator

There was an air leak into the vapour duct during Experiment Sk2 and this appeared to affect the BPE data collected during this run. Thus only the data from Experiment Sk1 was used for determining a correlation for BPE. The BPE response to concentration followed the predicted theoretical curve but with a slight offset. The temperature measurement point is 0.4 m below the bottom of the tube, and with the liquid first free falling from the tube and then running down an uninsulated duct, there should not be any superheat present (even at high concentrations).

Fouling and CIP effectiveness

Fouling of the heat transfer surface during milk runs could have been estimated from the change in differential pressure with time. However, due to factors such as variations in feed concentration, comparisons between runs would be difficult using this method. Comparison is easier if the fluid composition is constant. Therefore differential pressure

values determined on water at steady state, after rinsing and after CIP, were used to give an indication of both fouling rate and CIP effectiveness. Rinsing with warm water will remove some foulant material (Bird & Fryer, 1991), so this method only shows the effect on heat transfer of foulant material which requires the application of caustic and/or acid to remove.

The degree of fouling during Experiment Sk1 was slight (see Figure 31.3). Run B had by far the highest feed concentration (37% w/w) and thus the higher degree of fouling observed is not unexpected. After Run L, the feed flow rate was unstable which may explain the unusually high value obtained. The state of the plant after CIP was consistent for all runs indicating that the CIP was effective.

However, for Experiment Sk2, the degree of fouling during runs was high, and the effectiveness of the CIP was poor. After Run B the plant was not cleaned effectively and this meant that shortly into Run C, the plant fouled badly causing a massive drop in HTC (see Figure 31.5). The reasons for the increased fouling rates during Experiment Sk2 may be partly due to an increase in protein content (see Chapter 32). But is probably mostly due to the high temperature driving force / low feed flow combination and the presence of foam. The foam may form bubbles in the film and cause localised fouling of the heat transfer surfaces. The cleaning effectiveness may have been reduced by the lack of antifoam both in the milk and in the caustic. Antifoam had been added to the caustic in the past, but was not added to the solution used for Experiment Sk2.

The increase in fouling, observed before and after CIP for Runs H to J of Experiment Sk2, and then the dramatic decrease in fouling after CIP for Run K can be attributed to the following factors;

- an operator interface failure during the CIP period after Run H, which meant the plant had to be restarted after CIP;
- the concentrate flow meter had to be unblocked just prior to Runs I and J, which meant that there was poor concentrate flow control during CIP; and;
- after the CIP following Run K, the plant shut down due to a high temperature alarm and the plant was cleaned-in-place again prior to the "after CIP" measurement for Run K.

Use of antifoam

The addition of antifoam (see Section 8.5) to the feed stocks during Experiment Sk1 certainly helped maintain a degree of level control. The addition of antifoam, however,

may alter the fluid properties in a way which affects the HTC. For this reason, an attempt was made to add it to the separator so that the falling film did not contain antifoam. This did not prove effective in controlling foam. The antifoam would have just run down the wall of the separator vapour duct and perhaps a spray nozzle would have ensure better coverage. For Experiment Sk2, the level control problem was avoided by fixing the pump speed. The speed (75%) was chosen to ensure that flooding of the separator would not occur. This meant that no antifoam was required, and therefore, HTCs for *pure* skim milk could be obtained. In general, the HTCs obtained were lower (see Figure 31.6) than obtained for Experiment Sk1, but given the change in protein content and (more importantly) the problems encountered with fouling and CIP, no conclusion regarding antifoam can be drawn.

To create a stable foam, air or other non-condensable gases must be present, and some form of mixing of the liquid and air must occur. The presence of foam at the bottom of the calandria, suggests that there was a reasonably large air leak into that area of the plant which allowed air at sonic velocity to come in contact with the liquid stream. Once the foam formed, the small size of the pump suction line may have prevented it from breaking down. In commercial plants, foam is usually not a problem, even when using centrifugal pumps in scavenging mode. An exception is when the milk is first flashed after preheating, where the non-condensable gases on flashing can create foam. The Research Evaporator suction side lines need modification to allow the presence of foam to be visually monitored and to assist breakdown of the foam. Inspection through the sight glass in the pump's suction line, often showed no bubbles. This indicates that back leakage of air from the pump was not always the cause of foam.

Effect of preheat treatment

The effect of preheat treatment (see Figure 31.6) on the HTC appears to be insignificant. However, the poor quality of the data may hide a real effect. An increase in preheat treatment is known to increase the apparent viscosity (Bloore, 1981). However, at the concentration levels used in these experiments, the viscosity is low. The observed changes in apparent viscosity may only occur at higher concentrations due to a combination of pseudoplastic and thixotropic effects. With increasing heat treatment, the percentage of the whey protein that is denatured increases. This can be seen by the reduction in the whey protein nitrogen index (see Appendix I) which dropped (for Experiment Sk1) from 5.9 to 1.2 mg/g as the preheat treatment was increased from a low heat to a high heat treatment. This could be expected to reduce the formation of foam, but foam was a problem during all runs.

Comparison of experimental results with Chun & Seban's Nu_e correlations

Comparison of the experimental overall HTC results with values determined by integration of the local Nu_e correlations of Chun and Seban (1971) shows (see Figure 31.8) that the predictions are conservative. The flow regime varies from wavy-laminar to turbulent over the range of concentrations used due to the change in Pr_e. Therefore, the increasing conservativeness of the prediction may be, in part, due to the fact that Chun & Seban's model does not fully describe the transitional behaviour.

The combinations of $\bar{Re}_e$ and $\bar{Pr}_e$ used in Experiments Sk1 and Sk2 (see Figure 31.7) mean that they are highly correlated. By fitting equation 27.2 to the data from Experiment Sk1 (see Figure 31.9) the following correlation is obtained:

$$U = 2.356\, \bar{Re}_e^{0.77}\, \bar{Pr}_e^{0.65} \tag{31.2}$$

The exponent for $\bar{Re}_e$ of 0.77 was obtained with an r^2 of 0.99. The value of the exponent is less than that obtained for sucrose (1.05) which was expected because of the lower BPE of skim milk (experimentally $\bar{Re}_e$ is highly correlated with $\bar{BPE}$). When the experimental $\bar{Nu}_e$ is used instead of the overall HTC, the following correlation was obtained with a r^2 of 0.86:

$$\bar{Nu}_e = 0.02155\, \bar{Re}_e^{0.19}\, \bar{Pr}_e^{0.65} \tag{31.3}$$

The Re exponent is lower than the 0.4 suggested by Chun & Seban for turbulent flow, which is not surprising considering the integration procedure showed that most of the runs were operating under a predominately wavy-laminar flow regime where the $\bar{Re}_e$ exponent is negative. The data from Experiment Sk2 were not compared with the Chun & Seban correlations due to the poor CIP performance between runs.

Comparison with dimensionless group models developed for sucrose and water

The fit of Equations 26.4 and 26.5 to the Experiment Sk1 data is shown in Figures 31.10 and 31.11. Equation 26.4 provided the closer fit to the data but the reasons for the poor fit need to be investigated further.

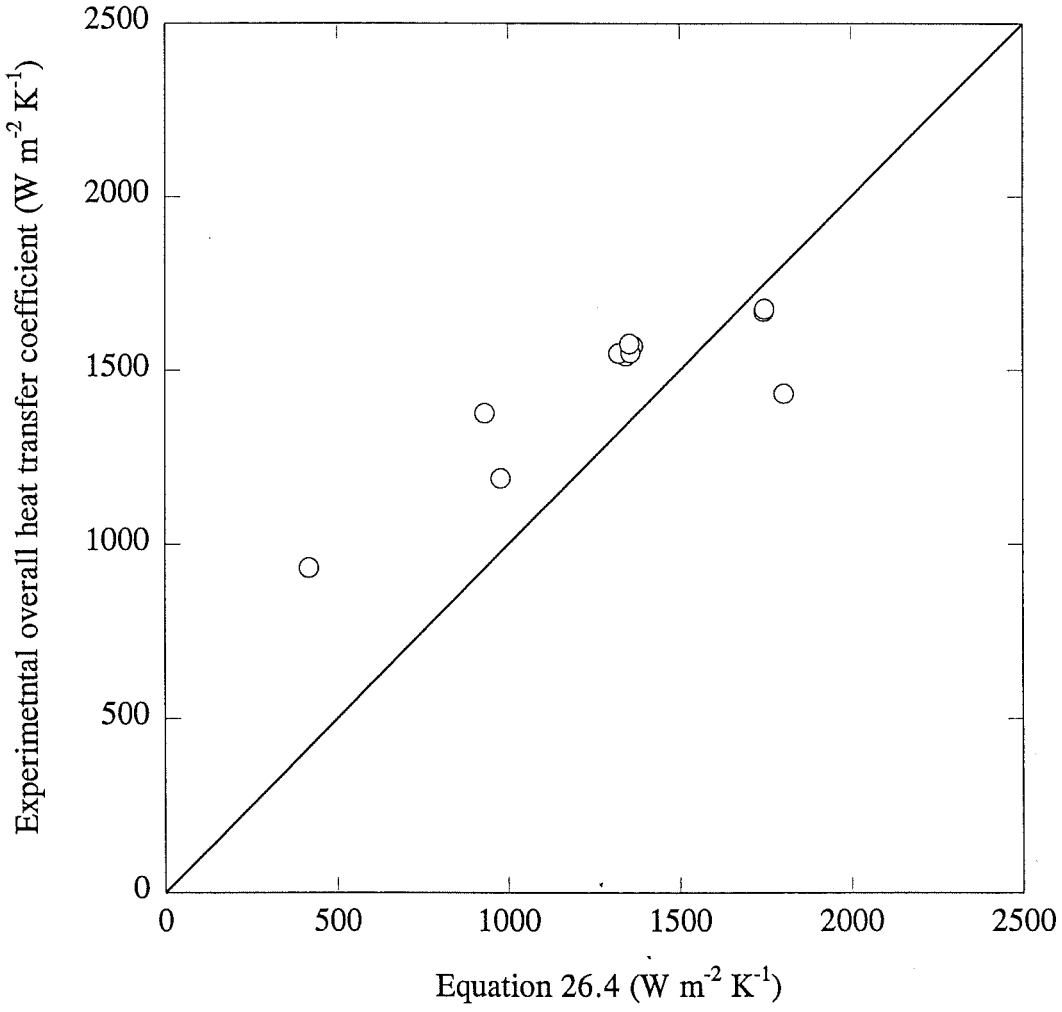

Figure 31.10: Fit of Equation 26.4 to Data from Experiment Sk1.

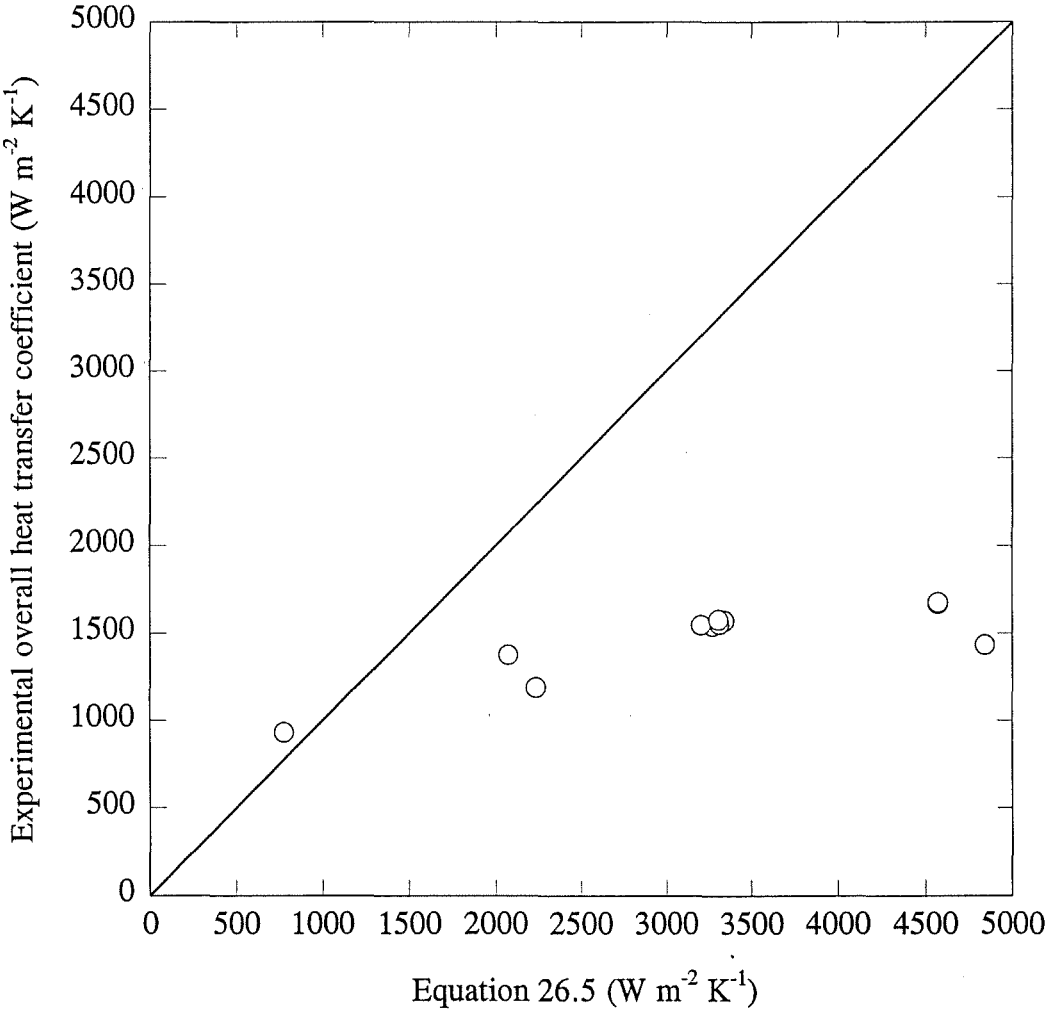

Figure 31.11: Fit of Equation 26.5 to Data from Experiment Sk1.

32 DISCUSSION - SKIM MILK EXPERIMENTS

Milk composition

The milk composition on a dry basis for each experiment is shown in Table 32.1. The compositions are all within the normal range of compositions found in New Zealand milk. The protein content in the milk was expected to increase at the end of the season so the higher protein content in Experiment Sk2 was not unexpected. The drop in protein content between Experiments Sk0 and Sk1 was probably due to the fact that milk from town milk supply herds was used for Experiment Sk1. Because of the change in protein, the viscosity of the milk in Experiment Sk2 was expected to be higher (Bloore, 1981) although this effect may only be noticeable at high concentrations (> 40% w/w). This may have contributed to the extra fouling observed in Experiment Sk2, but was probably swamped by other factors (see Section 31.2).

Table 32.1 Skim milk composition (dry basis) for Experiments Sk0, Sk1 and Sk2.

Component		Experiment Sk0	Experiment Sk1	Experiment Sk2
Ash (% w/w)		8.2	8.3	7.7
Lactose (% w/w)		53.0	53.1	52.0
Protein (% w/w)	Total	38.1	37.5	39.4
	Casein	-	28.7	30.4
	Whey Protein	-	7.3	7.3
Fat (% w/w)		0.77	1.08	0.87

Foam, antifoam and evaporator control

The use of antifoam proved to be essential to maintain even a poor degree of level control on the suction side of the concentrate pump. The need for level control is peculiar to the Research Evaporator due to the inability of single-stage, centrifugal pumps to meet the flow-head requirements. In commercial evaporators, centrifugal pumps are used and are run in scavenging mode avoiding the need for level control. With positive displacement pumps this is not desirable

and therefore some form of level control is required. Further work is required to find ways of avoiding foam interfering with level measurements before the Research Evaporator can be run effectively on skim milk, and certainly before using it in multiple effect or pass mode.

Further work

This work has only provided very limited HTC data for skim milk evaporation. There is a clear need for more understanding of the physical properties of milk with respect to composition and thermal history. Work is currently under way at the NZDRI in obtaining a fuller understanding of the viscosity of milk. Given advances in this area, the need for seasonal trials to determine the effect of seasonal variations would be reduced.

The Research Evaporator will be useful for concentrating milk under a wide range of conditions. This work illustrated the need to operate the evaporator in multiple effect mode to reduce the amount of milk required, and to reduce manpower requirements. Thus, a solution to the problems experienced in product transfer pumping needs to be found.

PART IV: HEAT TRANSFER IN THE PRESENCE OF NON-CONDENSABLE GASES

33 CONDENSATION IN THE PRESENCE OF NON-CONDENSABLE GASES

33.1 Early Works

Smith (1906a,b) determined that air should be rigorously excluded from low pressure steam condensers and proposed that a stable high concentration of air was formed near the condenser surface. Dalton's law of partial pressures was used to determine the bulk mole fraction of air and this was represented in graphical form by Morley (1912). Colburn & Hougen (1934) proposed a numerical solution for calculating the average overall HTC for a condenser. Allowance was made for the decrease in the temperature driving force, along the length of the condenser, due to the increase in the mole fraction of NCG.

Air is heavier than steam and thus, assuming liquid-like properties, would be expected to collect at the bottom of the apparatus. However, diffusion and macro steam flows due to condensation ensure that the air remains mixed with the steam. Northcroft (1943) noted that, in practice, the effect of density difference is negligible compared with other factors.

The air was considered to form a film on the condensing surface and Northcroft noted that a 0.025 mm thick air layer had the same resistance as a 480 mm thick piece of copper. Lyle (1947) also considered that most of the air would be mixed with the steam, but that there would be more air in remote corners (*i.e.* where flow is stagnate).

Cairns (1953) confirmed the Colburn & Hougen (1934) method by experiment for steam/air and chloroform/air mixtures and concluded that the diffusion of the vapour molecules through the gas film played an important part in the transfer of heat from a gas-vapour mixture.

33.2 De-aeration Vents

The presence and location of de-aeration vents was considered important by Northcroft (1943) to promote good condensation heat transfer. Khan (1972) determined that the venting rate should be based on maintaining a minimum vapour velocity of 1-1.5 m/s. No gross stratification of NCG was found, so the vent could be placed either at the top

or at the bottom.

33.3 Flat Plate Models and Experiments

Free convection

Sparrow & Eckert (1961) undertook a boundary-layer analysis of laminar film condensation on a short vertical plate. The effect of superheat and the presence of NCG were considered. The effect of free convection was not included in the analysis. On comparing their results with experimental results, they concluded that free convection did play an important role when NCG were present.

Sparrow & Lin (1964) produced a theoretical prediction of laminar film condensation in the presence of NCG. This theory included the effect of free convection, and a satisfactory agreement between theory and experiment was claimed. High concentrations of NCG were found to build up at the vapour/liquid interface, even at low bulk NCG levels. This reduces the film saturation temperature, and therefore the effective temperature driving force is reduced.

Slegers & Seban (1970) experimentally evaluated (on a 150 mm long flat plate) the laminar film condensation of steam containing small concentrations of air. The results obtained were 20% higher than Minkowycz & Sparrow (1966a) predicted, but this may be due to the presence of a small amount of forced flow convection. Al-Diwany & Rose (1973) determined experimentally the HTC for film condensation of steam on a vertical surface in the presence of air, argon, neon, and helium, under free convection conditions. The results obtained agreed quite closely with free convection boundary layer theory.

Diffusion

Minkowycz & Sparrow (1966a) used an analytical model to show that the HTC was reduced by as much as 50% at an air bulk mass fraction of 0.5%. The influence of NCG was accentuated at lower pressures. The reduction in heat transfer was attributed entirely to the diffusional resistance of the gas-vapour boundary layer.

Superheat

The effect of superheat was predicted to be negligible for pure steam condensation but was significant in the presence of NCG (Minkowycz & Sparrow, 1966a).

Interfacial resistance

The interfacial resistance was predicted to be negligible (Minkowycz & Sparrow, 1966a) and this was confirmed experimentally by Mills & Seban (1967).

Variable properties

The effect of variations in the fluid properties due to changes in temperature was considered by Minkowycz & Sparrow (1966b) and Poots & Miles (1967). The latter found that a reference temperature rule predicted the variable properties to within one percent for low and medium pressures.

Forced convection

The influence of NCG was found (Sparrow *et al*, 1967) to be less under forced convection conditions than under free convection conditions.

Denny & Mills (1969) developed a computer program to solve "the finite difference analogue of the conservation equations in boundary layer form for laminar film condensation". The validity of the extended Nusselt results was evaluated in terms of the effects of forced vapour flow, variable wall temperature, and variable fluid properties.

Patankar & Spalding (1967) presented "a general, impact, numerical, marching procedure for the solution of parabolic partial differential equations, with particular reference to those of the boundary layer". A non-dimensional stream function was employed as the independent variable across the layer. Denny *et al* (1971) used the general finite difference model of Patankar & Spalding (1967) to predict the laminar film condensation from a steam-air mixture undergoing forced flow down a vertical surface. The influence of NCG was most marked at low vapour velocities and at high NCG concentrations.

33.4 Measurement of Non-condensable Gases

The ways of determining the amount and composition of NCG in steam, milk and condensate streams in an evaporator are discussed in Appendix J. A preliminary set of methods is recommended for evaluation as a tool both for research and for commercial plant troubleshooting. The use of in-line pressure and temperature measurements for the determining the mole fraction of NCG in steam flowing through an evaporator de-aeration line was critically evaluated (see Appendix K). Calculations were carried out to determine the likely degree of error in the temperature and pressure measurements.

34 MODEL OF STEAM CONDENSATION IN THE PRESENCE OF NON-CONDENSABLE GASES

34.1 Previous Models

The presence of even low concentrations of non-condensable gases (NCG) has been shown to have a significant effect (Denny *et al*, 1971) on condensation heat transfer. The models developed by Denny and others however only consider a short (~ 150 mm) vertical plate under conditions of free and forced convection. The effects of upward forced convection, cylindrical coordinates and enclosure of the bulk vapour gas have not been considered. The gas phase equations presented here are based on the forms in Bird *et al* (1960).

34.2 Dimensions of System being Modelled

The third effect of the NZDRI Research Evaporator was instrumented to experimentally evaluate the effect of the presence of NCG on heat transfer. The third effect was chosen because it has a single tube of commercial diameter. The single tube made the steam side flow patterns easier to model. The features and dimensions of the steam side of the third effect is covered in Section 4.12.

34.3 Steam Side Flow Regions

The steam side can be split into a number of flow regions (see Figure 34.1).

(A) The steam entry region where the steam enters. Depending on the driving force and the boiling temperature, velocities in this region will be high. The vapour and liquid boundary layers on both the tube and steam jacket may be disturbed or even stripped off by the resultant turbulence.

(B) A region of forced convection above the steam entry point where the steam bulk flow is upward with an ever decreasing velocity.

(C) A region around the top de-aeration line entry where tangential flow patterns will be important.

(D) A region at the top of the calandria where free convection is the only driving force.

(E) A region of forced convection below the steam entry point where the steam bulk flow is downwards with an ever decreasing velocity.

(F) A region around the bottom de-aeration line entry where tangential flow patterns

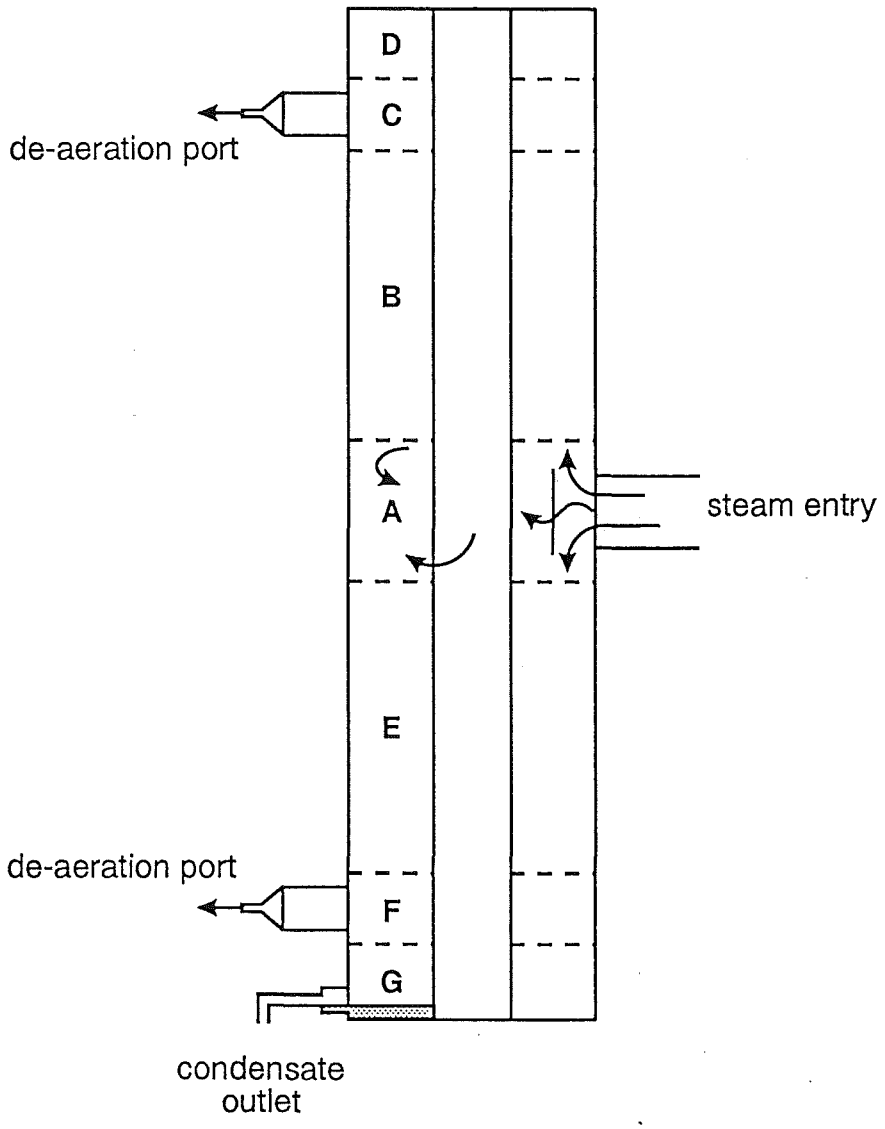

Figure 34.1: Steam-side Model Regions.

will be important.

(G) A region at the bottom of the calandria where free convection will be the only driving force.

(H) A region at the bottom of the calandria where heat will be transferred from a pool of condensate to the tube wall.

In all regions the flow of steam (and NCG) will be bounded by a liquid film on the tube wall and the steam jacket wall. Depending on the effectiveness of the insulation, the steam jacket wall may be (partially) covered by droplets, rivulets or a film.

34.4 Factors to Consider in Model Selection

The selection of an appropriate model should take into account the relative importance of each region. Clearly the majority of the heat transfer will occur in regions (B) and (E) and therefore the model chosen should match the conditions in these regions as closely as possible. Region (A) is relatively unimportant in terms of heat transfer because of its short length, but what happens within that region will have a dramatic effect on the heat transfer in regions (B) and (E). There are a number of scenarios to consider;

i. The steam mixing on entry strips off the vapour boundary layers off the walls and mixes the NCG rich boundary layer in with the bulk vapour flow. The NCG then travel with the bulk gas out of region (A). This effectively means that the bottom and top halves of the calandria can be considered to be isolated from one another with respect to the vapour phase.

ii. The steam entering strips off the vapour boundary layers and in addition strips off the liquid film on the tube wall and the droplets fall through the steam space. This means that bottom and top sections can be considered to be totally isolated from each other with respect to the condensate film as well as to the vapour phase.

iii. Both the vapour boundary layer and liquid films are unaffected by the steam entry.

Regions (C), (D), (F), (G) and (H) are relatively unimportant with regard to heat transfer. However (C) and (F), in particular, could have major non-condensable gas concentration gradients which may affect overall heat transfer rates.

34.4

34.5 Proposed Model

If Scenario i. is chosen then, as a first approximation, the system to be modelled can be split in three regions.

I. A region where steam from an upward bulk flow of vapour is condensing on a falling condensate film.

II. A region where steam from a downward bulk flow of vapour is condensing on a falling film of condensate.

III. A well mixed region at the steam entry point, extending for say 300 mm above and below the entry point centre line. This would allow some air from the top half to leave through the bottom de-aeration line.

The liquid film thickness in region (II) is dependent on the condensation in region (I) so ideally the model for region (I) should be solved first. The model must consider the cylindrical nature of the problem although tangential differences can be assumed to be negligible.

The bulk flow of steam through the annulus needs to be modelled so that the bulk flow velocity can be determined at any point. To simplify the problem, the steam jacket wall temperature can be assumed to be equal to that of the steam bulk temperature. That is, no heat transfer through the outer steam jacket wall and no condensate film formation. The product tube wall temperature will be assumed to be constant. The steam and air leaving the region of interest to go the de-aeration lines will have a velocity and concentration gradient which will be determined by the model.

34.6 Parabolic Technique

To solve the top half by a forward marching technique, requires iteration as the steam boundary conditions are defined at the bottom and the liquid boundary conditions are defined at the top ($\delta = 0$). One iterative method which could be used is to assume a steam flow in and a de-aeration rate and just march upwards until $\delta(L) = 0$. Then iterate by modifying the steam rate until L_model = L. This method assumes that all air entering the top half leaves through the top de-aeration line.

The conservation equations and boundary conditions used are found in Appendix O along with the finite difference approximations. A version of the numerical method procedure is shown in Appendix P and the FORTRAN code of the necessary physical properties in Appendix Q.

The variables which need to be solved for the vapour phase, as functions of r and z, are the two velocity vectors (u_r and u_z), the temperature (T) and the steam mass fraction (w_1). The inputs required were the wall temperature, inlet steam flow, composition and pressure (assumed to be at saturation temperature), the de-aeration (venting) rate and the calandria geometry. The film thickness at the bottom was estimated using Nusselt conditions, and initial profiles for u_r, u_z, T and w_1 and their first order partial derivatives with respect to z were assumed. The first large step in z, was split into a number of small steps, to allow the profiles to be established, before marching up the calandria.

A variety of alternative initial conditions were tried, including linear, $1\text{-}e^r$ and parabolic profiles for $u_z(r)$ and linear and $1\text{-}e^r$ profiles for water vapour mass faction, $w_1(r)$. After observing that the pressure drop over the calandria length was negligible in practice (see Appendix B) the pressure was assumed to be constant on the steam-side. In addition, setting the interfacial shear to zero was also tried.

To simplify the problem, the limiting case of no NCG was investigated using an appropriate subset of the conservation equations and boundary conditions. In this limiting case model, an effort was made to balance the radial and longitudinal velocity vectors across the steam-side at the bottom using the Thomas algorithm to solve the tri-diagonal system of linear equations. A further limiting case of upward flowing gas passing a downward flowing liquid film without condensation was also evaluated in an attempt to get a better initial velocity profile.

There was a similar lack of success with all the above work due to the fact that the parabolic forward marching technique can not cope with separated flows (Patankar, 1988a), *i.e.* it can not cope with negative velocities in the marching direction. This problem would not occur in the bottom half of the calandria shell, so the method could be used for that purpose, once the conditions at the centre-point of the calandria are determined.

34.7 Elliptic Technique

It now appears that solution of the top half will require the use of an elliptic procedure, in which essentially the whole region is solved at once. To ease computation, storage and time factors, the region can be iteratively solved using a tri-diagonal matrix algorithm to solve firstly row by row and then column by column until convergence is

achieved (Patankar, 1988b). The conservation and boundary conditions shown in Appendix O would still apply, but the finite difference approximations would differ from those shown.

34.8 Conclusion

The unfortunate choice of the parabolic method prevented the successful modelling of the top half of the steam side. The use of an elliptic procedure appears to be the best method to try next. Once the top half model is solved, the same method could be used for the much simpler bottom half. The description of the conservation equations and boundary conditions and the physical property code provided here will be a good starting point for the implementation of an elliptic model.

35 NON-CONDENSABLE GAS EXPERIMENTAL DESIGN AND PROCEDURE

35.1 Experimental Design

The standard operating conditions used during the work, except where expressly stated, were as stated in Section 13.1. Water was used as the feed stock for all runs. The NCG experiment work was split into five areas as outlined below.

De-aeration line blockage

The effect of de-aeration port location was determined dynamically (Experiment Nc1, 27 & 29 September 1991). There were three runs:

Run 1: Once the plant was stable with differential pressure control and with both de-aeration line valves open, the bottom de-aeration line valve was closed. The evaporation rate was monitored while maintaining a constant differential pressure. The initial conditions were as described in Section 13.1, except that the temperature driving force was 3.5°C, the feed flow rate was 113 kg h^{-1} and the feed temperature was 59°C.

Run 2: As for Run 1, except that the top de-aeration valve was closed instead of the bottom one. After the plant had stabilized with the valve closed, it was opened again.

Run 3: When the plant had almost reached its original condition after Run 2, the steam valve position was fixed and the bottom de-aeration line valve was closed. The evaporation rate and differential pressure were monitored while maintaining a constant steam valve position (73.8% open).

Air bleed experiment

Experiment Nc2 was an evolutionary experiment, carried out on 21-22 October 1991, looking at the effect of NCG concentration on heat transfer. The run conditions were chosen to determine:

(1) the effect of NCG concentration on differential pressure at constant evaporation rate, and,

(2) the effect of NCG concentration on the evaporation rate at constant differential pressure.

The de-aeration rate for the experiments was nominally 1% of the incoming steam flow

rate (de-aeration nozzle diameter 0.99 mm). But in practice, the de-aeration rate was actually a co-variant of either the differential pressure or the evaporation rate.

Wetting factor experiments

Experiments Wa9-Wa13 looked at the effect of de-aeration rate and NCG concentration over a range of boiling side liquid loadings (see Section 13.5). Two levels of de-aeration rate (nominally 0.8 and 6.5% w/w) were used, and at the lower de-aeration level, the effect of deliberate air addition to the steam was evaluated.

Differential pressure experiments

The experimental design for Experiments Wa14 and Wa23 is presented in Section 13.7. The de-aeration nozzles used for Experiment Wa14 were 0.99 mm in diameter, and for Experiment Wa23 were 3.2 mm in diameter.

Pressure rise leak tests

To determine the normal level of air leaks into the steam side of the Third Evaporator and to check the air flow rates through the air bleed nozzles a series of pressure rise tests were conducted (Experiment Nc3). The tests was carried out with no deliberate NCG addition and then with deliberate air addition through air bleed nozzles with nominal diameters of 0.2, 0.34 and 0.51 mm. Runs 1-5 were done on 23-24 October 1991 and Runs 6-12 between 30 October 1991 and 1 November 1991. The de-aeration nozzles were 0.99 mm in diameter.

Commissioning of non-condensable gas measurement apparatus

Experiment Nc4 consisted of a number of spot measurements of the NCG concentration in the de-aeration lines using the NCG measurement apparatus. The boiling side operating conditions varied considerably between measurements. The measurements were taken between 9 September 1991 and 27 March 1992.

35.2 Experimental Procedure

For Experiments Wa9-Wa14 and Wa23 the procedure used is described in Chapter 14.

For Experiments Nc1, Nc2 and Nc4, steps 1-8 of the water experimental procedure (see Chapter 14) were carried out. The controller set points were then manually changed as required for each run. The plant was shut down in the manner described in Chapter 14.

For experiment Nc3, both the condensate and de-superheat water drain lines were blanked off, and the steam valve and the de-superheat water supply line valve were closed. Before the first test, a vacuum was drawn on the plant and maintained for 3 h to evaporate off water in the plant. The de-aeration valves were then closed and, if required, the air bleed valve was opened. After the run, the air bleed was closed (if open) and the bottom de-aeration valve opened to bring the pressure down again before the next run.

35.3 Data Analysis

For Experiment Nc1, the overall heat transfer coefficient was determined as described in Chapter 12. For Experiments Nc2, Wa9-Wa14 and Wa23 the data analysis procedure was as described in Chapter 12 except for additional calculations to determine the NCG concentration in the steam and the de-aeration rates (see Section R3 of Appendix R). For Experiment Nc3 the data analysis procedure is found in Sections R1 and R2. The data analysis procedure for Experiment Nc4 is described in Sections R3 and R4.

36 NON-CONDENSABLE GAS EXPERIMENTAL RESULTS

The raw data for Experiments Nc2, Nc4 and Wa9-Wa13 are found in Appendix I.

36.1 Experiment Nc1: De-aeration Port Location

The change in the overall heat transfer coefficient (HTC) with time after closing a de-aeration valve is shown in Figures 36.1-36.2. The reduction of the overall HTC over the space of several hours is due to the gradual increase in the air fraction in one half of the calandria shell. The effect of closing either the top or bottom de-aeration port is essentially the same (see Figure 36.1), a reduction in overall HTC to 60% of its original value. When the port is opened again, the overall HTC rapidly regained its original value. The disturbances before and/or after each closure of a de-aeration port, prevented any useful comparison of the time constants for the process at constant differential pressure and at constant steam valve position.

36.2 Experiment Nc2: Effect of Inlet Air Concentration

Thirty experimental runs were done, but Runs 2 and 29 were unstable and Runs 4-15 were not analyzed after it was discovered that there was an additional leak through the bleed valve housing during these runs. The remaining run results are presented in Table 36.1. The effect of NCG concentration on the condensation rate is shown in Figure 36.3. A regression line fitted through the values obtained at a differential pressure of 2.93 kPa ("a" points on Figure 36.3), gave a y-intercept of 23.47 kg h^{-1}. The evaporation rate ratio (E/E_0) was then calculated for the "a" values and plotted along with heat transfer rate ratio (k/k_0) values extracted from Kessler (1987) in Figure 36.4.

36.3 Wetting Factor Experiments (Wa9-Wa13)

The overall heat transfer results are shown in Figure 36.5. Both the de-aeration rate and the addition of air have a marked effect on heat transfer. The percentage air entering with the steam and the de-aeration rates are based on the assumptions made for Experiment Nc2 (see Appendix R).

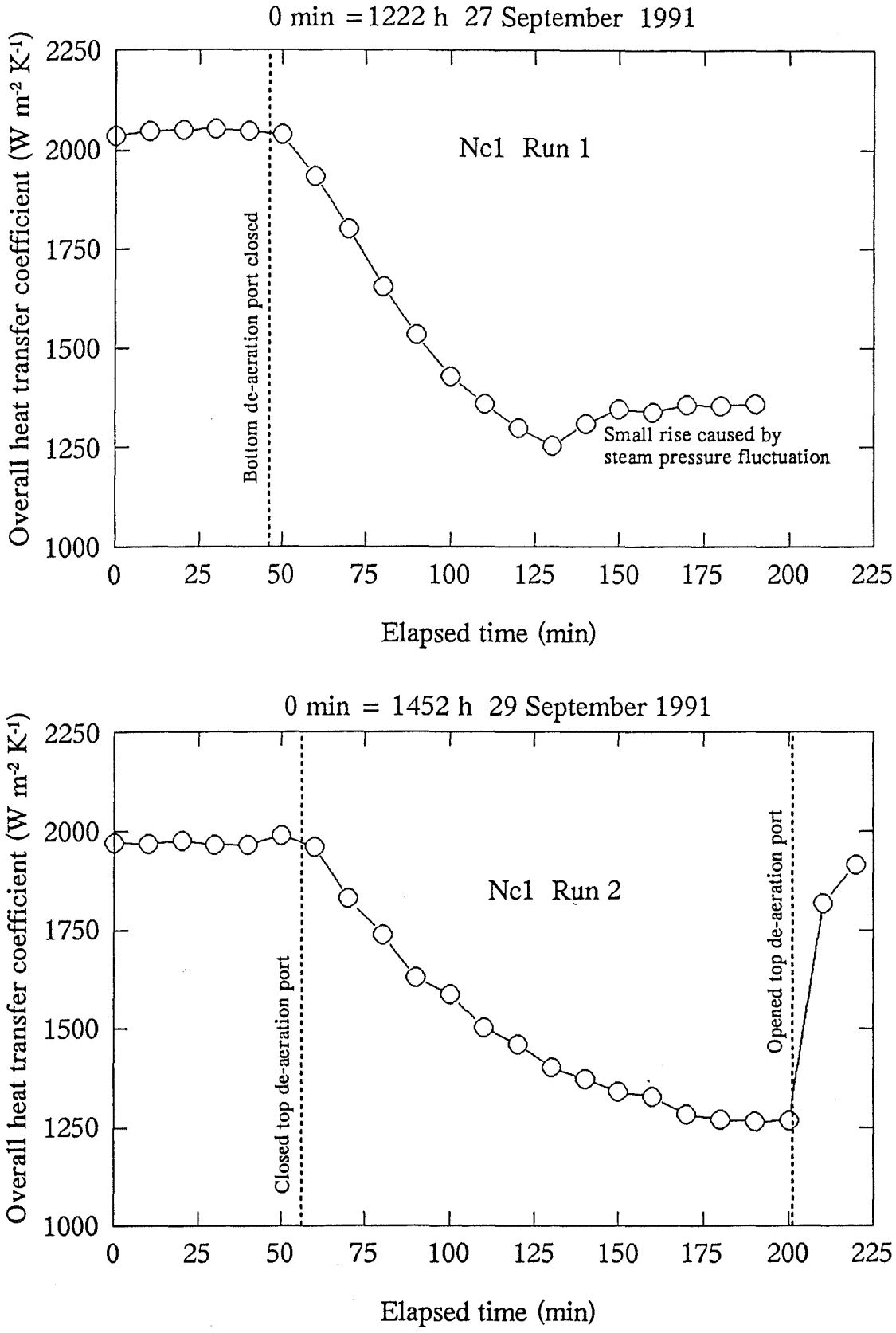

Figure 36.1: Dynamic Response to Closing a De-aeration Port at Constant Differential Pressure.

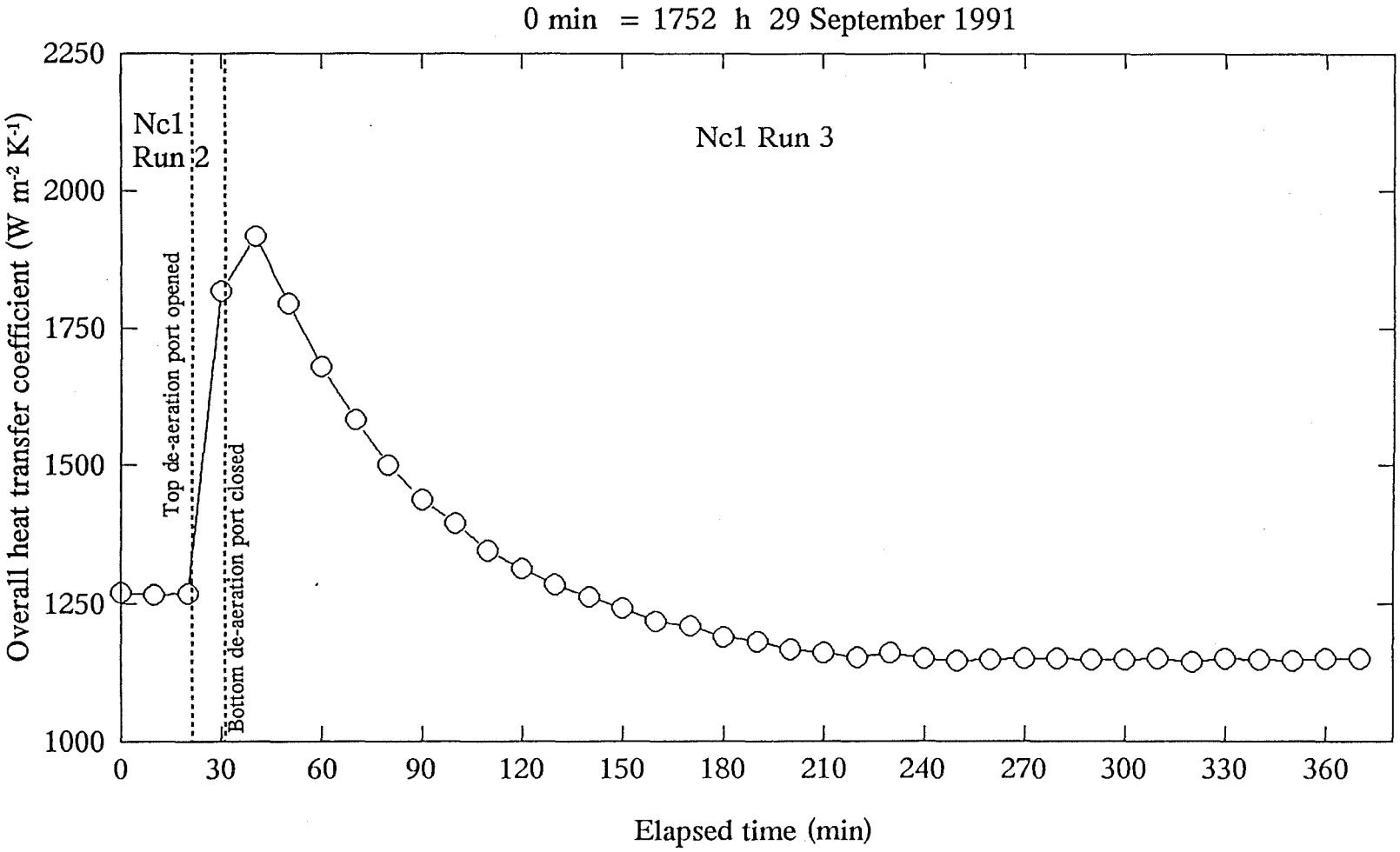

Figure 36.2: Dynamic Response to Closing a De-aeration Port at a Fixed Steam Valve Position.

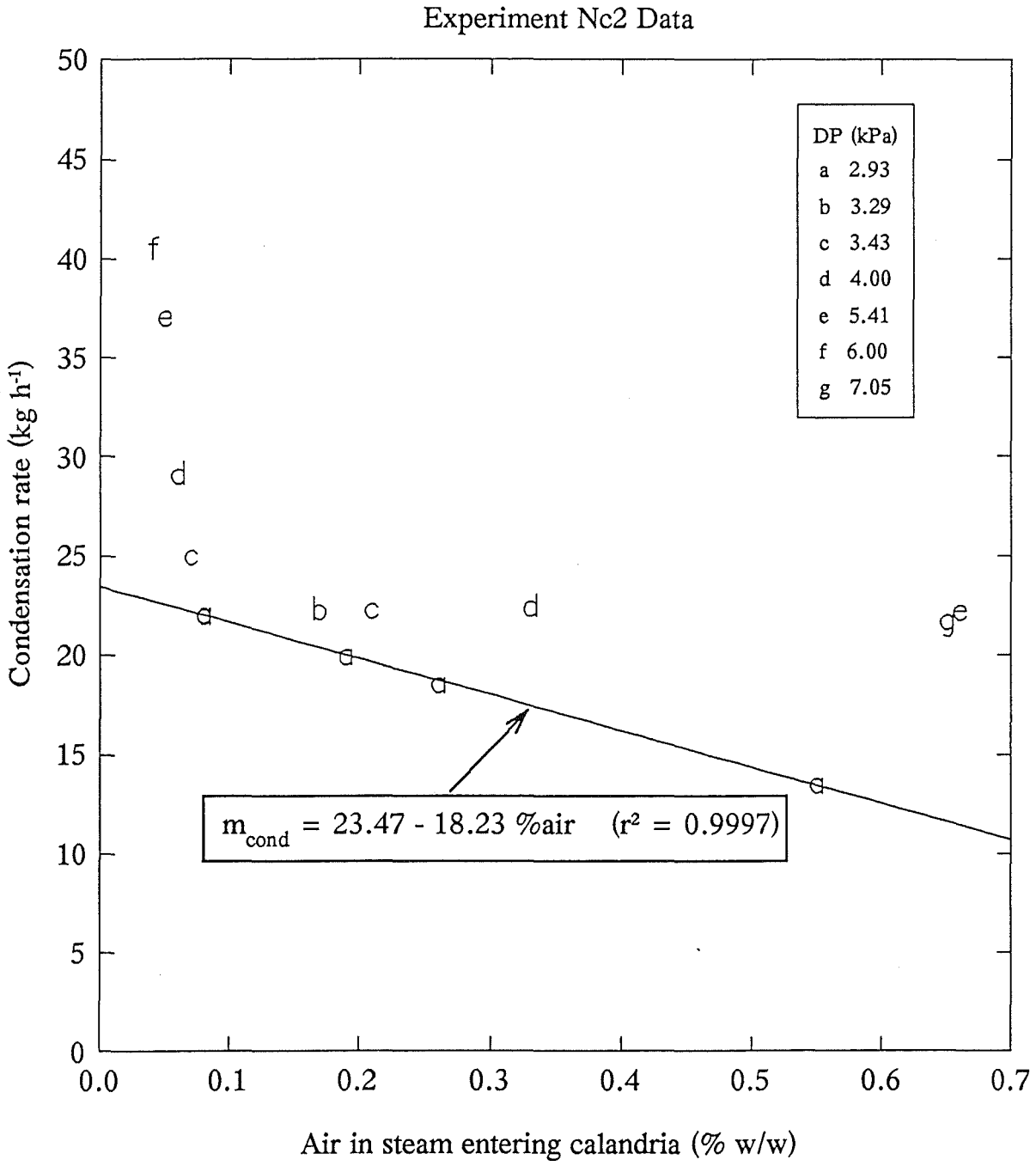

Figure 36.3: Effect of NCG Concentration on Condensation Rate at a Range of Differential Pressures (DP).

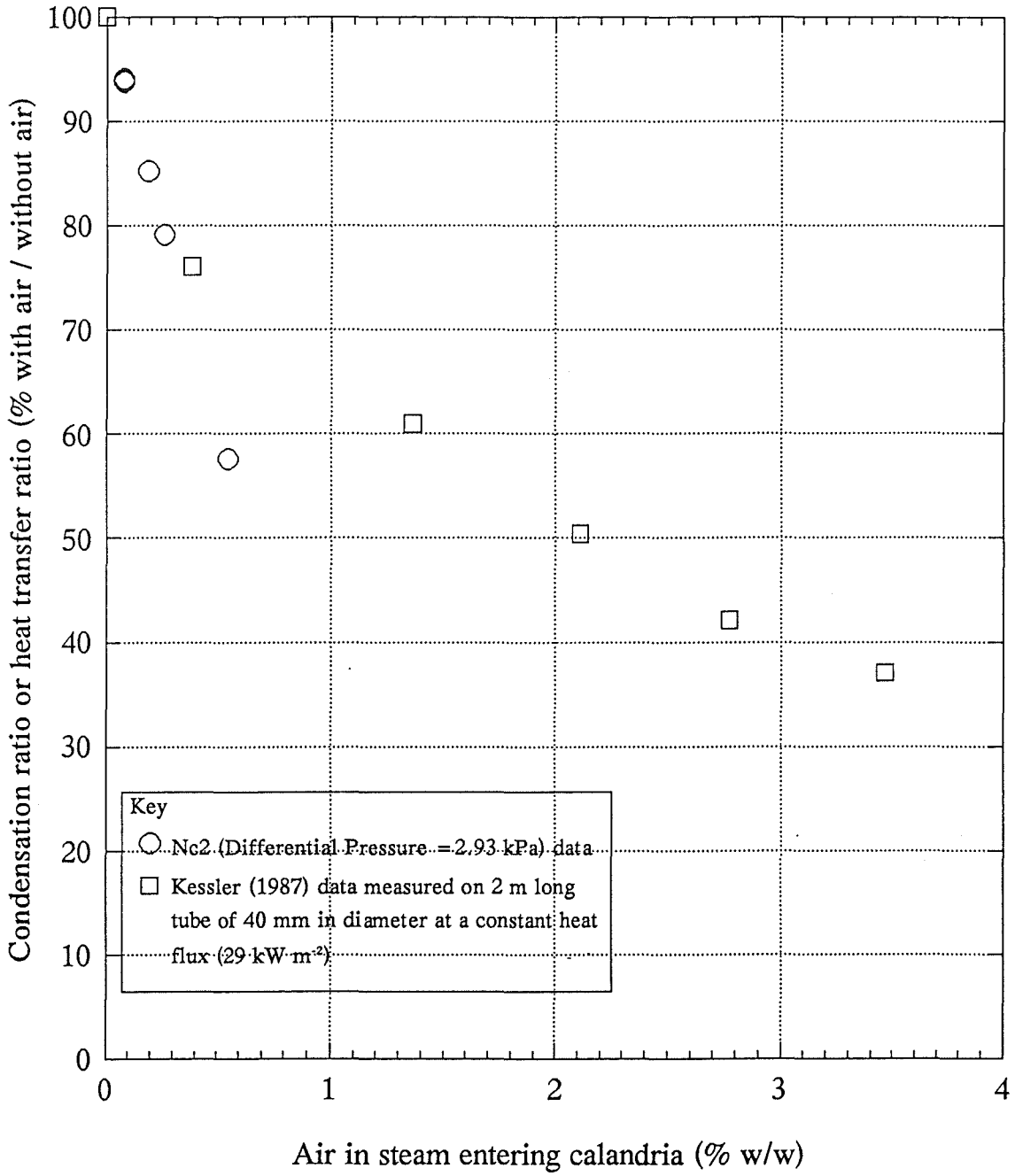

Figure 36.4: Comparison of Data from Experiment Nc2 and Kessler (1987).

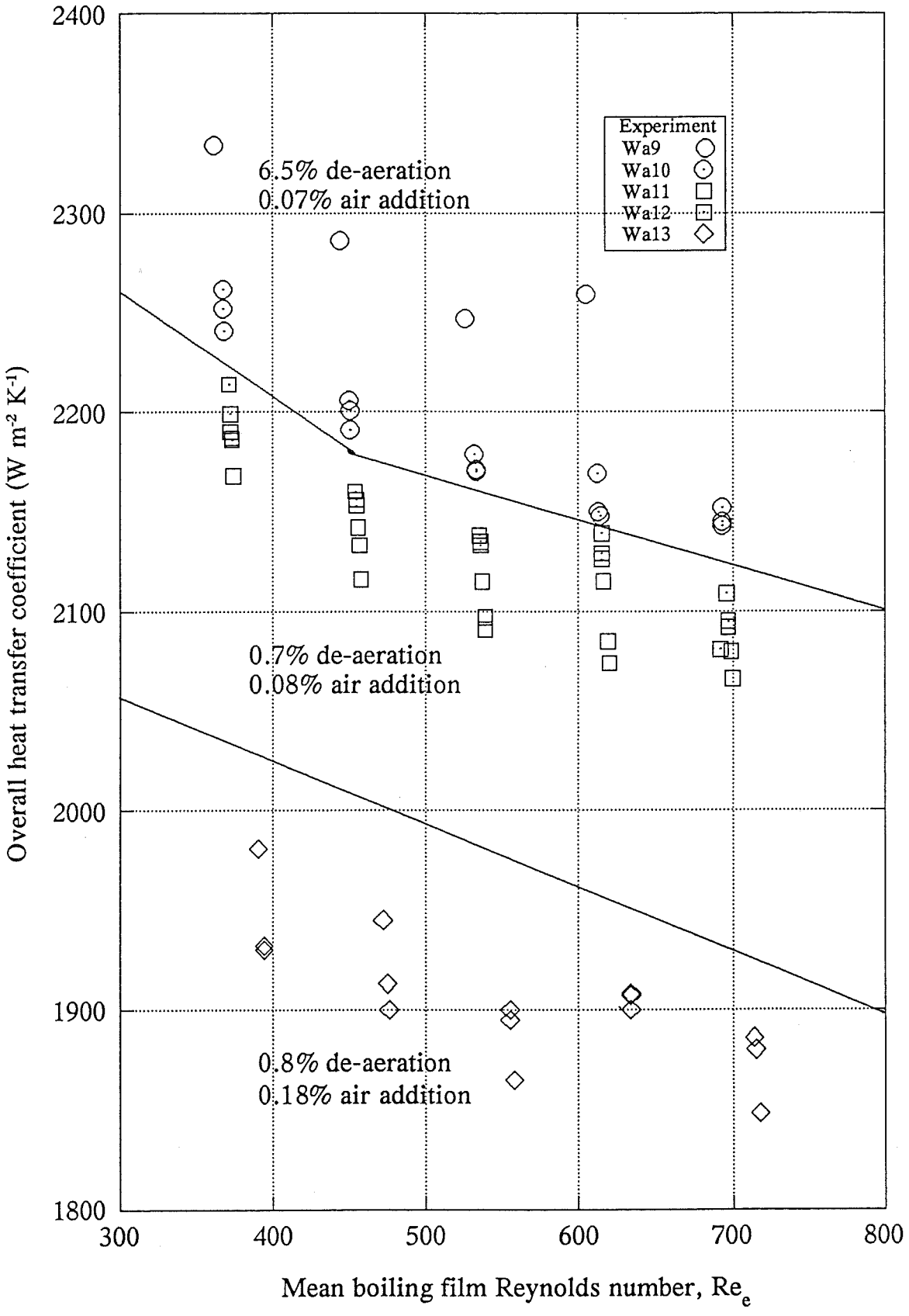

Figure 36.5: Overall Heat Transfer Coefficients for Experiments Wa9-Wa13.

Table 36.1: Selected Experiment Nc2 Results.

Run No	Bleed Nozzle	Differential Pressure (kPa)	Leakage Rate[a] (kg h^{-1})	De-aeration Rate[a,b] (kg h^{-1})	Condensation Rate (kg h^{-1})	Air In (%)	Vent rate (%)	Air Out (%)
1	000050	5.41	0.149	0.217	22.20	0.66	0.96	69.1
3	None	5.41	0.018	0.177	37.06	0.05	0.46	10.2
16	None	2.93	0.018	0.160	22.04	0.08	0.71	11.2
17	000009	3.29	0.038	0.168	22.24	0.17	0.74	22.6
18	000009	2.94	0.038	0.166	20.00	0.19	0.81	22.9
19	None	2.93	0.018	0.160	22.08	0.08	0.71	11.2
20	000012	3.44	0.049	0.173	22.30	0.21	0.75	28.4
21	000012	2.94	0.049	0.169	18.56	0.26	0.89	29.0
22	None	3.42	0.018	0.164	25.01	0.07	0.64	11.0
23	None	2.93	0.018	0.160	22.00	0.08	0.71	11.2
24	000021	4.00	0.076	0.184	22.38	0.33	0.80	41.3
25	000021	2.94	0.076	0.177	13.51	0.55	1.27	43.0
26	None	4.00	0.018	0.167	29.11	0.06	0.56	10.7
27	None	2.93	0.018	0.160	22.03	0.08	0.71	11.2
28	000050	7.05	0.149	0.226	21.73	0.65	0.99	65.9
30	None	6.00[c]	0.018	0.186	40.46	0.04	0.43	9.9

[a]Calculated flow rates assuming nozzle coefficient of 0.75 based on nominal diameter and that base leakage rate is 0.018 kg h^{-1} (see Section R2).
[b]De-aeration nozzles were SS0002 (0.99 mm in diameter, calculation procedure in Section R3.
[c]Absolute pressure was 19.92(3) kPa for all runs except this one (20.08 kPa).

36.4 Differential Pressure Experiments (Wa14 & Wa23)

The differential pressure results are reported and discussed in Chapter 19.

36.5 Experiment Nc3: Leakage Rate Tests

The differential pressure and absolute pressure trends for Runs 1-3 are shown in Figure 36.6. The steam side pressure rise data and the calculated leakage rates are included in Appendix R. Without deliberate air addition, the measured leakage rate varied between 0.009 to 0.018 kg h^{-1}. The nozzle coefficients determined from the experiment varied from 0.69 to 0.86 based on the nominal nozzle diameter and varied between 0.52 and 0.75 based on a measured nozzle diameter. Thus, a nozzle coefficient

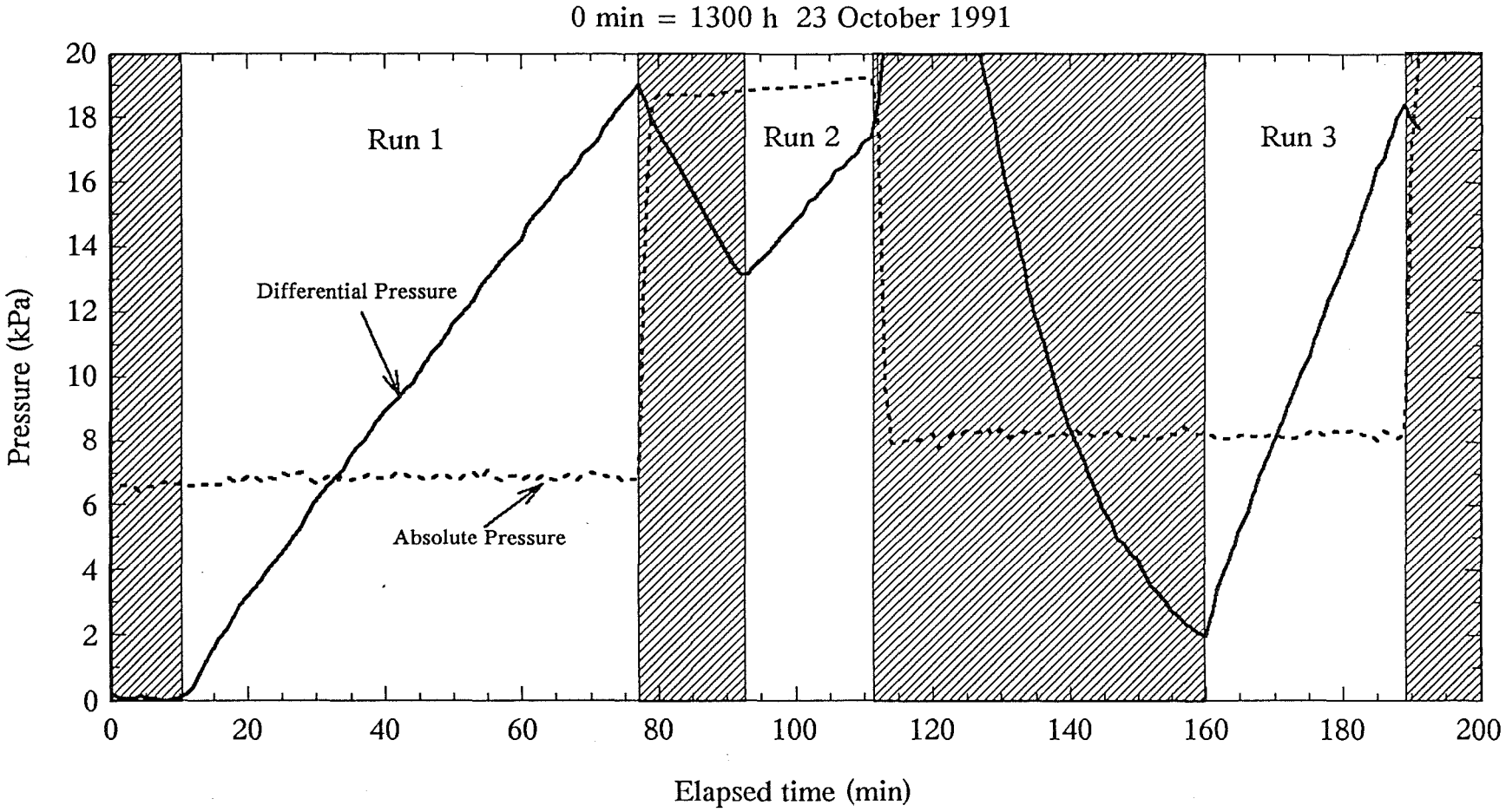

Figure 36.6: Leakage Test Trends (Experiment Nc3 Runs 1, 2 and 3).

of 0.75 based on the nominal nozzle diameter was assumed for calculating air addition rates for Experiment Nc2 and Wa13.

36.6 Experiment Nc4: Non-condensable Gas Measurement in De-aeration Lines

The observations made during the NCG commissioning trials are included in Appendix S. The NCG measurements made are tabulated in Table 36.2 along with the conditions under which each measurement was made. The change in absolute pressure inside the sample bottle when cooled is shown in Figures 36.7 and 36.8 for Measurements 5 and 6 respectively. For Nc4 Measurements 10, 11 and 12, the differential pressure measured at the bottom of the calandria, dropped significantly when the valves were open to sample the de-aeration line stream (see Figure 36.9).

Table 36:2 Experiment Nc4 NCG Measurements on De-aeration Lines.

Measurement No.	Plant Steam Side Conditions	Sampling Location and Duration	Cooling Method used	NCG Concentration (% v/v)	Comments
1	Top vent closed Vent diameter 3.2 mm No air bleed	Bottom vent line 16 min	dry ice plus a little water liquid nitrogen	6.1% 7.5%	Closed IN valve before OUT valve so initial pressure was low (15.1 kPa). Reduced pressure to 1.3 kPa with dry ice/water mixture, 0.78 kPa with liquid nitrogen.
2	Top vent closed Vent diameter 3.2 mm No air bleed	Bottom vent line 8.5 min	water plus dry ice liquid nitrogen	18.1% 7.9%	The temperature of the water/dry ice mixture only dropped to 5°C. This sample was pressurized with helium and analysed on the GC.
3	Both vents open Vent diameter 3.2 mm No air bleed	Bottom vent line 8 min	glycol plus dry ice liquid nitrogen	14.3% 11.7%	Wrong valves closed at end of sample, so low initial pressure.
4	Both vents open Vent diameter 3.2 mm No air bleed	Bottom vent line 7 min	glycol plus dry ice liquid nitrogen	5.4% 6.9%	Initial pressure determined from plant AP and DP measurements for Measurements 4-12. No compensation made for volume of lines to AP sensors.
5	Both vents open Vent diameter 3.2 mm No air bleed	Bottom vent line 10 min	glycol plus dry ice liquid nitrogen	6.3% 6.3%	There was a leak between the two valves on the line to the AP sensors during this measurement.
6	Both vents open Vent diameter 3.2 mm No air bleed	Top vent line 8 min	liquid nitrogen Glycol plus dry ice	0.5% 1.5%	The bottle was cooled with liquid nitrogen first, then put in glycol which froze onto the bottle. The frozen glycol was removed and a glycol dry mixture was then used.

Table 36:2 continued.

Measurement No.	Plant Steam Side Conditions	Sampling Location and Duration	Cooling Method used	NCG Concentration (% v/v)	Comments
7	Top vent closed Vent diameter 3.2 mm No air bleed	Bottom vent line 5 min	glycol with dry ice	0.9%	Temperature of glycol -0.1°C.
8	Top vent closed Vent diameter 3.2 mm Bleed diameter 0.51 mm	Bottom vent line 8.5 min	glycol with dry ice	4.3%	
9	Top vent closed Vent diameter 0.99 mm No air bleed	Bottom vent line 15 min	glycol with dry ice	1.9%	Temperature of glycol -2°C.
10	Top vent closed Vent diameter 0.99 mm Bleed diameter 0.51 mm	Bottom vent line 7 min	glycol with dry ice	81.0%	Temperature of glycol -0.6°C. In-line temperature and pressure measurements indicate an air concentration of 52.3%.
11	Top vent closed Vent diameter 0.99 mm Bleed diameter 0.51 mm	Bottom vent line 6 min	glycol with dry ice	83.4%	Temperature of glycol -1.9°C. In-line temperature and pressure measurements indicate an air concentration of 53.4%
12	Both vents open Vent diameter 0.99 mm Bleed diameter 0.51 mm	Bottom vent line 6 min	glycol with dry ice	69.4%	Temperature of glycol -3°C. In-line temperature and pressure measurements indicate an air concentration of 36.7%. Bypass closed before IN/OUT opened.

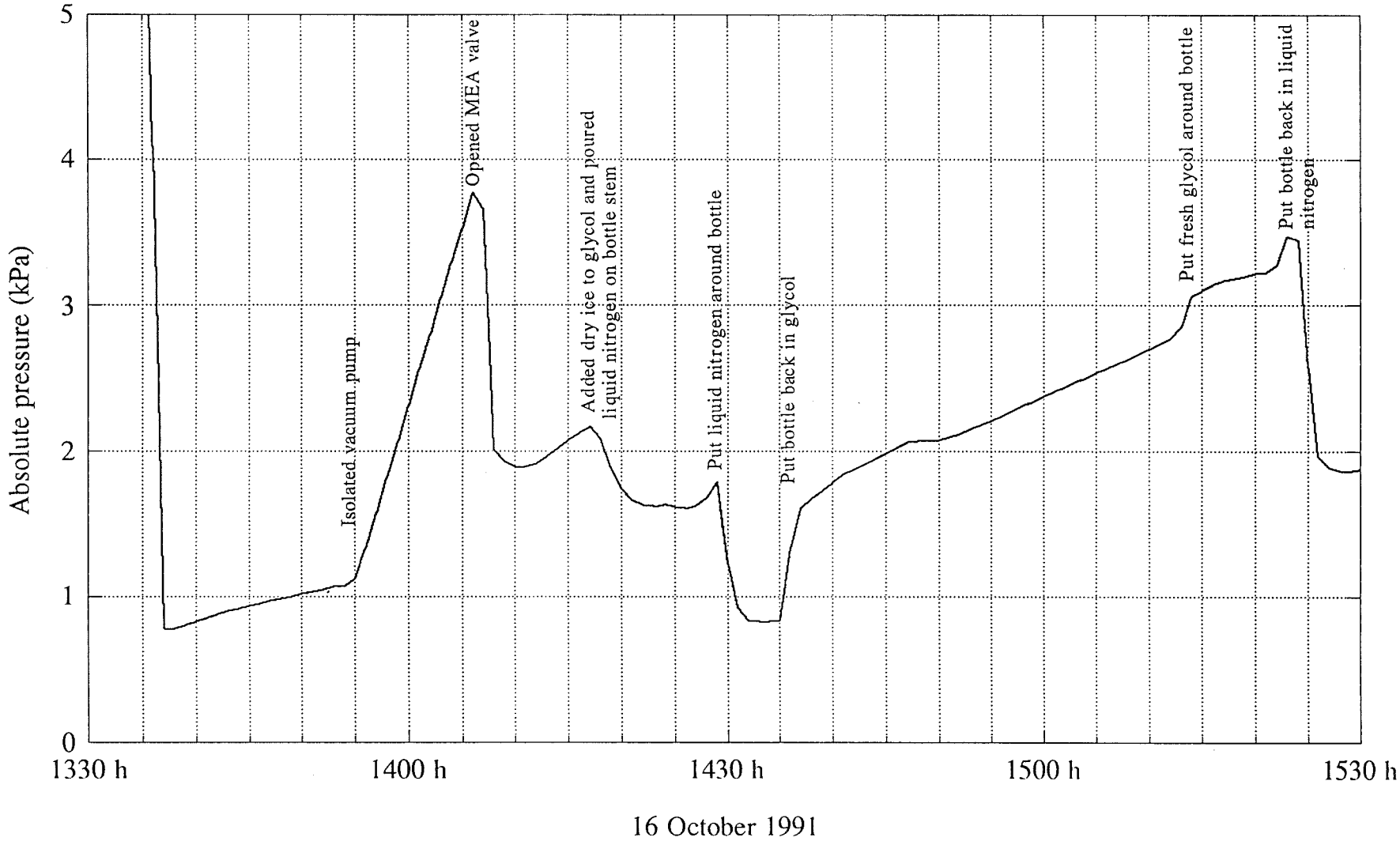

Figure 36.7: NCG Apparatus Absolute Pressure (0-7AP) Trend for Experiment Nc4 Measurement 5.

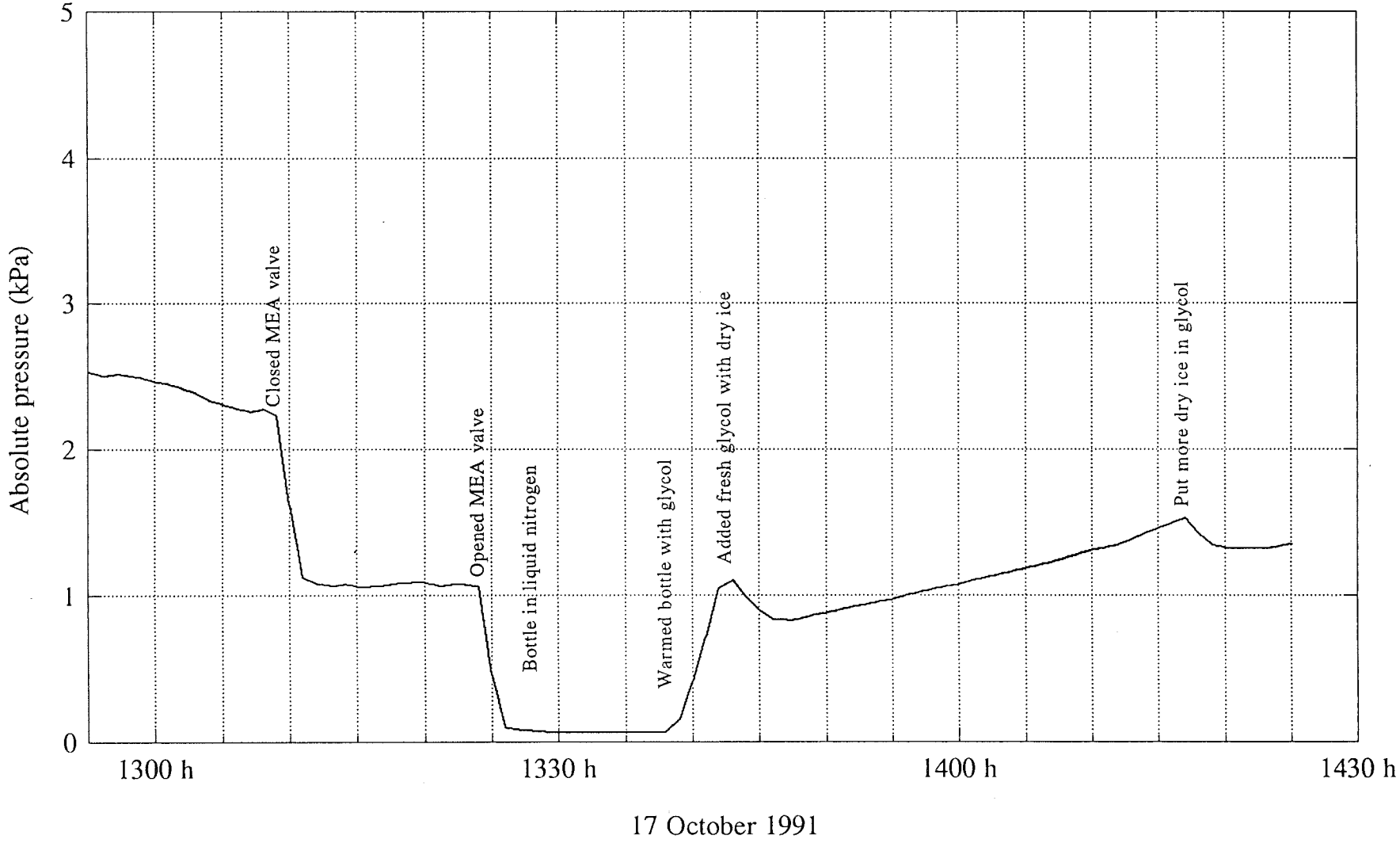

Figure 36.8: NCG Apparatus Absolute Pressure (0-7AP) Trend for Experiment Nc4 Measurement 6.

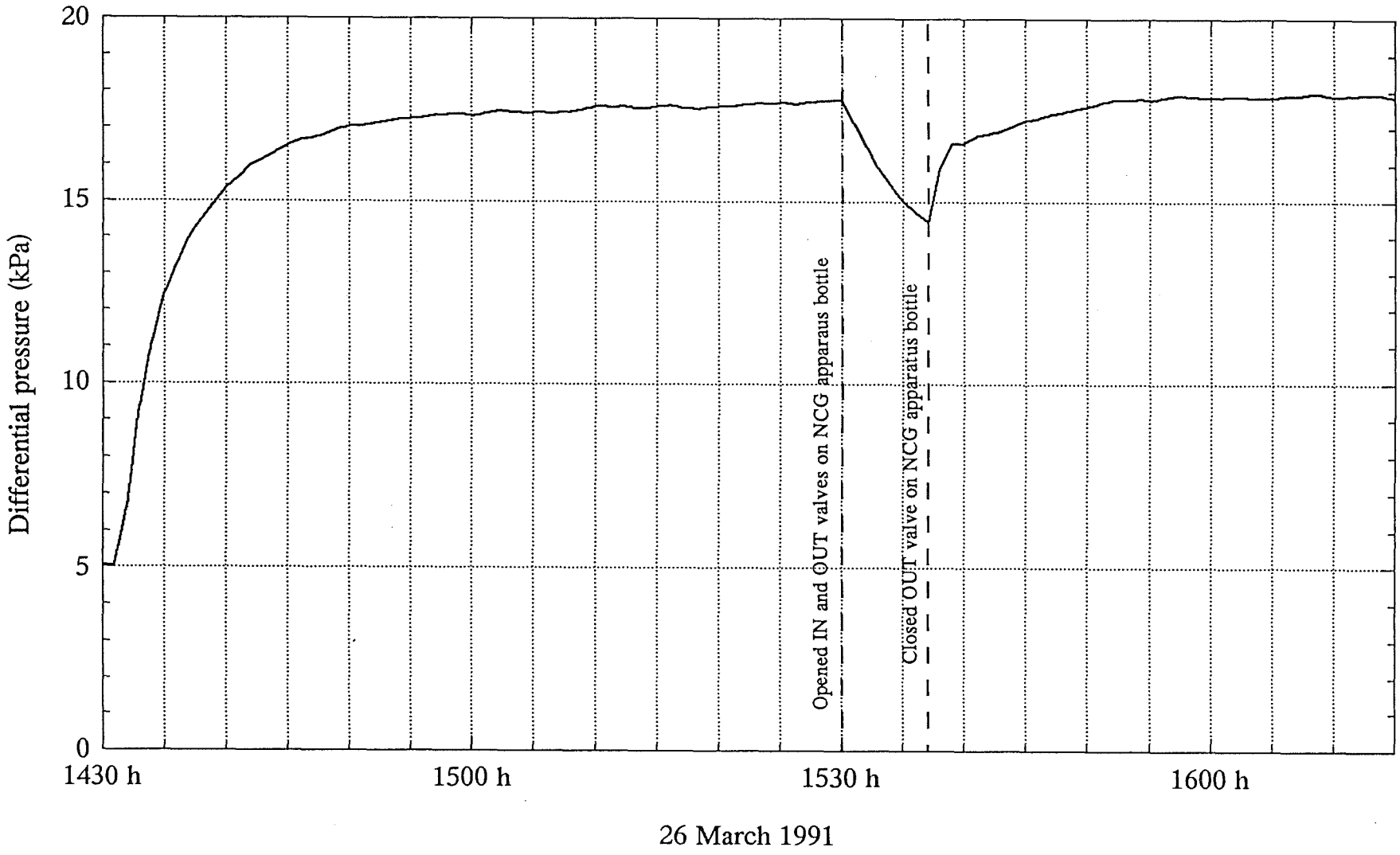

Figure 36.9: Bottom Differential Pressure Trend for Experiment Nc4 Measurement 10.

37 NON-CONDENSABLE GAS DISCUSSION

37.1 De-aeration Port Location

The effect of de-aeration port location was shown dramatically in Experiment Nc1. The result showed that very little condensation occurred in the half of the calandria which was not vented. Thus, de-aeration ports must be placed to minimise dead spaces where NCG concentrations can build up. The time it takes for the plant to stabilize, after closing a de-aeration port, gives a measure of the incoming NCG concentration (given that the stagnant volume is known). The time to regain stability, after opening the valve, gives a measure of the de-aeration rate. Thus, the closing and subsequent opening of a de-aeration port could be used to determine both the incoming NCG concentration and the de-aeration rate. However, the slow response to closure would present difficulties when testing commercial plants.

The similar results obtained when closing either the top or bottom port indicates that the amount of NCG leaving in the condensate is insignificant. This is not surprising as the solubility of NCG in water, when close to its boiling point and in contact with a vapour phase containing mostly steam, would be negligible.

37.2 Effect of De-aeration Rate

Reducing the de-aeration rate from 6.5% w/w to 0.7% w/w reduced the overall HTC by 4% (see Figure 36.5) to 13% (see Figure 19.3) at a temperature driving force of 3°C. At a low temperature driving force (1°C) the reduction in HTC was 43% (see Figure 19.3). Thus, the commercial rates of 1-1.5% may be suitable for plants running with greater than 3-4°C temperature driving force, but higher rates are recommended for MVR evaporators, which under turndown conditions run with temperature driving forces as low as 2°C.

37.3 Effect of the Presence of Non-condensable Gases in Steam

The presence of small qualities of NCG in the incoming steam had a dramatic effect on the overall HTC. The presence of 0.55% w/w air in steam reduces the condensation rate by 33% (see Figure 36.4). The results from Experiment Nc2 show a negative, linear relationship between NCG concentration and condensation rate (see Figure 36.3). Kessler (1987) however presents data which shows that the incremental effect of NCG

concentration decreased as the concentration increased (see Figure 36.4). The data reported by Kessler was obtained on a 2 m long, 40 mm diameter tube with the steam entering at the top and a de-aeration port at the bottom. The de-aeration rate was not given. If the de-aeration rate was high, there would not be a large vertical concentration gradient and thus the build up of a horizontal concentration gradient near the condensing surface would have provided the resistance to heat transfer. The heat transfer rate was fixed, so that the steam side pressure increased with increasing air concentration, and thus, presumably, the de-aeration rate also increased. In Experiment Nc2, there was a significant vertical concentration gradient as well as the horizontal concentration gradient near the condensing surface. The results presented in Figure 36.4 were obtained at a fixed steam side pressure and the de-aeration rate increased linearly with air concentration (see Table 36.1). The reason for the curvature reported by Kessler is not clear. One possibility is that the de-aeration port flow regime changed from subsonic to sonic as the air content increased, thus causing a non-linear increase in de-aeration rate.

The effective temperature driving force was calculated for the 2.93 kPa differential pressure data by multiplying the nominal temperature driving force (3 °C) by the ratio of condensation rate to condensation rate at 0% w/w air (23.47 kg h^{-1} obtained by extrapolation). From the effective temperature driving force, the steam partial pressure was determined, and then the air partial pressure by difference (see Table 37.1).

Table 37.1: Calculation of Mean Air Concentration from Condensation Rates.

Run	-	16/19/23/27	18	21	25
%Air In (% w/w)	0	0.08	0.19	0.26	0.55
%Air Out (% w/w)	0	11.2	22.9	29.0	43.0
Ratio of %Air Out over %Air In	-	140	121	112	78
Condensation rate (kg h^{-1})	"23.47"	22.04	20.00	18.56	13.51
Effective temperature driving force (°C)	3	2.82	2.56	2.37	1.73
Steam partial pressure (kPa)	22.89	22.71	22.44	22.25	21.62
Predicted mean air concentration (% w/w)	0	0.81	1.98	2.8	5.6
Ratio of mean over inlet concentration	-	10.2	10.4	10.9	10.2

The ratio of the predicted mean air concentration to the inlet air concentration was 10 which could be perhaps explained purely in terms of the vertical concentration gradient as the outlet air concentration was 78-140 times the inlet air concentration. Assuming a horizontal air concentration profile does exist in some sectors of the calandria, the predicted mean concentration suggests that there may be an area of the tube near the steam entry port where the vapour boundary layer is stripped off by turbulence. For Kessler's data the predicted mean concentration was 11-20 times the inlet air concentration. More work is required to establish the relative importance of the vertical and horizontal concentration gradients. Completion of the model described in Chapter 34 would provide a good starting point. The NCG concentration in the bulk steam will be highest at the ends of the calandria, so severe air inclusion may effectively reduce the length of tube available for condensation.

37.4 Measurement of Non-condensable Gas Concentration in Calandria Shell

The pressure rise test determined that the leakage rate without deliberate air addition was between 0.009 and 0.018 kg h^{-1} of air. The upper value was used for all further calculations, essentially because it was measured shortly after Experiment Nc2. The nominal diameter (with a nozzle coefficient of 0.75) was used to calculate air ingress rates because there was less variation between the coefficients (based on the nominal diameter) over the range of nozzle diameters tested. It is possible that the increase in the ratio of actual diameter to nominal diameter as the diameter reduces may have been done deliberately by Spraying Systems in order to maintain a constant nozzle coefficient.

37.5 Steam Side Measurements

Steam side pressure measurement

For the majority of the experimental work there were three differential pressure sensors mounted on the Third Evaporator. The three gave slightly different readings due to mounting location. When the effects of pressure drop due to friction and velocity and the difference in suction side head was accounted for (See Appendix B) the difference in the pressure at the top, bottom and middle of the calandria shell was insignificant. The entry differential pressure measurement which has been used in all calculations, had an error of +0.12 kPa, so the temperature driving forces were actually approximately 0.1°C lower than reported in this work.

Steam side temperature measurement

The surface temperature probes installed to measure the condensate temperature, the steam entry temperature and the top and bottom de-aeration temperatures consistently gave different readings (see Table 37.2) under conditions where air inclusion was minimal. As they were not calibrated in place, the variation could be due to mounting location and effectiveness of insulation. This is certainly the case for the condensate temperature (see Chapter 17).

Table 37.2: Comparison of Steam-Side Temperatures for Experiments Wa9-Wa13.

Experiment[a]	Operating Conditions	Steam Entry Temperature (°C)	Condensate Temperature (°C)	Top De-aeration Temperature (°C)	Bottom De-aeration Temperature (°C)
Wa9	De-aeration nozzle 3.2 mm No air bleed	62.6 (62.96)[b] [62.97][c]	60.7	61.4 (62.73) [62.85]	62.7 (62.73) [62.85]
Wa10	De-aeration nozzle 3.2 mm No air bleed	62.6 (62.96) [62.97]	60.5	61.4 (62.73) [62.85]	62.7 (62.73) [62.85]
Wa11	De-aeration nozzle 0.99 mm No air bleed	62.9 (62.96) [62.97]	60.0	61.5 (60.37) [61.68]	62.9 (60.37) [61.68]
Wa12	De-aeration nozzle 0.99 mm No air bleed	63.2 (62.96) [62.97]	60.2	62.0 (60.37) [61.68]	63.2 (60.37) [61.68]
Wa13	De-aeration nozzle 0.99 mm Air bleed nozzle 0.51 mm	63.1 (62.94) [62.95]	59.4	60.8 (57.33) [58.72]	62.5 (60.37) [58.72]

[a] Data presented is for Run 4 of each experiment, but temperatures were essentially the same for all runs.

[b] Figures in (..) are predicted temperatures determined as described in Section R3 assuming a base air leakage rate of 0.018 kg h^{-1}.

[c] Figures in [..] are predicted temperatures determined by assuming a base air leakage rate of 0.009 kg h^{-1}.

Determination of de-aeration flow rate

Each de-aeration line had a nozzle mounted in-line which operated under sonic flow conditions and controlled the flow rate through the de-aeration line. The nozzle profile was essentially orifice-like so the nozzle coefficient was approximately 0.75. The sonic flow would not be independent of downstream pressure, however, due to the varying area of the *vena contracta* (Grace & Lapple, 1951). In addition, the flow of NCG/steam mixtures through sonic nozzles has not be measured. The error in using a nozzle coefficient of 0.75 may be ± 15% and results presented here should be considered in this light.

37.6 Determining Non-condensable Gas Concentration from In-line Temperature and Pressure Measurements

Comparing the differences between the de-aeration entry temperatures between experiments, it is clear that;

- either the base air leakage rate varied significantly between runs, or,
- that the temperature measurements were not responsive to small changes in air concentration.

The variation in the steam entry temperature could be due to superheat but the presence of superheat in the de-aeration lines is unlikely. At higher air leakage rates, the de-aeration temperatures did change with air concentration (see Table 37.3). The results obtained suggest that the base air leakage rate (*i.e.* without deliberate air addition) was higher than 0.018 kg h^{-1} which is possible considering the NCG measurements were taken four months after the air leakage rate tests. The difference between the air concentrations determined by in-line temperature measurement and with those determined by pressure ratio (before and after cooling extracted sample to $<0°C$) could be due to a number of factors including;

- condensation in the line leading to the sampling apparatus, or,
- a long temperature probe time constant as the differential pressure dropped sharply at the beginning of the sampling period.

Table 37.3: Comparison of Methods of Determining Outlet Air Concentration for Runs 10, 11 and 12 of Experiment Nc4.

Run	Outlet Air Concentration (% v/v)		
	From Air Leakage Calculation[a]	From In-line Temperature and Pressure Measurement	From Pressure Ratio[b] Measurement
10	38.5 (50.2% w/w)	52.3	81.2
11	38.0 (49.7% w/w)	53.4	83.6
12	23.9 (33.6% w/w)	36.7	55.1

[a] Assuming a base air leakage rate of 0.018 kg h^{-1}
[b] Pressure measured after condensing vapour over initial pressure.

37.7 Determination of Non-condensable Gas Concentration by the Pressure Ratio Method

Extraction of a representative sample

The extraction of a representative sample from a de-aeration line without disturbing the process proved a complicated process. The location of the de-aeration ports meant that several metres of tubing was required to take the de-aeration stream to the sampling bottle and back again. After the bottle on the sample return line a de-aeration nozzle was mounted. Thus, when the de-aeration flow was switched to the sampling bottle, the de-aeration rate would stabilize at the same flow rate after the initial disturbance. Generally, the valves on the sampling line were opened first before the valve on the bypass line (with the normal de-aeration nozzle) was opened. The location of the bypass valve meant that for 8 s both de-aeration nozzles were open. During Runs 10 and 11 of Experiment Nc4, a drop in differential pressure occurred when the sample valves were opened, and it was thought that the extra flow had reduced the air concentration in the calandria. However, in Run 12, the bypass valve was closed first, and there still was a drop in differential pressure. Inspection of both nozzles revealed that they were identical (same nominal size) so the reason for the drop in differential pressure is not fully understood. A possibility is that the line to the sampling device cooled down significantly between samples due to heat losses and a build up of a high air concentration under stagnant flow conditions. When the flow was resumed, the incoming steam/air mixture condensed on the cold tube walls causing the de-aeration rate to increase, and possibly also ensuring that there was a higher air concentration in the sample bottle. The latter is a possible explanation for the high air concentration measurements obtained for Measurements 10, 11 and 12 (see Table 37.3). The use of heat tracing on the de-aeration lines would prevent condensation occurring, and should be considered when planning further work.

Preparation of sample bottle

The preparation of the bottle involved using a heating jacket maintained at 100°C, and pulling a vacuum on the bottle. The combination of heat and vacuum ensured that any residual water was boiled off. The neck of the bottle, the valve assembly and the lines to the absolute pressure sensors were not heated directly so some water could remain in these areas. To avoid condensation in the lines leading to the absolute pressure sensors, rerouting the line from the bottle to the vacuum pump should be considered for further work. The vacuum tightness was tested regularly during the trials and, on a couple of occasions, leaks were found. The bottle was made of stainless steel because the fact that

the fitters were experienced in working with stainless steel. This also ensured that CIP chemicals would not affect the bottle, although in practice the apparatus could have been shielded from CIP chemicals. The conductivity of stainless steel is poor ($k_{SS} \approx 13.4$ W m^{-1} K^{-1}) and perhaps the use of Aluminium ($k_{Al} = 204$ W m^{-1} K^{-1}) would have ensured that the neck and valve assembly would heat along with the bottle. The provision of heat tracing on the lines to the absolute pressure sensors might be considered for future work, so that the valve to the absolute pressure sensors could be open while collecting the sample. The temperature of the pressure sensors affects the pressure measurement, so if there was to be any major departure from ambient temperature for the sensor, its temperature would have to be monitored and the temperature correction curve obtained.

Cooling of the sample bottle

To determine the partial pressure of NCG in the sample, the steam has to be condensed. The partial pressure of steam over ice (sources: Rogers & Mayhew (1982) and Weast & Astle (1980, D195)) is plotted in Figure 37.1. The steam partial pressure has to be subtracted from the pressure measured after cooling to obtain the air partial pressure. Therefore, the temperature of the sample after cooling is critical, in order to determine firstly the steam vapour pressure, and to determine the density of the sample (from ideal gas laws). It was intended to measure the bottle temperature using a surface probe, but due to the poor conductivity of Stainless Steel, the neck of the bottle was still warm, even when half the bottle was in liquid nitrogen. Thus, only the coolant temperature could be measured. The temperature inside the bottle (chilled surfaces) could only be estimated. The measurement of temperature inside the bottle is difficult as the temperature measured is likely to be the probe wall temperature and conduction of heat from outside the vessel down the probe could introduce a considerable error. This needs to be overcome in any further work.

Coolants used were water/dry ice mixtures, glycol/dry ice mixtures and liquid nitrogen. The water/dry ice mixture proved unsatisfactory in that the time to cool the sample was excessive and the final temperature on one occasion was 5°C. A mixture of glycol and dry ice proved satisfactory in maintaining a coolant temperature of -3°C to -0.6°C. Thus, the temperature inside the bottle was estimated to be approximately 0°C. The liquid nitrogen provided rapid cooling but the temperature reached inside the bottle was unknown. A temperature of -50°C was assumed in order to calculate the air fraction

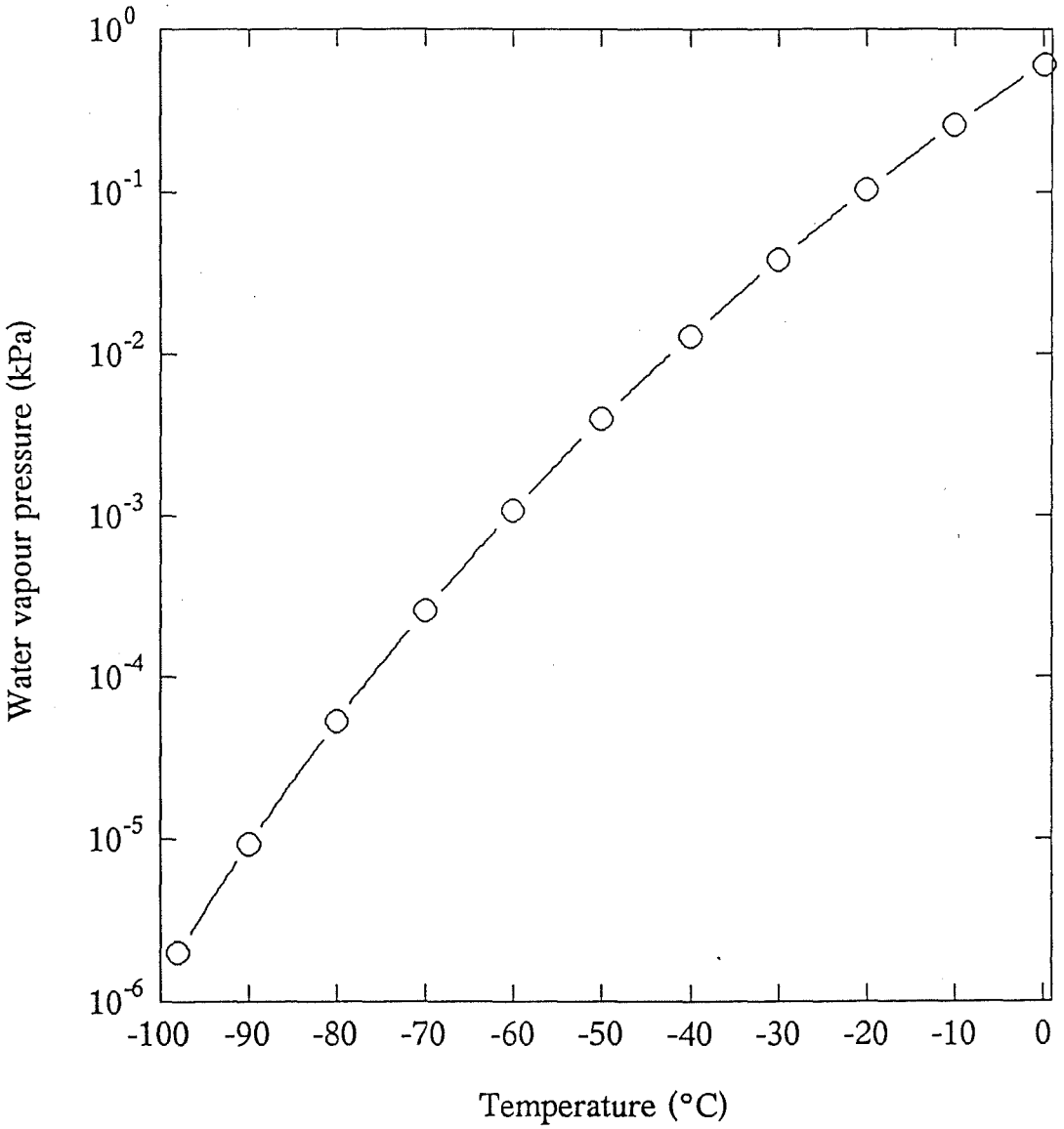

Figure 37.1: Vapour Pressure Over Ice (Sources: Rogers & Mayhew (1982) and Weast & Astle (1980, D195)).

(see Appendix R) but the temperature could have varied widely depending on the amount of water vapour present in the system and the speed at which it travelled to the cold surfaces. The carbon dioxide (freezing point -78°C) could have been frozen in some cases. This aside, the liquid nitrogen would have brought the temperature down to a level where the steam vapour pressure was insignificant, thus the temperature is only required to determine the density.

The average density of a gas sample at low pressure where the surface temperature of the sample container varies widely is a debatable point. The bottle was only partially immersed in the coolant. The water vapour would be expected to travel slowly to the cold surfaces and condense, but there may be a sizable temperature gradient within the bottle. In further work, the possibility of jacketing the entire bottle and fittings so that both coolants and heating mediums can be circulated around the entire apparatus should be considered. This would a feat of engineering, however, and care would have to be taken to ensure that the temperature of the absolute pressure sensors is within their operating range and that temperature compensation is made.

Pressure measurement during sampling and cooling

For Measurements 1-3, the line to the absolute pressure sensors was kept open during sample extraction and cooling of the sample. However, condensation in the lines proved difficult to remove, so for the remainder of the measurements the absolute pressure sensors were isolated until the sample was cooled. The residual pressure then had to be adjusted to account for the change in volume (see Appendix R). The residual pressure in the absolute pressure lines before the valve was opened was assumed to be the water vapour pressure. This was a reasonable assumption except when there was an air leak into the lines (Measurement 5).

Ease of measurements

The time to prepare the apparatus, extract and cool the sample was approximately 1 h at best. The use of multiple sampling containers may be a way of allowing a number of measurements to be taken quickly from a single source. The current apparatus is heavy and would not be practical for taking to commercial plants. Further work should consider ways of reducing the weight and bulk of the apparatus. A means of compressing the sample prior to cooling would improve the accuracy of the measurements.

37.8 Determination of Non-condensable Gas Concentration by Gas Chromatography

The addition of helium (the GC carrier gas) to the condensed sample to bring the sample to above atmospheric pressure looks promising. However, during this work, both an appropriately size bottle of pure helium and a test gas with the desired composition (see Section 8.7) proved unobtainable. Since then, both have arrived but the Research Evaporator is out of action, due to building alterations. The method used here, with some minor refinements to prevent contamination and ease sample extraction, appears suitable for checking the accuracy of the pressure ratio method and to provide a measure of composition.

37.9 Non-condensable Gas Measurement Conclusions

The in-line measurement of temperature and pressure proved unresponsive, perhaps due to the use of a surface temperature probe. Further work is required to evaluate the technique, but its use may be limited to measuring gross levels of air. For example, in the line to the vacuum pump. The extraction of a sample from a de-aeration line operating under vacuum proved difficult. Maintenance of vacuum tight equipment is an on-going problem. Heat tracing of all sample lines is required to ensure no condensation occurs prior to or during sampling. The whole bottle and fittings need to be chilled to ensure a constant temperature in the bottle after cooling. A suitable way of temperature measurement of the sample after cooling needs to be established. The extraction of a sample for GC analysis is feasible.

PART V: OVERVIEW

38 GENERAL DISCUSSION

38.1 Background and Objectives of PhD Programme

A research evaporator was designed and installed at the NZDRI in 1987 to undertake research into evaporator heat transfer and the fouling and cleaning of heat transfer surfaces. The plant was designed with tubes of commercial length and diameter, and with the appropriate total tube circumference in each pass to be able to mimic a modern commercial evaporator. To get the evaporator functioning correctly was seen to require an extensive amount of effort. The PhD programme was proposed to ensure that the work was done with minimal interruption. The programme as proposed was to determine heat transfer coefficients for skim milk and whole milk under a range of operating conditions and to conduct a seasonal trial to determine the effect of seasonal changes in milk on the evaporation process. The programme was to investigate the fouling of heat transfer surfaces but cleaning of the fouled surfaces was the subject of another programme of work.

The commissioning of the evaporator proved to be troublesome for a variety of reasons. Several instruments did not meet their manufacturer's specifications, the positive displacement pump performance was abysmal, and the original method for measuring the pump suction side level was flawed. The hysteresis of the control valves (Fisher) was found to be 10% of travel at best, so positioners had to be installed. The direct steam injection (DSI) unit fouled rapidly on skim milk and limited runs to 4-5 h when it was in operation.

Attempting to fix the above problems delayed the start of the experimental programme and meant that the first trials carried out were the seasonal trials on skim milk and whole milk during the 1990/91 dairy season. The action of foam and an unsuitable level measurement technique (capacitance probe) ensured that the flow rate between each pass of the evaporator was unstable and therefore these results are not reported in this work. The plant was modified before the 1991/92 season and a more suitable level measurement system (differential pressure) was tested. The process hall (in which the evaporator was situated) was to shut down in April 1992 for 6-9 months for refurbishment. This forced major modifications to the PhD experiment programme, to ensure completion of the experimental work before the closure. The plant was not running reliably as a five pass

evaporator, and the condenser was undersized, so the work was done using only one calandria at a time.

The approach taken was to investigate the effect of a large number of variables on water which had constant properties over the length of the tube, and then investigate the relevant variables on sucrose (because it was a Newtonian fluid, was readily available, and there was a reasonable amount of physical property information available) and then finally on skim milk (a non-Newtonian, thixotropic fluid with variable composition).

The required modifications to the Research Evaporator and the recommended direction of further work is discussed later.

38.2 Thickness of Boiling Film

The thickness of the film was estimated using Equations 10.1-10.2. Results for a range of conditions are shown in Table 38.1. The effect of ripples and a co-current vapour flow are not allowed for in Equation 10.1. Ripples would increase the area disturbed by the film, whereas the vapour flow would be expected to flatten the film against the wall. Thus the above analysis should give a reasonable estimate of the film thickness. Except at very high sucrose or skim milk concentrations, the film was less than 1 mm thick.

Table 38.1: Boiling Film Thickness at 60°C.

Fluid Type	Reynolds Number	Viscosity (kg m-2 s^{-1})	Film Thickness (mm)		$(1 - (d_v/d_{ID})^2)^a$ (%)	
			Laminar Flow Equation 10.1	Turbulent Flow Equation 10.2	For 23 mm tube	For 48 mm tube
Water	400-2800	0.463×10^{-3}	0.19-0.36	0.15-0.40	3.3-6.3	1.6-3.0
Sucrose 57% TS	120	6.95×10^{-3}	0.66	0.43	11.3	5.4
Sucrose 75% TS	9	0.104	1.6	0.68	26.3	12.9
Skim milk 48% TS	26	0.045	1.2	0.55	20.0	9.7

[a]Percentage of cross-sectional area taken up by liquid under laminar flow (Equation 10.1).

The data, presented in Table 38.1, represent the range experienced during the water experiments and the maximum levels encountered during the sucrose and skim milk experiments. The reduction in area for vapour flow is greater for the smaller tube and therefore the larger tube diameter is preferred. The vapour flow per tube will naturally

drop as the concentration increases (lower overall HTC) and therefore the increase in film thickness is unlikely to cause a greater pressure drop over the tube length.

38.3 Entry Effects

The boiling film flow on entering the tube takes some distance to stabilise itself under either laminar or turbulent flow. Struve (1969) demonstrated that when adding refrigerant R11 to the outside of a tube, the film flow was stable within 1 m of the entry point. The effect of a co-current vapour flow on the inside of the tube would be expected to reduce the length over which the entry effects occur. Thus as the tube length was 10 m or 15 m, the portion of the tube under entrance conditions could be considered insignificant. The degree of flash did not affect significantly the overall HTC which also confirms the insignificance of the entry effects. The entry effects may however play a main role in fouling which was not investigated in depth in this work.

38.4 Evaporation of Milk

This work only provided some preliminary data on heat transfer coefficients for skim milk at high tube liquid loadings. The results obtained compared poorly with the dimensional models from the sucrose and water work (see Figures 31.10 and 31.11).

The numerical model using the Chun & Seban local Nusselt number correlations provided conservative overall HTCs (see Figure 31.8) but is probably the best method to use for predicting the overall HTC. It is possible that the conservative predictions is due to the quality of the available physical property data. This is an important area for further work, especially in light of the non-Newtonian behaviour of milk. The composition of milk varies during the season and any physical property work should try to determine the effects of these changes.

The minimum allowable wetting factors to prevent rapid fouling of the heat transfer surfaces is a important area for further study, along with the study of CIP effectiveness.

38.5 Research Evaporator Modifications

The Research Evaporator requires modification to ensure steady product transfer flow rates and to provide preheat treatment. An additional condenser is ready for installation to increase the evaporation capacity. The foaming (due probably to air leaks) needs to be reduced or eliminated.

The selection of a suitable product pump is not a simple problem. The existing rotary lobe pumps have proved unable to cope with the duty, in particular the vacuum. This may be due to tiny air leaks through the dry seals, although no back flow of bubbles has been observed. A liquid seal would present problems as the potential for water leaking into the product would make the use of flow measurement for determining evaporation unreliable. The use of a multi-stage centrifugal pump would eliminate the need for level control but a sanitary pump may be hard to find and probably is expensive. The installation of a centrifugal pump to prime the positive lobe pump may be a solution.

The direct steam injection unit proved unsuccessful and experience gained on UHT pilot plants suggests it may be a factor of scale problem. A different device, where the steam is drawn in by the liquid flow, has apparently been proved successful on a pilot plant scale and will be considered as the next method to try.

39 CONCLUSIONS

A large body of experimental heat transfer data was obtained on well-instrumented, commercial sized evaporator tubes at commercial operating conditions. Data were obtained on water, sucrose solutions, and, skim milk concentrates. Variables investigated on water were tube liquid loading, temperature driving force, boiling temperature, feed temperature (degree of flash), tube diameter, and, steam-side factors. The steam-side factors looked at were the non-condensable gas concentration, the location of de-aeration ports and de-aeration flow rates. Variables evaluated on sucrose solutions were feed concentration, tube liquid loading, boiling temperature, temperature driving force, degree of flash on entry, and, tube diameter. For skim milk, the effects of pre-heat treatment and feed concentration were investigated.

The work confirmed the significant effect of the boiling temperature, the temperature driving force, the tube liquid loading, the non-condensable gas concentration in steam, the de-aeration rate and the de-aeration port location(s) on the overall heat transfer coefficient (HTC). The effect of the degree of flash on the overall heat transfer was insignificant on water and sucrose, which indicates that the entrance boiling film flow behaviour does not affect the overall HTC in long tube evaporators. A reduction in tube diameter was shown to reduce heat transfer due to increasing pressure drop over the tube length.

The local boiling Nusselt number correlations of Chun & Seban (1971) proved superior to those of Billet (1989) and fitted the water and sucrose experimental data well. The Billet correlations over-predicted the Nusselt number in the transitional zone, and their adjustment for Prandtl number did not extrapolate well outside the fitted range (1 to 10).

The presence of a local maximum overall heat transfer coefficient in the transitional flow regime was confirmed on water. Struve (1969) had obtained data on Refrigerant R11 which also exhibits a local maximum. This shows that the transitional flow behaviour is more complex than previously thought.

Heat transfer data were obtained at high Prandtl numbers (up to 250) under conditions which ensured large changes in both the local Reynolds number and the local Prandtl numbers over the length of the tube. Numerical integration of Chun & Seban local Nusselt number correlations over the length of the tube, demonstrated that mean Reynolds and Prandtl numbers could be

reasonably approximated by using linear means of entry and exit values.

The dramatic effect of the presence of low concentrations of non-condensable gases in condensing steam on the overall heat transfer coefficient was confirmed.

40 RECOMMENDATIONS FOR FURTHER WORK

The physical properties of milk under conditions found in evaporators needs to be investigated thoroughly. The work should identify the milk components which have a significant effect on the specific physical property, so that the effect of variations in milk stream composition due to seasonal changes and processing can be allowed for.

The Research Evaporator needs to be modified so that it can be run successfully as a five pass evaporator. This will enable work to carried out looking at the effect of fluid composition, thermal history, liquid loading and concentration on the overall heat transfer coefficient, fouling rates and cleaning-in-place requirements.

The development of a simple apparatus to measure a local boiling film heat transfer coefficient of the fluid leaving an evaporator pass should be considered as a means of obtaining data which could be used to improve the Chun & Seban correlations for Nu_e in the transition region.

The modelling of NCG concentration profiles in the steam side of the calandria using an elliptic technique should be considered. The feasibility of installing thermocouples inside the calandria shell to measure local temperatures should also be investigated.

Work is required to verify the boiling regime for milk over the range of temperature driving forces used in commercial evaporators.

REFERENCES

Al-Diwany, H K & Rose, J W (1973). Free convection film condensation of steam in the presence of non-condensing gases. *International Journal of Heat and Mass Transfer*, **16**, 1359-1369.

Al-Zubaidi A A J (1987). Sea water desalination in Kuwait - A report on 33 years experience. *Desalination*, **63**, 1-55.

Åsblad A & Berntsson T (1990). Surface evaporation of turbulent falling films. *International Journal of Heat and Mass Transfer*, **34**, 3, 835-841.

Baloh T (1984). Wärmeübergang im verdampferrohr. *Zuckerindustrie*, **109**, 10, 916-921.

Bloore C G (1981). A quality control system for the manufacture of spray dried milk powders. *PhD thesis*, Massey University, Palmerston North, New Zealand.

Billet R (1989). *Evaporation Technology - Principles, Applications, Economics.* VCH Verlagsgescllschaft mbH, Weinheim, Germany.

Bird M R & Fryer P J (1991). An experimental study of the cleaning of surfaces fouled by whey proteins. *Trans IChemE*, **69**, Part C, 13-21.

Bird R B, Stewart W E & Lightfoot E N (1960). *Transport Phenomena.* John Wiley & Sons, Inc., New York.

Buckingham J H (1973). *Kinematic viscosities of reconstituted skim milk.* Physics and Engineering Laboratory, Department of Science and Industrial Research, New Zealand, Report No 444.

Cairns, R C (1953). The condensation of vapour from gas-vapour mixtures. *Chemical Engineering Science*, **2**, 127-138.

Castellan, G W (1972). *Physical Chemistry*. 2nd edn., Addison-Wesley Publishing Co, Reading.

Chun K R & Seban R A (1971). Heat transfer to evaporating liquid films. *ASME Journal of Heat Transfer*, **93**, 391-396.

Chun K R & Seban R A (1972). Performance prediction of falling-film evaporators. *ASME Journal of Heat Transfer*, **94,** 432-436.

Chun M H & Kim K T (1990). Assessment of the new and existing correlations for laminar and turbulent flow film condensations on a vertical surface. *International Communications in Heat and Mass Transfer*, **17**, 431-441.

Colburn A P & Hougen O A (1934). Design of cooler condensers for mixtures of vapors with noncondensing gases. *Industrial and Engineering Chemistry*, **26**, 1178-1182.

Coulson J M & Richardson J F (1968). *Chemical Engineering - Volume Two Unit Operations*. 2nd edn., Pergamon Press, Oxford.

Creamer, L (1988). The proteins and minerals of milk. *Dairy Science Summer School - Application of Science to Dairy Manufacture*, Dairy Technology Society (NZ) Inc., Palmerston North, 23-29.

Denny, V E & Mills, A F (1969). Nonsimilar solutions for laminar film condensation on a vertical surface. *International Journal of Heat and Mass Transfer*, **12**, 965-979.

Denny, V E, Mills, A F & Jusionis, V J (1971). Laminar film condensation from a steam-air mixture undergoing forced flow down a vertical surface. *Journal of Heat Transfer, Trans. ASME (C)*, **93**, 3, 297-304.

Fergusson P H (1989). Developments in the evaporation and drying of dairy products. *Journal of the Society of Dairy Technology*, **42**, (4), 94-101.

Gordon W G & Kalan E B (1974). Proteins of milk. In *Fundamentals of Dairy Chemistry* (Webb B H, Johnson A H & Alford J A, Eds., 2nd edn., AVI Publishing Company Inc., Westport, Connecticut.), 87-124.

Grace H P & Lapple C E (1951). Discharge coefficients of small-diameter orifices and flow nozzles. *Trans. ASME*, **73**, 639-647.

Gray R M (1981). Technology of skimmed milk evaporation. *Journal of the Society of Dairy Technology*, **34**, (2), 53-57.

Grey I K (1988). The gross composition of milk and factors that influence it. *Dairy Science Summer School - Application of Science to Dairy Manufacture*, Dairy Technology Society (NZ) Inc, Palmerston North, 23-29.

Hall C W & Hedrick T I (1966). *Drying of Milk and Milk Products*, AVI Publishing Company Inc., Westport Connecticut.

Hill B M (1993). *Personal communication*, Microbiologist, New Zealand Dairy Research Institute.

Houšová J (1970). Přestup tepla při varu v odparkách se stékajícím filmem. *Prûmysl Potravin,* **21**, (1), 7-12.

Incropera F P & DeWitt D P (1990). *Fundamentals of Heat and Mass Transfer*, 3rd edn., John Wiley & Sons, New York.

Janssen P W M (1989). *Research Evaporator Control System Operation Manual*, Engineering Services Section, New Zealand Dairy Research Institute, Palmerston North.

Jebson R S & Iyer M (1991). Performances of falling film evaporators. *Journal of Dairy Research*, **58**, 29-38.

Jebson R S (1992, 1994). *Personal communications*, Food Technology, Massey University, Palmerston North.

Johnson A H (1974). The composition of milk. In *Fundamentals of Dairy Chemistry* (Webb H W, Johnson A H & Alford J H Eds., 2nd edn., AVI Publishing Co, Westport Connecticut.), 1-57.

Kessler H G (1987). Multistage evaporation and water vapour recompression with special emphasis on high dry matter content, product losses, cleaning and energy savings. *Milk - The vital force. Proceedings of the 22nd International Dairy Congress, The Hague, Sept 29 - Oct 3 1986*, D. Reidel Publishing. Co., Dordrecht, 545-558.

Khan, R A (1972). Effect of noncondensables in sea water evaporators. *Chemical Engineering Progress*, **68**, 7, 79-80.

Knipschildt M E (1986). Drying of milk and milk products. In *Modern Dairy Technology, Volume 1, Advances in Milk Processing* (Robertson R K, Ed.), Elsevier Applied Science Publishers, London.

Linke W (1953). *Kältetechnik*, **5**, 275

Liu Y J, Deng W Y, Liu Y, Xu Y R & Chong Y O (1991). Experimental study on the heat transfer to milk in a falling film evaporator. *Proceedings of the 19th Australasian Chemical Engineering Conference, Newcastle, Australia*, **1**, 536-541.

Lyle, O (1947). *The Efficient Use of Steam*. His Majesty's Stationary Office, London, 276-286.

Mackereth (1987). Unpublished notes taken while on study leave at APV Anhydro A/S, Copenhagen, Denmark.

Mackereth (1990). Unpublished data from acceptance test on MVR evaporator at Inglewood.

Mills, A F & Seban, R A (1967). The condensation coefficient of water. *International Journal of Heat and Mass Transfer*, **10**, 1815-1827.

Minkowycz, W J & Sparrow, E M (1966a). Condensation heat transfer in the presence of noncondensables, interfacial resistance, superheating, variable properties, and diffusion. *International Journal of Heat and Mass Transfer*, **9**, 1125-1144.

Minkowycz, W J & Sparrow, E M (1966b). Free convection heat transfer to steam under variable property conditions. *International Journal of Heat and Mass Transfer*, **9**, 1145-1147.

Mojonnier T & Troy H C (1925). *Technical Control of Milk Products*, 2nd edn., Mojonnier Bros. Co., Chicago, Illinois., 122.

Morley, T B (1912). Properties of air and steam mixtures in relation to condensing plant. *Engineering*, 76-77.

Müller-Steinhagen H (1989). Heat transfer & heat exchanger design. *Continuing Education Seminar notes*, Chemical and Materials Engineering Department, University of Auckland, Auckland.

Nicol W M (1968). Boiling point elevation of pure sucrose solutions. *International Sugar Journal*, **70**, 199-202.

Northcroft, L G (1943). Air in steam. *Power and Works Engineer*, **38**, 442, 77-78.

Nusselt W (1916). Die oberflächkondensation des wasserdampfes. *Ver. Deutscher Ing. Zeit*, **60**, 541-546.

Pancoast H M & Junk W R (1980). *Handbook of Sugars*, 2nd edn., AVI Publishing Co, Westport, Connecticut.

Parry R M (1974). Milk coagulation and protein denaturation. In *Fundamentals of Dairy Chemistry* (Webb H W, Johnson A H & Alford J H Eds., 2nd edn., AVI Publishing Co, Westport Connecticut.), 603-611.

Patankar, S V & Spalding, D B (1967). A finite-difference procedure for solving the equations of the two-dimensional boundary layer. *International Journal of Heat and Mass Transfer*, **10**, 1389-1411.

Patankar, S V (1988a). Parabolic systems: Finite-difference method I. In *Handbook of Numerical Heat Transfer* (Minkowycz W J, Sparrow E M, Schneider G E & Pletcher R H, Eds., John Wiley & Sons, New York.), 89-115.

Patankar, S V (1988b). Elliptic systems: Finite-difference method I. In *Handbook of Numerical Heat Transfer* (Minkowycz W J, Sparrow E M, Schneider G E & Pletcher R H, Eds., John Wiley & Sons, New York.), 215-240.

Poots, G & Miles, R G (1967). Effects of variable physical properties on laminar film condensation of saturated steam on a vertical plate. *International Journal of Heat and Mass Transfer*, **10**, 1677-1692.

Rogers G F C & Mayhew Y R (1982). *Thermodynamic and Transport Properties of Fluids - SI Units*, 3rd edn., Basil Blackwell, Oxford.

Slegers, L & Seban, R A (1970). Laminar film condensation of steam containing small concentrations of air. *International Journal of Heat and Mass Transfer*, **13**, 1941-1947.

Smith, J A (1906a). Experiments on surface condensation. *Engineering*, 395-399.

Smith, J A (1906b). Air in relation to the surface condensation of low-pressure steam. *The Engineer (London)*, 75-76.

Snoeren T H M, Brinkhuis J A, Damman A J & Klok H J (1984). Viscosity and age-thickening of skim-milk concentrate. *Neth. Milk Dairy J.*, **38**, 43-53.

Sparrow, E M & Eckert, E R G (1961). Effects of superheated vapor and noncondensable gases on laminar film condensation. *American Institute of Chemical Engineers Journal*, **7**, 3, 473-477.

Sparrow, E M & Lin, S H (1964). Condensation heat transfer in the presence of a noncondensable gas. *Journal of Heat Transfer, Trans. ASME (C)*, **86**, 430-436.

Sparrow, E M, Minkowycz, W J & Saddy, M (1967). Forced convection condensation on the presence of noncondensables and interfacial resistance. *International Journal of Heat and Mass Transfer*, **10**, 1829-1845.

Struve, H (1969). Der wärmeübergang an einen verdampfenden rieselfilm. *VDI-Forschungsheft 534*, VDI-Verlag, Düsseldorf.

Trinh, T K (1993). *Personal communication*, New Zealand Dairy Research Institute.

Wassner L (1981). Wärmetechnische auslegung von fallfilmverdampfern; Theorie und Anwendung. *Forschung im ingenieurwesen*, **47**, 4, 125-130.

Weast R C & Astle M J - Eds. (1980). *CRC Handbook of Chemistry and Physics*, 60th edn., CRC Press Inc., Boca Raton, Florida.

Wood P W (1982). *Physical Properties of Dairy Products.* 2nd edn., Dairy Division of the Ministry of Agriculture and Fisheries, Wellington, Report No T2/82.